Universidade do Minho
Escola de Engenharia

Vitor Manuel Correlo da Silva

Development of New Chitosan Based BiodegradableBlends for Bone and Cartilage Tissue Engineering

Agosto 2009

Development of New Chitosan Based Biodegradable Blends for Bone and Cartilage Tissue Engineering
Vitor Manuel Correlo da Silva
UMinho | 2009

Universidade do Minho
Escola de Engenharia

Vitor Manuel Correlo da Silva

Development of New Chitosan Based Biodegradable Blends for Bone and Cartilage Tissue Engineering

Tese de Doutoramento em Ciência e Tecnologia
de Materiais: Engenharia de Tecidos - Materiais Híbridos

Trabalho efectuado sob a orientação do
Professor Rui Luís Gonçalves dos Reis
Professor Nuno João Meleiro Alves das Neves
Professor Mrinal Bhattacharya

Agosto 2009

To my mother, my wife and my son

ACKNOWLEDGEMENTS.

In the last few years I had the privilege of knowing and working with many exceptional and talented people that directly and indirectly contributed to the accomplishment of the work described in this thesis. To them, I would like to deeply express my gratitude and dedicate this thesis.

My first acknowledgments are made to my supervisor Prof. Rui Reis, which gave me the privilege of being a part of the 3B's Group some years ago. This thesis is the corollary of his advises, confidence and way of thinking that always transmitted to me since the period that I arrived on his group to start the graduation thesis. During this period he always transmitted me motivation and as natural leader showed me that it is always possible to do better. His accomplishments, professionalism and leadership are a motivation and make me feel privileged by working under his supervision.

To Prof. Nuno Neves, for his knowledgeable and careful supervision of my work. He showed always to be available and, above all, he constantly gave me important advices and inputs that resulted in the improvement of my work. I'm also thankful to Prof. Nuno for the time that he patiently lost with me explaining me how to overcome my limitations and doubts.

To Prof. Mrinal Bhattacharya, my co-supervisor, for guiding my scientific work and helping me on the processing lab during the first extrusion learning stages. I really enjoyed all our discussions around science and about the American way of thinking (and about football…). I also acknowledge the way Prof. Mrinal received me at the University of Minnesota that made me feel like at home during my stay at USA.

During the development of this thesis was had the fortune of make friends that with their intelligence, professionalism and friendship where an inspiration for me. To them, Rui Amandi, Ana Leite, Miguel Oliveira, Patricia Malafaya, João Oliveira, Emanuel Fernandes, Susana Silva and Tiago Silva I would like to express my deep gratitude.

I wish to give my sincere thanks to Luciano Boesel that even being abroad was always a good friend and was one of the first persons helping me when I arrived on the 3B's research group.

Additionally, I would like to use this opportunity to thank the following people for their help and support throughout the PhD thesis: Ana Rita Pinto, Paula Sol, Elisabete Pinho and Marta Silva.

I am also sincerely grateful to Alexandra Marques for being a good friend and for the help and supot on understanding the biocompatibility phenomenum.

I acknowledge Adriano Pedro for being a good friend, help me secure the data and provide a valuable assistance for solving problems with my laptop.

I cannot forget and express particular gratitude to the members of the 3B's management team especially, Ariana Santos, Virginia, Fátima, Berta and even being absent Tánia Alves,.

I would also like to express my gratitude to many people that made my work easier throughout these years. I would like to acknowledge the support of the technicians at the University of Minho, namely Francisco Mateus, Serafim Sampaio, João Paulo Peixoto, Manuel Escourido, Mauricio Malheiro and Elsa Ribeiro.

To the Portuguese Foundation for Science and Technology for the financial support through a PhD grant (SFRH/BD/22455/2005). This work was also partially supported by the EU project GENOSTEM (LSHB-CT-2003-503161).

I'm especially grateful to my dear friends Nuno Ferreira, Luisa Lestra, Manuel Vaz, Conceição Ferreira and Iola Rodrigues for the good moments that they provide me. I am a lucky person to have you around as friends.

My complete thankfulness to my family, namely my mother, my grandmother, my brother, my sisters in law Idalina and Carla, my brother in law Medeiros, Claudia's grandfather Sr. Sousa, Claudia's parents Sr. Correia e D. Clarisse, my nieces Margarida, Ana Claudia e Mariana, for their unconditional love and care. They represent the good port that I can reach in the good and bad moments. I could never accomplish this stage without their support. This thesis is dedicated to them.

By last, my final words go out to my dearest wife Claudia. For her love, patience, dedication and for letting me be part of her life. She is the light and inspiration that makes my life better. To her I dedicate this thesis.

Development of new chitosan based biodegradable blends for bone and cartilage tissue engineering

ABSTRACT.

A number of natural origin polymers are being employed in tissue engineering strategies. Natural origin polymers offer the advantage of being similar to macromolecular substances, which the biological environment is prepared to recognize and to deal with metabolically. Another attractive characteristic of natural polymers is their ability to be degraded by naturally occurring enzymes, implying that the implant will be degraded and eventually metabolized by physiological mechanisms. Chitosan, a mucopolysaccharide, is the alkaline deactylated product of chitin and has structural similarities to glycosaminoglycans, thus, mimicking their functional behaviour. Moreover, it is reported to be typically non-toxic, biodegradable, and biocompatible. Chitosan exhibit a range of properties that make it suitable for use as alternatives to currently used biomaterials, but its mechanical properties and processability are less than ideal which precludes its use as material in load bearing applications. The development of hybrid materials that combine naturally occurring polymers with biocompatible synthetic polymers is expected to be able to minimize the mismatch of mechanical properties and to preserve the functional biocompatibility. However, little research has been conducted in the melt blending of synthetic polyester and chitosan. The main objectives of this thesis were to: i) compound and evaluate the properties of chitosan and biodegradable aliphatic polyesters blends and composites processed using melt based technologies; ii) study the water absorption and degradation characteristics of the produced blends and composites; iii) produce chitosan-based scaffolds with different architectures by melt based technologies.; iv) evaluate their potential cytotoxic behaviour and to conduct direct contact assays aiming to validate their potential use in bone or cartilage tissue engineering applications.

The first step of this thesis experimental work was to melt blend chitosan with poly-ε-caprolactone (PCL), poly(butylene succinate) (PBS), poly(lactic acid) (PLA), poly(butylene terephthalate adipate) (PBTA), and poly(butylene succinate adipate) (PBSA). For the chitosan/PBS blend, the amount of chitosan was varied from 25% to 70% by weight. The remaining polyesters had 50% of chitosan by weight. The morphology, tensile and thermal properties of the produced blends were evaluated.

Composites consisting of hydroxyapatite, chitosan, and aliphatic polyester were also compounded using a twin-screw extruder. The polyesters used were the same applied in blends preparation. The mass fraction of chitosan ranged from 17.5 to 45%, while that of HA ranged from 10 to 30%. The tensile

properties (tensile strength and tensile modulus), thermal properties, and morphological properties of the composites were evaluated. Ternary blends often lead to complex morphology and poor properties.

The water absorption and degradation of the developed chitosan-based blends and composites were also evaluated, since these properties are critical for their possible applications as biomaterials. These studies revealed that chitosan content significantly affects the water uptake, weight loss and mechanical properties of the developed blends. The weight loss also directly correlates with the HA content being higher for higher HA amount present in the composite.

Novel scaffolds made from chitosan-based blends and composites were produced by the melt-based routine involving compression molding and salt leaching. The scaffolds were made with different pore sizes and porosity, aiming at applications in bone and cartilage tissue engineering. Cytotoxicity evaluation were carried out using standard tests, revealing that L929 cells had comparable metabolic activities to that obtained for the negative control.

Chitosan based fibers and chitosan fiber mesh scaffolds could also be prepared by melt processing (solvent-free) to be used as tissue engineering templates. Biological assessment was performed in direct contact assays, using a human osteosarcoma cell line (SaOs-2). Cells showed remarkable cell colonization, not only at the surface but also in the inner porous structure of the different scaffolds. Furthermore, the cells showed high indexes of viability in all the scaffold types.

The motivation for this thesis was to develop and to produce a new range of chitosan based scaffolds using novel polymeric blends and composites in an established and reproducible melt processing technology. Most of the approaches reported in the literature to produce scaffolds from chitosan-based blends or composites involve the use of solvents, being this work the first that reports the successful use of a melt-based route. Moreover, the methodologies used are very versatile and avoid the drawbacks associated with solvents and allows for producing a large variety of scaffolds with a wide range of porosities and pore morphologies using different polymers.

Desenvolvimento de novas misturas biodegradáveis à base de quitosano para ser usadas em engenharia de tecidos do osso e cartilagem

RESUMO.

Um número cada vez maior de polímeros de origem natural tem sido utilizado em estratégias de engenharia de tecidos. Estes oferecem a vantagem de serem similares a substâncias macromoleculares, cujo sistema biológico está preparado para reconhecer e lidar metabolicamente. Outra característica interessante dos polímeros naturais é a possibilidade de serem degradados por enzimas existentes no organismo, levando a que o implante seja degradado e eventualmente metabolizado por mecanismos fisiológicos. O quitosano é um produto obtido pela desacetilação alcalina da quitina e tem similaridades estruturais com os glicosaminoglicanos, ou seja, mimetiza o seu comportamento funcional. Além disso, é descrito como sendo tipicamente não-tóxico, biodegradável e biocompatível. O quitosano exibe um espectro de propriedades que o tornam adequado para ser utilizado como alternativa aos biomateriais usados correntemente. Mas as suas propriedades mecânicas e processabilidade não são as ideais limitando a sua utilização em aplicações sujeitas a esforços elevados. É expectável que o desenvolvimento de materiais híbridos, combinando polímeros de origem natural com polímeros sintéticos biocompatíveis, minimize a incompatibilidade das propriedades mecânicas e preserve a sua biocompatibilidade funcional. Pouca ou nenhuma investigação tem sido desenvolvida focando o desenvolvimento de misturas de quitosano com poliésteres utilizado tecnologias baseadas na fusão. Uma vez identificada esta lacuna, os principais objectivos desta tese foram: i) produzir e determinar as propriedades de misturas e compósitos à base de quitosano com poliésteres alifáticos processados por tecnologias baseadas na fusão; ii) estudar as características de absorção de água e degradação das misturas e compósitos produzidos; iii) preparar scaffolds à base de quitosano com diferentes arquitecturas utilizando tecnologias baseadas na fusão; iv) avaliar o seu potencial comportamento citotóxico e conduzir ensaios de contacto directo com o objectivo de validar o potencial de serem utilizados em aplicações para engenharia de tecidos do osso ou cartilagem.

O primeiro passo desta tese em termos de trabalho experimental consistiu em misturar, por técnicas de fusão, quitosano com policaprolactona (PCL), polibutileno succinato (PBS), polibutileno succinato co-adipato (PBSA), polibutileno teraftalato co-adipato (PBTA) e poli (ácido láctico) (PLA). As quantidades de quitosano utilizadas na preparação das misturas de quitosano/PBS variaram entre 25% e 70% em peso. Aos restantes poliésteres foi adicionado 50% em peso de quitosano. As propriedades térmicas e mecânicas e respectiva morfologia das misturas produzidas foram avaliadas.

Compósitos contendo hidroxiapatite (HA), quitosano e poliéster alifático foram preparados utilizando uma extrusora duplo fuso. Os poliésteres utilizados foram os mesmos das misturas anteriormente preparadas. A fracção mássica do quitosano variou entre 17.5% e 45%, enquanto a da HA variou entre 10% e 30%. As propriedades mecânicas à tracção, propriedades térmicas, e propriedades morfologias dos compósitos foram determinadas. As misturas ternárias apresentaram uma morfologia complexa e propriedades mecânicas abaixo do previsto.

O comportamento em termos de absorção de água e degradação das misturas e compósitos à base de quitosano foi determinado uma vez que estas propriedades são criticas na utilização de biomateriais. Estes estudos revelaram que a quantidade de quitosano utilizado afectou significativamente a absorção de água, perda de peso e propriedades mecânicas das misturas produzidas. O perda de peso apresentou também uma relação directa com a quantidade de HA sendo maior nos compósitos preparados com maior quantidade de HA.

Foram produzidos scaffolds com as misturas e compósitos à base de quitosano utilizando métodos baseados na fusão, nomeadamente moldação por compressão com lixiviação de sal. Os scaffolds foram produzidos com diferentes porosidades e diferentes tamanhos de poros com o objectivo de serem utilizados em estratégias de engenharia de tecidos do osso ou cartilagem. Foram realizados ensaios de citotoxicidade usando testes padrão, tendo as células L929 apresentado uma actividade celular semelhante à do controlo negativo.

Fibras e scaffolds, à base de fibras, foram também desenvolvidas por tecnologias baseadas na fusão (sem solventes) para serem utilizados em estratégias de engenharia de tecidos. Foram realizados ensaios biológicos de contacto directo utilizando uma linha celular derivada de osteosarcoma humano (SaOs-2). As células apresentaram uma colonização notável, não apenas na superfície mas também no interior dos scaffolds. Além disso, as células apresentaram altos índices de viabilidade celular em todo o tipo de scaffolds.

A motivação desta tese foi o desenvolvimento e produção de um novo tipo de scaffolds à base de quitosano utilizando novas misturas e compósitos com recurso a tecnologias baseadas na fusão. A maior parte das estratégias descritas na literatura para produção de scaffolds à base de quitosano envolve o uso de solventes, sendo este o primeiro trabalho que descreve o uso com sucesso de tecnologias apenas baseadas na fusão. Além disso, as metodologias usadas demonstraram ser muito versáteis evitando as desvantagens normalmente associadas aos solventes e permitiram a produção de scaffolds uma variabilidade alargada de porosidades e morfologia de poros.

TABLE OF CONTENTS.

LIST OF ABBREVIATIONS.

2-D	two-dimensional;
3-D	three-dimensional;
A	
ALP	alkaline phosphatase;
B	
BA	blowing agent
BCP	biphasic calcium phosphate;
C	
CaP	calcium phosphate
Ch	chitosan;
CPC	calcium phosphate cement;
D	
DD	degree of deacetylation;
DNA	deoxyribonucleic acid;
E	
ECM	extracellular matrix;
ECs	human endothelial cells
E_s	secant modulus;
F	
FDA	US food and drug administration;
G	
GAGs	glycosaminoglycans;
GAM	gene-activated matrices;
H	
HA	hydroxylapatite;
hMSCs	human mesenchymal stem cells;
HPLC	high performance liquid chromatography;
I	
L	
M	
Mimics®	Materialise interactive medical image control system;
μg	micrograms;
μL	microliters;
μm	micrometers;
μ-CT	micro-computed tomography;
N	
O	
OECs	outgrowth endothelial cells
P	
PDLLA	poly(DL-lactic acid)
PEO	polyethylene oxide;
PGA	poly(glycolic acid);
PHA	polyhydroxyalkanoates;
PHB	polyhydroxybutyrate;
PLGA	poly(lactide-*co*-glycolide);
PLLA	poly-(L-lactic acid);
R	
ROS	rat osteosarcoma
RP	rapid prototyping
S	
SaOs-2	human osteoblast-like cells;
SBF	simulated body fluid;
SCA	starch-cellulose acetate;
SEM	scanning electron microscopy;
SEVA-C	starch-ethylene-vinyl alcohol;
SPCL	starch-polycaprolactone;
SPLA	starch-poly(lactic acid);
T	
TCPS	tissue culture polystyrene;
TGA	thermogravimetric analysis;
TGF-β	transforming growth factor beta;
U	
UV	ultraviolet;
V	
VEGF	vascular endothelial growth factor;
W	
WLs	weight loss;
WAs	water absorption;
X	
XRD	X-ray diffraction;
Z	
Z	zeta potential;

LIST OF FIGURES.

LIST OF TABLES.

SHORT *CURRICULUM VITAE*.

Vitor Manuel Correlo da Silva was born in 1974 in Sobradelo da Goma – Póvoa de Lanhoso, Portugal. Nowadays, he lives in Braga and works, as a researcher, in the 3B's Research Group, Department of Polymer Engineering at University of Minho, Headquarters of the European Institute of Excellence on Tissue Engineering and Regenerative Medicine at Avepark, Caldas das Taipas - Guimarães, Portugal. This research group is directed by its founder, Professor Rui L. Reis. This group has been considered as excellent by the Portuguese Foundation for Science and Technology, and is one of the associated units of the Institute for Biotechnology and Bioengineering.

His background includes a graduation in Materials Engineering from University of Minho that he finished with a final graduation mark of 14 (0-20 scale). During the final year of his degree, he developed is final research project on the theme "Optimization of the processing conditions of biodegradable polymers for medical application" in the Department of Polymer Engineering, University of Minho, Portugal. This work was supervised by Professor Rui L. Reis and co-supervised by Prof. Nuno M. Neves.

In 2004, he formally started his PhD at the 3B's Research Group under the scope of the Genostem project. In 2005, he received a grant from the Portuguese Foundation for Science and Technology (FCT) which enabled him to perform work at the University of Minnesota, USA, under the local supervision of Prof. Mrinal Bhattacharya.

As a researcher in the 3B's Research Group, he has been involved in the writing, preparation, and supporting management of several grant proposals both at National and European levels. He was also involved in the development and writing of the business plan of STEMMATERS which is the biotechnological spin-off of the 3B's Research Group that has been awarded in 2007 with the National Award for Entrepreneurship (START). He is also member since the foundation (2004) of the DNAPC (Departament of New Applications and/or Products in/with Cork) group.

As a result of his research efforts within the field of tissue engineering and regenerative medicine, presently he is author or co-author of more than 12 publications in international journals, 3 book chapters and approximately 33 communications (as oral presenter/poster presenter) in international meetings.

LIST OF PUBLICATIONS.

The research work carried out during the PhD period resulted in the following publications:

INTERNATIONAL JOURNALS WITH REFEREE, AS FIRST AUTHOR

Correlo VM, Bhattacharya M, Neves NM and Reis RL, 2009, Natural origin polymers and processing methods for scaffolds preparation and their use in bone or cartilage tissue engineering applications, *submitted*

Correlo VM, Costa-Pinto AR, Sol P, Covas JA, Bhattacharya M, Mano JF, Neves NM and Reis RL, 2009, Melt processing of chitosan-based fibers and fiber-mesh scaffolds for the engineering of connective tissues, Acta Biomaterialia, *submitted*

Correlo VM, Boesel LF, Pinho ED, Costa-Pinto AR, Alves da Silva ML, Bhattacharya M, Mano JF, Neves NM and Reis RL, 2008, Melt-based compression moulded scaffolds from chitosan-polyester blends and composites: morphology and mechanical properties, Journal of Biomedical Materials Research: Part A, **DOI - 10.1002/jbm.a.32221,** *in press*

Correlo VM, Pinho ED, Pashkuleva I, Bhattacharya M, Neves NM and Reis RL, 2007, Water absorption and degradation characteristics of chitosan-based polyesters and hydroxyapatite composites, Macromolecular Bioscience, **7(3)**:354-363

Correlo VM, Boesel LF, Bhattacharya M, Mano JF, Neves NM and Reis RL, 2005, Hydroxyapatite reinforced chitosan and polyester blends for biomedical applications, Macromolecular Materials and Engineering, **290(12)**:1157-1165

Correlo VM , Boesel LF, Bhattacharya M, Mano JF, Neves NM and Reis RL, 2005, Properties of melt processed chitosan and aliphatic polyester blends, Materials Science and Engineering A - Structural Materials Properties Microstructure and Processing, **403(1-2)**: 57-68

BOOK CHAPTERS AND CONFERENCE PROCEEDINGS WITH REFEREE, AS FIRST AUTHOR

Correlo VM , Gomes ME, Tuzlakoglu K, Oliveira JM, Malafaya PB, Mano JF, Neves NM and Reis RL, 2007, Tissue Engineering Using Natural Polymers, In Biomedical Polymers , eds. Mike Jenkins, Woodhead publishing Ltd , Cambridge, 197-217

Correlo VM, Sol PC, Novikoff S, Neves NM and Reis RL, 2008, Novel PHB/PCL Scaffolds Produced by Melt Base Technologies, Tissue Engineering: Part A, **14** : 890

INVITED LECTURES

Correlo VM, Neves NM and Reis RL, Polímeros biodegradáveis de origem natural para engenharia de tecidos do osso e cartilagem, JORTEC 2009, Lisboa, Portugal, May 2009.

ORAL PRESENTATIONS IN INTERNATIONAL MEETINGS, AS FIRST AUTHOR

Correlo VM, Pinho ED, Bhattacharya M, Mano JF, Neves NM and Reis RL, Novel Melt Processable Chitosan/Polyester Blends and Composites: Extensive Characterization Aiming at There Biomedical Application, Euromat 2005 - European Congress on Advanced Materials and Processes, Prague, Czech Republic, September 2005.

POSTER PRESENTATIONS IN INTERNATIONAL MEETINGS, AS FIRST AUTHOR

Correlo VM, Martins A, Bhattacharya M, Charbord P, Reis RL and Neves NM, Production of porous scaffolds for bone and cartilage tissue engineering, Genostem 2nd Workshop on Mesenchymal Stem Cells Enginnering for ConectiveTissue Disorders, Porto, Portugal, January 2006

Correlo VM, Boesel LF, Costa-Pinto AR, Bhattacharya M, Reis RL and Neves NM, Novel 3-D Chitosan/Polyester Scaffolds for Bone and Cartilage Tissue Engineering, 19th European Conference on Biomaterials, Sorrento, Italy, September 2005

Correlo VM, Boesel LF, Costa-Pinto AR, Bhattacharya M, Mano JF, Neves NM and Reis RL, Melt Processing Chitosan/ Poly-å-caprolactone Blends to be used in Bone Tissue Engineering, 3rd EPF Summer School, Saint-Dié-des-Vosges, France, May 2005

INTERNATIONAL JOURNALS WITH REFEREE, AS CO-AUTHOR

Alves da Silva ML, Crawford A, Mundy JM, **Correlo VM**, Sol PC, Bhattacharya M, Hatton PV, Reis RL and Neves NM, 2009, Chitosan/ Polyester – Based Scaffolds For Cartilage Tissue Engineering: Assessment of Extracellular Matrix Formation, *submitted*

Oliveira JT, Crawford A, Mundy JL, Sol PC, **Correlo VM**, Bhattacharya M, Neves NM, Hatton PV, Reis RL, 2009, Novel Melt-Processable Chitosan-Polybutylene Succinate Fibre Scaffolds for Cartilage Tissue Engineering, Journal of Biomaterials Science, Polymer Edition, *submitted*

Costa-Pinto A. R., **Correlo VM**, Sol PC, Bhattacharya M, Charbord P, Delorme B, Reis RL and Neves NM, 2009, Osteogenic Differentiation of Human Bone Marrow Mesenchymal Stem Cells Seeded on Melt based Chitosan scaffolds for Bone Tissue Engineering Applications, Biomacromolecules, **10(8)**: 2067-2073

Costa-Pinto AR, Salgado AJ, **Correlo VM**, Sol PC, Bhattacharya M, Charbord P, Reis RL and Neves NM, 2008, Adhesion, proliferation, and osteogenic differentiation of a mouse mesenchymal stem cell line (BMC9) seeded on novel melt-based chitosan/polyester 3D porous scaffolds, Tissue Engineering Part A, **14 (6)**: 1049-1057

Oliveira JT , **Correlo VM**, Sol PC, Costa-Pinto AR, Malafaya PB, Salgado AJ, Bhattacharya M, Charbord P, Neves NM and Reis RL, 2008, Assessment of the Suitability of Chitosan/PolyButylene Succinate Scaffolds Seeded with Mouse Mesenchymal Progenitor Cells for a Cartilage Tissue Engineering Approach , Tissue Engineering - Part A, **14(10)**: 1651-1661

Silva SP, Sabino MA, Fernandes EM, **Correlo VM**, Boesel LF and Reis RL, 2005, Cork: properties, capabilities and applications, International Materials Reviews, **50 (6)**: 345-365

BOOK CHAPTERS AND CONFERENCE PROCEEDINGS WITH REFEREE, AS CO-AUTHOR

Sousa RA, **Correlo VM**, Chung S, Neves NM, Mano JF and Reis RL, 2008, Processing of thermoplastic natural-based polymers: an overview of starch based blends, In Handbook of Natural-based Polymers for Biomedical Applications, eds. Neves NM, Mano JF, Gomes ME, Marques AP, Azevedo HS, Reis RL, Cambridge, 85-105

Marchiori-Silva V, Han SW, Novikoff S, Semedo P, Reis RL, **Correlo VM**, Lisboa BCG, Camara NOS, 2008, Polyhydroxybutyrate (PHB) from sugar cane as biomaterial for bone tissue engineering using mesenchymal stem cells derived from human dental pulp, International Journal of Artificial Organs, **31(7)**: 600

Sangwon Chung, Martins A, **Correlo VM**, Oliveira JT, Marques AP, Neves NM, Mano JF, Sousa RA and Reis RL, 2008, Dependence of cell proliferation on the morphology of starch based scaffolds for tissue engineering, Tissue Engineering – Part A, **14**: 718

Alves da Silva ML, Martins A, Costa, P. F., **Correlo VM**, Sol PC, Bhattacharya M, Rougier N, Reis RL and Neves NM, 2008, Cartilage Tissue Engineering Using a Flow Perfusion Bioreactor, Tissue Engineering: Part A, **14**: 708

Alves da Silva ML, Crawford A, Mundy JM, **Correlo VM**, Sol PC, Hatton PV, Reis RL and Neves NM, 2007, Novel Chitosan/ Poly (Butylene Succinate) Scaffolds For Cartilage Tissue Engineering, Tissue Engineering: Part A, **13(7)**: 1735

Pinto AR, **Correlo VM**, Bhattacharya M, Charbord P, Reis RL and Neves NM, 2006, Behaviour of human bone marrow mesenchymal stem cells seeded on fiber bonding chitosan polyester based for bone tissue engineering scaffolds, Tissue Engineering, **12 (4)**: 1019

Bhattacharya M, Reis RL, **Correlo VM** and Boesel LF, 2005, Material Properties of Biodegradable Polymers, In Biodegradable Polymers for Industrial Applications, eds. Ray Smith, Woodhead Publishing , Cambridge, 336-356

ORAL PRESENTATIONS IN INTERNATIONAL MEETINGS, AS CO-AUTHOR

Costa-Pinto AR, **Correlo VM**, Sol PC, Battacharya M, Martins A, Costa, PF and Neves NM, The Culture of Human Mesenchymal Stem Cells on Chitosan based Scaffolds in a Multi-Chamber Flow Perfusion Bioreactor for Bone Tissue Engineering , 2nd TERMIS World Congress in conjunction with 2009 Seoul Stem Cell Symposium, Seoul, Korea (south), September 2009

Pires RA, Silva SP, Aroso IM, Fernandes EM, **Correlo VM**, Mano JF and Reis RL, Cork as a source of added-value chemicals, 1st IBB Scientific Meeting, Faro, Portugal, May 2009

Alves da Silva ML, Martins A, Costa, PF, **Correlo VM**, Sol PC, Bhattacharya M, Rougier N., Reis RL and Neves NM, Cartilage tissue engineering using a flow perfusion bioreactor, TERMIS-EU, Porto, Portugal, June 2008

Sangwon Chung, Martins A, **Correlo VM**, Oliveira JT , Marques AP, Neves NM, Mano JF, Sousa RA and Reis RL, Dependence of cell proliferation on the morphology of starch based scaffolds for tissue engineering, TERMIS-EU, Porto, Portugal, May 2008

Costa-Pinto AR, **Correlo VM**, Sol PC, Bhattacharya M, Charbord P, Delorme B, Reis RL and Neves NM, Osteogenic differentiation of Human Mesenchymal Stem Cells cultured onto chitosan melt based scaffolds , TERMIS-AP, Tokyo, Japan, December 2007

Alves da Silva ML, Crawford A, Mundy JM, **Correlo VM**, Sol PC, Bhattacharya M, Hatton PV, Reis RL and Neves NM, Novel Chitosan/ Poly (Butylene Succinate) Scaffolds For Cartilage Tissue Engineering, TERMIS-EU, London, United Kingdom, September 2007

Alves da Silva ML, Costa-Pinto A. R., Crawford A, Mundy JM, **Correlo VM**, Sol PC, Bhattacharya M, Hatton PV, Reis RL and Neves NM, The Potential of Chitosan-Based Scaffolds for Bone and Cartilage Tissue Engineering, Genostem 3rd Workshop on Mesenchymal Stem Cells Enginnering for Conective Tissue Disorders, Barcelona, Spain, Barcelona, Spain, February 2007

Costa-Pinto AR, **Correlo VM**, Sol PC, Bhattacharya M, Charbord P, Reis RL and Neves NM, Adult Human Mesenchymal Stem cells seeded in Natural-Polymer based Scaffolds for Bone and Cartilage Tissue Engineering, ESF-EMBO Symposium Conference on Stem Cells in Tissue Engineering, Sant Feliu de Guixols, Spain, October 2006

Costa-Pinto A. R., **Correlo VM**, Sol PC, Bhattacharya M, Charbord P, Reis RL and Neves NM, Study of the Osteogenic Behaviour of Adult Stem Cells and Novel Melt-Processable Chitosan-Polyester Based Scaffolds for Bone Tissue Engineering, Regenerate World Congress on Tissue Engineering and Regenerative Medicine-TERMIS, Pittsburgh, United States of America, April 2006

Costa-Pinto AR, **Correlo VM**, Bhattacharya M, Charbord P, Reis RL and Neves NM, Behaviour of Human Bone Marrow Mesenchymal Stem Cells Seeded on Fiber Bonding Chitosan Polyester based for Bone Tissue Engineering Scaffolds, 8th TESI Annual Meeting, Shanghai, China, October 2005

Costa-Pinto AR, Salgado AJ, **Correlo VM**, Oliveira JT , Bhattacharya M, Charbord P, Reis RL and Neves NM, Evaluation of the Adhesion, Proliferation and Differentiation of a Mouse Mesenchymal Stem Cell line on Novel Chitosan/Polyester Based Scaffolds, ESB 2005-19th European Conference on Biomaterials, Sorrento, Italy, September 2005

Oliveira JT , Salgado AJ, **Correlo VM**, Costa-Pinto A. R., Bhattacharya M, Charbord P, Neves NM and Reis RL, Preliminary Assessment of the Behaviour of Chitosan/Poly(Butylene Succinate) Scaffolds Seeded with Mouse Mesenchymal Stem Cells for Cartilage Tissue Engineering, European Society for Biomaterials 2005/19th European Conference on Biomaterials, Sorrento, Italy, September 2005

Oliveira JT , Salgado AJ, **Correlo VM**, Costa-Pinto A. R., Bhattacharya M, Charbord P, Neves NM and Reis RL, Preliminary Assessment of the Potential of Chitosan/Polyester Based Scaffolds for Bone and Cartilage Tissue Engineering, Society for Biomaterials 2005 / 30th Annual Meeting and Exposition: New Applications and Technologies, Memphis, Tennessee, United States of America, April 2005

POSTER PRESENTATIONS IN INTERNATIONAL MEETINGS, AS CO-AUTHOR

Costa-Pinto AR, **Correlo VM**, Sol PC, Battacharya M, Martins A, Costa, P. F. and Neves NM, The Culture of Human Mesenchymal Stem Cells on Chitosan based Scaffolds in a Multi-Chamber Flow Perfusion Bioreactor for Bone Tissue Engineering , 2nd TERMIS World Congress in conjunction with 2009 Seoul Stem Cell Symposium, Seoul, Korea (south), September 2009

Silva SP, Aroso IM, Fernandes EM, Pires RA, **Correlo VM** and Reis RL, New products and applications based on cork, 1st IBB meeting, Faro, Portugal, May 2009

Alves da Silva ML, **Correlo VM**, Sol PC, Bhattacharya M, Rougier N., Hatton PV, Reis RL and Neves NM, Chitosan-based scaffolds for cartilage tissue engineering , Genostem 2007: Mesenchymal Stem Cells International Symposium, Montpellier, France, November 2007

Costa-Pinto AR, **Correlo VM**, Sol PC, Bhattacharya M, Charbord P, Delorme B, Reis RL and Neves NM, In vivo testing of chitosan based scaffolds for bone tissue engineering, Genostem 4th Workshop on Mesenchymal Stem Cells Enginnering for Connective Tissue Disorders, Montpellier, France, October 2007

Alves da Silva ML, Crawford A, Mundy JM, **Correlo VM**, Sol PC, Bhattacharya M, Hatton PV, Reis RL and Neves NM, Evaluation of Bovine Articular Chondrocytes When Seeded into Chitosan/ Poly (Butilene Succinate) Scaffolds, Cartilage Biology and Pathology, Ventura, United States of America, March 2007

Costa-Pinto AR, **Correlo VM**, Sol PC, Bhattacharya M, Charbord P, Reis RL and Neves NM, Engineering three-dimensional bone tissue in vitro using chitosan melt based biodegradable scaffolds and hBMSCs, GENOSTEM General Assembly 2007, Barcelona, Spain, February 2007

Alves da Silva ML, Crawford A, Mundy JM, **Correlo VM**, Sol PC, Bhattacharya M, Hatton PV, Reis RL and Neves NM, Evaluation of Extracelullar Marrix Formation on Chitosan-Based Scaffolds Using a Bovine Articular Chondrocytes Model for Articular Cartilage, Genostem 3rd Workshop on Mesenchymal Stem Cells Enginnering for Conective Tissue Disorders, Barcelona, Spain, February 2007

Silva SP, Fernandes EM, Aroso IM, Pires RA, **Correlo VM** and Reis RL, Microscopy techniques as tools for the characterization of cork and the development of new cork applications , XLI Congresso da Sociedade Portuguesa de Microscopia, Braga, Portugal, December 2006

Costa-Pinto AR, **Correlo VM**, Bhattacharya M, Charbord P, Reis RL and Neves NM, Human Bone Marrow Mesenchymal Stem Cells Differentiation when seeded onto Novel Chitosan-Polyesters fiber

mesh Scaffolds: A Bone Tissue Engineering Approach, 1st Annual Meeting of Portuguese Society for Stem Cells and Cell Therapy (SPCE-TC), Madeira, Portugal, May 2006

Oliveira JT , **Correlo VM**, Crawford A, Mundy JM, Bhattacharya M, Neves NM, Hatton PV and Reis RL, Novel Chitosan-Polyester Scaffolds Seeded With Bovine Articular Chondrocytes For Cartilage Tissue Engineering, 2006 Regenerate World Congress on Tissue Engineering and Regenerative Medicine, Pittsburgh, Pennsylvania , United States of America, April 2006

Costa-Pinto AR, **Correlo VM**, Bhattacharya M, Charbord P, Reis RL and Neves NM, Study of the Osteogenic Behaviour of Primary Cultures of Human Bone Marrow MSCs seeded onto Chitosan-Polyester based Scaffolds, Genostem 2nd Workshop on Mesenchymal Stem Cells Enginnering for Conective Tissue Disorders, Porto, Portugal, January 2006

Oliveira JT, Alves da Silva ML, **Correlo VM**, Bhattacharya M, Charbord P, Reis RL and Neves NM, Chondrogenic Differentiation of a Mouse Bone Marrow Derived Mesenchymal Progenitor Cell Line (BMC9) and a Primary Culture of Human Mesenchymal Stem Cells (hMSCs) onto Chitosan/Polyester Based Scaffolds, Genostem 2nd Workshop on Mesenchymal Stem Cells Engineering Connective Tissues Disorders, Porto, Portugal, January 2006

Oliveira JT, **Correlo VM**, Crawford A, Mundy JM, Bhattacharya M, Neves NM, Hatton PV and Reis RL, Chitosan-Polyester Scaffolds Seeded with Bovine Articular Chondrocytes for Cartilage Tissue Enginnering Applications(P127), Artificial Organs, pg. 774, vol.29, nº9, European Society for Artificial Organs (ESAO), Bologne, Italy, October 2005

Oliveira JT, **Correlo VM**, Crawford A, Mundy JM, Bhattacharya M, Neves NM, Hatton PV and Reis RL, Chitosan-Poly(Butylene Succinate) Fiber Scaffolds Are Suitable For Cartilage Tissue Enginnering Applications , United Kingdom Society for Biomaterials 2005 , Nottingham, United Kingdom, June 2005

Santos TC, Marques AP, **Correlo VM**, Bhattacharya M, Neves NM, Castro AG and Reis RL, Novel melt-processed chitosan-polyester blends for orthopaedic applications and its interactions with osteoblast-like cells, 6th International Symposium on Frontiers in Biomedical Polymers, Granada, Spain, June 2005

Oliveira JT, Salgado AJ, **Correlo VM**, Costa-Pinto A. R., Bhattacharya M, Charbord P, Neves NM and Reis RL, Preliminary Assessment of the Behaviour of Chitosan/Polyester Scaffolds Seeded with Mouse Mesenchymal Stem Cells for Cartilage and Bone Tissue Engineering, 1st Meeting of the Portuguese Society for Stem Cells and Cell Therapies , Lisbon, Portugal, January 2005

INTRODUCTION TO THE THESIS FORMAT.

This thesis divided into four sections containing eight different chapters, with five of them being experimental research. According to the 3B's Research Group long-ago implemented philosophy, the thesis format is based on published or submitted papers, including the introduction section (a review paper). The contents of each chapter are summarized below.

SECTION 1 (Chapter I)

The first chapter of this thesis is based on a review paper and presents a comprehensive overview on the most promising biodegradable natural origin polymers intended for bone and cartilage tissue engineering scaffolding applications. Their chemical structure and several other properties are also discussed. In Chapter are highlighted also the processing methods used on the preparation of foams or meshes from these polymers and their application on the context of cartilage and bone tissue engineering.

SECTION 2 (Chapter II)

Chapter II fully describes the materials studied and the experimental work procedures followed during this work. The main objective was to complement the information given in each of the following experimental chapters.

SECTION 3 (Chapter III to VII)

The chapters included within this section are based on the series of related papers that resulted from research work already published or submitted for publication.

Chapter III describes the melt based processing methods used for the preparation of chitosan based blends. The mechanical, thermal and morphological characterization of the developed blends is also discussed herein.

Chapter IV reports the processing of chitosan/polyester/HA composites using melt based routes. Results from their extensive characterization regarding mechanical, thermal and morphological properties are also presented and discussed.

Chapter V aims at reporting on the water absorption and degradation of the newly developed polymer blends and composites since these properties are critical for their possible applications as biomaterials. The water uptake and the degradation properties, as measured by the loss in tensile strength, were evaluated as a function of time.

Chapter VI describes the production of novel scaffolds made from chitosan based blends and composites produced by the melt-based routine involving compression molding and salt leaching. This Chapter shows how it was possible to prepare scaffolds with different macroscopic architecture using a melt-based approach by changing both the amount and average particle size of the porogen agent used. The mechanical and thermal properties, as well as, the morphology of the produced scaffolds are also discussed. Cytotoxic evaluation of developed scaffolds, by means of MTS tests, is also reported.

Chapter VII report the production of chitosan based fibers and chitosan fiber mesh scaffolds by melt processing (solvent-free) to be used as tissue engineering templates. Its mechanical and morphological characterization are also discussed. Biological assessments were also performed in direct contact assays, using a human osteosarcoma cell line (SaOs-2).

SECTION 4 (Chapter VIII)

This thesis ends with Chapter VIII, which is the summary and conclusions of the research work under the scope of this thesis.

SECTION 1.

CHAPTER I.

Natural origin polymers and processing methods for scaffolds preparation and their use in bone or cartilage tissue engineering applications

CHAPTER I.

Natural origin polymers and processing methods for scaffolds preparation and their use in bone or cartilage tissue engineering applications

Abstract

Typical tissue engineering approach require the use of 3D porous scaffolds that will act as a temporary substrate for cells providing appropriate mechanical, structural and biological environments for tissue repair and regeneration. There has been an extensive research on the application of biodegradable polymers, both of synthetic or natural origin, in this field for the preparation of 3D porous structures. Due to several advantages including, their enzymatic or hydrolytic degradation, biological and chemical similarities to natural tissues, natural origin polymers are of special interest for scaffolds production. This paper provides a review of the most promising biodegradable natural origin polymers intended for bone and cartilage tissue engineering scaffolding applications. Their chemical structure and several other properties are also discussed. This review highlights also the processing methods used on the preparation of foams or meshes from these polymers and their application on the context of cartilage and bone tissue engineering.

This chapter is based on the following publication: **Correlo VM,** Bhattacharya M, Neves NM and Reis RL, 2009, Natural origin polymers and processing methods for scaffolds preparation and their use in bone or cartilage tissue engineering applications, *submitted*

---

1. INTRODUCTION

Bone and cartilage injuries, manly resulting from an increasingly aged population, degenerative diseases or traumatic accidents, compromise significantly the quality of life of humanity resulting in a significant socio-economic increasing problem. Many repair techniques have been suggested over the past decades. However almost all of them failed to produce long-lasting tissue repair. Current options to treat these injuries are unsatisfactory as they rely on the use of autografts, allografts, and an assortment of synthetic or biomimetic materials and devices. Each of these options has significant limitations, such as the need for second site of surgery, limited supply, inadequate size and shape, and the morbidity associated with donor site [1, 2]. Thus, all these limitations lead to the need for the development of innovative approaches to aid skeletal repair and reconstruction. It is in this context that in the last decades tissue engineering emerged as an alternative approach to the repair and regenerate damaged human tissues, avoiding the need for a permanent implant [3-5]. Tissue engineering has potential to address these needs and treatment concepts based on those techniques. The engineered substitute should structurally and morphologically resemble the native tissue and be able to perform similar biological functions eliminating problems of donor site scarcity, immune rejection and pathogen transfer.

Tissue engineering can be subdivided into different strategies, the most used strategy applied for the creation of hard tissue (such as, bone and cartilage) substitutes combines the use living cells, biologically active molecules and temporary three-dimensional (3-D) porous scaffolds [6]. For this approach, cells are isolated from the patient, expanded, seeded and cultured *in vitro* into an appropriate scaffold prior to implantation. After implantation, the cell matrix construct should be remodeled into native tissue. Since tissue engineering scaffolds will act as a temporary substrate for cells and provide the temporary support for tissue reconstruction, the challenge for their design include the fulfillment of a number of requirements, namely: (i) must be biocompatible not provoking any adverse reaction to the organism after implantation; (ii) possess appropriate mechanical properties that should be compatible with the ones of the adjacent tissue when implanted; (iii) should have adequate porosity, pore size and interconnectivity to allow cell migration, transporting of gases, metabolites, nutrients and signal molecules both within the scaffold and between the scaffold and the local environment; (iv) must be biodegradable allowing to be metabolized by biological processes at a rate compatible with the rate of tissue growth while sustaining mechanical integrity over periods of time varying from a few weeks to several months [7].

The supporting structures that have emerged in the last few decades as possible forms for tissue engineering can be divided into scaffolds and matrices. The scaffold is usually consider as a microporous three dimensional structure, in which a cell suspension can be seeded having the opportunity to attach to the free surfaces of the material, and the media, with nutrients and other agents, can circulate. The matrices, which are gels, and more specifically hydrogels, involving a network of structural, usually cross-linked, molecules, within a water-based viscous matrix [8]. Since load bearing applications requires porous structures with improved mechanical performance we believe that scaffolds can be more indicated for connective tissue engineering applications than matrices from hydrogels. For that reason, this review will not include hydrogels, and special attention will be given to natural polymers and processing methods used on the production of sponges and fibrous scaffolds. The state of the art regarding their application on cartilage or bone tissue engineering application will be also reviewed.

2. NATURAL BASED POLYMERS

Natural polymers are widely spread in nature. Those polymers are formed during the growth cycles of many organisms, being obtained from renewable sources like plants, animals or micro-organisms. A large variety of natural polymers are available with special potential interest on scaffolds production due to, as natural components of living structures, their biological and chemical similarities to natural tissues. Moreover, natural polymers have the advantage of being prone or susceptible to enzymatic or hydrolytic degradation which may indicate the greater propensity of these materials to be metabolized by the physiological mechanism [9].

Many different natural polymers were already used as biomaterials and can be broadly categorized in eight different categories, namely: (1) polysaccharides, (2) proteins, (3) polyhydroxyalkanoates, (4) polythioesters, (5) polyanhydrides, (6) polyisoprenoids, (7) lignin, and (8) nucleic acids [10]. We have however decided that his review will give special emphasis only to polymers belonging to the three first classes manly because they are the polymers mostly used on the preparation of sponges and fibrous mesh scaffolds for bone and cartilage tissue engineering applications. This review will describe also the chemical structure, main properties and processing methods used to produce them.

2.1. STARCH

Starch is the predominant energy storing compound in many plants. It can be found in storage organs such as roots and tubers in a granular form. Most of the granules are oval and granule size can vary

from 1 to 110 μm depending on the starch source [11]. By far the largest source of starch is corn (maize) with other commonly used sources being wheat, potato, tapioca and rice.

The structure and composition of native starches varies with the botanical sources, but all granules consist of two types of α-glucan polymers, amylose and amylopectin [11, 12]. Amylose, the minor constituent, is defined as a relative long, linear polymer consisting mainly of α(1→4) linked D-glucopyranosyl units. Amylopectin, the major component, is a branched polysaccharide composed of hundreds of short (1→4)-α-glucan chains, which are interlinked by (1→6)-α -linkages [11-13]. Figure 1.1 shows the typical structure of amylose and amylopectin macromolecules.

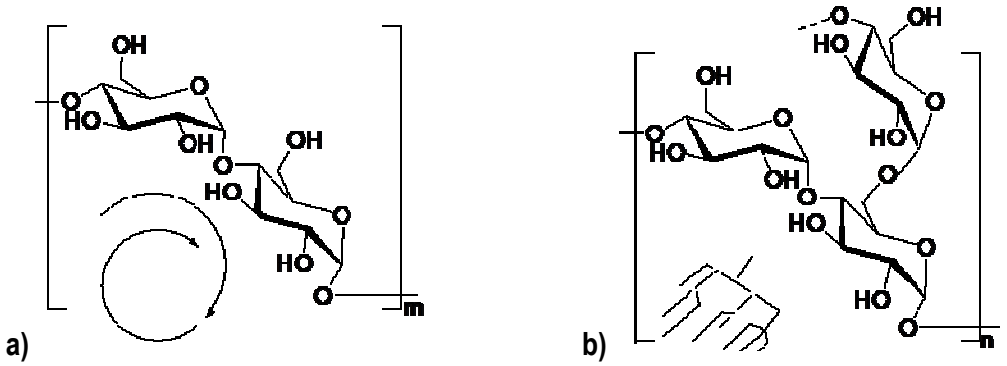

Figure 1.1. a) Amylose and b) amylopectin structures.

Starch contributes with 50–70% of the energy in the human diet, providing a direct source of glucose, which is an essential substrate in brain and red blood cells for generating metabolic energy [14]. The human body can degrade starch by using specific enzymes including α-amylase present in saliva and also in the blood plasma. Starch degradation products are oligosaccharides that can be metabolized to produce energy. Other enzymes involved in starch degradation are β-amylase, α-glucosidases, and other debranching enzymes [15].

The crystallinity of native starch granules can vary from about 15% for high-amylose starches to about 45–50% for waxy starches [14]. The processing of native starch to be used on varied applications requires to disrupt and melt the semicrystalline granular structure of native starches. The modification method is usually referred as gelatinization. Gelatinization occurs during heating in the presence of

sufficient moisture. In those conditions the starch granules absorb water and swell losing irreversibly their crystallinity and structural organization [10].

Products from pure starch or from thermoplastic starch (starch with disrupted granular structure), are usually brittle and moisture sensitive, thus strongly limiting their potential fields of application. One possible way to overcome these limitations is to blend starch with other biodegradable polymers. Several polymeric systems were already obtained by blending native maize starch with: i) ethylene-vinyl alcohol (SEVA-C); ii) cellulose acetate (SCA); polycaprolactone (SPCL) and iv) poly(lactic acid) (SPLA) [16]. These blends have been originally proposed by Rui L. Reis and his collaborators at U. Minho as alternatives for hard tissue applications [17-20].

Starch based blends and composites were shown to be non-cytotoxic and potentially biocompatible [21, 22] and were proposed for several biomedical applications, including bone cements [23], drug delivery systems [24], bone fixation devices [25], and tissue engineering scaffolding [26-28].

2.1.1. Processing methods

Due to the thermoplastic behavior of the starch based blends and composites it is possible to produce 3-D porous scaffolds using traditional melt based technologies, such as compression moulding combined with particulate leaching [29] and injection moulding [30, 31] or extrusion with blowing agents [29, 32]. This offers the unique advantage of avoiding the use of solvents that sometimes are detrimental for the biomedical field.

Gomes *et al.* [29] produced scaffolds from a blend of starch with cellulose acetate (SCA) by method consisting on extrusion with different types and amounts of blowing agents. The porous structure of the samples results from the gases released by the thermal decomposition of the blowing agents (BA) during processing. Thus, by using different types and amounts of BA it was possible to obtain scaffolds with different porosities in the range of 50-500 μm.

The same approach was used to produce scaffolds from a blend of corn starch/ethylene-vinyl alcohol (SEVA-C) [32]. The developed porous structures had 60% porosity with pore sizes between 200 and 900 μm with an acceptable degree of interconnectivity. The limitation of this method is the difficulty in controlling the pore size and interconnectivity between the pores.

Gomes *et al.* [29] used other melt based technology, compression moulding and particulate leaching, to produce scaffolds from the same starch based blend (SCA). The obtained scaffolds possessed an open network of pores through the sample with sizes ranging from 10 to 500 μm and a porosity of about 50%. The advantage of this technique is the possibility of tightly control the percentage of porosity and pore size simply by varying the amount and size of the leachable particles.

SPCL (starch with ε-polycaprolactone, 30:70%) and SPLA (starch with poly(lactic acid), 30:70%) based scaffolds were prepared by a fibre-bonding process using fibres obtained by melt-spinning [27]. The two types of scaffolds produced by this method exhibited a typical fibre-mesh structure, with a fibre diameter of roughly 180 μm for SPCL and 210 μm for SPLA, with highly interconnected pores and a porosity of approximately 75%. Both types of scaffolds exhibited better mechanical performance than most scaffolds obtained from other biodegradable polymers aimed at tissue engineering applications. Moreover, using fiber bonding method, different porosities of the fiber meshes scaffolds can be obtained using different amounts (by weight) of fibers [33].

Duarte *et al.* proposed the use of supercritical fluid technology - supercritical immersion precipitation - as a clean and environmentally friendly approach to prepare scaffolds from starch and poly(l-lactic acid) blends [26] and composites [34] for tissue engineering applications. The obtained matrices are highly porous and interconnected and their morphology can be considered as a bicontinuous structure composed of macropores (∼75 μm) and micropores with sizes ranging from 10 to 20 μm and the surfaces appear very rough. Therefore, the impregnation with Bioglass® did not affect the porosity or interconnectivity of the starch based scaffolds [34]. From the results obtained it was also possible to conclude that pressure was the parameter that most affected the porosity, interconnectivity and pore size of the prepared scaffodls [26]. The supercritical fluid technology can be also used to prepare drug-loaded starch-based porous scaffolds in a one-step process [35]. Scaffolds prepared by this method and loaded with dexamethasone showed a sustained release over 21 days and had morphology comparable to the unloaded ones.

A novel hierarchical starch-based scaffold, obtained by a combination of rapid prototyping (RP) and electrospinning techniques, was developed aiming to overcome the high number of cells needed to attain sufficient adherent cells to the RP scaffolds [36]. These scaffolds were characterized by a 3D structure of parallel aligned rapid prototyped microfibres (average fibre diameter, 300 μm), periodically intercalated by randomly distributed electrospun nanofibres (fibre diameters in the range 400 nm–1.4

μm). The interest of those systems was to improve the cell seeding efficiency of the systems obtained by RP.

2.1.2. Starch in bone tissue engineering applications

Several studies reported in the literature have shown that starch based scaffolds can be used on bone tissue engineering strategies by promoting the attachment, proliferation and differentiation of bone marrow stromal cells [33, 37] and endothelial cells [38]. It has been also demonstrated that the use of starch-based scaffolds, in conjunction with fluid flow bioreactor culture, minimize diffusion constraints and provide mechanical stimulation to the marrow stromal cells, leading to enhancement of differentiation toward development of bone-like mineralized tissue [33].

Nevertheless, for a bone cell-scaffold construct to be successful it is necessary the establishment of a functional vasculature. With this objective, Santos *et al.* [38] demonstrated that starch based fiber mesh scaffolds are an excellent substrate for the growth of human endothelial cells (ECs) required for the vascularization process. These findings, coupled with those reported for bone marrow cells, suggest that starch based scaffolds may have a high potential for use as a scaffold material for vascularized bone tissue engineering applications.

Very recently, it was shown that prevascular structures were induced by co-culturing outgrowth endothelial cells (OECs) with primary osteoblasts on SPCL scaffolds, which were achieved without additional supplementation of culture medium with angiogenic growth factors [39]. Additionally, in cellular constructs consisting of OECs and primary osteoblasts on SPCL implanted subcutaneously into a nude mouse model, OECs formed vascular structures closely associated with the scaffold material and embedded in a rich extracellular matrix produced by the primary osteoblasts.

Aiming to simulate the conditions found *in vivo*, Martins *et al.* [40] studied simultaneously the influence of α-amylase and lipase on the degradation of SPCL fiber meshes as a function of immersion time and on the osteodifferentiation of rat marrow stromal cells. Results indicated that culture medium supplemented with enzymes enhanced cell proliferation after 16 days of culture and that lipase positively influenced osteoblastic differentiation of MSCs and promoted matrix mineralization. Furthermore, *in vivo* studies have also shown that different starch-based scaffolds (SCA, SEVA-C, and SEVAC/CaP) implanted into bone defects created on the distal femur were well integrated in the defect site and surrounding marrow,

indicating their biocompatibility, and that the early connective tissue occupying the bone/scaffold interface could be characterized as an early form of bone [41].

2.1.3. Starch in cartilage tissue engineering applications

Oliveira *et al.* [42] tested the suitability of using corn starch-polycaprolactone (SPCL) scaffolds for on cartilage tissue engineering approaches. With that intention, bovine articular chondrocytes were seeded on SPCL and poly(glycolic acid) (PGA) non-woven scaffolds under dynamic conditions. The results have showed that SPCL scaffolds can support bovine articular chondrocytes adhesion, proliferation and differentiation. Moreover, contrarily to PGA scaffolds that presented a central area of cells depletion, which can be a result of acidic by-products release from their hydrolytic degradation, inefficient cells penetration or necrosis induced by high cellular densities, starch based scaffolds presented homogeneous cell colonization throughout the scaffold structure.

In a different study, electrospun polycaprolactone (PCL) and starch-compounded PCL (SPCL) nanofiber meshes were used to evaluate extracellular matrix (ECM) formation by bovine articular chondrocytes (BACs) and their performance compared [43]. The data did not show obvious qualitative or quantitative differences between the two materials; nevertheless, the authors consider advantageous to use SPCL, not only because of its natural-based composition, but also because it allows for greater control of the degradation kinetics and further functionalization of its structure.

2.2. CHITOSAN

Chitosan is obtained from the alkaline deacetylation of the biopolymer chitin, the second most abundant organic materials, which can be found in shells of marine crustaceans and cell walls of fungi [44]. Structurally, chitosan is a linear polysaccharide consisting of N-glucosamine (deacetylated unit) and N-acetyl glucosamine (acetylated unit) units linked by $\beta(1\rightarrow4)$ glycosidic bonds (Fig. 1.2). The degree of deacetylation (DD) is the glucosamine / N-acetyl glucosamine ratio and usually can vary, depending on the source, from 30% to 95%. The degree of crystallinity of chitosan is manly controlled by the degree of deacetylation being maximum for both chitin (i.e. 0% deacetylated) and fully deacetylated forms (100% chitosan) and minimum for intermediate degrees of deacetylation [45].

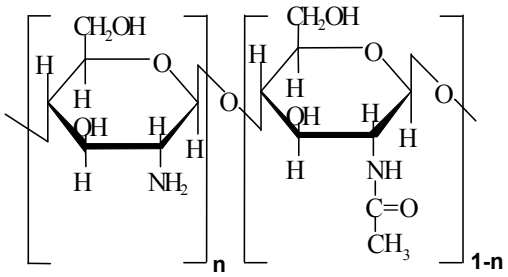

Figure 1.2. Chemical structure of chitosan

Chitosan is degraded by enzymatic hydrolysis being lysozyme the primary agent of *in vivo* degradation [46]. The degradation rate is inversely related to the percentage of crystallinity which is, as referred, controlled mainly by the degree of deacetylation. Highly deacetylated forms (e.g. 85%) exhibit the lowest degradation rates and may last several months *in vivo* [47]. The degradation products are chitosan oligosaccharides of variable length.

Chitosan is normally insoluble in neutral or basic pH conditions. However, it is soluble in weak or dilute acids (pH<6), and can be easily processed into films and porous scaffolds [48].

Chitosan is biocompatible evoking minimal foreign body reaction, with little or no fibrous encapsulation when implanted as scaffold [49]. Much of the potential of chitosan as biomaterial for tissue engineering can be partially justify by its structural similarity to glycosaminoglycans (GAGs), as it possesses the same glucosamine residues, which are the major components of the extracellular matrix of cartilage [47]. Since GAGs properties include many specific interactions with growth factors, receptors and adhesion proteins, this suggests that the analogous structure in chitosan may also have related bioactivities [50]. Moreover, chitosan's cationic nature also allows it to interact with anionic GAGs, proteoglycans and other negatively charges species. This property can be of great interest since it may serve as a mechanism for retaining or accumulating these molecules within a tissue scaffold during colonization or after implantation [48].

2.2.1. Processing methods

A very interesting property of chitosan is that it can be transformed into 3-D high porous structures with high degree of interconnectivity using several technologies. For example, porous scaffolds can be produced by lyophilizing a frozen solution of chitosan powder dissolved in acetic acid [48, 51]. The obtained scaffolds had a porosity of ~80% and a median pore diameter of ~68 μm. The mean pore diameters can be controlled within the range of 1-250 μm by varying the freezing conditions [48]. The main limitation of those structures is that the mechanical properties are very low for connective tissue applications.

Abdel-Fattah *et al.* [52] used chitosans with different degrees of deacetylation to produce chitosan microspheres and of 3-D porous chitosan matrices via a sintered microsphere technique. The median pore size and porosity level of the obtained scaffolds was ~200 μm and ~20%, respectively. The porosity of the scaffolds was considered to be too low and was attributed to the large size of the microspheres. A similar particle aggregation approach was followed by Malafaya *et al.* [53] to produced chitosan-based scaffolds intended to promote neo-vascularization. Quantitative analysis of porosity, pore size and interconnectivity were accessed by microCT. The obtained results were ~28%, ~265 μm and 95% respectively. Moreover, it was concluded that porosity morphology of the scaffolds produced by this technique will allow for tissue ingrowth resembling those of trabecular bone, if this application is considered. The main limitation of this technique is the level of porosity that may be considered too low.

Wet spinning is one of the mostly used methods to produce natural fibres, and was used to prepared chitosan fibres and 3-D fibre meshes [54]. The obtained scaffolds had an average pore size in the range of 100-500 μm which is ideal for bone related applications.

Until very recently, the methods to produce chitosan scaffolds were based on the use of solvents. Nevertheless, Correlo *et al.* [55] produced chitosan/polyester 3D porous scaffolds suitable for supporting the adhesion, proliferation, and osteogenic differentiation of mouse MSCs [56] using for the first time melt based processing technologies. All the scaffolds were produced by melt based compression moulding followed by salt leaching. By using this technique it was possible to obtain scaffolds with distinct properties concerning porosity, pore size, interconnectivity and mechanical performance by varying the porogen particle size and amount and by varying the ratio and type of aliphatic polyester used in the blend.

In a different concept, Martins *et al.* [57] reported the production of chitosan based scaffolds with the ability to form a porous structure in situ due to the attack by specific enzymes present in the human body (α-amylase and lysozyme). The *in vitro* formation of pores, controlled by the location of the "sacrifice" phase (native starch), was evident, although pore formation is expected to occur more rapidly *in vivo*, due to the presence of other enzymes and cells.

2.2.2. Chitosan in bone tissue engineering applications

In vitro tests have shown that chitosan based scaffolds support the adhesion and proliferation of osteoblasts [54, 58]. Costa-Pinto *et al.* [56] confirmed that chitosan/polyester based scaffolds support adhesion, viability/proliferation and osteogenic differentiation of a mouse mesenchymal stem cell line (BMC-9) and therefore may be used for cell-based therapies in the bone tissue engineering field.

The inclusion of bioactive ceramics in the scaffold composition can confer osteoconductive and even osteoinductive properties to the final structure that will guide bone formation. *In vitro* studies have shown that the use of chitosan based scaffolds prepared with biphasic calcium phosphate (BCP) for culture of MSCs and preosteoblasts increased bone tissue formation [59]. In a different study, the incorporation of hydroxyapatite (HA) into chitosan-gelatin composite scaffolds promoted *in vitro* initial adhesion and enhanced osteogenic differentiation of hMSC [60]. Porous scaffolds from collagen-chitosan-hydroxyapatite were characterized by possessing high histocompatibility and suitable material to be use as bone substitute [61]. Nano-hydroxyapatite/chitosan/carboxymethyl cellulose composites have shown promising properties to be used as bone repair materials [62]. Moreover, *in vivo* studies have shown that a composite consisting of calcium phosphate cement (CPC), chitosan fibres and gelatin displays the ability to form new bone more rapidly, with faster bioresorption, than pure CPC [63].

Several reports on the literature have shown that the development of apatite coatings on polymeric scaffolds using biomimetic approaches enhance the cell adhesion and proliferation, being an interesting method to enhance biomaterials properties aimed for bone tissue engineering applications [64-66]. Chitosan based fiber mesh scaffolds with a bone-like apatite coating have shown to posses higher cell adhesion and proliferation as compared to the uncoated samples [66]. Mineralized chitosan scaffolds with hydroxyapatite nanocrystals at its surface and within the pore channels induce the formation of extracellular matrix but did not significantly influenced the growth of human osteoblasts (SaOs-2) [65].

The performance of tissue engineering constructs can be greatly enhanced through the incorporation of bioactive agents. Chitosan scaffolds have been modified with RGDS enhancing the rat osteosarcoma (ROS) cells attachment [67]. In a different study, chitosan/collagen scaffold loaded adenoviral vector encoding human bone morphogenetic proteins (BMP7) were implanted into defects on both sides of the mandible [68]. The results have shown that the scaffold containing Ad-BMP7 exhibited the higher ALP activity, and the expression of osteopontin and bone sialoprotein were up-regulated. Moreover, in defects around implant, the bone formation in Ad-BMP7 scaffolds was greater than that in other scaffolds. In addition, *in vivo* analysis using a mouse implantation model have shown that although there was a large migration of neutrophils into the implantation area, there were minimal signs of any inflammatory reaction to the chitosan scaffolds, demonstrating that chitosan has a high degree of biocompatibility in this animal model [49]. Recently, chitosan based scaffolds implanted into rat muscle-pockets shown a mild inflammatory response commonly observed in the implantation of foreign bodies *in vivo* [53]. In addition, neo-vascularization of the implants created by new blood vessels formation was clear even after only 2 weeks of implantation. This process evolved significantly for a longer periods of time, showing that the scaffolds characteristics were favourable to obtain integration with the host tissue.

2.2.3. Chitosan in cartilage tissue engineering applications

The structural and chemical similarity of chitosan with GAGs makes it an interesting candidate material to be used on cartilage tissue engineering applications. Studies conducted with chitosan scaffolds and porcine chondrocytes have shown that these scaffolds supported cell attachment and maintenance of the typical rounded cell morphology, suggesting that they can be a useful alternative to synthetic ones [51].

The intrinsic properties of chitosan (cationic nature and hydrophilicity) are often explored by blending it with other synthetic biodegradable polymers, namely with aliphatic polyesters. Wu *et al.* [69] demonstrated that PDLLA/chitosan scaffolds exhibited higher attachment, proliferation and spreading of chondrocytes compared to pure PDLLA ones. Similar results were obtained with chitosan-PLGA composite fibrous matrices [70]. In a different study, PLLA microspheres coated with chitosan, exhibited stronger ability to promote cell attachment and proliferation, and maintain the secretion function of the chondrocytes (especially the ones with larger chitosan amount) [71]. Scaffolds produced from chitosan and polybutylene succinate blends using melt based technologies have shown to be appropriate for

supporting cell growth and differentiation using chondrogenic differentiation medium, suggesting that they should be considered for further studies in the cartilage tissue engineering field [72].

The combination of gene therapy and tissue engineering have been paid much attention as a novel approach to treat cartilage defects. Guo *et al.* [73, 74] produced gene-activated matrices (GAM) by incorporating plasmid DNA into chitosan-gelatin scaffolds. Chondrocytes cultured on these GAM maintained their round shape and cell clusters were surrounded with extracellular matrix composed of proteoglycans and type II collagen. In addition, *in vivo* studies have shown that chitosan-gelatin three-dimensional scaffolds containing plasmid DNA encoding TGF-β1 facilitated new cartilage tissue production when implanted into cartilage defects of rabbit knee joints [73]. In a different study, autologous MSCs modified with the TGF-β1 gene were seeded into chitosan scaffolds and then implanted into the full-thickness articular cartilage defects of rabbits' knees [75]. Twelve weeks after implantation, the defects were filled with regenerated hyaline-like cartilage tissue suggesting that the repair of cartilage defects can be enhanced by TGF-β1 gene-modified-tissue engineering of cartilage on the basis of a strategy using MSCs, chitosan, and liposomal transfection.

An *in vivo* study using a large animal model revealed that when oMSC were seed in presence of chitosan-based scaffold and TGFβ-3 can be differentiated into chondrocyte-like cells surrounded by a hyaline-like cartilaginous matrix that was integrated to the host cartilage [76].

2.3. COLLAGEN

Collagen is the most abundant structural protein in the connective tissue's extracellular matrices and acts as the natural scaffold for cell attachment in the body. It gives mechanical stability, strength and toughness to a range of tissues. In special cases like bone and dentin the stiffness is improved by the inclusion of minerals [77].

The hallmark of a collagen is a molecule that consists of three polypeptide chains (α chains), each having a general amino acid motif of (-Gly-X-Y)n, where the residues for X and Y are frequently the amino acids propline (Pro) and hydroxyproline (Hyp) being Gly-Prol-Hyp the most common triplet found in collagen [78, 79]. This repeating sequence allows the chains to form a right-handel triple-helical structure, with all glycine residues buried within the core of the protein, and the residues X and Y exposed on the surface [78, 80]. The individual triple helices are usually arranged in fibrils which provide high tensile strength.

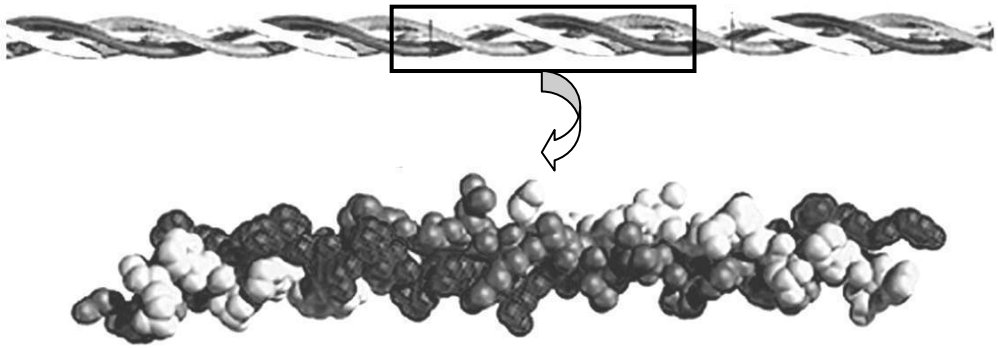

Figure 1.3. Overall collagen structure a) van der Waals model of the helical structure of collagen and b) three single chains intertwined into a triple-stranded helix. (adapted from [78])

To date, more than 20 genetically distinct types of collagen have been identified. Collagens I-V are the five major types being type I collagen the most abundant form and can be isolated from adult connective tissues, including skin, tendons, and bone [79]. Type II can be found in cartilage, the developing cornea, and in the vitreous body of the eye [81]. It can be isolated and purified from various animal species by enzyme treatment being bovine collagen the most commonly used type of collagen. Nevertheless, as alternative to the possible complications that can occur from using bovine origin collagen (risks of bovine spongiform encephalopathy – BSE - transmission), porcine collagen [82] or, even more safer, collagen from marine sources [83] are often used on scaffolds production. Human recombinant collagen has also become available and can be used in scaffolds manufacturing [84]. Collagen possesses several advantages including biodegradability, low immunogenicity, and the ability to promote cellular attachment and growth making it an attractive component of tissue engineering scaffolds [85]. In the human body, collagen is degraded largely through the activity of the metalloprotease collagenase and some serine proteases [9]. By altering the degree to which it is crosslinked, it is possible to adapt the mechanical properties and degradation rate of collagen. Furthermore, the abundance of functional groups along its polypeptide backbone makes it highly receptive to the binding of genes, growth factors and other biological molecules [86].

2.3.1. Processing methods

Collagen has been widely used to prepare scaffolds for bone and cartilage tissue engineering. The most used process to produce collagen scaffolds is freeze-drying. This process consists in freezing an aqueous solution of collagen followed by the sublimation of the ice crystals by vacuum at low temperature. 3D scaffolds consisting of mineralised collagen type I, with a composition that mimics extracellular matrix of bone tissue, were generated by a freeze drying process, whereas the pore size could be controlled by temperature and the freezing velocity [87].

An improved method was developed by O'Brien and co-workers [88] consisting on using a lyophilisation or freeze-drying process whereby a suspension of collagen and glycosaminoglycans (GAG) in acetic acid is cooled at a constant rate to a final temperature of freezing to produce collagen-GAG scaffolds with homogeneous pore structure. It was also found that by varying the final freezing temperatures, a range of homogeneous collagen-GAG scaffolds with varying mean pore sizes could be produced [89]. In a different study, Chen *et al.* used a freeze-drying technique to produce PLGA-collagen hybrid meshes by forming collagen microsponges in the opening of PLGA knitted meshes [90, 91]. Recently, Kanungo *et al.* [92] produced collagen-GAG scaffolds with varying mineral content via a triple co-precipitation method followed by freeze-drying. Although the scaffolds have shown to possess pore size adequate for bone growth, the mechanical properties were lower than those of mineralized scaffolds made by other techniques, as well as cortical and cancellous bone. In a different study, solvent casting/particulate leaching process was used to produce PLGA-collagen scaffolds [93]. These scaffolds are characterized by being ease to fabricate and by possessing a porous structure with a consistent interconnectivity throughout the entire scaffold.

Electrospinning was used to produce a 3-D nanofibrous matrix of Type I collagen aiming to mimic as close as possible the native extracellular matrix (ECM) [94]. The electrospinning process consists on using an electrical field gradient to pull a charged polymer solution towards a grounded collector, resulting in a non-oven mesh of nanofibres.

To overcome some limitations of scaffolds related with cell migration and nutrients diffusion constrains, collagen and collagen-hydroxyapatite scaffolds were produced combining critical point drying and solid freeform technologies [95, 96]. These methods allow controling the pore size, biodegradation and mechanical properties of the produced scaffolds and the incorporation of microchannels vasculature on their interior that can overcome the diffusion limitations of current foam scaffolds [97]. *In vitro* and *in vivo*

studies demonstrated that these scaffolds supported osteogenesis and chondrogenesis using HBMSCs and that the introduction of microchannels to scaffolds architecture enhanced chondrogenesis [98]. Aiming to generate scaffolds closely resembling the natural extracellular matrix components of bone, this processing method has been modified to produce collagen-hydroxyapatite scaffolds [99].

Microfabrication is a promising technique for generating high-precision scaffolds. Chin *et al.* [100] developed a microfabrication strategy, based on gelling collagen-based components inside a microfluidic device, that produces well-controlled pore sizes inside the scaffold. This approach has some disadvantages including the need for dehydrating the scaffold before peeling and the delicate handling required for thin hydrogel structures.

Lui *et al.* [101] produced a gradient collagen/nano-HA composite scaffold, with a Ca-rich side and a Ca-depleted side, aiming applications in tissues with gradient properties, such as osteochondral bone.

The controlled release of signaling molecules, such as growth factors from the scaffolds is critical for tissue repair, by providing cell guidance and development. PLGA- based microspheres encapsulating a model protein were imbedded in collagen and collagen/HA scaffolds [102].

2.3.2. Collagen in bone tissue engineering applications

Collagen type I is the major organic component of the ECM in bone and can play an important role in bone tissue engineering. Type I collagen (bovine) is the basis of several commercial products including Collapat II®, Healos®, Collagraft® and Biostite® among others [81]. Several studies demonstrated that the use of type I collagen matrices can promote osteogenic differentiation and mineralization of marrow stromal cells and human adipose stem cells [94, 103, 104]. In a different study, it was demonstrated that a collagen scaffold (Gingistat®) is suitable for supporting MSC distribution and their commitment to form bone tissue [105]. The *in vitro* evaluation of the degradation time of the collagen sponge (degraded in 4–5 weeks) suggested that its use in *in vivo* experiments may be hindered by the scaffold's complete dissolution prior to the healing process and bone formation is completed.

Tierney *et al.* [106] examined the effects of varying collagen concentration and crosslink density on the biological, structural and mechanical properties of collagen-GAG scaffolds for bone tissue engineering. The results indicated that doubling the collagen content to 1% and dehydrothermally crosslinking the scaffold at 150 ºC for 48 h has enhanced mechanical and biological properties of the scaffold making it more attractive for use in bone tissue engineering.

Aiming to mimic the microstructure and composition of the extracellular matrix of bone, several studies have been conducted to produce scaffolds based on collagen type I combined with hydroxyapatite [98, 107, 108]. These collagen–HA composite scaffolds supported the osteogenic differentiation of human bone marrow-derived stromal cells (hBMSCs) both *in vitro* and *in vivo*. Additionally, extensive new osteoid formation of the implant was observed in the areas of vasculature, *in vivo*. In a different study it was demonstrated that porous nanocomposite scaffolds containing collagen fibres and synthetic apatite nanocrystals successfully healed critical-sized defects in the femur of Wistar rats and on the tibia of Yorkshire-Landrace pigs [108].

2.3.3. Collagen in cartilage tissue engineering applications

Cartilage tissue engineering methods involving scaffolds made from collagen hold great promise for the treatment of cartilage defects. Negri *et al.* [109] have shown that human articular cartilaginous cells can multiply and grow on type I collagen substrate with production of extracellular matrix. Buma *et al.* [110] evaluated the effect of cross-linked type I and type II collagen matrices, with and without attached chondroitin sulfate, on the tissue response after 4 and 12 weeks of *in vivo* implantation. This study allows concluding that different types of collagen matrices induce different tissue responses in full-thickness articular cartilage defects, suggesting that a composite matrix consisting of a deep layer of type I collagen and a more superficial layer of type II collagen may provide the needed conditions for cartilage regeneration.

Dorotka *et al.* have shown that although the collagen matrix was an adequate environment for BMSC *in vitro*, only the matrices seeded with autologous cells in combination with microfracture created the conditions that facilitate hyaline-like cartilage regeneration *in vivo* [111, 112]. The successful control of the cartilage tissue shape was reported by using rabbit bone marrow cells seeded on collagen sponge scaffold and cultured in a rotating wall vessel (RWV) bioreactor [113]. Moreover, it was demonstrated that the use of a collagen scaffold enhanced the glycosaminoglycan (GAG) content, strengthened the compression strength of the product and shortened the culture period necessary before tissue transplantation.

The production, *in vitro*, of cartilaginous constructs with varying degrees of maturity (e.g., with different GAG content) may be advantageous for cartilage tissue engineering strategies. Pfeiffer *et al.* [114] demonstrated that it is possible to control the degree of maturation of tissue-engineered cartilaginous

constructs. The cross-linking density of type II collagen scaffolds was proposed to be determinant for the GAG density of chondrocyte-seeded constructs.

Sato *et al.* [115] seeded PLLA sponges and PLLA–collagen hybrid sponges with bovine articular chondrocytes and implanted them in athymic nude mice. The *in vivo* studies have shown that cartilaginous tissue was more widely formed and more homogeneously distributed in the PLLA–collagen hybrid sponge than in the PLLA sponge throughout implantation period. More recently, Chan *et al.* [116] developed self-assembled injectable collagen-human mesenchymal stem cell (hMSC) microspheres by microencapsulation. An *in vivo* implantation study conducted using the developed collagen-hMSC microspheres shown the fabrication of cartilage-like tissue micro-masses with good host tissue integration [117].

The promising result using collagen based scaffolds to promote cartilage regeneration conduct to their use in clinical cases [118-120].

2.4. POLYHYDROXYALKANOATES

Poly([R]-hydroxyalkanoates) (PHA) are a family of polyesters that can be produced by a large number of bacteria as carbon storage compound under metabolic stress, such as limitation of an essential nutrient [121, 122]. PHA chemical and physical properties depend on the monomeric composition that is determined by the producing microorganism and their nutrition [121]. PHA is composed of 3-, 4- or rarely 5-hydroxy fatty acid monomers, which form linear polyesters. The general chemical structure is shown in Figure 1.4.

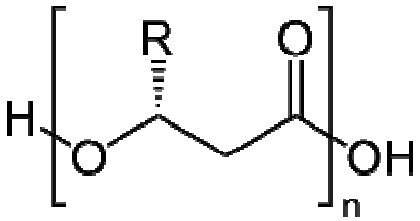

Figure 1.4. General structure of poly ([R]-hydroxyalkanoates)

To date, more than 100 different monomers have been reported, nevertheless most of the studies are focused on poly 3-hydroxybutyrate (PHB), the simplest and first to be discovered. [123]. PHB is a semi-crystalline thermoplastic with a melting temperature of~177 ºC and glass transition temperature of ~4ºC. It can be processed by melting or by solvent based technologies [122]. PHB is a relatively stiff and brittle material what limits their application [124]. To overcome the limitation in properties and the narrow processing window of PHB, many studies have proposed the use of copolymers of 3-hydroxybutyrate and 3-hydroxyvalerate (PHBV), poly 4-hydroxybutyrate (P4HB), and copolymers of 3-hydroxybutyrate and 3-hydroxyhexanoate (PHBHHx) [125].

In general PHA are biodegradable, with good biocompatibility [124]. PHA can be degraded in 3-9 months by many microorganisms into carbon dioxide and water. Their primary breakdown products 3-hydroxyacids that are naturally found in the human body (R-3-hydroxybutyric acid is a normal constituent of blood). However, PHB has a rather low degradation in the body due to its high crystallinity. Thus, medical studies are more focused on the co-polymer PHBV), which being less crystalline undergoes degradations at a much faster rate [123].

2.4.1. Processing methods

Electrospinning was used to produce ultrafine mats from PHB, PHBV, and their 50/50 w/w blend to be used as bone scaffolds [126]. In a different study electrospinning was used to fabricate nanofibers with an average diameter of 300-500nm, and nanofibrous membranes from PHBHHx [127]. An improved method, consisting on combining conventional electrospinning with a gas-jet was developed to produce PHB based scaffolds containing nanosized hydroxyapatite and possessing an extracellular matrix-like topography [128].

PHBV and PHBV/HA composite scaffolds can be fabricate using the emulsion freezing/freeze-drying technique [129]. These scaffolds were characterized by being highly porous, with pore size ranging from several microns to around 300 μm, and interconnected porous structure. Moreover, the incorporation of HA besides rendering osteoconductivity, lowered the crystallinity of PHBV matrix and enhanced the mechanical properties of the composite scaffolds.

PHBHHx scaffolds were prepared by directional freezing and phase-separation [130]. The scaffolds were characterized by possessing uniaxial microtubular structure able of guiding cell growth and by possessing anisotropic mechanical properties. Moreover, it was possible to adjust the structure and

mechanical properties of the scaffolds by changing the PHBHHx concentration, solvent and freezing temperature. In a different study, Wang *et al.* [131] produced PHBHHx scaffolds using a solvent-lyophilizing method. The scaffolds had a non-directional porous structure, with an average pore size of 100 µm and a porosity of 90%.

PHB and PHBHHx scaffolds with or without addition of HA can be produced by combining solvent casting with salt leaching [132, 133]. In a different study, PHBV scaffolds were prepared by combining freeze-drying and particulate leaching aiming to create a scaffold with high porosity and uniform pore sizes [134]. The produced scaffolds were further treated with rf-oxygen plasma to modify their surface chemistry and hydrophilicity. The results have shown that the pore size, porosity and pore morphology could be controlled by the polymer concentration, presence and size of leachable solutes and surface modification. Sun *et al.* [135] used a solvent free technique consisting on compression moulding, thermal processing and salt particulate leaching method to produce PHBV scaffolds. The obtained scaffold exhibited macroporous structure with interconnected open pores with size varying from 30 µm to 300 µm and a porosity of 80% ± 1.2. A similar approach was followed to prepare composite scaffolds of PHBV with bioactive wollastonite [136].

2.4.2. Polyhydroxyalkanoates in bone tissue engineering applications

It has been shown that PHB scaffolds seeded with human maxillary osteoblasts can induce ectopic bone formation [137]. Rat marrow osteoblasts were cultured on PHBV scaffolds and bone formation was investigated *in vitro* over a period of 60 days [138]. The results have shown that osteoblasts could grow inside the scaffolds and lead to mineralization making them suitable to be used one bone tissue engineering.

The *in vitro* biocompatibility of PHB, PHBHHx and PLA scaffolds for growth of osteoblasts was studied and compared [132]. It was found that PHBHHx had the best performance on attachment and proliferation of bone marrow cells than PLA scaffolds.

More recently, it was also demonstrated that 3-hydroxybutyrate (3HB), one of the degradation products of PHA, supported *in vitro* differentiation of murine osteoblast MC3T3-E1 in direct proportion to its concentration [139]. This study also revealed that 3HB administration can become an effective agent against osteoporosis.

Incorporation of HA into PHA allows the production of bioactive and biodegradable composite scaffolds for bone tissue engineering applications. *In vitro* studies have shown that PHB scaffolds containing nanosized hydroxyapatite had positive effects on attachment, proliferation and differentiation of BMSCs [128]. Similar results were obtained by Wang *et al.* [133], that has shown that the addition of HA to PHB increased mechanical properties and osteoblast responses including cell growth and alkaline phosphatase activity. Nevertheless, in the case of composite scaffolds made from PHBHHx the addition of HA had an adverse effect.

2.4.3. Polyhydroxyalkanoates in cartilage tissue engineering applications

Sun *et al.* [135] studied the possibility of using PHBV matrices on cartilage tissue engineering applications and the results have shown that that the chondrocytes maintained their activity, fully expressed their phenotype and produced the extracellular matrix after incubation *in vitro* on the scaffolds for 7 days. In a different study, PHBV and collagen containing calcium phosphate (CaP–Gelfix®) scaffolds were implanted into a full thickness cartilage defects (4.5 mm in diameter and 4 mm in depth) at the patellar groove on the right and left knees of eight rabbits [140]. The *in vivo* results shown that PHBV matrices seeded wit chondrocytes presented early cartilage formation resembling normal articular cartilage and revealed minimal foreign body reaction and better healing response than CaP–Gelfix®.

Deng *et al.* studied the possibility of using PHB and PHB/PHBHHx scaffolds on the growth of chondrocyte culture [141, 142]. The results showed that chondrocytes proliferated better on the PHB/PHBHHx scaffolds than on PHB ones [142]. Moreover, results obtained by combining second-harmonic generation imaging technique, with confocal fluorescence microscopy revealed that PHBHHx in PHB scaffold provided better surface properties for anchoring type II collagen filaments and their penetration into internal layers of the scaffolds [141].

Very recently, Wang *et al.* [131] evaluated the potential of PHBHHx scaffolds using an rabbit articular cartilage defect model and concluded that these scaffolds provided a favorable environment for chondrocytes' proliferation, migration and differentiation, both *in vitro* and *in vivo*. This study has shown that after 16 weeks of *in vivo* implantation, it was possible to achieved successful full thickness cartilage repair using PHBHHx scaffolds seeded with allogeneic chondrocytes.

2.5. SILK FIBROIN

Silks are natural fibrous proteins produced by a variety of species, including lepidoptera, scorpions and spiders. Silks differ widely in composition, structure and properties depending on the specific source. The most extensively characterized silks are from the domesticated silkworm, *Bombyx mori*, that have been the primary silk-like material used in biomedical applications particularly as sutures [143, 144].

Silkworm silk is composed of a filament core protein termed fibroin (the major component), and sericin a water-soluble glue-like protein that bind the fibroin fibers together [145]. Silk fibroin is a hydrophobic glycoprotein and consists of heavy and light chain polypeptides of~350 and ~25kDa, respectively, linked by a disulfide bond [146, 147]. The light chain, which is linked to the heavy chain, plays only a marginal role in the fiber. The larger heavy chain is glycine (Gly) rich and most of its amino acid composition consists of glycine (Gly), alanine (Ala), and serine (Ser) [148].

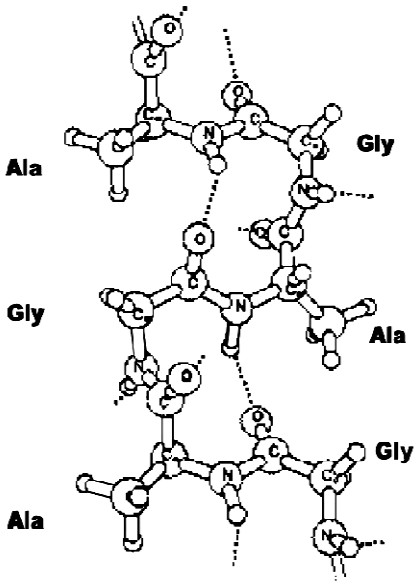

Figure 1.5. The conformation of a repeated β-turn type II – like molecules as a model for silk I proposed by Asakura *et al.* (adapted from [149])

In the solid state, silk fibroin from *B. mori* can assume two distinct crystalline structures, namely silk I (before spinning) and silk II (after spinning) [149]. Structure determination of silk I was difficult because

any attempt to study it caused a conversion of the silk I form to the silk II form. A structural model (Fig. 1.5) was proposed by Asakura *et al.* that can be called as a repeated β-turn type II structure [149]. Regarding the silk II structure, although there are some reports suggesting the possession of some intrinsic structural disorder, they are basically in accordance with Marsh's antiparallel β-sheet model based on a fiber diffraction study [150].

The motivation in using fibroin in biomedical and tissue engineering applications derives from the unique mechanical properties of these fibers, the versatility in its processing, as well as its biocompatibility and low inflammatory response [144, 151-153]. Immunogenic reactions to silk sutures have been largely attributable to the sericin proteins [153]. Twenty-five to thirty percent of the silk cocoons are composed of sericins that can be removed by boiling the material in an alkaline solution to obtain purified silk fibroin [154]. While silk is a FDA approved biomaterial defined by the US Pharmacopeia as non-degradable, fibroin is proteolytically degrade with predictable long-term degradation characteristics [143, 155]. The susceptibility to proteolytic hydrolysis of silk fibroin structures can be enhanced by using all-aqueous process for their preparation [156]. More recently, *in vivo* studies have also demonstrated that besides the processing method, the processing variables (silk fibroin concentration and pore size) also affected the degradation rate [151].

2.5.1. Processing methods

It is well known that silk fibroin can be processed into various products with different morphologies by using different methods (versatile processability). Nazarov *et al.* [157] used three fabrication techniques, freeze-drying, salt leaching and gas foaming, to form porous three-dimensional silk biomaterial matrixes. Freeze-dried scaffolds, processed with 15% methanol or 15% 2-propanol, at -20 or -80 °C, presented highly interconnected and porous structures with pores pore size with diameters of 50 ± 20 μm. Moreover, some of the scaffolds formed two layers, an upper more porous flakelike layer and a bottom layer that was more condensed and compact. The salt leached scaffolds used NaCl as a porogen, formed pores with sizes of 202 ± 112 μm. Although the pores were larger in comparison to those generated by the freeze-drying method, the pore structure was not as highly interconnected. Scaffolds formed by gas foaming (ammonium bicarbonate was used as the porogen) showed a highly interconnected open pore morphology with diameters in the range of 155 ± 114 μm. Furthermore, the gas foamed process did not leave a skin layer on the surface of the scaffold allowing to conclude that the scaffolds formed by gas foaming were the best of the matrices prepared. Aiming to avoid the use of

organic solvents or harsh chemicals, Kim *et al.* [156] reported the formation of 3-D silk fibroin porous scaffolds prepared by an all-aqueous process. By adjusting the concentration of silk fibroin in water and the particle size of NaCl used in the process it was possible to control the morphological and functional properties of the scaffolds.

A salt leaching method with sieved NaCl crystals was used by Hofmann *et al.* [158] aiming to engineer 3D silk fibroin scaffolds with separate domains of different pore diameters on a single scaffold. The produced scaffolds had mixed pore sizes with pore diameters of 112–224 μm on one side and 400–500 μm on the other side of the scaffold and a porosity of ~95%.

Due to the high surface area, fibers with nanoscale diameters can provide benefits on tissue engineering applications. Thus, electrospinning has been used in the fabrication of silk-based biomaterial scaffolds and to improve the processibility of silk solutions, polyethylene oxide (PEO) can be blended with the aqueous solution of fibroin [159]. Moreover, biomimetic alignment of fibers can be achieved using a cylindrical target and controlled as a function of its speed during electrospinning of a silk fibroin solution blended with PEO [160]. However, nanofibrous scaffolds developed through electrospinning technique might have structural limits for cell proliferation because pore size is too small for the cells to grow inside. Aiming to overcome this limitation, nanofibrous silk fibroin scaffolds were prepared via electrospinning followed by a salt-leaching method [161]. The obtained scaffolds had uniformly distributed pores and high porosity (about 94%), but low pore interconnectivity, with various pore size (58–930 μm).

Recently, direct ink writing was used to fabricate microperiodic scaffolds of regenerated silk fibroin [162]. The method consisted on extruding a ink (fibroin solution) in a layer-by layer fashion through a fine nozzle to produce a 3D array of silk fibroin fibers with 5 μm in diameter that are much finer than those produced by other rapid prototyping methods.

2.5.2. Silk fibroin in bone tissue engineering applications

Silk fibroin is an attractive biomaterial in which mechanical performance and biological interactions are major factors for success including bone tissue engineering. Silk fibroin scaffolds have been shown to be suitable substrates to engineer bone-like tissue *in vitro* [163, 164]. Human mesenchymal stem cells (hMSCs) cultured on porous and three-dimensional silk scaffolds were differentiated into bone depositing cells *in vitro*, which resulted in the formation of a trabecular-like network of tissue-engineered

bone structures [165]. It was also demonstrated that, the implantation of silk fibroin scaffolds cultured with human mesenchymal stem cells pre-differentiated along an osteoblastic lineage promoted bone formation in critical sized cranial [165] and mid-femoral segmental [166] defects.

Aiming to improve bone tissue engineering outcomes, BMP-2 was loaded in porous silk fibroin scaffolds [167]. The results have shown that BMP-2 induced hMSCs to undergo osteogenic differentiation when the seeded scaffolds were cultured in medium supplemented with osteogenic stimulants. Moreover, when implanted in critical sized cranial defects in mice, scaffolds loaded with BMP-2 and seeded with hMSCs resulted in significant bone ingrowth. *In vitro* bone formation from hMSCs was significantly improved by incorporating functional factors, such as BMP-2 and a bone-like mineral hydroxyapatite into silk fibroin scaffolds [168, 169].

Bone is a complex hierarchical structure having variable pore sizes. Aiming at mimicking the physiological tissue morphology, Hofmann *et al.* [158] engineered different bone-like structures using scaffolds with small pores (112–224 mm) in diameter on one side and large pores (400–500 mm) on the other. Analysis conducted using microCT revealed that the pore structures of the newly formed tissue and suggested that the structure of tissue-engineered bone was controlled by the underlying scaffold geometry.

One of the major challenges on bone repair and regeneration is vascularization. One of the currently approaches to improve the vascularization of bone tissue engineered constructs is the pre-vascularization by including endothelial cells. Outgrowth endothelial cells (OECs), isolated and expanded from heterogeneous human peripheral blood cultures were investigated regarding their ability to serve as an autologous cell source for the endothelialization of 3-D silk fibroin scaffolds [170]. Results have shown both a close interaction of OECs with the scaffolds and the formation of microvessel-like structures induced by angiogenic stimuli involved in the processes of neo-vascularization. More recently, Fuchs *et al.* [171] have shown that OECs in co-culture with human primary osteoblasts on silk fibroin scaffolds formed highly organized pre-vascular structures.

2.5.3. Silk fibroin in cartilage tissue engineering applications

Meinel *et al.* [172] studied the used highly porous, slowly degrading HFIP-derived silk fibroin scaffolds and human mesenchymal stem cells (hMSCs) for *in vitro* cartilage tissue engineering and compared the results with unmodified and crosslinked collagen scaffolds. The results have demonstrated that hMSCs

attachment, proliferation, and metabolic activity were markedly better on slowly degrading silk than on fast-degrading collagen scaffolds. Similar results were obtained with hMSCs cells seeded on silk fibroin and collagen scaffolds and cultured in serum-free chondrogenic medium [173].

In a different study 3-D aqueous-derived silk fibroin scaffolds (prepared by salt leaching) have been successfully used for *in vitro* cartilage tissue engineering using adult mesenchymal stem cells (MSCs) [174] and adult human chondrocytes (hCHs) [175].

Surface treatments can benefit the fabrication of scaffolds with modified surface for tissue engineering. Treating electrospun nanofibrous silk fibroin scaffolds with microwave-induced argon plasma significantly increased the attachment, proliferation and GAG synthesis of chondrocytes [161].

Selecting the appropriate cell source for cartilage tissue engineering may be challenging. Tığlı *et al.* [176] studied the chondrogenic potential in a 3D culture of human chondrocytes, human embryonic stem cells and mesenchymal stem cells (derived from human embryonic stem cells, bone marrow and adipose tissue). The cells were cultured with or without BMP6 on silk fibroin and chitosan scaffolds. BMP6-modified silk fibroin scaffolds cultured with MSCs (derived from human embryonic stem cells) are suggested as the most promising system to use for cartilage regeneration. However, since chondrogenesis was incomplete and was not homogeneous throughout scaffold, further studies optimizing the *in vitro* culture conditions, such as using dynamic cultivation were suggested. The potential of silk fibroin scaffolds loaded with insulin-like growth factor I (IGF-I) was also explored in the context of cartilage tissue engineering [177]. hMSC were seeded on unloaded and IGF-I loaded scaffolds in TGF-β supplemented medium. Chondrogenic differentiation of hMSC was observed only on IGF-I loaded scaffolds suggesting their potential to be used on cartilage tissue engineering.

3. FINAL REMARKS

As described, considerable effort has been directed towards the development of scaffolds using natural polymers. Various remarkable achievements were reported both for bone and for cartilage tissue engineering. Nevertheless, the use of natural polymers still has some disadvantages that limit their application. The predominant hydrophilic nature, which results in inherent fast degradation rates. Also the poor mechanical performance limits the use of natural polymers on load bearing applications like bone and cartilage tissue engineering. Moreover, they can induce undesirable immune response due to the presence of impurities and endotoxins (depending on their source). Another aspect is that their

properties may differ from batch to batch during large-scale isolation procedures due to the difficulty to accurately control the processing techniques.

Some of these disadvantages can be significantly improved by blending the natural derived polymers with other biodegradable polymers from synthetic origin. Nevertheless, new systematic methods including methods for production, purification, controlling material properties should be developed for designing better natural-based materials. The possibility of producing natural based polymers with improved physical, chemical and biological properties could improve the outcomes of bone and cartilage tissue engineering applications.

REFERENCES

1. Salgado, A.J., *et al.*, Bone and Articular CartilageTissue Engineering: The Biological Components, in Biodegradable Systems in Tissue Engineering and Regenerative Medicine, R.L. Reis and J. San Roman, Editors. 2005, CRC Press: Boca Raton.
2. van Gaalen, S., *et al.*, Tissue engineering of bone, in Textbook on Tissue Engineering, C. Van Blitterswijk, *et al.*, Editors. 2007, Elsevier: Amsterdam. p. 559-610.
3. Nesic, D., *et al.*, Cartilage tissue engineering for degenerative joint disease. Advanced Drug Delivery Reviews, 2006. 58(2): p. 300-322.
4. Chung, C. and J.A. Burdick, Engineering cartilage tissue. Advanced Drug Delivery Reviews, 2008. 60(2): p. 243-262.
5. Mistry, A.S. and A.G. Mikos, Tissue engineering strategies for bone regeneration, in Regenerative Medicine Ii: Clinical and Preclinical Applications. 2005. p. 1-22.
6. Hutmacher, D.W., *et al.*, State of the art and future directions of scaffold-based bone engineering from a biomaterials perspective. Journal of tissue engineering and regenerative medicine, 2007. 1(4): p. 245-260.
7. Harrison, K., Introduction to polymeric scaffolds for tissue engineering, in Biomedical polymers, M. Jenkins, Editor. 2007, Woodhead publishing Lts: Cambridge. p. 1-32.
8. Williams, D., Biocompatibility, in Textbook on Tissue Engineering, C. Van Blitterswijk, *et al.*, Editors. 2007, Elsevier: Amsterdam. p. 255-278.
9. Gomes, M.E., *et al.*, Natural Polymers in tissue engineering applications, in Textbook on Tissue Engineering, C. Van Blitterswijk, *et al.*, Editors. 2007, Elsevier: Amsterdam. p. 145-192.

10. Sousa, R.A., *et al.*, Processing of thermoplastic natural-based polymers: an overview of starch based blends, in Handbook of Natural-based Polymers for Biomedical Applications, N.M. Neves, *et al.*, Editors. 2008, CRC Press: Cambridge.
11. Hoover, R., Composition, molecular structure, and physicochemical properties of tuber and root starches: a review. Carbohydrate Polymers, 2001. 45(3): p. 253-267.
12. Tester, R.F., J. Karkalas, and X. Qi, Starch - composition, fine structure and architecture. Journal of Cereal Science, 2004. 39(2): p. 151-165.
13. Buléon, A., *et al.*, Starch granules: structure and biosynthesis. International Journal of Biological Macromolecules, 1998. 23(2): p. 85-112.
14. Copeland, L., *et al.*, Form and functionality of starch. Food Hydrocolloids, 2009. 23(6): p. 1527-1534.
15. Martins, A.M., *et al.*, Towards Osteogenic Differentiation of Marrow Stromal Cells and *In vitro* Production of Mineralized Extracellular Matrix onto Natural Scaffolds, in Biological Interactions on Materials Surfaces: Understanding and Controlling Protein, R. Bizios and D. Puleo, Editors. 2008, Springer: San Diego.
16. Reis, R.L. and A.M. Cunha, Starch and Starch Based Thermoplastics, in Encyclopedia of Materials Science and Technology, K.H. Jurgen Buschow, *et al.*, Editors. 2001, Elsevier Science: Amesterdam. p. 8810-8816.
17. Reis, R.L. and A.M. Cunha. Characterization of two biodegradable polymers of potential application within the biomaterials field. in 12th European Conference on Biomaterials. 1995. Oporto, Portugal.
18. Reis, R.L., *et al.*, Mechanical behavior of injection-molded starch-based polymers. Polymers for Advanced Technologies, 1996. 7(10): p. 784-790.
19. Reis, R.L., *et al.*, Structure development and control of injection-molded hydroxylapatite-reinforced starch/EVOH composites. Advances in Polymer Technology, 1997. 16(4): p. 263-277.
20. Reis, R.L., *et al.* Processing and *in vitro* degradation of starch/EVOH thermoplastic blends. in Cambridge Polymer Conference - Partnership in Polymers. 1996. Cambridge, England.
21. Marques, A.P., R.L. Reis, and J.A. Hunt, The biocompatibility of novel starch-based polymers and composites: *in vitro* studies. Biomaterials, 2002. 23(6): p. 1471-1478.
22. Marques, A.P., R.L. Reis, and J.A. Hunt, An *in vivo* study of the host response to starch-based polymers and composites subcutaneously implanted in rats. Macromolecular Bioscience, 2005. 5(8): p. 775-785.

23. Boesel, L.F., J.F. Mano, and R.L. Reis, Optimization of the formulation and mechanical properties of starch based partially degradable bone cements. Journal of Materials Science-Materials in Medicine, 2004. 15(1): p. 73-83.
24. Balmayor, E.R., *et al.*, Preparation and characterization of starch-poly-[epsilon]-caprolactone microparticles incorporating bioactive agents for drug delivery and tissue engineering applications. Acta Biomaterialia, 2009. 5(4): p. 1035-1045.
25. Sousa, R.A., *et al.*, Injection molding of a starch/EVOH blend aimed as an alternative biomaterial for temporary applications. Journal of Applied Polymer Science, 2000. 77(6): p. 1303-1315.
26. Duarte, A.R.C., J.F. Mano, and R.L. Reis, Preparation of starch-based scaffolds for tissue engineering by supercritical immersion precipitation. The Journal of Supercritical Fluids. In Press, Corrected Proof.
27. Gomes, M.E., *et al.*, Starch-poly(epsilon-caprolactone) and starch-poly(lactic acid) fibre-mesh scaffolds for bone tissue engineering applications: structure, mechanical properties and degradation behaviour. Journal of Tissue Engineering and Regenerative Medicine, 2008. 2(5): p. 243-252.
28. Salgado, A.J., *et al.*, Effects of Starch/Polycaprolactone-based Blends for Spinal Cord Injury Regeneration in Neurons/Glial Cells Viability and Proliferation. Journal of Bioactive and Compatible Polymers, 2009. 24(3): p. 235-248.
29. Gomes, M.E., *et al.*, Alternative tissue engineering scaffolds based on starch: processing methodologies, morphology, degradation and mechanical properties. Materials Science and Engineering: C, 2002. 20(1-2): p. 19-26.
30. Neves, N.M., A. Kouyumdzhiev, and R.L. Reis, The morphology, mechanical properties and ageing behavior of porous injection molded starch-based blends for tissue engineering scaffolding. Materials Science and Engineering: C, 2005. 25(2): p. 195-200.
31. Gomes, M.E., *et al.*, A new approach based on injection moulding to produce biodegradable starch-based polymeric scaffolds: morphology, mechanical and degradation behaviour. Biomaterials, 2001. 22(9): p. 883-889.
32. Salgado, A.J., O.P. Coutinho, and R.L. Reis, Novel starch-based scaffolds for bone tissue engineering: Cytotoxicity, cell culture, and protein expression. Tissue Engineering, 2004. 10(3-4): p. 465-474.

33. Gomes, M.E., *et al.*, Influence of the porosity of starch-based fiber mesh scaffolds on the proliferation and osteogenic differentiation of bone marrow stromal cells cultured in a flow perfusion bioreactor. Tissue Engineering, 2006. 12(4): p. 801-809.
34. Duarte, A.R.C., *et al.*, Processing of novel bioactive polymeric matrixes for tissue engineering using supercritical fluid technology. Materials Science and Engineering: C. In Press, Accepted Manuscript.
35. Duarte, A.R.C., J.F. Mano, and R.L. Reis, Dexamethasone-loaded scaffolds prepared by supercritical-assisted phase inversion. Acta Biomaterialia. In Press, Corrected Proof.
36. Martins, A., *et al.*, Hierarchical starch-based fibrous scaffold for bone tissue engineering applications. Journal of Tissue Engineering and Regenerative Medicine, 2009. 3(1): p. 37-42.
37. Gomes, M.E., *et al.*, Effect of flow perfusion on the osteogenic differentiation of bone marrow stromal cells cultured on starch-based three-dimensional scaffolds. Journal of Biomedical Materials Research Part A, 2003. 67A(1): p. 87-95.
38. Santos, M.I., *et al.*, Response of micro- and macrovascular endothelial cells to starch-based fiber meshes for bone tissue engineering. Biomaterials, 2007. 28(2): p. 240-248.
39. Fuchs, S., *et al.*, Contribution of outgrowth endothelial cells from human peripheral blood on *in vivo* vascularization of bone tissue engineered constructs based on starch polycaprolactone scaffolds. Biomaterials, 2009. 30(4): p. 526-534.
40. Martins, A.M., *et al.*, The Role of Lipase and alpha-Amylase in the Degradation of Starch/Poly(epsilon-Caprolactone) Fiber Meshes and the Osteogenic Differentiation of Cultured Marrow Stromal Cells. Tissue Engineering Part A, 2009. 15(2): p. 295-305.
41. Salgado, A.J., *et al.*, *In vivo* response to starch-based scaffolds designed for bone tissue engineering applications. Journal of Biomedical Materials Research Part A, 2007. 80A(4): p. 983-989.
42. Oliveira, J.T., *et al.* A cartilage tissue engineering approach combining starch-polycaprolactone fibre mesh scaffolds with bovine articular chondrocytes. in 20th Conference of the European-Society-for-Biomaterials. 2006. Nantes, FRANCE.
43. da Silva, M.A., *et al.*, Evaluation of Extracellular Matrix Formation in Polycaprolactone and Starch-Compounded Polycaprolactone Nanofiber Meshes When Seeded with Bovine Articular Chondrocytes. Tissue Engineering Part A, 2009. 15(2): p. 377-385.
44. Shi, C.M., *et al.*, Therapeutic potential of chitosan and its derivatives in regenerative medicine. Journal of Surgical Research, 2006. 133(2): p. 185-192.

45. Kim, I.Y., *et al.*, Chitosan and its derivatives for tissue engineering applications. Biotechnology Advances, 2008. 26(1): p. 1-21.
46. Vårum, K.M., *et al.*, *In vitro* degradation rates of partially N-acetylated chitosans in human serum. Carbohydrate Research, 1997. 299(1-2): p. 99-101.
47. Di Martino, A., M. Sittinger, and M.V. Risbud, Chitosan: A versatile biopolymer for orthopaedic tissue-engineering. Biomaterials, 2005. 26(30): p. 5983-5990.
48. Madihally, S.V. and H.W.T. Matthew, Porous chitosan scaffolds for tissue engineering. Biomaterials, 1999. 20(12): p. 1133-1142.
49. VandeVord, P.J., *et al.*, Evaluation of the biocompatibility of a chitosan scaffold in mice. Journal of Biomedical Materials Research, 2002. 59(3): p. 585-590.
50. Suh, J.K.F. and H.W.T. Matthew, Application of chitosan-based polysaccharide biomaterials in cartilage tissue engineering: a review. Biomaterials, 2000. 21(24): p. 2589-2598.
51. Nettles, D.L., S.H. Elder, and J.A. Gilbert, Potential use of chitosan as a cell scaffold material for cartilage tissue engineering. Tissue Engineering, 2002. 8(6): p. 1009-1016.
52. Abdel-Fattah, W.I., *et al.*, Synthesis, characterization of chitosans and fabrication of sintered chitosan microsphere matrices for bone tissue engineering. Acta Biomaterialia, 2007. 3(4): p. 503-514.
53. Malafaya, P.B., *et al.*, Morphology, mechanical characterization and *in vivo* neo-vascularization of chitosan particle aggregated scaffolds architectures. Biomaterials, 2008. 29(29): p. 3914-3926.
54. Tuzlakoglu, K., *et al.*, Production and characterization of chitosan fibers and 3-D fiber mesh scaffolds for tissue engineering applications. Macromolecular Bioscience, 2004. 4(8): p. 811-819.
55. Correlo, V.M., *et al.*, Melt-based compression-molded scaffolds from chitosan-polyester blends and composites: Morphology and mechanical properties. 2008. p. NA.
56. Costa-Pinto, A.R., *et al.*, Adhesion, proliferation, and osteogenic differentiation of a mouse mesenchymal stem cell line (BMC9) seeded on novel melt-based chitosan/polyester 3D porous scaffolds. Tissue Engineering Part A, 2008. 14(6): p. 1049-1057.
57. Martins, A.M., *et al.*, Natural origin scaffolds with in situ pore forming capability for bone tissue engineering applications. Acta Biomaterialia, 2008. 4(6): p. 1637-1645.
58. Fakhry, A., *et al.*, Chitosan supports the initial attachment and spreading of osteoblasts preferentially over fibroblasts. Biomaterials, 2004. 25(11): p. 2075-2079.

59. Sendemir-Urkmez, A. and R.D. Jamison, The addition of biphasic calcium phosphate to porous chitosan scaffolds enhances bone tissue development *in vitro*. Journal of Biomedical Materials Research Part A, 2007. 81A(3): p. 624-633.
60. Zhao, F., *et al.*, Effects of hydroxyapatite in 3-D chitosan-gelatin polymer network on human mesenchymal stem cell construct development. Biomaterials, 2006. 27(9): p. 1859-1867.
61. Wang, Y., *et al.*, Synthesis and characterization of collagen-chitosan-hydroxyapatite artificial bone matrix. Journal of Biomedical Materials Research - Part A, 2008. 86(1): p. 244-252.
62. Liuyun, J., *et al.*, Preparation and properties of a novel bone repair composite: Nano-hydroxyapatite/chitosan/carboxymethyl cellulose. Journal of Materials Science: Materials in Medicine, 2008. 19(3): p. 981-987.
63. Pan, Z.H. and P.P. Jiang, Assessment of the suitability of a new composite as a bone defect filler in a rabbit model. Journal of Tissue Engineering and Regenerative Medicine, 2008. 2(6): p. 347-353.
64. Kong, L.J., *et al.*, A study on the bioactivity of chitosan/nano-hydroxyapatite composite scaffolds for bone tissue engineering. European Polymer Journal, 2006. 42(12): p. 3171-3179.
65. Manjubala, I., *et al.*, Growth of osteoblast-like cells on biomimetic apatite-coated chitosan scaffolds. Journal of Biomedical Materials Research Part B-Applied Biomaterials, 2008. 84B(1): p. 7-16.
66. Tuzlakoglu, K. and R.L. Reis, Formation of bone-like apatite layer on chitosan fiber mesh scaffolds by a biomimetic spraying process. Journal of Materials Science-Materials in Medicine, 2007. 18(7): p. 1279-1286.
67. Ho, M.H., *et al.*, Preparation and characterization of RGD-immobilized chitosan scaffolds. Biomaterials, 2005. 26(16): p. 3197-3206.
68. Zhang, Y.F., *et al.*, Combination of scaffold and adenovirus vectors expressing bone morphogenetic protein-7 for alveolar bone regeneration at dental implant defects. Biomaterials, 2007. 28(31): p. 4635-4642.
69. Wu, H., *et al.*, Proliferation of chondrocytes on porous poly(DL-lactide)/chitosan scaffolds. Acta Biomaterialia, 2008. 4(1): p. 76-87.
70. In, K.S., *et al.*, Homogeneous chitosan-PLGA composite fibrous scaffolds for tissue regeneration. Journal of Biomedical Materials Research - Part A, 2008. 84(1): p. 247-255.
71. Lao, L., *et al.*, Chitosan modified poly(l-lactide) microspheres as cell microcarriers for cartilage tissue engineering. Colloids and Surfaces B: Biointerfaces, 2008. 66(2): p. 218-225.

72. Oliveira, J.T., *et al.*, Assessment of the suitability of chitosan/polybutylene succinate scaffolds seeded with mouse mesenchymal progenitor cells for a cartilage tissue engineering approach. Tissue Engineering - Part A., 2008. 14(10): p. 1651-1661.
73. Guo, T., *et al.*, Gene-activated matrices for cartilage defect reparation. International Journal of Artificial Organs, 2006. 29(6): p. 612-621.
74. Guo, T., *et al.*, Porous chitosan-gelatin scaffold containing plasmid DNA encoding transforming growth factor-beta 1 for chondrocytes proliferation. Biomaterials, 2006. 27(7): p. 1095-1103.
75. Guo, C.A., *et al.*, Novel gene-modified-tissue engineering of cartilage using stable transforming growth factor-beta 1-transfected mesenchymal stem cells grown on chitosan scaffolds. Journal of Bioscience and Bioengineering, 2007. 103(6): p. 547-556.
76. Mrugala, D., *et al.*, Phenotypic and functional characterisation of ovine mesenchymal stem cells: Application to a cartilage defect model. Annals of the Rheumatic Diseases, 2008. 67(3): p. 288-295.
77. Fratzl, P., Collagen: Structure and Mechanics, an Introduction, in Collagen, Structure and Mechanics, P. Fratzl, Editor. 2008, Springer: New York. p. 1-12.
78. Chau, D.Y.S., R.J. Collighan, and M. Griffin, Collagen: Structure and modification for Biomedical applications in Trends in Biomaterials Research, P.J. Pannone, Editor. 2007, Nova Science Publishers, Inc.: New York p. 143-190.
79. Beckman, M.J., K.J. Shields, and R.F. Diegelmannm, Collagen, in Encyclopedia of Biomaterials and Biomedical Engineering, G.E. Wnek and G.L. Bowlin, Editors. 2008, Taylor & Francis, Inc.: New York. p. 628-638.
80. Hulmes, D.J.S., Collagen Diversity, Synthesis and Assembly, in Collagen, Structure and Mechanics, P. Fratzl, Editor. 2008, Springer: New York. p. 15-41.
81. Wahl, D.A. and J.T. Czernuszka, Collagen-hydroxyapatite composites for hard tissue repair. European Cells & Materials, 2006. 11: p. 43-56.
82. Mimura, T., *et al.*, A novel exogenous concentration-gradient collagen scaffold augments full-thickness articular cartilage repair. Osteoarthritis and Cartilage, 2008. 16(9): p. 1083-1091.
83. Song, E., *et al.*, Collagen scaffolds derived from a marine source and their biocompatibility. Biomaterials, 2006. 27(15): p. 2951-2961.
84. Wang, Y., *et al.*, Bone regeneration by using scaffold based on mineralized recombinant collagen. Journal of Biomedical Materials Research Part B-Applied Biomaterials, 2008. 86B(1): p. 29-35.

85. Lee, C.H., A. Singla, and Y. Lee, Biomedical applications of collagen. International Journal of Pharmaceutics, 2001. 221(1-2): p. 1-22.
86. Harley, B.A.C. and L.J. Gibson, *In vivo* and *in vitro* applications of collagen-GAG scaffolds. Chemical Engineering Journal, 2008. 137(1): p. 102-121.
87. Gelinsky, M., *et al.*, Porous three-dimensional scaffolds made of mineralised collagen: Preparation and properties of a biomimetic nanocomposite material for tissue engineering of bone. Chemical Engineering Journal, 2008. 137(1): p. 84-96.
88. O'Brien, F.J., *et al.*, Influence of freezing rate on pore structure in freeze-dried collagen-GAG scaffolds. Biomaterials, 2004. 25(6): p. 1077-1086.
89. O'Brien, F.J., *et al.*, The effect of pore size on cell adhesion in collagen-GAG scaffolds. Biomaterials, 2005. 26(4): p. 433-441.
90. Chen, G., *et al.*, Cell adhesion of bone marrow cells, chondrocytes, ligament cells and synovial cells on a PLGA-collagen hybrid mesh. Materials Science and Engineering: C, 2004. 24(6-8): p. 867-873.
91. Chen, G., J. Tanaka, and T. Tateishi, Osteochondral tissue engineering using a PLGA-collagen hybrid mesh. Materials Science and Engineering: C, 2006. 26(1): p. 124-129.
92. Kanungo, B.P., *et al.*, Characterization of mineralized collagen-glycosaminoglycan scaffolds for bone regeneration. Acta Biomaterialia, 2008. 4(3): p. 490-503.
93. Lee, S.J., *et al.*, *In vitro* evaluation of a poly(lactide-co-glycolide)-collagen composite scaffold for bone regeneration. Biomaterials, 2006. 27(18): p. 3466-3472.
94. Sefcik, L.S., *et al.*, Collagen nanofibres are a biomimetic substrate for the serum-free osteogenic differentiation of human adipose stem cells. Journal of tissue engineering and regenerative medicine, 2008. 2(4): p. 210-220.
95. Sachlos, E., D. Gotora, and J.T. Czernuszka, Collagen scaffolds reinforced with biomimetic composite nano-sized carbonate-substituted hydroxyapatite crystals and shaped by rapid prototyping to contain internal microchannels. Tissue Engineering, 2006. 12(9): p. 2479-2487.
96. Sachlos, E., *et al.*, Novel collagen scaffolds with predefined internal morphology made by solid freeform fabrication. Biomaterials, 2003. 24(8): p. 1487-1497.
97. Wahl, D.A., *et al.* Controlling the processing of collagen-hydroxyapatite scaffolds for bone tissue engineering. in 20th Conference of the European-Society-for-Biomaterials. 2006. Nantes, FRANCE.

98. Dawson, J.I., *et al.*, Development of specific collagen scaffolds to support the osteogenic and chondrogenic differentiation of human bone marrow stromal cells. Biomaterials, 2008. 29(21): p. 3105-3116.
99. Sachlos, E., *et al.*, The impact of critical point drying with liquid carbon dioxide on collagen-hydroxyapatite composite scaffolds. Acta Biomaterialia, 2008. 4(5): p. 1322-1331.
100. Chin, C.D., K. Khanna, and S.K. Sia, A microfabricated porous collagen-based scaffold as prototype for skin substitutes. Biomedical Microdevices, 2008. 10(3): p. 459-467.
101. Liu, L., *et al.*, Degradation Behavior and biocompatibility of nanohydroxyapatite/silk fibroin composite scaffolds. Acta Chimica Sinica, 2008. 66(16): p. 1919-1923.
102. Ungaro, F., *et al.*, Microsphere-integrated collagen scaffolds for tissue engineering: Effect of microsphere formulation and scaffold properties on protein release kinetics. Journal of Controlled Release, 2006. 113(2): p. 128-136.
103. Byrne, E.M., *et al.*, Gene expression by marrow stromal cells in a porous collagen-glycosaminoglycan scaffold is affected by pore size and mechanical stimulation. Journal of Materials Science-Materials in Medicine, 2008. 19(11): p. 3455-3463.
104. Kakudo, N., *et al.*, Bone tissue engineering using human adipose-derived stem cells and honeycomb collagen scaffold. Journal of Biomedical Materials Research Part A, 2008. 84A(1): p. 191-197.
105. Donzelli, E., *et al.*, Mesenchymal stem cells cultured on a collagen scaffold: *In vitro* osteogenic differentiation. Archives of Oral Biology, 2007. 52(1): p. 64-73.
106. Tierney, C.M., *et al.*, The effects of collagen concentration and crosslink density on the biological, structural and mechanical properties of collagen-GAG scaffolds for bone tissue engineering. Journal of the Mechanical Behavior of Biomedical Materials. In Press, Corrected Proof.
107. Bernhardt, A., *et al.*, Mineralised collagen - an artificial, extracellular bone matrix - improves osteogenic differentiation of bone marrow stromal cells. Journal of Materials Science-Materials in Medicine, 2008. 19(1): p. 269-275.
108. Pek, Y.S., *et al.*, Porous collagen-apatite nanocomposite foams as bone regeneration scaffolds. Biomaterials, 2008. 29(32): p. 4300-4305.
109. Negri, S., *et al.*, Tissue engineering: chondrocyte culture on type 1 collagen support. Cytohistological and immunohistochemical study. Journal of tissue engineering and regenerative medicine, 2007. 1(2): p. 158-159.

110. Buma, P., *et al.*, Cross-linked type I and type II collagenous matrices for the repair of full-thickness articular cartilage defects--A study in rabbits. Biomaterials, 2003. 24(19): p. 3255-3263.
111. Dorotka, R., *et al.*, Marrow stimulation and chondrocyte transplantation using a collagen matrix for cartilage repair. Osteoarthritis and Cartilage, 2005. 13(8): p. 655-664.
112. Dorotka, R., *et al.*, Repair of articular cartilage defects treated by microfracture and a three-dimensional collagen matrix. Biomaterials, 2005. 26(17): p. 3617-3629.
113. Ohyabu, Y., *et al.*, Cartilage tissue regeneration from bone marrow cells by RWV bioreactor using collagen sponge scaffold. Materials Science and Engineering: C. In Press, Corrected Proof.
114. Pfeiffer, E., *et al.*, The effects of glycosaminoglycan content on the compressive modulus of cartilage engineered in type II collagen scaffolds. Osteoarthritis and Cartilage, 2008. 16(10): p. 1237-1244.
115. Sato, T., *et al.*, Evaluation of PLLA-collagen hybrid sponge as a scaffold for cartilage tissue engineering. Materials Science and Engineering: C, 2004. 24(3): p. 365-372.
116. Chan, B.P., *et al.*, Self-assembled collagen-human mesenchymal stem cell microspheres for regenerative medicine. Biomaterials, 2007. 28(31): p. 4652-4666.
117. Hui, T.Y., *et al.*, *In vitro* chondrogenic differentiation of human mesenchymal stem cells in collagen microspheres: Influence of cell seeding density and collagen concentration. Biomaterials, 2008. 29(22): p. 3201-3212.
118. Adachi, N., *et al.*, Lateral compartment osteoarthritis of the knee after meniscectomy treated by the transplantation of tissue-engineered cartilage and osteochondral plug. Arthroscopy-the Journal of Arthroscopic and Related Surgery, 2006. 22(1): p. 107-112.
119. Andereya, S., *et al.*, Treatment of patellofemoral cartilage defects utilizing a 3D collagen gel: Two-year clinical results. Zeitschrift Fur Orthopadie Und Unfallchirurgie, 2007. 145(2): p. 139-145.
120. Andereya, S., *et al.*, First clinical experiences with a novel 3D-collagen gel (CaReS (R)) for the treatment of focal cartilage defects in the knee. Zeitschrift Fur Orthopadie Und Ihre Grenzgebiete, 2006. 144(3): p. 272-280.
121. Furrer, P., M. Zinn, and S. Panke, Polyhydroxyalkanoate and its potential for biomedical applications, in Natural-based Polymers for Biomedical Applications, N.M. Neves, *et al.*, Editors. 2008, Woodhead Publishing Ltd.: Cambridge. p. 416-445.
122. Chen, G.G.-Q., Polyhydroxyalkanoates, in Biodegradable Polymers for Industrial Applications, R. Smith, Editor. 2005, Woodhead Publishing Ltd.: Cambridge. p. 32-56.

123. Zinn, M., B. Witholt, and T. Egli, Occurrence, synthesis and medical application of bacterial polyhydroxyalkanoate. Advanced Drug Delivery Reviews, 2001. 53(1): p. 5-21.
124. Chen, G.-Q. and Q. Wu, The application of polyhydroxyalkanoates as tissue engineering materials. Biomaterials, 2005. 26(33): p. 6565-6578.
125. Nair, L.S. and C.T. Laurencin, Biodegradable polymers as biomaterials. Progress in Polymer Science, 2007. 32(8-9): p. 762-798.
126. Sombatmankhong, K., *et al.*, Bone scaffolds from electrospun fiber mats of poly(3-hydroxybutyrate), poly(3-hydroxybutyrate-co-3-hydroxyvalerate) and their blend. Polymer, 2007. 48(5): p. 1419-1427.
127. Cheng, M.-L., *et al.*, Processing and characterization of electrospun poly(3-hydroxybutyrate-co-3-hydroxyhexanoate) nanofibrous membranes. Polymer, 2008. 49(2): p. 546-553.
128. Guan, D., *et al.*, Attachment, proliferation and differentiation of BMSCs on gas-jet/electrospun nHAP/PHB fibrous scaffolds. Applied Surface Science, 2008. 255(2): p. 324-327.
129. Sultana, N. and M. Wang. Fabrication of HA/PHBV composite scaffolds through the emulsion freezing/freeze-drying process and characterisation of the scaffolds. in 5th Asian-Australian Conference on Composite Materials (ACCM-5_. 2006. Hong Kong, PEOPLES R CHINA.
130. Lin, F., *et al.*, Deposition behavior and properties of silk fibroin scaffolds soaked in simulated body fluid. Materials Chemistry and Physics, 2008. 111(1): p. 92-97.
131. Wang, Y., *et al.*, Evaluation of three-dimensional scaffolds prepared from poly(3-hydroxybutyrate-co-3-hydroxyhexanoate) for growth of allogeneic chondrocytes for cartilage repair in rabbits. Biomaterials, 2008. 29(19): p. 2858-2868.
132. Wang, Y.-W., Q. Wu, and G.-Q. Chen, Attachment, proliferation and differentiation of osteoblasts on random biopolyester poly(3-hydroxybutyrate-co-3-hydroxyhexanoate) scaffolds. Biomaterials, 2004. 25(4): p. 669-675.
133. Wang, Y.-W., *et al.*, Evaluation of three-dimensional scaffolds made of blends of hydroxyapatite and poly(3-hydroxybutyrate-co-3-hydroxyhexanoate) for bone reconstruction. Biomaterials, 2005. 26(8): p. 899-904.
134. Köse, G.T., *et al.*, Macroporous poly(3-hydroxybutyrate-co-3-hydroxyvalerate) matrices for bone tissue engineering. Biomaterials, 2003. 24(11): p. 1949-1958.
135. Sun, J., *et al.*, Macroporous poly(3-hydroxybutyrate-co-3-hydroxyvalerate) matrices for cartilage tissue engineering. European Polymer Journal, 2005. 41(10): p. 2443-2449.

136. Li, H. and J. Chang, Fabrication and characterization of bioactive wollastonite/PHBV composite scaffolds. Biomaterials, 2004. 25(24): p. 5473-5480.
137. Mai, R., *et al.*, Ectopic bone formation in nude rats using human osteoblasts seeded poly(3)hydroxybutyrate embroidery and hydroxyapatite-collagen tapes constructs. Journal of Cranio-Maxillofacial Surgery, 2006. 34(Supplement 2): p. 101-109.
138. Köse, G.T., *et al.*, Bone generation on PHBV matrices: an *in vitro* study. Biomaterials, 2003. 24(27): p. 4999-5007.
139. Zhao, Y., *et al.*, The effect of 3-hydroxybutyrate on the *in vitro* differentiation of murine osteoblast MC3T3-E1 and *in vivo* bone formation in ovariectomized rats. Biomaterials, 2007. 28(20): p. 3063-3073.
140. Köse, G.T., *et al.*, Tissue engineered cartilage on collagen and PHBV matrices. Biomaterials, 2005. 26(25): p. 5187-5197.
141. Deng, Y., *et al.*, Poly(hydroxybutyrate-co-hydroxyhexanoate) promoted production of extracellular matrix of articular cartilage chondrocytes *in vitro*. Biomaterials, 2003. 24(23): p. 4273-4281.
142. Deng, Y., *et al.*, Study on the three-dimensional proliferation of rabbit articular cartilage-derived chondrocytes on polyhydroxyalkanoate scaffolds. Biomaterials, 2002. 23(20): p. 4049-4056.
143. Altman, G.H., *et al.*, Silk-based biomaterials. Biomaterials, 2003. 24(3): p. 401-416.
144. Wang, Y., *et al.*, Stem cell-based tissue engineering with silk biomaterials. Biomaterials, 2006. 27(36): p. 6064-6082.
145. MacIntosh, A.C., *et al.*, Skeletal tissue engineering using silk biomaterials. Journal of Tissue Engineering and Regenerative Medicine, 2008. 2(2-3): p. 71-80.
146. Tanaka, K., K. Mori, and S. Mizuno, Immunological Identification of the Major Disulfide-Linked Light Component of Silk Fibroin. Journal of Biochemistry, 1993. 114(1): p. 1-4.
147. Kundu, S.C., *et al.*, Natural protective glue protein, sericin bioengineered by silkworms: Potential for biomedical and biotechnological applications. Progress in Polymer Science, 2008. 33(10): p. 998-1012.
148. Zhou, C.Z., *et al.*, Silk fibroin: Structural implications of a remarkable amino acid sequence. Proteins-Structure Function and Genetics, 2001. 44(2): p. 119-122.
149. Yao, J.M., Y. Nakazawa, and T. Asakura, Structures of Bombyx mori and Samia cynthia ricini silk fibroins studied with solid-state NMR. Biomacromolecules, 2004. 5(3): p. 680-688.
150. Yao, J. and T. Asakura, Silks, in Encyclopedia of Biomaterials and Biomedical Engineering, G.E. Wnek and G.L. Bowlin, Editors. 2008, Taylor & Francis, Inc.: New York. p. 2442-2449.

151. Wang, Y., *et al.*, *In vivo* degradation of three-dimensional silk fibroin scaffolds. Biomaterials, 2008. 29(24-25): p. 3415-3428.
152. Meinel, L., *et al.*, The inflammatory responses to silk films *in vitro* and *in vivo*. Biomaterials, 2005. 26(2): p. 147-155.
153. Panilaitis, B., *et al.*, Macrophage responses to silk. Biomaterials, 2003. 24(18): p. 3079-3085.
154. Vepari, C. and D.L. Kaplan, Silk as a biomaterial. Progress in Polymer Science, 2007. 32(8-9): p. 991-1007.
155. Horan, R.L., *et al.*, *In vitro* degradation of silk fibroin. Biomaterials, 2005. 26(17): p. 3385-3393.
156. Kim, U.-J., *et al.*, Three-dimensional aqueous-derived biomaterial scaffolds from silk fibroin. Biomaterials, 2005. 26(15): p. 2775-2785.
157. Nazarov, R., H.J. Jin, and D.L. Kaplan, Porous 3-D scaffolds from regenerated silk fibroin. Biomacromolecules, 2004. 5(3): p. 718-726.
158. Hofmann, S., *et al.*, Control of *in vitro* tissue-engineered bone-like structures using human mesenchymal stem cells and porous silk scaffolds. Biomaterials, 2007. 28(6): p. 1152-1162.
159. Jin, H.-J., *et al.*, Human bone marrow stromal cell responses on electrospun silk fibroin mats. Biomaterials, 2004. 25(6): p. 1039-1047.
160. Meinel, A.J., *et al.*, Optimization strategies for electrospun silk fibroin tissue engineering scaffolds. Biomaterials, 2009. 30(17): p. 3058-3067.
161. Baek, H.S., *et al.*, Enhanced chondrogenic responses of articular chondrocytes onto porous silk fibroin scaffolds treated with microwave-induced argon plasma. Surface and Coatings Technology, 2008. 202(22-23): p. 5794-5797.
162. Ghosh, S., *et al.*, Direct-write assembly of microperiodic silk fibroin scaffolds for tissue engineering applications. Advanced Functional Materials, 2008. 18(13): p. 1883-1889.
163. Meinel, L., *et al.*, Bone tissue engineering using human mesenchymal stem cells: Effects of scaffold material and medium flow. Annals of Biomedical Engineering, 2004. 32(1): p. 112-122.
164. Meinel, L., *et al.*, Engineering bone-like tissue *in vitro* using human bone marrow stem cells and silk scaffolds. Journal of Biomedical Materials Research Part A, 2004. 71A(1): p. 25-34.
165. Meinel, L., *et al.*, Silk implants for the healing of critical size bone defects. Bone, 2005. 37(5): p. 688-698.
166. Meinel, L., *et al.*, Silk based biomaterials to heal critical sized femur defects. Bone, 2006. 39(4): p. 922-931.

167. Karageorgiou, V., *et al.*, Porous silk fibroin 3-D scaffolds for delivery of bone morphogenetic protein-2 *in vitro* and *in vivo*. Journal of Biomedical Materials Research Part A, 2006. 78A(2): p. 324-334.
168. Kim, H.J., *et al.*, Bone tissue engineering with premineralized silk scaffolds. Bone, 2008. 42(6): p. 1226-1234.
169. Li, C., *et al.*, Electrospun silk-BMP-2 scaffolds for bone tissue engineering. Biomaterials, 2006. 27(16): p. 3115-3124.
170. Fuchs, S., *et al.*, Outgrowth endothelial cells isolated and expanded from human peripheral blood progenitor cells as a potential source of autologous cells for endothelialization of silk fibroin biomaterials. Biomaterials, 2006. 27(31): p. 5399-5408.

171. Fuchs, S., *et al.*, Dynamic processes involved in the pre-vascularization of silk fibroin constructs for bone regeneration using outgrowth endothelial cells. Biomaterials, 2009. 30(7): p. 1329-1338.
172. Meinel, L., *et al.*, Engineering cartilage-like tissue using human mesenchymal stem cells and silk protein scaffolds. Biotechnology and Bioengineering, 2004. 88(3): p. 379-391.
173. Hofmann, S., *et al.*, Cartilage-like tissue engineering using silk scaffolds and mesenchymal stem cells. Tissue Engineering, 2006. 12(10): p. 2729-2738.
174. Wang, Y., *et al.*, *In vitro* cartilage tissue engineering with 3D porous aqueous-derived silk scaffolds and mesenchymal stem cells. Biomaterials, 2005. 26(34): p. 7082-7094.
175. Wang, Y., *et al.*, Cartilage tissue engineering with silk scaffolds and human articular chondrocytes. Biomaterials, 2006. 27(25): p. 4434-4442.
176. T, R.S., *et al.*, Comparative chondrogenesis of human cell sources in 3D scaffolds. 2009. p. n/a.
177. Uebersax, L., H.P. Merkle, and L. Meinel, Insulin-like growth factor I releasing silk fibroin scaffolds induce chondrogenic differentiation of human mesenchymal stem cells. Journal of Controlled Release, 2008. 127(1): p. 12-21.

SECTION 2.

CHAPTER II.

Materials and methods

CHAPTER II.

Materials and methods

The main porpose of this chapter is to describe in more detail the materials used, the experimental techniques and the characterization methodologies employed that allowed to obtained results presented in this thesis and that will be provided further, in Section 3. Along with Chapter I, it aims to be a guideline of the rationale for this research, namely on the aspects related with the selection of the materials, on the processing routes used, and characterization process adopted.

1. MATERIALS

1.1. CHITOSAN

Chitosan is obtained from the alkaline deacetylation of the biopolymer chitin, the second most abundant organic materials, which can be found in shells of marine crustaceans and cell walls of fungi [1]. Structurally, chitosan is a linear polysaccharide consisting of N-glucosamine (deacetylated unit) and N-acetyl glucosamine (acetylated unit) units linked by β(1→4) glycosidic bonds (Fig. 2.1). The degree of deacetylation (DD) is the glucosamine / N-acetyl glucosamine ratio and usually can vary, depending on the source, from 30% to 95%. The degree of crystallinity of chitosan is manly controlled by the degree of deacetylation being maximum for both chitin (i.e. 0% deacetylated) and fully deacetylated forms (100% chitosan) and minimum for intermediate degrees of deacetylation [2].

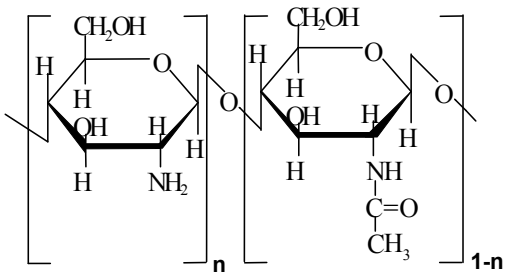

Figure 2.1. Chemical structure of chitosan

Chitosan and its derivates have attracted attention for potential application in the biomedical field because of their various advantages including biocompatibility, biodegradability, hydrophilicity and anti-microbial activity as well as bioadherence and cell affinity. However the use of chitosan as material for load bearing applications has been limited by its mechanically weak features especially in the weat state. The development of hybrid materials that combine naturally occurring polymers with biocompatible synthetic polymers is expected to minimize the mismatch of mechanical properties and preserve biocompatibility.

The chitosan used for production of the blends reported on this thesis was The chitosan, supplied by France Chitin, (Orange, France), and had a degree of deacetylation of approximately 85%.

1.2. ALIPHATIC POLYESTERS

Synthetic polymers used in the biomaterials field include biodegradable aliphatic polyesters, such as polyhydroxybutyrate and its copolymer polyhydroxybutyrate-co-valerate, poly(lactic acid), poly(glycolic acid), poly-ε-caprolactone, and their copolymers. The ester bonds in these synthetic polymers hydrolyze to nontoxic natural metabolites and are eliminated from the body via respiration [3].

A series of biodegradable polyesters using 1,4 butane diol and succinic acid has been produced using polycondensation reaction. Polybutylene succinate, known under the trade name Bionolle 1000 (Showa Highpolymer, Japan), is available in melt flow indexes ranging from 1-50 and can be used for a wide range of applications. A corresponding co-polyester of succinic and adipic acid is also available (Bionolle 3000, Showa Highpolymer, Japan). Bionolle 1000 has a melt temperature of 115 ºC while Bionolle 3000 has a melt temperature of 85 ºC. The 1000 series is more crystalline and takes longer to degrade. Bionolle plastics have been found to degrade in compost, soil, fresh water, and sea water though the time taken for degradation varies. Both the 1000 and 3000 series are relatively stable during processing [4]. Nevertheless, to our knoladge, these polymers were never used in biomedical applications.

The polyesters used on this thesis include poly(lactic acid) (PLA), poly-ε-caprolactone (PCL), poly(butylene succinate) (PBS), poly(butylene succinate adipate) (PBSA) and poly(butylene terephthalate adipate) (PBTA). Polycaprolactone resins PCL 787 (MFI~4), commercially available as TONE™ polymer, were obtained from Union Carbide Chemicals and Plastics Division, Bound Brook, New Jersey. Eastar Bio Copolyester 14766™, a butanediol, adipate, and terephthalate copolymer (MFI~20), was obtained from Eastman Chemical Company, Kingsport, Tennessee. Bionolle™ 1050, a polybutylene succinate copolymer (MFI~50), and Bionolle™ 3001, a poly(butylene succinate adipate) copolymer (MFI~1.0) were obtained from Showa Highpolymer Co. Ltd., Tokyo, Japan. The characteristics of the various polyesters are summarized in Table 2.1.

Table 2.1. Material properties of polyesters used in this study.

	PCL 787 [a]	PBS [b]	PBSA [c, *]	PBTA [d]	PLA [e]
MELT INDEX	4	50	1	20	-
MN (X 10^{-5})	0.64	0.34	0.46	0.43	1.54
MW (X 10^{-5})	1.24	0.89	0.91	0.78	2.52

* from [5]
[a] poly-ε-caprolactone
[b] poly(butylene succinate)
[c] poly(butylene succinate adipate)
[d] poly(butylene terephthalate adipate)
[e] poly(lactic acid)

1.3. HYDROXYAPATITE (HA)

HA is a bioactive material, i.e. a material that elicits a specific biological response at the interface of the material, facilitating the osteointegration of implants due to the formation of bond between tissues and the material [6]. HA is also an osteoconductive material, acting as a bioconductive pathway that supports the ingrowth of bony tissue [7, 8]. For these reasons and due to its similar chemical structure to the inorganic composition of human bone, HA is often used in bone reconstruction.

The objectives of using HA as a filler material for chitosan based polymeric materials were: i) to assure the bioactive behaviour of the composite and ii) to improve the mechanical properties of the composite by providing the simultaneous stiffening of the polymer matrix. Hydroxyapatite (grade Capital S) [3 μm<d<6 μm] used on this thesis was obtained from Plasma Biotal Ltd, Tideswell, England.

2. PROCESSING METHODS

All the studies reported on this thesis were performed on moulded specimens processed according to at least one of the following processing methods:

2.1. EXTRUSION COMPOUNDING

In order to achieve a high degree of mixing in the compounded materials, all the blends and composites used on the thesis were produced in a twin screw extruder. The chitosan/polyester blends containing less than 70% chitosan were compounded in a counter rotating twin-screw extruder (Carvex, Lisbon, Portugal). The only exception to this was when blends of chitosan (50% by weight) were compounded with B3001. Higher chitosan content pushed the torque in the counter rotating extruder close to the

maximum. Alternately, throughput had to be reduced to keep the torque below the upper threshold. Hence, blends containing 70% chitosan were compounded in a co-rotating twin-screw extruder [Leistriz LSM 36] to improve mixing. Since the torque was close to the maximum limit of the machine, this blend (70% chitosan/30% PBS) was processed with the die removed and with addedwater/glycerol to enhance plasticization. The various blend compositions studied and processing conditions used are summarized in Table 2.2.

The composites were compounded in a co-rotating twin-screw extruder [Leistriz LSM 36]. Similarly to blends with high chitosan content, extrusion of chitosan based composites pushed the torque in the extruder close to the maximum. Hence, each composition had 5% by weight of plasticizer (glycerol) to reduce the torque. The various processing conditions used for compounding the different composite are summarized in Table 2.3. For both cases (blends and composites), the extruded strands were ground by a Coloritron grinder using 5 mm diameter pellets.

Table 2.2. Processing conditions used for various blends composition studied.

MATERIAL	PROCESSING CONDITIONS			
	TEMPERATURE PROFILE	SCREW SPEED (RPM)	DIE TEMPERATURE (°C)	TYPE OF MACHINE USED
25Ch-75PBS [a]	160/160/160	15	160	Counter Rotating
50Ch-50PBS [b]	160/160/160	15	160	Counter Rotating
50Ch-50PBTA [c]	160/160/160	15	160	Counter Rotating
50Ch-50PCL [d]	160/160/160	15	160	Counter Rotating
50Ch-50PBSA [e]	160 in all zones	100	160	Co-rotating
50Ch-50PLA [f]	175 in first 4 zones, 180 rest of the zones	100	180	Co-rotating
70Ch-30PBS [g]	70/90 and 160 in the rest of the zones	100	-	Co-rotating

[a] Blend containing 25% by weight of chitosan and 75% by weight of PBS
[b] Blend containing 50% by weight of chitosan and 50% by weight of PBS
[c] Blend containing 50% by weight of chitosan and 50% by weight of PBTA
[d] Blend containing 50% by weight of chitosan and 50% by weight of PCL
[e] Blend containing 50% by weight of chitosan and 50% by weight of PBSA
[f] Blend containing 50% by weight of chitosan and 50% by weight of PLA
[g] Blend containing 70% by weight of chitosan and 30% by weight of PBS

Table 2.3. Processing conditions used for compounding the various composites studied.

MATERIAL	PROCESSING CONDITIONS		
	TEMPERATURE PROFILE (°C)	SCREW SPEED (RPM)	TYPE OF MACHINE USED
70PBS-30HA [h]	80/120/140/150/165/175	100	Co-rotating
17.5Ch-52.5PBS-30 HA + 5% glycerol [i]	80/120/140/150/165/175	100	Co-rotating
45Ch-45PBS-10HA + 5% glycerol [j]	80/120/140/150/165/175	100	Co-rotating
40Ch-40PBS-20HA + 5% glycerol [l]	80/120/140/150/165/175	100	Co-rotating
35Ch-35PBS-30HA + 5% glycerol [m]	80/120/140/150/165/175	100	Co-rotating
35Ch-35PBTA-30HA + 5% glycerol [n]	80/120/140/150/165/175	100	Co-rotating
35Ch-35PCL-30HA + 5% glycerol [o]	80/120/140/150/165/175	100	Co-rotating
35Ch-35PLA-30HA + 5% glycerol [p]	175 in first 4 zones, 180 rest	100	Co-rotating

[h] Composite containing 70% by weight of PBS and 30% by weight of hydroxyapatite
[i] Composite containing 17.5% by weight of chitosan, 52.5% by weight of PBS and 30% by weight of hydroxyapatite, processed with 5% by weight of glycerol
[j] Composite containing 45% by weight of chitosan, 45% by weight of PBS and 10% by weight of hydroxyapatite, processed with 5% by weight of glycerol
[l] Composite containing 40% by weight of chitosan, 40% by weight of PBS and 20% by weight of hydroxyapatite, processed with 5% by weight of glycerol
[m] Composite containing 35% by weight of chitosan, 35% by weight of PBS and 30% by weight of hydroxyapatite, processed with 5% by weight of glycerol
[n] Composite containing 35% by weight of chitosan, 35% by weight of PBTA and 30% by weight of hydroxyapatite, processed with 5% by weight of glycerol
[o] Composite containing 35% by weight of chitosan, 35% by weight of PCL and 30% by weight of hydroxyapatite, processed with 5% by weight of glycerol
[p] Composite containing 35% by weight of chitosan, 35% by weight of PLA and 30% by weight of hydroxyapatite, processed with 5% by weight of glycerol

2.2. CONVENTIONAL INJECTION MOULDING

The blends and composites were injection molded using an ENGEL injection molding machine to produce tensile test bars. The tensile bars had a neck cross-section area of 2mm×4mm and a neck length of 20 mm (Figure 2.2).

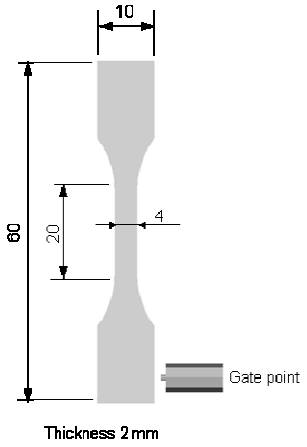

Figure 2.2. Dumbbell shaped tensile bar of 60mm length, a constant rectangular cross-section of 4x2mm and 20mm of reference length.

The conditions used for molding the blends and composites are summarized in Table 2.4 and 2.5, respectively. The mold was held at a constant temperature of 22 ºC for all compositions except for PLA where the mold temperature was raised to 30 ºC.

Table 2.4. Injection molding processing conditions for blends.

MATERIAL	INJECTION SPEED (mm/s)	HOLDING PRESSURE (BAR)	BARREL TEMP. (°C)	MOULD TEMP. (°C)
PBS [a]	30	50	90-120-120-140	22
PBSA [b]	30	120	80-100-120-130	22
PBTA [c]	30	50	90-120-120-140	22
PCL [d]	80	80	70-90-100-110	22
PLA [e]	30	30	155-170-180-190	30
25Ch-75PBS [f]	25	20	110-130-150-160	22
50Ch-50PBS [g]	30	80	110-130-150-160	22
50Ch50PBTA [h]	20	30	110-130-150-160	22
50Ch-50PCL [i]	40	20	110-130-150-160	22
50Ch-50PBSA [j]	65	100	110-130-150-160	22
50Ch-50PLA [l]	70	25	150-155-155-160	30
70Ch-30PBS [m]	80	50	110-130-150-160	22

[a] poly(butylene succinate)
[b] poly(butylene succinate adipate)
[c] poly(butylene terephthalate adipate)
[d] poly-ε-caprolactone
[e] poly(lactic acid)
[f] Blend containing 25% by weight of chitosan and 75% by weight of PBS
[g] Blend containing 50% by weight of chitosan and 50% by weight of PBS
[h] Blend containing 50% by weight of chitosan and 50% by weight of PBTA
[i] Blend containing 50% by weight of chitosan and 50% by weight of PCL
[j] Blend containing 50% by weight of chitosan and 50% by weight of PBSA
[l] Blend containing 50% by weight of chitosan and 50% by weight of PLA
[m] Blend containing 70% by weight of chitosan and 30% by weight of PBS

Table 2.5. Injection molding processing conditions for composites.

MATERIAL	INJECTION SPEED (mm/s)	HOLDING PRESSURE (BAR)	BARREL TEMP. (°C)
70PBS-30HA [h]	28	40	90-120-120-140
17.5Ch-52.5PBS-30 HA + 5% glycerol [i]	28	20	110-130-150-160
45Ch-45PBS-10HA + 5% glycerol [j]	26	20	110-130-150-160
40Ch-40PBS-20HA + 5% glycerol [lz]	32	20	110-130-150-160
35Ch-35PBS-30HA + 5% glycerol [m]	30	20	110-130-150-160
35Ch-35PBTA-30HA + 5% glycerol [n]	22	25	110-130-150-160
35Ch-35PCL-30HA + 5% glycerol [o]	42	20	110-130-150-160

[h] Composite containing 70% by weight of PBS and 30% by weight of hydroxyapatite
[i] Composite containing 17.5% by weight of chitosan, 52.5% by weight of PBS and 30% by weight of hydroxyapatite, processed with 5% by weight of glycerol
[j] Composite containing 45% by weight of chitosan, 45% by weight of PBS and 10% by weight of hydroxyapatite, processed with 5% by weight of glycerol
[l] Composite containing 40% by weight of chitosan, 40% by weight of PBS and 20% by weight of hydroxyapatite, processed with 5% by weight of glycerol
[m] Composite containing 35% by weight of chitosan, 35% by weight of PBS and 30% by weight of hydroxyapatite, processed with 5% by weight of glycerol
[n] Composite containing 35% by weight of chitosan, 35% by weight of PBTA and 30% by weight of hydroxyapatite, processed with 5% by weight of glycerol
[o] Composite containing 35% by weight of chitosan, 35% by weight of PCL and 30% by weight of hydroxyapatite, processed with 5% by weight of glycerol

2.3. FIBERS PRODUCTION

The chitosan based fibers presented on chapter VI Blends of chitosan with poly(butylene succinate) (Ch-PBS) at two different ratios (25/75 wt% and 50/50wt%) and blends of chitosan with poly(butylene terephthalate adipate) (Ch-PBTA) (50/50 wt%) previously compound were extruded into fibers, by using a prototype single screw micro-extruder (Figure 2.3) [9] coupled to a capillary die. Although the machine is capable of producing extrudates with only a few grams of material in powder form, it was designed to induce thermo-mechanical stresses of the same order of magnitude of those developed in bigger machines. Moreover, the screw contains a multi-pass barrier section that greatly improves the dispersive mixing capacity. The extrudates were air-cooled without any significant stretch and winded. The extruder operating conditions are summarized in Table 2.6.

a)

b)

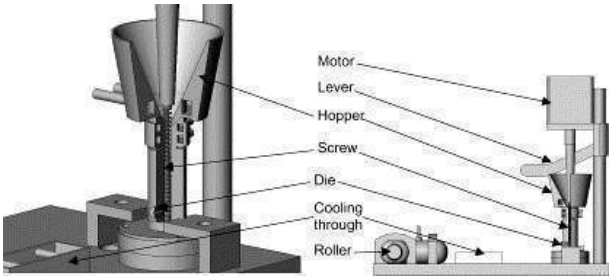

Figure 2.3. a) The micro-extruder and b) its layout (adapted from [9])

Table 2.6. Processing conditions of chitosan based fibers using a micro-extruder.

COMPOSITION	BARREL TEMPERATURE (°C)	SCREW SPEED (RPM)
25Ch-75PBS [a]	140-150	35
50Ch-50PBS [b]	140-155	35
50Ch-50PBTA [c]	155-160	35

[a] Blend containing 25% by weight of chitosan and 75% by weight of PBS
[b] Blend containing 50% by weight of chitosan and 50% by weight of PBS
[c] Blend containing 50% by weight of chitosan and 50% by weight of PBTA

2.4. SCAFFOLDS PRODUCTION – FIBER BONDING

The scaffolds presented in Chapter VII were fabricated into mesh structures by a fiber compression method. Briefly, the extruded fibers from the blends 50Ch-50PBS and 50Ch-50PBTA were chopped in 1 cm long sections and loaded into a mould. The mould is heated above the melting temperature (T_m) of the thermoplastic composite during a specific time period. The next step involves applying pressure to

allow the fibers to weld at the junctions forming a stable fiber mesh structure. The porous mesh structure is further cut into 1.5 mm thick discs, with diameter of 7 mm.

2.5. SCAFFOLDS PRODUCTION – COMPRESSION MOULDING/PARTICULATE LEACHING

The chitosan/polyester blends and composites used for the production of the scaffolds described in Chapter VI were compounded in a twin-screw extruder and details of the processing conditions were previously described (topic 2.1 of this chapter). For scaffolds production, the compounded blends or composites were ground, mixed with salt, loaded into a mold that was further heated, and compression molded into discs. The salt content was 60 and 80% by weight for blends and 60 and 70% by weight for composites containing hydroxyapatite (HA). Salt was obtained from a local grocery store. The group of the larger range of NaCl particles (250–500 μm) was obtained by sieving the raw material. The second group (63–125 μm) was obtained by grinding the raw material that was further sieved. The composition of the scaffolds produced from chitosan-polyester blends and composites are shown in Tables 2.7 and 2.8, respectively.

The aim of using two different salt amounts and two different salt particle size ranges was to produce scaffolds with varying amounts of porosity and pore sizes and analyze the effect of these parameters on the morphology and mechanical of the developed scaffolds. Some scaffolds were selected to analyze the effect of compression-molding processing method on the crystallinity and thermal properties of the polyester part.

The compression-molded discs were further sliced to obtain cubes with nominal dimensions of 5 mm. The cubes were then immersed in distilled water to leach out the porogen. The water was replaced daily. Preliminary studies had shown that immersing for a period of 6 days would enable the entire salt to leach out. The cubes were dried to constant weight and used for further testing.

Table 2.7. Composition of the scaffolds produced from chitosan-polyester blends and salt particle size ranging from 63 - 125μm or 250 -500μm.

COMPOSITION	SALT PARTICLE SIZE (μm)	SALT CONTENT (WT%)
25C-75PBS [a]	63-125	60
		80
	250-500	60
		80
50C-50PBS [b]	63-125	60
		80
	250-500	60
		80
50C-50PBTA [c]	63-125	60
		80
	250-500	60
		80
50C-50PCL [d]	63-125	60
		80
	250-500	60
		80
70C-30PBS [e]	63-125	60
		80
	250-500	60
		80

[a] Blend containing 25% by weight of chitosan and 75% by weight of PBS
[b] Blend containing 50% by weight of chitosan and 50% by weight of PBS
[c] Blend containing 50% by weight of chitosan and 50% by weight of PBTA
[d] Blend containing 50% by weight of chitosan and 50% by weight of PCL
[e] Blend containing 70% by weight of chitosan and 30% by weight of PBS

Table 2.8. Composition of scaffolds containing hydroxyapatite produced using salt particles with size ranging from 250μm - 500μm.

COMPOSITION	SALT PARTICLE SIZE (μm)	SALT CONTENT (WT%)
70PBS-30HA [h]	250-500	60 70
17.5Ch-52.5PBS-30HA [i]	250-500	60 70
45Ch-45PBS-10HA [j]	250-500	60 70
40Ch-40PBS-20HA [l]	250-500	60 70
35Ch-35PBS-30HA [m]	250-500	60 70
35Ch-35PCL-30HA [n]	250-500	60 70
35Ch-35PBTA-30HA [o]	250-500	60 70

[h] Composite containing 70% by weight of PBS and 30% by weight of hydroxyapatite
[i] Composite containing 17.5% by weight of chitosan, 52.5% by weight of PBS and 30% by weight of hydroxyapatite
[j] Composite containing 45% by weight of chitosan, 45% by weight of PBS and 10% by weight of hydroxyapatite
[l] Composite containing 40% by weight of chitosan, 40% by weight of PBS and 20% by weight of hydroxyapatite
[m] Composite containing 35% by weight of chitosan, 35% by weight of PBS and 30% by weight of hydroxyapatite
[n] Composite containing 35% by weight of chitosan, 35% by weight of PCL and 30% by weight of hydroxyapatite
[o] Composite containing 35% by weight of chitosan, 35% by weight of BTA and 30% by weight of hydroxyapatite

3. CHARACTERIZATION METHODS

3.1. MECHANICAL PROPERTIES

3.1.1. Tensile tests

The tensile properties of the chitosan based blends and composites were determined using a Universal tensile testing machine (Instron 4505 Universal Machine, USA). The tested specimens were dumbbell shaped tensile bars. Tensile force was taken as the maximum force in the force-deformation curve. Tensile modulus was estimated from the initial slope of the stress–strain curve. Samples were conditioned at room temperature for at least 48 h before testing. A crosshead speed

of 5mm min^{-1} was used up to a deformation of 1.5% after which the speed increased to 50 $mm.min^{-1}$. The values reported were the average of at least five specimens.

The tensile properties of the produced fibers were determined using a Universal tensile testing machine (Intron 5540 Universal Machine, USA). A crosshead speed of 5 $mm.min^{-1}$ was used up to rupture of the fiber. The results presented are the average of the testing of 10 specimens.

For each tensile test, the following mechanical properties, which are graphically defined in Figure 2.4, were determined:

i) the secant modulus at 1 % strain (E_s), defined as the slope of the line from the origin to the point corresponding to 1 % strain on the stress-strain curve of the material;

ii) the ultimate tensile strength (UTS), defined as the maximum tensile stress developed in the material during the tensile test;

iii) the strain at break point (ε_b), defined as the maximum strain of the material, i.e. elongation at the failure point of the material.

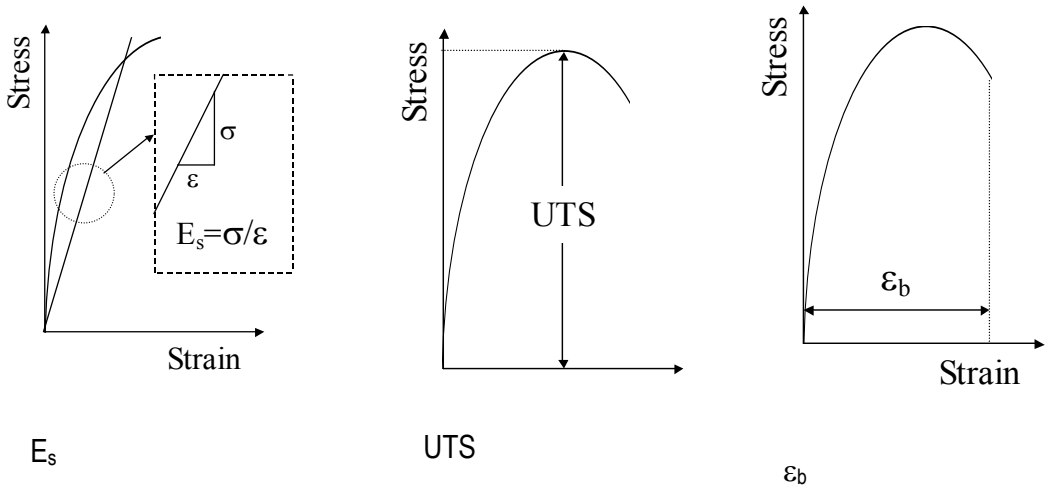

Figure 2.4. Graphical definition of the secant modulus at 1 % strain (Es), the ultimate tensile strength (UTS), and the strain at break point (εb), being σ the stress and ε the strain.

3.1.2. Compression tests

The compression testes of the developed chitosan based fiber mesh scaffolds were performed using a Universal tensile testing machine (Instron 4505 Universal Machine, USA). The tests were performed under compression loading using a crosshead speed of 2 $mm.min^{-1}$ and the results presented are the average of at least five specimens.

The mechanical properties of the scaffolds obtained by compression moulding/particulate leaching were determined by performing uniaxial compression tests on the cubic scaffolds using a Universal tensile testing machine (Instron 4505 Universal Machine, USA). Each specimen measured 5 mm in the direction of testing and was 5 mm square in cross-section. A crosshead speed of 2 $mm.min^{-1}$ was used in the compression tests.

On both cases, samples were conditioned at room temperature for at least 48 h before testing. The values reported are the average of at least five specimens per condition. The compressive modulus was determined in the most linear region of the stress–strain graph using the secant method. In the cases that the yield stress was not clear it was calculated as the stress at the intersection of a line drawn parallel to the linear region and intercepting the *x*-axis at 1% strain.

3.2. DIFFERENTIAL SCANNING CALORIMETRY

The DSC experiments were performed in a Perkin-Elmer DSC7 apparatus, using a water-cooling accessory and nitrogen as a purge gas (flux gas of ca. 20 $cm^3\ min^{-1}$). Both temperature and heat flux were calibrated with Indium (99.99999% purity) at a scanning rate of 20 $ºCmin^{-1}$. The samples were obtained by cutting a small piece of material (with ca. 10 mg weight) in the central region of the injection parts. An effort was made to maintain the geometry of the different samples, in order to keep the same thermal resistance. All the experiments were performed at 20 $ºCmin^{-1}$, starting from room temperature. Only the first run was analyzed, which reflects not only the materials contained in the samples, but also the general morphology developed during processing.

3.3. WIDE ANGLE *(WAXS)* AND SMALL ANGLE *(SAXS)* X-RAY SCATTERING

WAXS and SAXS experiments were performed using Xray synchrotron radiation (transmission mode) at the Soft Condensed Matter A2 beam line at HASYLAB (DESY) synchrotron facility in Hamburg (Germany). The experimental setup includes a MARCCD detector for acquiring two dimensional SAXS

patterns (sample-to-detector distance being 280 cm) and a linear detector for 1D WAXS measurements (distance 23 cm). Cu-Kα radiation, with a wavelength of λ = 0.154 nm, was employed for both SAXS and WAXS measurements. The injection moulded samples were fixed vertically and the patterns were acquired at room temperature.

3.4. OPTICAL MICROSCOPY

To analyze the chitosan distribution on the polymer matrix, tensile bars of each blend were stained with a 0.10 (w/v) Eosin solution for 10 min at 32±0.5 ºC. Stained samples were examined by light microscopy (Olympus BH-2) in reflection mode. Photographs of the stained surface were obtained using a microscope digital camera Olympus DP11. Images of the cross-section were obtained by cryogenically fracturing the tensile bar. The fractured surface was smoothened using a glass knife for optical clarity.

To analyze the chitosan phase distribution within the fibers, cross sections were prepared and analyzed in a procedure similar to the one reported for the tensile bars. Chitosan based fibers were mounted in epoxy resin. After the curing stage, thin slices of material were removed from the surface of the fibers entrapped in the epoxy resin using a microtome. The procedure continued until approximately half the diameter of the fibers was sliced. After this procedure, the fibers with the exposed surface were stained with a 0.10 (w/v) eosin solution for 10 min at 32±0.5 ºC. Stained samples were examined by light microscopy (Olympus BH-2) in reflection. Photomicrographs of the stained surfaces were obtained using a digital camera Olympus DP11 directly mounted in the microscope.

3.5. SCANNING ELECTRON MICROSCOPY

The morphological characterization of the blends was made using a Leica-Cambridge S-360 (UK) scanning electron microscope (SEM). All the samples were sputter-coated with gold. Several different analyses of the cross-section of the tensile bars were made. These include (i) observations after the tensile tests; (ii) observations after immersing the samples in liquid nitrogen for 1 min and fracturing the sample in the testing zone to analyze the brittle fracture; and (iii) observations after cryogenically-fractured surfaces were etched with 1% acetic acid for 3 h or 1 day. The objective was to dissolve the chitosan since not enough phase contrast between the filler and polyester was obtained in the SEM images. In addition, the extrudates were also observed under SEM.

The cross-section of all the developed scaffolds (both produced by fiber bonding and by compression moulding/particulate leaching) was analyzed using a Leica-Cambridge S-360 scanning electron microscope (SEM) for preliminary assessments on the morphology of the scaffolds. All the samples were sputtercoated with gold prior to SEM observations.

3.6. MICRO-COMPUTED TOMOGRAPHY

Recently, micro-computed tomography (μCT) was employed for the observation and analysis of 3-D porous scaffolds [10]. Its advantages include the fact that it is a nondestructive technique that allows analysis the scaffold interior as opposed to SEM that requires sectioning. μCT allows visualizing and measuring the complete three-dimensional volume of the structures without any further sample preparation or chemical fixation.

Both types of chitosan-based scaffolds were analyzed using a high-resolution μCT Skyscan 1072 scanner (Skyscan, Kontich, Belgium).

In Chapter VI, μCT evaluation of the polymeric scaffolds was carried out by analyzsing four scaffolds of each condition were scanned in high-resolution mode of 8.7 μm *x/y/z* and an exposure time of 1792 ms. The energy parameters defined in the scanner were 63 keV with a current of 157 μA. Isotropic slice data were obtained by the system and reconstructed in 2-D images. These slice images were compiled and analyzed to render 3-D images and obtain quantitative architecture parameters. A μCT analyzer and a μCT Volume Realistic 3-D Visualization, both from SkyScan, were used as image processing tools for both μCT reconstruction and to create/visualize the 3-D representation. Regions of interest (square of 4.5x4.5 mm^2) were selected in each slice image and thresholded to eliminate background noise. This threshold (to distinguish polymer material from pore voids) was chosen and maintained constant for all the scanned specimens and samples. The threshold was also inverted to obtain pore volume and to analyze both the pore morphology and its interconnectivity.

For the chitosan-based fiber mesh scaffolds (Chapter VII), five scaffolds of each condition were scanned in high resolution mode using a pixel size of 8.24μm and integration time of 2.0 ms. The X-ray source was set at 80 keV of energy and 124 μA of current. For all the scanned specimens representative data sets of 150 slices were transformed into binary using a dynamic threshold of 60-255 (grey values) to distinguish polymer material from pore voids. This data was used for morphometric analysis (CT Analyser v1.5.1.5, SkyScan). 3-D virtual models of representative regions in the bulk of the scaffolds

were also created, visualized and registered using both image processing softwares (ANT 3-D creator v2.4, SkyScan).

3.7. WATER ABSORPTION STUDIES

The water absorption tests described in Chapter V were conducted using injection moulded tensile bars that were previously dried in a vacuum oven at 50 ºC until a constant weight was obtained. These samples were immersed in an isotonic solution of NaCl 0.154 M (9 $g.l^{-1}$) and pH 7.4 at 37 ºC for periods of 1, 3, 7, 14, 30, and 60 days (6 specimens of each blend for each period of immersion). The samples were then removed at specific intervals, gently blotted with tissue paper to remove the excess water on the surface, and the weight recorded. This process was repeated at several time intervals.

The percentage of water absorption (WAs) after each time of immersion (t) was calculated by means of using equation 2.1,

$$WAs,t = [(m_{w,t}-m_i)/ m_i] \times 100 \qquad (2.1)$$

Where leaching was found to occur, the data were corrected to account for the weight loss. The parameters D, Φ, and ψ were estimated for the data by non-linear regression routine (provided in Kaleidagraph, Synergy Software, Reading, PA, USA) based on a modified Levenberg–Marquardt algorithm.

3.8. DEGRADATION STUDIES

The injection-molded samples from the different chitosan based blends and composites were immersed in an isotonic saline solution for periods of 1, 3, 7, 14, 30, and 60 d. A solution of 40 ml was used for three samples (one batch). Two batches were used for each selected immersion period. At the end of each immersion period, the solution pH was measured. The weight loss was determined by drying the samples to constant weight and comparing to their initial weight.

The percentage of weight loss of the samples (WLs) after each time of immersion (t) was calculated using equation 2.2,

$$WLs,t = [(m_{d,t}-m_i)/ m_i] \times 100 \qquad (2.2)$$

The tensile bars from the water absorption tests above were subjected to tensile testing using an Instron Universal Tensile Testing Machine (Instron 4505 Universal Machine, USA). The test conditions are described in the section 3.1.1 of this Chapter.

3.9. CONTACT ANGLE

The static contact angle measurements were obtained by the sessile drop method using a contact angle meter OCA15+ with a high-performance image processing system (DataPhysics Instruments, Germany). The liquid (glycerol or CH_2I_2, 1 µl, HPLC grade) was added by a motor-driven syringe at room temperature. Five samples of each material were used, and six measurements were carried out for each sample. The data presented in Chapter V are an average of five readings. The polarity of the surface and the surface tension were calculated using Kaelble's equation:

4. *In vitro* BIOLOGICAL TESTING

4.1. CELL CYTOTOXICITY ASSAYS

A rat lung fibroblast cell line -L929-, acquired from the European Collection of Cell Cultures, was used to perform cytotoxicity tests on the scaffolds prepared by compression moulding/particulate leaching (Chapter VI). Cells were grown as monolayers in Dulbecco's modified eagle's medium (Sigma, St. Louis, MO) supplemented with 10% fetal bovine serum (Biochrom, Berlin, Germany) and 1% of antibiotic–antimycotic mixture (10,000 U/mL penicillin G sodium; 10,000 U/mL streptomycin sulphate; 25 µg/mL amphotericin B) (Gibco, Invitrogen, USA). Trypsin/EDTA (0.25% w/v trypsin/0.02% EDTA, Sigma) was used to detach the cells from the culture flasks before the experiments were conducted. Cells were seeded in 96-well plates (n = 6) at a density of 1.8 x 10^4 cells/well and incubated for 24 h at 37 ºC, in a humidified atmosphere with 5% CO_2.

The ratio of material weight to extract fluid was constant and equal to 0.25 g/mL. Latex rubber was used as a positive control of cell death, because it has a strong cytotoxic effect leading to extensive cell death. The ratio of latex material outer surface to extraction fluid was 2.5 cm^2/mL. Culture medium was

used as negative control of cytotoxicity, considered to be the ideal situation of cell growth. Test scaffolds (*n* = 6) and positive control were extracted for 24 h at 37 ºC, using complete culture medium as the extraction fluid. Before the tests, culture medium was removed from wells with cells adhered, and an identical volume (200 µL) of extraction fluid was added. The cells were left to proliferate in the extract fluid for 72 h. After this period, the extraction fluid was removed, and the serum-free culture medium without phenol red and a substrate-3-(4,5-dimethylthiazol-2-yl)-5(3-carboxymethoxyphenyl)-2(4-sulfofenyl)-2*H*-tetrazolium (MTS; CellTiter 96 One solution Cell Proliferation Assay kit; Promega, Madison, WI), in a proportion of 5:1, was added to each well. This reaction is based on the reduction of MTS, into a brown formazan product by an enzyme—dehydrogenase—active in all viable cells.

Cells were then incubated for 3 h at 37 ºC in a humidified atmosphere containing 5% CO_2. After this period, optical density (OD) was measured with a plate reader (Biotek, model Synergy HTi) at 490 nm. The mean OD value obtained was standardized taking into account the values for the negative control.

4.2. CELL CULTURE

A human osteoblast cell line (SaOS-2) was used to conduct the cell culture studies on the fiber mesh scaffolds (Chapter VII). Cells were grown as monolayer cultures in a culture medium consisting of DMEM medium, 10% FBS and 1% antibiotic/antimycotic mixture. When the adequate cell number was obtained, cells were detached with trypsin, centrifuged and ressuspended in cell culture medium. Cells were seeded at a density of 2,5x105cells/scaffold under static conditions, using for this purpose 1mL of cell suspension. Two hours after seeding, the cell seeded scaffolds were changed into new plates and 1 ml of culture medium was added to each well. The cell seeded scaffolds were maintained in a humidified atmosphere at 37ºC, containing 5% CO_2 during the remaining testing period.

4.2.1.Cell adhesion and morphological analysis by SEM

Cell adhesion, morphology and average distribution at the surface and at the bulk of the scaffolds were also analysed by SEM, after 24, 48, 72 hours and 7 days of culture. Cell-seeded scaffolds were washed in 0.15 M phosphate buffered saline and fixed in 2.5% glutaraldehyde in phosphate buffered saline. After rinsing 3 times in phosphate buffered saline, the constructs were dehydrated using a series of graded ethyl alcohols (30, 50, 70, 90, 100% ethanol) for 15 minutes each, twice. The samples were further subjected to 2 changes for 15 minutes each with 100% hexamethyldisilazane (HDMS; Electron Microscopy Sciences, Washington, USA). Finally HDMS was removed and let to air dry for 2h.

Afterwards, the constructs were sputter coated with gold (JEOL JFC-1100) and analyzed with a Leica Cambridge S360 scanning electron microscope (UK).

4.2.2. Cell viability by MTS assay

Cell viability was assessed after 24, 48, 72 hours and 7 days, using the MTS test. Cells cultured onto tissue culture polystyrene (TCPS) with standard culture medium were used as negative control. At each time point, cell-seeded scaffolds (*n*=3) were rinsed in 0.15M phosphate buffered saline (Sigma) and immersed in a mixture consisting of serum-free cell culture medium and MTS reagent at 5:1 ratio and incubated for 3h at 37 ºC in a humidified atmosphere containing 5% CO2. After this, 200 µl (*n*=3) were transferred to 96 well plates and the optical density (O. D.) determined at 490 nm.

REFERENCES

1. Shi, C.M., et al., Therapeutic potential of chitosan and its derivatives in regenerative medicine. Journal of Surgical Research, 2006. 133(2): p. 185-192.
2. Kim, I.Y., et al., Chitosan and its derivatives for tissue engineering applications. Biotechnology Advances, 2008. 26(1): p. 1-21.
3. Kim, B.S. and D.J. Mooney, Development of biocompatible synthetic extracellular matrices for tissue engineering. Trends in Biotechnology, 1998. 16(5): p. 224-230.
4. Bhattacharya M., et al., Material Properties of Biodegradable Polyme, in Biodegradable Polymers for Industrial Applications, R. Smith, Editor. 2005, Woodhead Publishing Cambridge. p. 336-356.
5. Wang, Y. and J.F. Mano, Biodegradable Poly(L-lactic acid)/Poly(butylene succinate-co-adipate) blends: Miscibility, morphology, and thermal Behavior. Journal of Applied Polymer Science, 2007. 105(6): p. 3204-3210.
6. Kusakabe, H., et al., Osseointegration of a hydroxyapatite-coated multilayered mesh stem. Biomaterials, 2004. 25(15): p. 2957-2969.
7. Boyde, A., et al., Osteoconduction in large macroporous hydroxyapatite ceramic implants: evidence for a complementary integration and disintegration mechanism. Bone, 1999. 24(6): p. 579-589.
8. Chang, B.-S., et al., Osteoconduction at porous hydroxyapatite with various pore configurations. Biomaterials, 2000. 21(12): p. 1291-1298.

9. Covas, J.A. and P. Costa, A miniature extrusion line for small scale processing studies. Polymer Testing, 2004. 23(7): p. 763-773.
10. Ho, S.T. and D.W. Hutmacher, A comparison of micro CT with other techniques used in the characterization of scaffolds. Biomaterials, 2006. 27(8): p. 1362-1376.

SECTION 3.

CHAPTER III.

Properties of melt processed chitosan and aliphatic polyester blends

CHAPTER III.

Properties of melt processed chitosan and aliphatic polyester blends

Abstract

Chitosan was melt blended with poly--caprolactone (PCL), poly(butylene succinate) (PBS), poly(lactic acid) (PLA), poly(butylene terephthalate adipate) (PBTA), and poly(butylene succinate adipate) (PBSA). For the chitosan/PBS blend, the amount of chitosan was varied from 25% to 70% by weight. The remaining polyesters had 50% of chitosan by weight. Addition of chitosan to PBS or PBSA tends to depress the melting temperature of the polyester. The crystallinity of the polyesters (PCL, PBS, PBSA) containing 50% chitosan decreased. Adding chitosan to the blends decreased the tensile strength but increased the tensile modulus. Chitosan displayed intermediate adhesion to the polyester matrix. Microscopic results indicate that the skin layer is polyester rich, while the core is a blend of chitosan and polyester. Fractured surface of chitosan blended with a high T_g polymer, such as PLA, displayed a brittle fracture. Blends of chitosan with PCL, PBTA, or PBSA display fibrous appearances at the fractured surface due to the stretching of the polymer threads. Increasing the amount of chitosan in the blends also reduced the ductility of the fractured surface. The chitosan phase agglomerated into spherical domains or were clustered into sheaths. Pull-out of chitosan particles is evident in tensile-fractured surfaces for blends of chitosan with ductile polymers but absent in the blends with PLA. PBS displays a less lamellar orientation when compared to PCL or PBSA. The orientation of the polyesters (PCL, PBSA) does not seem to be affected by the addition of chitosan. The two main diffraction peaks observed using WAXS are unaffected by the addition of chitosan.

This chapter is based on the following publication: **Correlo VM ,** Boesel LF, Bhattacharya M, Mano JF, Neves NM and Reis RL, 2005, Properties of melt processed chitosan and aliphatic polyester blends, Materials Science and Engineering A - Structural Materials Properties Microstructure and Processing, **403(1-2)**: 57-68

---

1. INTRODUCTION

A number of natural polymers are being employed as biomaterials. Naturally occurring polymers include collagen, chitin, silk, alginate, starch, and elastin. Natural polymers offer the advantage of being similar to macromolecular substances, which the biological environment is prepared to recognize and to deal with metabolically. Problems associated with the stimulation of chronic inflammatory reaction and toxicity by synthetic polymers are largely suppressed or eliminated by using natural polymers. On the other hand, natural polymers are frequently quite immunogenic. Another attractive characteristic of natural polymers is their ability to be degraded by naturally occurring enzymes, implying that the implant will be degraded and eventually metabolized by physiological mechanisms. Thus, useful properties can be obtained by blending natural and synthetic polymers.

Synthetic polymers used in the biomaterials field include biodegradable aliphatic polyesters, such as polyhydroxybutyrate and its copolymer polyhydroxybutyrate-co-valerate, poly(lactic acid), poly(glycolic acid), poly-ε-caprolactone, and their copolymers. The ester bonds in these synthetic polymers hydrolyze to nontoxic natural metabolites and are eliminated from the body via respiration [1]. Synthetic biodegradable polymers used as biomaterials range in tensile strength from 16 to 50 MPa and modulus from 400 to 3000MPa [2].

Chitin is a biopolymer found in nature and is mainly derived from the exoskeletons of crustaceans, insects and mollusks, and the cell walls of microorganisms [3]. Like cellulose, chitin is a glucose-based, unbranched polysaccharide. However, it differs from cellulose at the C_2 carbon, where instead of a hydroxyl group, chitin has an acetamide residue. Chitosan (α(1→4)-2-amino-2-deoxy-β-D-glucan), a mucopolysaccharide, is the alkaline deactylated product of chitin and has structural similarities to glycosaminoglycans, thus, mimicking their functional behavior. Chitosan is reported to be non-toxic, biodegradable, and biocompatible [4, 5].

Solution blending of chitin and chitosan with synthetic polymers has been studied. Graft copolymerization of chitosan with acrylonitrile, methylmethacrylate (MMA), methacrylic acid, 2-hydroxyethylmethacrylate (HEMA), and acryl-amide has been reported in the literature. Similarly, styrene, vinyl acetate, acrylamide, MMA, and HEMA, have also been grafted on chitosan. Grafting of chitosan with N,N' dimethylaminoethylmethacrylate (DMAEMA) has also been reported [6–10]. The tensile strength, crystallinity, and degree of swelling of grafted chitosan films decreased with increased levels of grafting with synthetic polymers. The grafted films showed improved thermal stability. Functional groups

have been grafted on chitosan powder to increase its solubility [11]. Blends of polyurethane-chitosan were prepared using the solvent casting method [12], and the mechanical properties were evaluated. Poor phase properties were reported. Hybrid materials of chitosan with polynosic (viscose rayon) were generated by a mechanical blending method. Chitin and chitosan were reacted with 1,6-diisocyanatohexane (poly-urea{urethanes}) in DMA-LiCl solutions and their properties evaluated [13]. Biodegradable films of chitosan containing polyethylene glycol (PEG) or polyvinyl alcohol (PVA) were prepared by mixing PEG or PVA with a solution of chitosan acetate, and films were prepared by the casting method [2, 14]. Homogenous films with increased value of initial temperature of thermal degradation were produced.

Little research has been conducted in the melt blending of synthetic polyester and chitosan. The objective of this research was to evaluate the properties of chitosan and biodegradable aliphatic polyesters (poly-ε-caprolactone (PCL), poly(butylene succinate) (PBS), poly(lactic acid) (PLA), poly(butylene terephthalate adipate) (PBTA), and poly(butylene succinate adipate) (PBSA). The tensile properties (tensile strength and tensile modulus) and thermal properties of the blends were evaluated. The amount of chitosan in the blends containing PBS was varied at 25%, 50%, and 70%. For the remaining polyester, the chitosan content was at 50%. The tensile and thermal properties were evaluated. The morphology of fractured and etched surfaces was evaluated using scanning electron microscopy (SEM). Optical microscopy was used to distinguish the stained chitosan phase in the blend. Small angle X-ray scattering (SAXS) and wide angle X-ray scattering (WAXS) were used to study the effect of processing on both the lamellar and crystalline structure of these blends.

2. MATERIALS AND METHODS

2.1. MATERIALS

The polyesters used include poly-ε-caprolactone (PCL), poly(butylene succinate) (PBS), poly(lactic acid) (PLA), poly(butylene terephthalate adipate) (PBTA), and poly(butylene succinate adipate) (PBSA). The chitosan used had a degree of deacetylation of approximately 85%. Polycaprolactone resins PCL 787 (MFI~4), commercially available as TONE™ polymer, were obtained from Union Carbide Chemicals and Plastics Division, Bound Brook, New Jersey. Eastar Bio Copolyester 14766™, a butanediol, adipate, and terephthalate copolymer (MFI~20), was obtained from Eastman Chemical Company, Kingsport, Tennessee. Bionolle™ 1050, a polybutylene succinate copolymer

(MFI~50), and Bionolle™ 3001, a poly(butylene succinate adipate) copolymer (MFI~1.0) were obtained from Showa Highpolymer Co. Ltd., Tokyo, Japan.

2.2. PROCESSING

The chitosan/polyester blends containing less than 70% chitosan were compounded in a counter rotating twin-screw extruder (Carvex, Lisbon, Portugal). The only exception to this was when blends of chitosan (50% by weight) were compounded with B3001. Higher chitosan content pushed the torque in the counter rotating extruder close to the maximum. Alternately, throughput had to be reduced to keep the torque below the upper threshold. Hence, blends containing 70% chitosan were compounded in a co-rotating twin-screw extruder [Leistriz LSM 36] to improve mixing. Since the torque was close to the maximum limit of the machine, this blend (70% chitosan/30% PBS) was processed with the die removed and with addedwater/glycerol to enhance plasticization. The various blend compositions studied and processing conditions used are summarized in Table 3.1.

Table 3.1. Processing condition used for various blends composition studied.

MATERIAL	PROCESSING CONDITIONS			
	TEMPERATURE PROFILE	SCREW SPEED (RPM)	DIE TEMPERATURE (°C)	TYPE OF MACHINE USED
25Ch-75PBS [a]	160/160/160	15	160	Counter Rotating
50Ch-50PBS [b]	160/160/160	15	160	Counter Rotating
50Ch-50PBTA [c]	160/160/160	15	160	Counter Rotating
50Ch-50PCL [d]	160/160/160	15	160	Counter Rotating
50Ch-50PBSA [e]	160 in all zones	100	160	Co-rotating
50Ch-50PLA [f]	175 in first 4 zones, 180 rest of the zones	100	180	Co-rotating
70Ch-30PBS [g]	70/90 and 160 in the rest of the zones	100	-	Co-rotating

[a] Blend containing 25% by weight of chitosan and 75% by weight of PBS
[b] Blend containing 50% by weight of chitosan and 50% by weight of PBS
[c] Blend containing 50% by weight of chitosan and 50% by weight of PBTA
[d] Blend containing 50% by weight of chitosan and 50% by weight of PCL
[e] Blend containing 50% by weight of chitosan and 50% by weight of PBSA
[f] Blend containing 50% by weight of chitosan and 50% by weight of PLA
[g] Blend containing 70% by weight of chitosan and 30% by weight of PBS

The extruded strands were ground using a Coloritron grinder using 5mm diameter pellets. The blends were injection molded using an ENGEL injection molding machine to produce tensile test bars. The tensile bars had a neck cross-section area of 2mm×4mm and a neck length of 20 mm. The conditions used for molding are summarized in Table 3.2. The mold was held at a constant temperature of 22 ºC for all compositions except for PLA where the mold temperature was raised to 30 ºC.

Table 3.2. Injection molding processing conditions for blends.

MATERIAL	INJECTION SPEED (mm/s)	HOLDING PRESSURE (BAR)	BARREL TEMP. (°C)	MOULD TEMP. (°C)
PBS [a]	30	50	90-120-120-140	22
PBSA [b]	30	120	80-100-120-130	22
PBTA [c]	30	50	90-120-120-140	22
PCL [d]	80	80	70-90-100-110	22
PLA [e]	30	30	155-170-180-190	30
25Ch-75PBS [f]	25	20	110-130-150-160	22
50Ch-50PBS [g]	30	80	110-130-150-160	22
50Ch50PBTA [h]	20	30	110-130-150-160	22
50Ch-50PCL [i]	40	20	110-130-150-160	22
50Ch-50PBSA [j]	65	100	110-130-150-160	22
50Ch-50PLA [l]	70	25	150-155-155-160	30
70Ch-30PBS [m]	80	50	110-130-150-160	22

[a] poly(butylene succinate)
[b] poly(butylene succinate adipate)
[c] poly(butylene terephthalate adipate)
[d] poly-ε-caprolactone
[e] poly(lactic acid)
[f] Blend containing 25% by weight of chitosan and 75% by weight of PBS
[g] Blend containing 50% by weight of chitosan and 50% by weight of PBS
[h] Blend containing 50% by weight of chitosan and 50% by weight of PBTA
[i] Blend containing 50% by weight of chitosan and 50% by weight of PCL
[j] Blend containing 50% by weight of chitosan and 50% by weight of PBSA
[l] Blend containing 50% by weight of chitosan and 50% by weight of PLA
[m] Blend containing 70% by weight of chitosan and 30% by weight of PBS

2.3. MECHANICAL PROPERTIES

The tensile properties were determined using a Universal tensile testing machine (Instron 4505 Universal Machine, USA). Tensile force was taken as the maximum force in the force-deformation curve. Tensile modulus was estimated from the initial slope of the stress–strain curve. Samples were conditioned at room temperature for at least 48 h before testing. A crosshead speed of 5mm min^{-1} was used up to a deformation of 1.5% after which the speed increased to 50mm min^{-1}. The values reported were the average of at least five specimens.

2.4. DIFFERENTIAL SCANNING CALORIMETRY

The DSC experiments were performed in a Perkin-Elmer DSC7 apparatus, using a water-cooling accessory and nitrogen as a purge gas (flux gas of ca. 20 cm^3 min^{-1}). Both temperature and heat flux were calibrated with Indium (99.99999% purity) at a scanning rate of 20 ºCmin^{-1}. The samples were obtained by cutting a small piece of material (with ca. 10 mg weight) in the central region of the injection parts. An effort was made to maintain the geometry of the different samples, in order to keep the same thermal resistance. All the experiments were performed at 20 ºCmin^{-1}, starting from room temperature. Only the first run was analyzed, which reflects not only the materials contained in the samples, but also the general morphology developed during processing.

2.5. OPTICAL MICROSCOPY

To analyze the chitosan distribution on the polymer matrix, tensile bars of each blend were stained with a 0.10 (w/v) Eosin solution for 10 min at 32±0.5 ºC. Stained samples were examined by light microscopy (Olympus BH-2) in reflection mode. Photographs of the stained surface were obtained using a microscope digital camera Olympus DP11. Images of the cross-section were obtained by cryogenically fracturing the tensile bar. The fractured surface was smoothened using a glass knife for optical clarity.

2.6. SCANNING ELECTRON MICROSCOPY

The morphological characterization of the blends was made using a Leica-Cambridge S-360 scanning electron microscope (SEM, UK). All the samples were sputter-coated with gold. Several different analyses of the cross-section of the tensile bars were made. These include (i) observations after the tensile tests; (ii) observations after immersing the samples in liquid nitrogen

for 1 min and fracturing the sample in the testing zone to analyze the brittle fracture; and (iii) observations after cryogenically-fractured surfaces were etched with 1% acetic acid for 3 h or 1 day. The objective was to dissolve the chitosan since not enough phase contrast between the filler and polyester was obtained in the SEM images. In addition, the extrudates were also observed under SEM.

2.7. WIDE ANGLE *(WAXS)* AND SMALL ANGLE *(SAXS)* X-RAY SCATTERING

WAXS and SAXS experiments were performed using Xray synchrotron radiation (transmission mode) at the Soft Condensed Matter A2 beamline at HASYLAB (DESY) synchrotron facility in Hamburg (Germany). The experimental setup includes a MARCCD detector for acquiring two dimensional SAXS patterns (sample-to-detector distance being 280 cm) and a linear detector for 1D WAXS measurements (distance 23 cm). Cu-Kα radiation, with a wavelength of λ = 0.154 nm, was employed for both SAXS and WAXS measurements. The injection moulded samples were fixed vertically and the patterns were acquired at room temperature.

3. RESULTS AND DISCUSSION

3.1. THERMAL PROPERTIES

The normalized DSC scans of PLA-based materials are shown in Fig. 3.1a. The injected pure PLA exhibits a glass transition at 62.0 ºC (midpoint), with $\Delta C_p(T_g)$ = 0.305 J g^{-1}. The endothermic peak at 65 ºC is associated with structural relaxation. In fact, the amorphous fraction of the material is in its glassy state at room temperature. Hence, in this non-equilibrium condition, the enthalpy will slowly relax towards its equilibrium values. At higher temperatures, the cold-crystallization is observed at T_c = 107.3 ºC and the melting at T_m = 155.3 ºC. The integration of the heat flux curve comprising both processes (between 99 and 174 ºC) gave 6.5 J g^{-1}. This small value indicates that the material is essentially amorphous. This was confirmed by wide-angle X-ray scattering (data not shown).

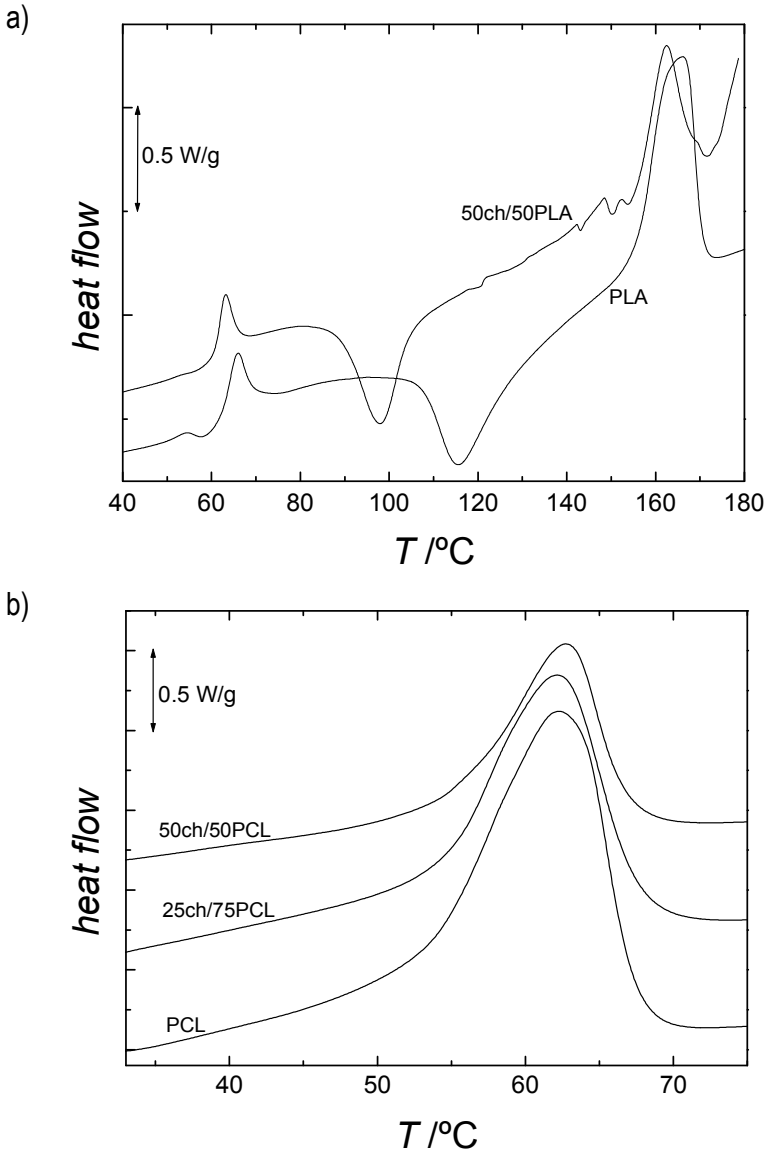

Figure 3.1. Representative DSC thermograms, obtained at 20 ºCmin^{-1} of (a) both PLA and 50ch-50PLA materials and (b) PCL-based materials.

The blend of PLA with 50 wt% chitosan has as slightly lower T_g (60.1 ºC) than the pure polyester. This may be due to the more aggressive processing conditions (higher torque) that were needed to produce the blend. The higher torque would have induced a higher thermal degradation on PLA and, hence, a greater decrease on the molecular weight. However, the biggest difference lies in the onset of the coldcrystallization process, which occurs at T_c = 89.2 ºC. This may indicate that chitosan acts as a nucleating agent, promoting a faster crystallization of PLA; however, the differences could be also associated with the higher decrease of the molecular weight of PLA during the processing of the blend.

No significant changes are observed in the melting temperature between PLA and the blend with chitosan (155.3 and 155.7 ºC, respectively), indicating that similar lamellae populations are produced during cold crystallization in the two materials.

Table 3.3 - Melting temperature and heat of fusion of the different samples analysed by DSC, and the corresponding crystallinity degree within the synthetic polymer component.

SAMPLE	T_m /ºC	ΔH /J.g-1	X%*
PCL [a]	51.9	69.2	41.7
25Ch-75PCL [b]	53.5	44.6	35.8
50Ch-50PCL [c]	55.2	25.9	31.2
PBS [d]	107.2	73	66.2
25Ch-75PBS [e]	103.4	55.5	67.1
50Ch-50PBS [f]	102.4	31.7	57.5
70Ch-30PBS [g]	104.6	23.1	69.8
PBSA [h]	83.7	40.2	-
50Ch-50PBSA [i]	77.2	16.2	-

*crystallinity in the polyester fraction
[a] poly-ε-caprolactone
[b] Blend containing 25% by weight of chitosan and 75% by weight of PCL
[c] Blend containing 50% by weight of chitosan and 50% by weight of PCL
[d] poly(butylene succinate)
[e] Blend containing 25% by weight of chitosan and 75% by weight of PBS
[f] Blend containing 50% by weight of chitosan and 50% by weight of PBS
[g] Blend containing 70% by weight of chitosan and 30% by weight of PBS
[h] poly(butylene succinate adipate)
[i] Blend containing 50% by weight of chitosan and 50% by weight of PBSA

The DSC results on the PCL-based materials (Fig. 3.1b), in the region of the melting temperature of the polymer that include pure PCL, and blends with different chitosan contents (to study the effect of the polysaccharide) is summarized in Table 3.3. From the enthalpy values, the degree of crystallinity of the PCL component in the samples was calculated from the known PCL content and by assuming that the heat of fusion of completely crystalline PCL is 166 J g^{-1} [15]. The melting temperature tends to increase slightly with increasing chitosan content. In a separate study, an opposite behavior was observed for PCL/chitosan blends prepared by solvent casting [16]. The crystallinity of PCL tends to decrease with

increasing chitosan content, similar to that observed in the work of Honma *et al.* [16]. This was attributed to hydrogen bond interactions between the carbonyl groups of the polyester and -OH and -NH_2 groups in chitosan. Such interactions occur in the amorphous state, thus, suppressing the extent of crystallization of the PCL domains.

There is a general tendency for the depression of T_m with increasing chitosan content, except for the blend with 70% by weight of chitosan (Table 3.3). The degree of crystallinity of the PBS component was calculated from the known theoretical value of ΔH_m for 100% crystalline PBS, that was estimated to be 110.3 J g^{-1}, calculated on the basis of the group contribution method proposed by Van Krevelen [17]. In the PBS-based material there is a general tendency for the depression of T_m with increasing chitosan content, except for the blend with 70 wt% of chitosan (Table 3.3). The same trend was observed in blends of poly(3-hydroxybutyrate) and chitosan [18] and was attributed to strong intermolecular interactions between chitosan and the polyester chains, resulting in thinner lamellar thickness crystals. The chitosan/PBSA blends also exhibit a decrease in melting temperature (Table 3.3). The addition of 25% and 70% chitosan progressively increases the crystalline content of PBS, this behavior being the opposite of that observed for PCL. However, the introduction of 50% by weight of chitosan in PBS or in PBSA has a depressing effect on the degree of crystallinity of the polyesters. This may be an indication that the physical and thermal properties of such kinds of blends may not exhibit regular trends with the compositions, as the processing conditions may also have an important effect on the performance of the final materials.

3.2. MECHANICAL PROPERTIES

The processing parameters for compounding and injection molding are summarized in Tables 3.1 and 3.2. It is well known that extrusion compounding parameters, such as screw profile, barrel temperature, and residence time, affect the morphology of blends. Similarly, several injection molding processing parameters, such as injection speed, packing pressure, barrel temperature, and mold temperature, may affect the tensile properties. In this study, no attempt was made to optimize properties. Rather, the conditions were selected for ease of processing and visual acceptance of molded parts.

Tensile strength, tensile modulus, and ultimate elongation are shown in Table 3.4. A typical stress–strain curve for the unfilled polyesters is shown in Fig. 3.2. The deformation is accompanied by the formation of a neck (except for PLA), where the true stress monotonically increases with the strain. Addition of chitosan led to a decrease in the tensile strength. This decrease is the smallest for PBTA

and the largest for PBSA and PLA. Also, the level of decrease is insignificant for samples containing 25% and 50% chitosan in PBS.

Table 3.4. Tensile properties of various polyesters and their blends.

MATERIALS	TENSILE STRENGTH (MPa)	TENSILE MODULUS (GPa)	ELONGATION (%)
PBS [a]	38.6±1.3	0.611±0.01	264±29
PLA [b]	82±2.1	2.4±0.13	6.18±1.1
PCL [c]	27.3±0.8	0.378±0.02	674±36
PBTA [d]	20.2±0.3	0.0817±0.01	1075±37
PBSA [e]	41.4±1.1	0.348±0.01	311±20
25Ch-75PBS [f]	28.7±0.8	1.11±0.02	6.4±0.6
50Ch-50PBS [g]	30.5±0.8	1.98±0.03	2.66±0.21
70Ch-30PBS [h]	21.3±1.6	3.2±0.14	1.37±0.036
50Ch-50PCL [i]	21.1±0.9	1.84±0.07	5±0.28
50Ch-50PBTA [j]	17.9±0.18	0.722±0.02	8.05±0.88
50Ch-50PLA [l]	54.3±7.5	3.74±0.19	1.97±0.37
50Ch-50PBSA [m]	26.4±2.3	1.74±0.04	4.33±3.05

[a] poly(butylene succinate)
[b] poly(lactic acid)
[c] poly-ε-caprolactone
[d] poly(butylene terephthalate adipate)
[e] poly(butylene succinate adipate)
[f] Blend containing 25% by weight of chitosan and 75% by weight of PBS
[g] Blend containing 50% by weight of chitosan and 50% by weight of PBS
[h] Blend containing 70% by weight of chitosan and 30% by weight of PBS
[i] Blend containing 50% by weight of chitosan and 50% by weight of PCL
[j] Blend containing 50% by weight of chitosan and 50% by weight of PBTA
[l] Blend containing 50% by weight of chitosan and 50% by weight of PLA
[m] Blend containing 50% by weight of chitosan and 50% by weight of PBSA

However, when the chitosan content is increased to 70%, there is a further decrease in tensile strength from 28.7 to 21.3 MPa. The higher decrease in tensile strength with PLA is partly because PLA has been observed to be very sensitive to degradation during processing [19,20]. The presence of moisture has a particularly severe effect at higher temperatures because it induces hydrolysis. While PLA

samples were dried prior to processing, the chitosan samples were used as received and had a moisture content of 6.9% on a dry weight basis.

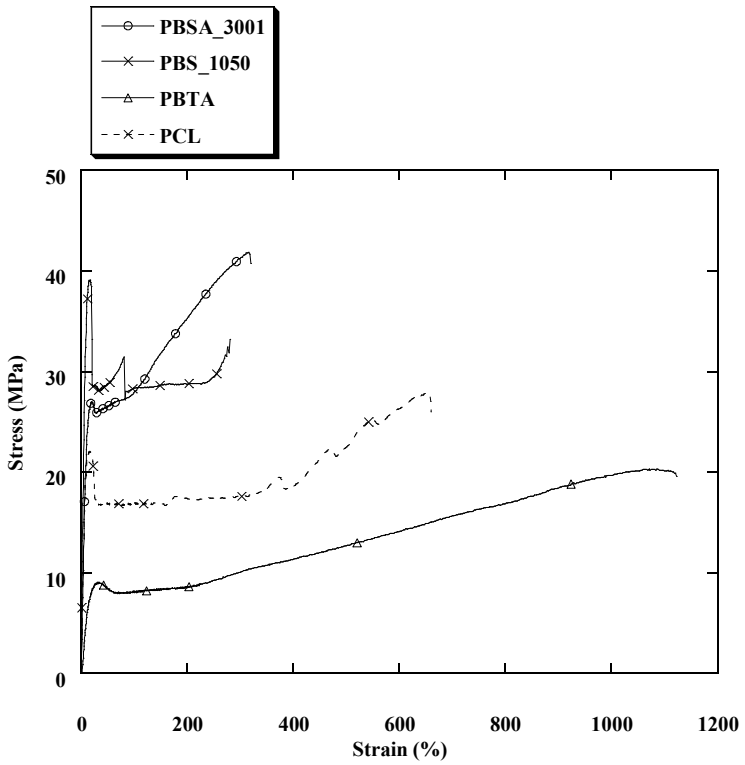

Figure 3.2. Stress versus strain curves for pure polyesters.

The decrease in tensile strength is partially due to the thermodynamic immiscibility and inherent incompatibility between chitosan and polyester. The mechanical performance of a filled polymer depends on the strength and modulus of the filler. Yield strength of a heterogeneous polymer blend or composite is dependent on the yield strength of the matrix, the decrease of effective load bearing cross-section, and the interfacial adhesion between the matrix and the filler and its ability to transfer stresses across the interface [21]. Lack of adhesion led to the formation of pores due to the debonding of the fibers upon the application of stress in a particulate-filled material. Similar incompatibility has been observed between other natural polymers and polyesters [22–24].

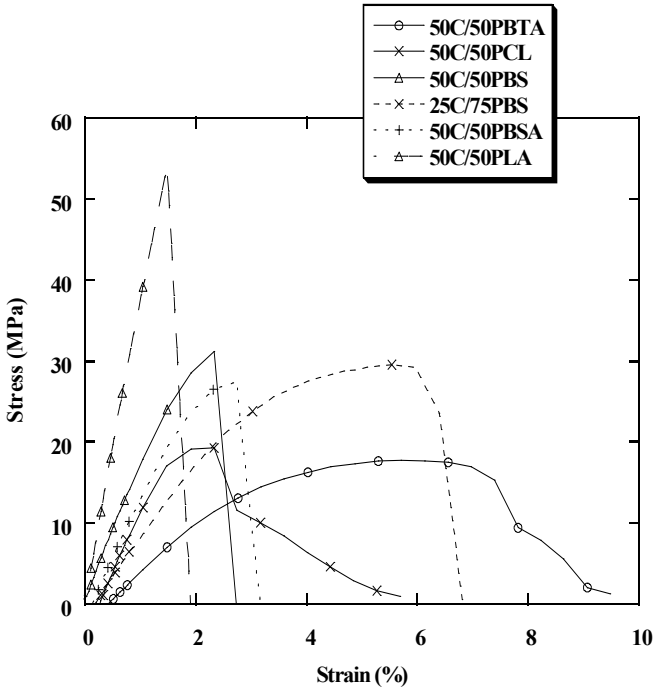

Figure 3.3. Stress versus strain curves for blends of polyester and chitosan.

Thus, because of the decrease in tensile properties upon the addition of chitosan, the blends used in this study can be characterized as having a reduced adhesive interaction between the chitosan and the polyesters. As the load is applied to the blend, the lack of interfacial adhesion between the chitosan and the polyester will limit the load transfer process. The lower the chitosan–matrix adhesion, the lower will be the stress at which debonding occurs, as the fibers are unable to reinforce the composite. There appears to be some adhesion between the two phases, as the tensile strength is unaffected when the chitosan content is increased from 25% to 50%. The decrease in properties when the chitosan content is increased to 70% by weight can be attributed to inadequate mixing. It should also be noted that the plasticizer would have an adverse effect on the strength of the blends. At high chitosan content (70%), the torque experienced was high enough that the die had to be removed when compounding. Also, at higher chitosan content, the filler inclusions form aggregates. These aggregates can lead to failure at lower stresses. Since the bonds between the filler particles are weaker than those between filler and the matrix, cavities would be formed, resulting in failure at lower stresses.

The shape of the stress–strain curve is affected by the addition of chitosan. For pure polymer (except for PLA), the behavior is similar to that of ductile polymers (Fig. 3.2). PLA is the only polymer with a glass

transition greater than room temperature and, hence, displayed brittle failure. PBSA, PBTA, and PCL all show strain hardening. In the case of PBS, tensile stress showed an upper yield point followed by a drop in stress due to a reduction in the cross-sectional area due to necking. After yielding, the stress dropped and remained at a constant value for the duration of cold drawing (necking extension). The deformation mechanism of polymer filled with particles depends on the relationship between the strength and the yield stress of the unfilled polymer [25]. If the strength of the unfilled polymer is lower than its yield stress, an increase in particle content leads to an embrittlement of the polymer. This would appear to be the case for blends of chitosan and PBS. For both 50% chitosan and PBS and 50% chitosan and PLA, failure occurs at low strains, and the material fails immediately after stress reaches maximum.

The elongation of break shows a marked decrease upon the addition of chitosan (Table 3.4). There is approximately a two order of magnitude decrease in the elongation upon the addition of 25% chitosan. However, the elongation is less affected as the chitosan content is increased from 25% to 70%. According to Dubnikova et al. [26], there is a critical filler volume fraction (φ) below which the samples deform by necking. Beyond this critical value, there is negligible shrinkage of the cross-sectional area. For aluminum hydroxide filled PP, the authors observed for certain filler dimensions that elongations were independent of filler content $\varphi > 0.2$. The elongations at failure for all blend compositions are of the same order of magnitude. While the pure polyesters underwent plastic deformation, the blends with 50% PBS displayed brittle failure, and those with 50% PBTA, 50% PBSA, 50% PCL and 75% PBS had uniform yield (Fig. 3). Chitosan/PLA blends displayed brittle failure. The deformation and failure of the composites occurred without any shrinkage of cross-sectional area, including those with uniform yield.

The modulus increased with increased chitosan content (Table 3.4). This suggests that there is sufficient stress transfer across the polyester-chitosan interface. The chitosan filler in the matrix restrains the movement of the polyester phase near the vicinity of each particle, contributing to an increase in the modulus. The increase in modulus was the highest for blends with PBTA and lowest for blends containing PLA. When a relatively softer matrix is reinforced by a high modulus filler, the polymer adjacent to the filler particle is highly restrained; this enables a major portion of the load to be carried by the filler.

3.3. OPTICAL MICROSCOPY

It is well known that processing conditions affect the morphology of the molded part. Furthermore, in this study, samples of different compositions could not be molded under the same molding conditions. The processing of the materials, included a blending stage in a twin-screw extruder, was followed by grinding and subsequent injection moulding of test bars. Optical microscopy of injection molded samples is shown in Figs. 3.4.

The staining with eosin was effective in identifying the chitosan domains in the blends. It appears that there is an adequate mixing of the polyester/chitosan blends. The optical microscopy micrographs were obtained both at the surface of injection molded tensile bar specimens (Fig. 3.4a) and on cross-sections of cryogenically-fractured samples (Fig. 3.4b). The morphology of the molded samples was observed to be heterogeneous and displayed a skin-core distribution. The skin is composed almost entirely of polyester. Located below this polyester skin is the chitosan dispersed in the polyester, as is clearly observed in Fig. 3.4b.

a) 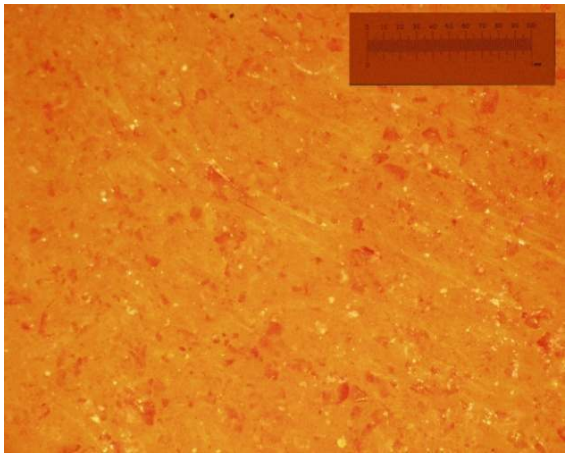 b) 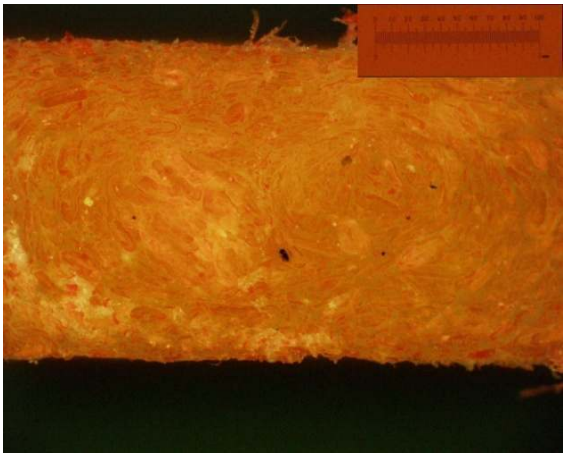

Figure 3.4 – (a) Optical micrograph of the surface of injection molded tensile bar of blends containing 50% chitosan and 50% PBSA; (b) Optical micrograph of cryogenically-fractured cross-section of blends containing 50% chitosan and 50% PBSA.

In all the cases examined, including the high chitosan (70%) containing blends, it is observed that chitosan remained dispersed in a continuous phase of polyester. This is expected since the chitosan

particles do not melt. As the chitosan contents increased in the blends from 25% up to 70%, there is not a proportional morphology evolution in the images of injection molded surfaces.

The observation of the cross-sections show a much clearer correlation between chitosan content and the area stained red (chitosan) in the images. This is an indication that the chitosan domains tend to be enclosed in the inner regions of moldings and confirms the earlier observation that the continuous phase consists of polyester and the dispersed phase is composed of chitosan domains. The distribution of chitosan domains in the cross-section images is controlled by the flow pattern. A circumferential and symmetric alignment of the domains with respect to the central point of the cross-section and defining a skin/core structure characteristic of injection mouldings is observed. In the blends with higher chitosan (70%), the distinct skin/core structure and the symmetric alignment is less visible, probably because of agglomeration of chitosan domains leading to chitosan-rich clusters.

Though difficulties were experienced in using optimal extruder configuration (reverse mixing element and use of die) due to high torque and viscous dissipation, an experiment was conducted to extrude blends of 50% chitosan and 50% PBSA using a reverse mixing element and a die. Optical micrographs of this blend indicate that the chitosan is much more distributed, as observed by the stained image of the chitosan domains (figure not shown). The mixing element in the extruder seems to enhance the quality of the mixing, however, it also causes a large increase in the torque required to process the materials, hindering its use in all other blends. The use of this reverse mixing element in the screw seems to be more effective in the dispersive mixing than in the distributive mixing.

3.4. SCANNING ELECTRON MICROSCOPY

Injection molded and extruded samples etched with acetic acid and observed under SEM also confirm the findings from optical microscopy that the chitosan is located preferentially under the skin. Of the components involved in this study, chitosan dissolves in dilute acetic acid, while the polyesters (except PLA) were relatively stable in acetic acid. The observations of the surface and of cross-section images indicate that the chitosan domains are 100–300 µm long with thicknesses in the order of 15–30 µm. It has been reported [27] that chitosan exists in the form of fibers that have thickness of around 120A°. SEM micrograph of chitosan powders (as received from the manufacturer and used in the blends without any modification) indicates that the thickness of the particles is much greater than that reported by Cartier et al. [27]. This would indicate that chitosan fibers are agglomerated into thicker particles prior to processing, giving the appearance of sheath-like structure. Due to insufficient torque during

processing, these particles are unable to completely disperse into individual fibers. It is possible to observe some variation of the chitosan domain size, most probably because of local variation of mechanical energy dissipation during processing. The clustered chitosan fibers are bent and appear to be compliant enough to adapt their geometry to the stresses experienced during processing, without breaking.

The SEM of injection molded specimens after tensile failure when stretched in the machine direction of chitosan/PBS blends as a function of chitosan content are shown in Fig. 3.5. Agglomerated chitosan fibers under SEM are present in the form of thin sheath-like structures which have dimensions in the 10–20 μm range or agglomerated ellipsoidal particles with dimensions in the 100–150 μm range. The thickness of the chitosan sheath varied with the composition; the higher the chitosan content, the thicker the sheath. We were unable to etch samples containing 70% chitosan by weight as they collapsed. The formation of sheaths (Fig. 3.5b) is an indication of the bundling of agglomerated chitosan fibers.

In general, chitosan domains of oblong shape are dispersed in the polyester matrix. The macroscopic deformation initially localized at the weakest point in the specimen. Debonding between the dispersed chitosan particles and the polyester matrix is apparent in the SEM images because of the lack of adhesion. This lack of adhesion results in interfacial slippage between the chitosan and the polyester matrix, leading to voids and cavitations. The holes resulting from the particle pull-out from the matrix is evident in most of the compositions (except in the case of chitosan/PLA). In addition to holes, thin wedges are also apparent in the matrix (Fig. 3.5c).

These wedges are a result of agglomerated chitosan fibers removed from the matrix. In some blends, these agglomerated fibers stack up, leading to the formation of sheaths (Fig. 3.5b). This gives rise to cluster-like morphology of the dispersed phase. The stresses generated during the processing were unable to destroy these structures. The formation of these sheaths decreases the aspect ratio of the fillers and can lead to significant decreases in reinforcement efficiency [28–30].

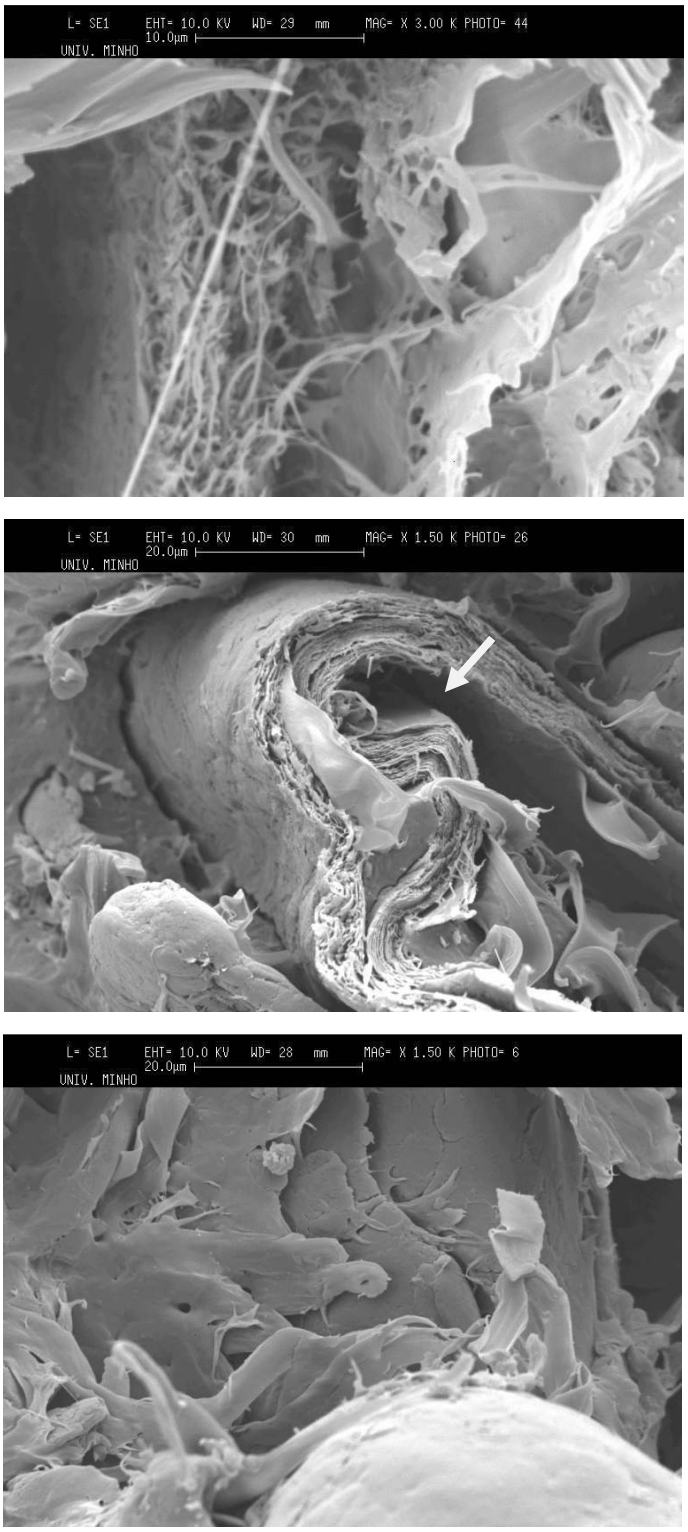

Figure 3.5. Scanning electron micrographs of tensile surfaces of chitosan and PBS (a) 25% chitosan; (b) 50% chitosan (the arrow denotes the sheath of chitosan); and (c) 70% chitosan.

a)

b)

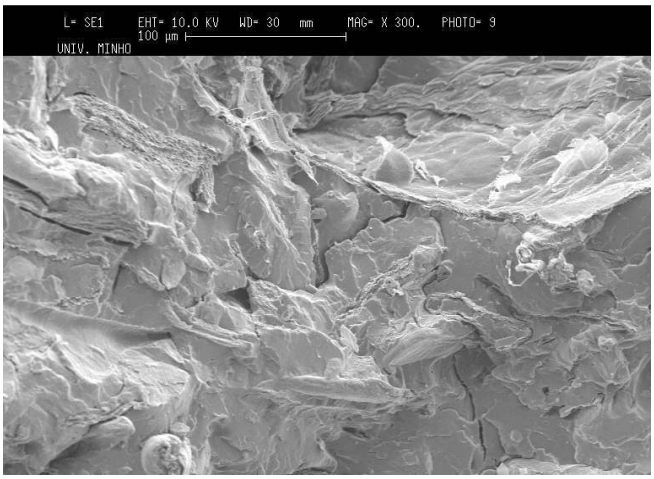

Figure 3.6. Scanning electron micrographs of tensile surfaces of chitosan and PBS (a) 25% chitosan; (b) 50% chitosan (the arrow denotes the sheath of chitosan); and (c) 70% chitosan.

The tensile-fractured surface of 25Ch-75PBS and 50Ch-50PBS shows the formation of fine fibrous structure (Fig. 3.5a). The polyester domains are elongated into fine fibrils of submicron dimensions in the core layers of the blend. Fibrous structures were also observed for 50% chitosan blended with PBTA (Fig. 3.6a) and PCL, though the diameters of the fibers were considerably larger (of micron scale) than those observed in blends containing PBS and PBSA. This would indicate that there is localized micronecking and fibrillation even in blends containing as high as 50% by weight of chitosan.

For chitosan/PLA blends (figure not shown), the upper and lower surfaces appeared smooth, with little evidence of any protrusion or loose chitosan particles. The number of cavities in chitosan/PLA is also

sharply lower, as well as of smaller diameter, than those observed in blends of other polyester with similar chitosan content. This is due to the mode of failure where the chitosan particle undergoes minimal deformation. For the more ductile polymers (PCL, PBTA and PBSA), the fibrous appearance of the surface is due to the stretching of the surrounding polymer threads and their subsequent failure. As the chitosan content is increased in chitosan/ PBS blends, the surface becomes smoother, indicating a decline in ductility.

It is also evident that the number of cavities in the cross-section of the extruded samples (figure not shown) are much lower than those in the tensile-fractured surface. The cryogenically-fractured tensile bar surfaces for most blends are relatively smooth compared to those tensile bar surfaces subjected to tensile fracture (Fig. 3.6a and b). For chitosan/PLA-fractured surfaces (figure not shown), it is observed that stacks of chitosan sheaths, inadequately dispersed, have induced local breakage. Cavities were also observed in the extruded specimens of the blends. The cavities that exist in extruded samples are probably due to foaming as a result of the presence of moisture.

The cavities showed both spherical and ellipsoidal form and had a size distribution. In addition, cavities of differing sheath thickness are also observed. The cavitation is more apparent in the blend containing 25% chitosan than in the blend containing 70% chitosan (Fig. 3.5a versus Fig. 3.5c). This difference is due to the mode of failure of the two samples. The 70% chitosan-containing blend fractures in the brittle mode, where there is very little deformation. The 25% chitosan-containing blend has a higher elongation (Fig. 3.5a). The blend containing 50% chitosan, as expected, shows an intermediate behavior.

The surfaces of some of the cavities are relatively smooth, indicating a lack of complete adhesion. Also, there appeared to be a lack of wetting between the chitosan fiber and the polyester. Bundles of sheaths were also observed in the samples (Fig. 3.6b), indicating local domains where mixing was insufficient. The diameter of the bundles increased as the concentration of chitosan increased. This is attributed to fiber agglomeration. The effect is similar to that reported for fiber reinforced polymers. The packing density of randomly oriented fiber is low. When the volume fraction of fiber being compounded is greater than its natural packing density, the fiber must either break into shorter fragments or form bundles to conform to space filling requirements [31]. Fiber breakage can be achieved by increasing the pressure. However, we were limited by maximum amperage of the extruder motor. The addition of as little as 25% chitosan increased torque significantly over what was required to process the synthetic polyester. This necessitated a decrease in screw speed (hence pressure) as well as adjusting screwprofile (such as no reverse element) and the removal of the die to further decrease the pressure.

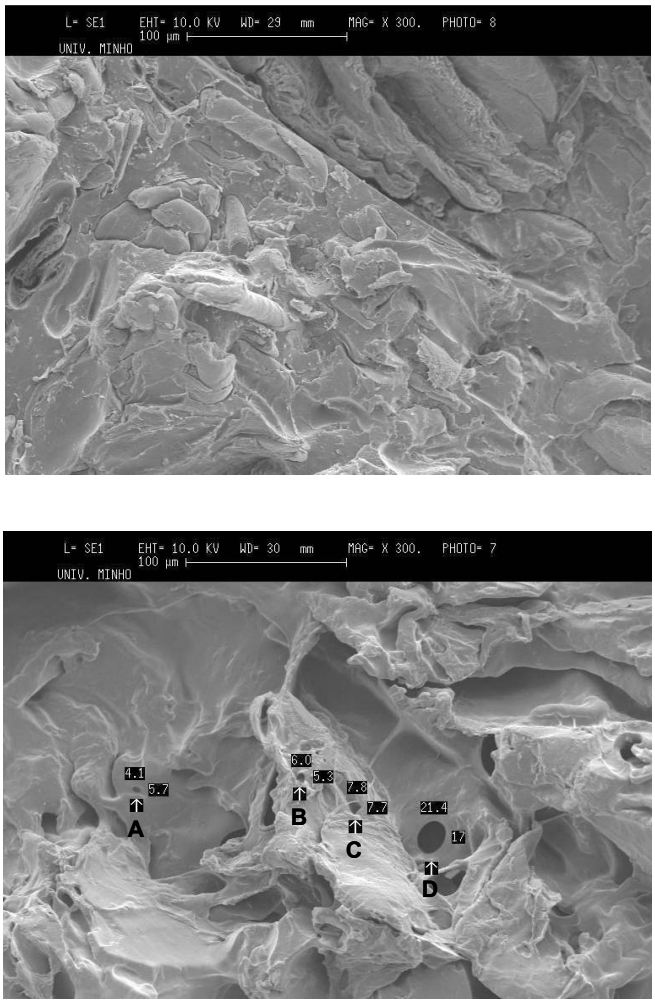

Figure 3.7. Blends of 50% chitosan and 50% PCL: (a) Cryogenically fractured and (b) cryogenically fractured and etched in 1% aqueous acetic acid for 3 h (A: 4.1×5.7 µm; B: 6.0×5.3 µm; C: 7.8×7.7 µm; D: 21.5×17.0 µm).

To identify the dispersion of chitosan domains in the blend matrix, a set of samples were etched by immersing in an acetic acid solution and observed under SEM. Chitosan is soluble in 1% acetic acid solution. A cryogenically-fractured surface of 50% chitosan and PCL with and without etching is shown in Fig. 3.7. The cavities observed in these etched samples are those of chitosan. The particle size of chitosan ranges from 15–145 µm. A range of cavity dimensions dispersed randomly in the etched samples was observed. The shapes of these cavities range from spherical to those resembling stacked sheaths. The dimensions and shapes of the holes correspond to those observed for unprocessed chitosan powder under SEM. It is also possible that there is some agglomeration of chitosan particles in

the blends, leading to hole dimensions larger than those observed for unprocessed chitosan powder under SEM. The cavities are not normal to the fracture surfaces, indicating that the chitosan agglomerates do not necessarily align themselves in the direction of flow.

3.5. SMALL-ANGLE X-RAY SCATTERING

Further insights on the microstructure at the lamellae scale can be obtained from SAXS. Selected 2-D SAXS patterns of injection molded parts are shown in Fig. 3.8.

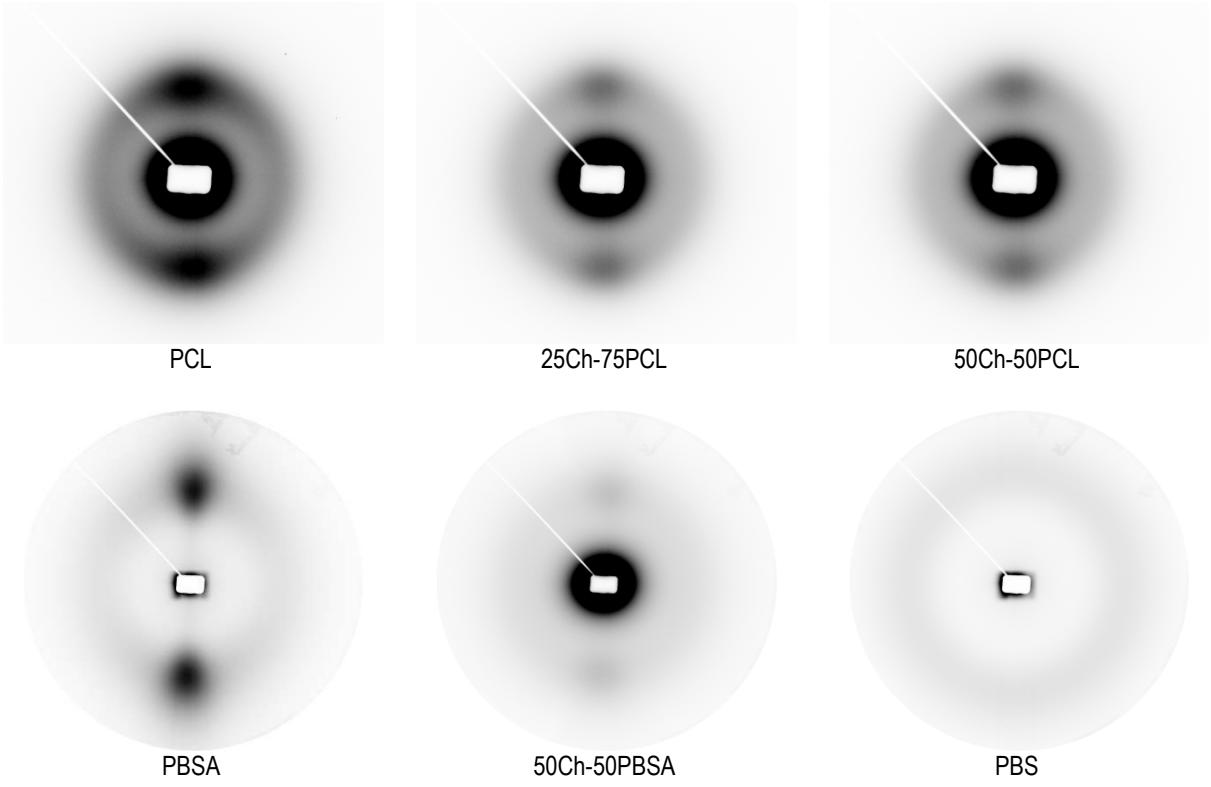

Figure 3.8. 2-D-SAXS patterns of injection-moulded samples.

All materials exhibited the typical scattering features associated with the electron density contrast between the alternating crystalline and amorphous layers. PCL displays a noticeable orientation of its lamellar morphology in the direction of the melt flow inside the mold. The inclusion of 25% and 50% by weight of chitosan seems not to affect this orientation; only the intensity of the diffraction pattern

decreases, as expected. PBSA samples also exhibit a strong anisotropy, also in the direction of the melt flow. However, the lamellar structure, although maintaining this orientation, is strongly depressed with the inclusion of 50% weight of chitosan.

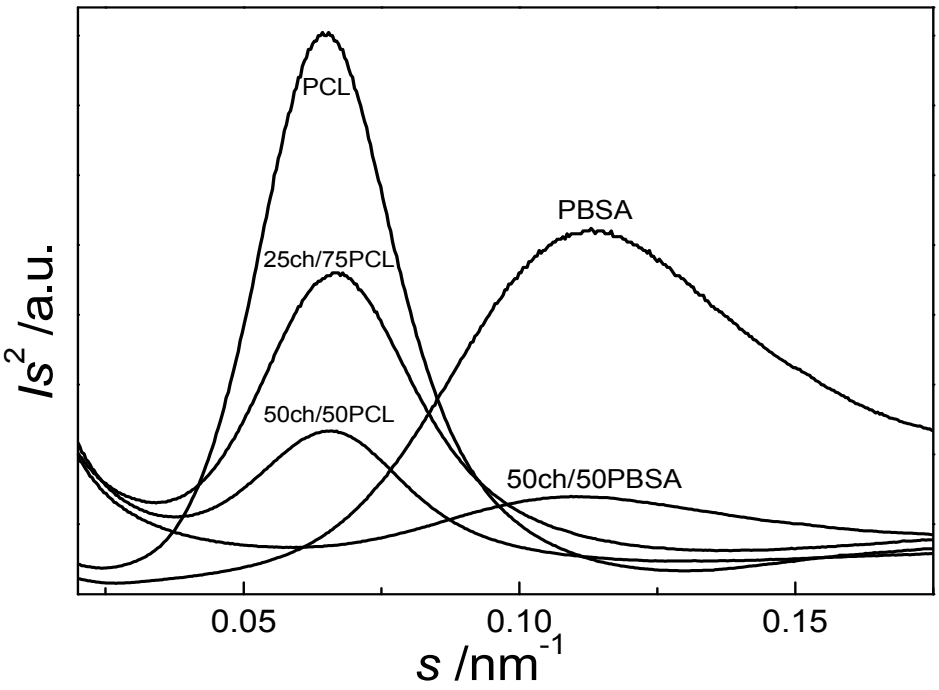

Figure 3.9. Lorentz-corrected SAXS profiles of some PCL and PBSA-based samples.

The 2-D SAXS patterns of the PBS parts do not exhibit the anisotropy found in the other materials. It should also be mentioned that despite the relative high degree of crystallinity of PBS (relative, for example, to PCL), the intensity of the SAXS pattern is quite low, probably indicating that the lamellar organization is not as efficient as in PCL.

The 2-D patterns were integrated (using the X-ray software, version 1.0) to estimate the intensity as a function of the scattering vector, s. Lorentz-corrected scattering profiles analyzed for some materials is shown in Fig. 3.9. In the low angular regions, a typical increase of the intensity is detected, which, due to the low signal, indicated that no regular heterogeneous structures are present with dimensions larger than the crystalline and amorphous layers.

As expected, the intensity of the main diffraction peaks decreased strongly with the incorporation of chitosan, as the total crystallinity (and, thus, the development of crystalline lamellae) is depressed. The position of the peaks was used to calculate the average long period, L=1/smax. For the PCL-based materials, we found that L ranged between 14.9 and 15.3 nm, with no particular trend with the chitosan content. Also for the PBSA and 50% chitosan and 50% PBSA materials, a similar long period was found (8.8 and 9.0 nm, respectively) for the lamellar structure of the polyester. From the results of the PBS system, we conclude that the average long period is always lower here than in PBSA, being near 7.5 nm, independently of the chitosan content. The results shown in Fig. 3.9 clearly indicate that the addition of the polysaccharide on the studied polyesters does not significantly affect the morphology developed at the lamellar scale.

3.6. WIDE-ANGLE X-RAY SCATTERING

Representative WAXS patterns on some selected PCLand PBS-based materials are shown in Fig. 3.10.

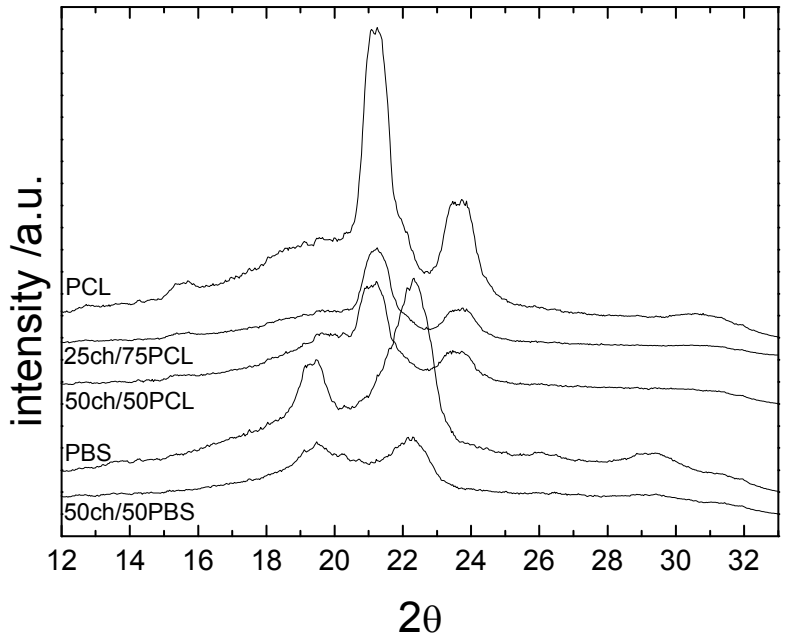

Figure 3.10. : WAXS patterns of some PCL- and PBS-based samples where the effect of the addition of chitosan is investigated.

In the first case, two main diffractions, at 2θ around 21º and 23º, attributed to the (1 1 0) and (2 0 0) planes in PCL are detected [32]. Neither peak changes their position upon blending with chitosan.

Moreover, the half-width of both peaks are maintained, indicating that the PCL crystal sizes are also maintained when chitosan is added. It is interesting to compare these results with those obtained by Honma *et al.* [16], where blends of PCL with chitin and chitosan were prepared by solvent casting. For solvent cast blends, they observed differences in the interplanar spacings of the (1 1 0) planes with the inclusion of the polysaccharides, the b axes of the PCL orthorhombic unit cell being more spread out in the blends. However, no differences were found in the spaces of the (2 0 0) planes [16]. It can therefore be concluded that considerable molecular interaction occurs between PCL and chitosan when the blend is processed by solvent-casting, influencing the crystalline development of PCL. By contrast, in the PCLblends prepared by injection molding, it seems that these interactions are weaker, as no influence in the crystalline morphology is detected in either the crystal unit (probed by WAXS) or lamellar (probed by SAXS) length scales.

The diffraction diagrams for the PBS-based injection molded parts (Fig. 3.10) display a peak at 2θ ≈19.3º, assigned to the (11-1) and (0 0 2) planes, a peak of (1 1 0) at 2θ ≈22.2º, with a shoulder at lower angles (better defined in the blends and composites) associated with the (0 1 2) planes, a peak of (12-1) at 2θ ≈25.9º and a peak of (1 1 1) at 2θ ≈29º. An electron diffraction study showed that PBS chains crystallize in monoclinic crystal lattice, with a = 0.523 nm, b = 0.908 nm, c = 1.079 nm, and β = 123.87º [33]. It can be seen in Fig. 3.10 that the position of the diffraction peaks is not altered with the introduction of chitosan, as observed previously for the PCL system. Only the intensity of the peaks is altered due to the loss of total crystallinity (with the blending with chitosan).

4. CONCLUSIONS

Chitosan, an important biomaterial, can be melt blended with several biodegradable polyesters to produce materials with a range of acceptable properties. Addition of chitosan to PLA decreased the glass transition temperature as well as the temperature of the onset of crystallization. For chitosan/PCL blends, the degree of crystallinity decreased with increased chitosan content. When the chitosan content in PBS increased, the melting temperaturewas found to decrease. For blends containing 25% and 70% chitosan, the crystallinity of the PBS increased, while at the intermediate chitosan content (50%), it decreased.

The tensile strength decreased with increased chitosan content while the modulus increased. A small amount of chitosan content caused a significant decrease in the elongation. No neckingwas observed in the filled polymers. These blends displayed a skin core morphology. Chitosan domains tend to be

enclosed in the inner regions of moldings, confirming the observation that the continuous phase consists of polyester and the dispersed phase is composed of chitosan domains. In all the blend compositions, the distribution of chitosan domains in the cross-section images seems to be controlled by the flow pattern, leading to a nearly radial and symmetric distribution of the domains with respect to the central point of the cross-section. Dispersed chitosan particles agglomerate to sheaths as the chitosan content is increased. The size distribution of chitosan observed in the blends is consistent with the range of sizes observed for pure chitosan under SEM. Qualitatively, the average particle size seems to decrease after processing, particularly in the 25% chitosan blends. This is probably due to the stresses experienced during extrusion, milling and subsequent injection moulding. There is some debonding between the chitosan platelets and the polyester matrix, as evident in the SEM of the tensile-fractured surfaces. Platelet pull-out results in holes in most of the matrices. The only exception is chitosan/PLA blends whose crosssection showed little evidence of any protrusion or loose chitosan particles. As the chitosan content is increased in chitosan/PBS blends, the fracture surface becomes smoother, indicating a decrease in ductility. Blends of chitosan with PCL, PBTA, or PBSA display fibrous appearance at the fractured surface due to the stretching of the polymer threads.

When cryogenically-fractured surfaces are etched with acetic acid to remove chitosan, cavities corresponding to dimensions of chitosan platelets are evident. These cavities have smooth surfaces, indicating that the chitosan fibers do not completely adhere to the polyester matrix. Some cryogenically-fractured surfaces of blends show fibrillar polymer structure. These polyesters display SAXS patterns that are consistent with a typically lamellar morphology. The lamellar orientation of the polyesters (PCL, PBSA) are unaffected by the addition of chitosan. However, the addition of chitosan does suppress the lamellar development. PBS, on the other hand, while crystalline, displays a more isotropic orientation. The intensity of the main diffraction peaks decreased with the incorporation of chitosan, as the total crystallinity is reduced. The two main diffraction peaks in PCL, observed using WAXS, are unaffected by the addition of chitosan. Similarly, the inclusion of HA does not influence the position of the diffraction peaks of PCL. The X-ray diffraction results confirm the morphological observations that the chitosan and the polyester are phase-separated systems.

REFERENCES

1. Kim, B.S. and D.J. Mooney, Development of biocompatible synthesis extracellular matrices for tissue engineering. Trends in Biotechnology, 1998. 16 (5): p. 224–230.
2. Engleberg, I. and J. Kohn, Physico-mechanical properties of degradable polymers used in medical applications: a comparative study. Biomaterials,1991. 12: p. 292–304.
3. Muzzarelli, R.A.A., Enzymatic synthesis of chitin and chitosan, in: Chitin, Pergamon Press, Oxford, 1977, p. 5–17.
4. Chandy, T. and C.P. Sharma, Chitosan as a biomaterial. Biomaterial Artificial Cells and Artificial Organs, 1990. 18: p. 1–24.
5. Goosen, M.F.A., Appplications of Chitin and Chitosan, Technomic Publishing Co. Inc., Pennsylvania, 1997.
6. Singh, D.K. and A.R. Ray, Radiation-induced grafting of N,N-dimethylaminoethylmethacrylate onto chitosan films. Journal of Applied Polymer Science, 1997. 66(5): p. 869–877.
7. D.K. Singh, A.R. Ray, Graft copolymerization of 2-hydroxyethylmethacrylate onto chitosan films and their blood compatibility. Journal of Applied Polymer Science, 1994. 53: p. 1115–1121.
8. Blair, H.S., *et al.*, Chitosan and modified chitosan membranes I. Preparation and characterisation. Journal of Applied Polymer Science, 1987. 33(2): p. 641–656.
9. Lagos, A. and J. Reyes, Grafting onto chitosan. I. Graft copolymerization of methyl methacrylates onto chitosan with Fenton's reagent (Fe2+-H2O2) as a redox initiator. Journal of Polymer Science Part A: Polymer Chemistry, 1988. 26(4): p. 985–991.
10. Shigeno, Y., K. Kondo and K. Takemoto, Functional monomers and polymers. 90. Radiation-induced graft polymerization of styrene onto chitin and chitosan. Journal of Macromolecular Science, Part A: Pure and Applied Chemistry, 1982. A17: p. 571–583.
11. Yoshikawa, S., T. Takeshi and N. Tsubokawa, Grafting reaction of living polymer cations with amino groups on chitosan powder. Journal of Applied Polymer Science, 1998. 68(11): p. 1883–1889.
12. Gong, P., *et al.*, Synthesis and characterization of polyurethane-chitosan interpenetrating polymer networks. Journal of Applied Polymer Science, 1998. 68(8): p. 1321–1329.
13. Muzzarelli, R.A.A., P. Ilari and M.B. Tomasetti, Chitin-based poly(urea-urethane)s. Journal of Biomaterials Science, Polymer Edition, 1994. 6(6): p. 541–547.

14. Chandy, T. and C.P. Sharma, Prostaglandin E1-immobilized poly(vinyl alcohol)-blended chitosan membranes: Blood compatibility and permeability properties. Journal of Applied Polymer Science, 1992. 44(12): p. 2145–2156.
15. Chen, H.L., L.J. Li and T.L. Lin, Formation of segregation morphology in crystalline/amorphous polymer blends: Molecular weight effect. Macromolecules, 1998. 31(7): p. 2255–2264.
16. Honma, T., T. Senda and Y. Inoue, Thermal properties and crystallization behaviour of blends of poly(-caprolactone) with chitin and chitosan. Polymer International, 2003. 52(12): p. 1839–1846.
17. van Krevelen, D.W., Properties of Polymers, Elsevier, Amsterdam, 1990.
18. Cheung, M.K., K.P.Y. Wan and P.H.Yu, Miscibility and morphology of chiral semicrystalline poly-(R)-(3-hydroxybutyrate)/chitosan and poly-(R)-(3-hydroxybutyrate-co-3-hydroxyvalerate)/chitosan blends studied with DSC, 1H T1 and T1 CRAMPS. Journal of Applied Polymer Science, 2002. 86(5): p. 1253–1258.
19. Ramkumar, D.H.R., and M. Bhattacharya, Steady shear and dynamic properties of biodegradable polyesters. Polymer Engineering and Science, 1998. 38(9): p. 1426–1435.
20. Jamshidi, K., S.H. Hyon and Y. Ikada, Thermal characterization of polylactides. Polymer, 1988. 29(12): p. 2229–2234.
21. Pukanszky, B., F.H.J. Maurer and J.W. Boode, Impact testing of polypropylene blends and composites. Polymer Engineering and Science, 1995. 35(24): p. 1962-1971.
22. Mani, R., and M. Bhattacharya, Properties of injection moulded blends of starch and modified biodegradable polyesters. European Polymer Journal, 2001. 37(3): p. 515–526.
23. Jacob, J., M. Bhattacharya, Properties of reactively blended soy protein and modified polyesters. Polymer International, 1999. 48(11): p. 1165–1172.
24. Vaidya, U.R., and M. Bhattacharya, Properties of blends of starch and synthetic polymers containing anhydride groups. Journal of Applied Polymer Science, 1994. 52(5): p. 617–628.
25. Bazhenov, S., The effect of particles on failure modes of filled polymers. Polymer Engineering and Science, 1995. 35(10): p. 813–822.
26. Dubnikova, I.L., V.G. Oshmyan and A.Ya. Greenberg, Mechanisms of particulate filled polypropylene finite plastic deformation and fracture. Journal of Materials Science, 1997. 32(6): p. 1613–1622.
27. Cartier, N., A. Domard and H. Chanzy, Single crystals of chitosan. International Journal of Biological Macromolecules, 1990. 12(5): p. 289–294.

28. Fornes, T.D., and D.R. Paul, Modeling properties of nylon 6/clay nanocomposites using composite theories. Polymer, 2003. 44(17): p. 4993–5013.
29. Clements, B.E., and E.M. Mas, Dynamic mechanical behavior of filled polymers. I. Theoretical developments. Journal of Applied Physics, 2001. 90 (11): p. 5522–5534.
30. Mas, E.M., and B.E. Clements, Dynamic mechanical behavior of filled polymers. II. Applications. Journal of Applied Physics, 2001. 90 (11): p. 5535–5541.
31. Evans, K.E., and A.G. Gibson, Prediction of the maximum packing fraction achievable in randomly oriented short-fibre composites. Composites Science and Technology, 1986. 25(2): p. 149–162.
32. Chatani, Y., *et al.*, Structural studies of polyesters. III. Crystal structure of poly-ε-caprolactone. Polymer Journal, 1970. 1(5): p. 555-562.
33. Ihn, K.J., E.S. Yoo and S.S. Inn, Structure and morphology of poly(tetramethylene succinate) crystals. Macromolecules, 1995. 28(7): p. 2460–2464.

CHAPTER IV.

Hydroxyapatite reinforced chitosan and polyester blends for biomedical applications

CHAPTER IV.

Hydroxyapatite reinforced chitosan and polyester blends for biomedical applications

Abstract

Hydroxyapatite, chitosan, and aliphatic polyester were compounded using a twin-screw extruder. The polyesters include poly(e-caprolactone) (PCL), poly(lactic acid) , poly(butylene succinate) (PBS), and poly(butylene terephthalate adipate). The mass fraction of chitosan ranged from 17.5 to 45%, while that of HA ranged from 10 to 30%. These composites were injection molded and evaluated for thermal, morphological, and mechanical properties. The addition of hydroxyapatite decreased the crystallinity in chitosan/PBS blends, while in blends containing chitosan/PCL, the crystallinity increased. Addition of hydroxyapatite significantly decreased the tensile strength and elongation of polyester/hydroxyapatite composites as well as chitosan/polyester/hydroxyapatite composites with elongations undergoing decreases over an order of magnitude. The tensile strength of the composite was dictated by the adhesion of HA to the chitosan/ olyester matrix. The tensile strength of composites containing hydroxyapatite could be predicted using the Nicolai and Narkis equation for weak filler adhesion ($K \approx 1.21$). Tensile-fractured and cryogenically-fractured surface indicates extensive debonding of hydroxyapatite crystals from the matrix, indicating weak adhesion. The adhesion of hydroxyapatite was higher for pure polyester than those containing chitosan and polyester. The modulus of the composites registered modest increase. The two main diffraction peaks observed using WAXS are unaffected by the amount of chitosan or hydroxyapatite.

This chapter is based on the following publication: **Correlo VM**, Boesel LF, Bhattacharya M, Mano JF, Neves NM and Reis RL, 2005, Hydroxyapatite reinforced chitosan and polyester blends for biomedical applications, Macromolecular Materials and Engineering, **290(12)**:1157-1165

1. INTRODUCTION

Chitin, an unbranched polysaccharide derived from the exoskeletons of crustaceans, insects, and mollusks, and the cell walls of microorganisms [1] is finding increased use in biomedical applications. Chitosan, a linear amino polysaccharide obtained by de-acetylation of chitin, and chitin possesses the inherent physical and biological characteristics that may render them useful as a component in hard tissue replacement material. Chitin's role in the exoskeleton of crustaceans is analogous to that of collagen in bone, being the fibrous matrix acting as template for the development of inorganic calcium material. Due to their good biological activity (providing affinity and surface chemistry ideal for contact with cells), biocompatibility, and biodegradability, chitosan and its derivatives have attracted attention for potential applications in the field of biomedical polymers [2]. These biomolecules have been reported to have applications as anticoagulants, wound-healing accelerators, wound dressing, artificial bone, and in drug delivery systems [3].

A large number of synthetic polymers have found varying uses in biomedical industries. These are summarized in several monographs, symposium proceedings, and texts [4,5]. While naturally occurring polymers exhibit a range of properties that make them suitable for use as alternatives to currently used biomaterials, they have less than ideal mechanical properties which precludes their use as materials in load bearing applications. The development of hybrid materials that combine naturally occurring polymers with biocompatible synthetic polymers is expected to minimize the mismatch of mechanical properties and preserve biocompatibility.

Hydroxyapatite (HA) is often added to orthopedic devices to induce osteoconductivity or bone-bonding ability. Few, if any, synthetic polymers are osteoconductive. Hydroxyapatite, because of its similar chemical structure to the inorganic composition of human bone, is often used in bone reconstruction. Several studies have shown the bone bonding ability of HA [6–8]. Hydroxyapatite has also been evaluated as a reinforcing agent with polymers such as HDPE [9–11], PLLA[12], PMMA [13–15], PHB homopolymer and P(HB-HV) copolymers [16,17], starch [18,19], and polyester-ether [20] to form bioactive compounds. In addition to increasing the modulus, apatites have biocompatibility with several cell types such as osteoblasts, osteoclasts, fibroblasts, and periodontal ligament cells that are found in calcified tissues [21–23].

In an earlier paper [24], we reported on the properties of composites of chitosan and aliphatic polyesters. The objective of this research was to evaluate the properties of hydroxyapatite, chitosan, and

biodegradable aliphatic polyesters poly-ε-caprolactone (PCL), poly(lactic acid) (PLA), poly(butylene succinate) (PBS), and poly(butylene terephthalate adipate) (PBTA). The tensile properties (tensile strength and tensile modulus), thermal properties, and morphological properties of the composites were evaluated. Ternary blends often lead to complex morphology and affect properties.

2. MATERIALS AND METHODS

2.1. MATERIALS

The chitosan, supplied by France Chitin, (Orange, France), had a degree of deacetylation of approximately 85%. The polyesters used include poly-ε-caprolactone) (PCL), Poly- (butylene succinate) (PBS), poly(lactic acid) (PLA), and poly(butylene terephthalate adipate) (PBTA). Polycaprolactone resin PCL 787, commercially available as TONE™ Polymer, was obtained from Union Carbide Chemicals and Plastics Division, Bound Brook, New Jersey. Eastar Bio Copolyester 14766™, a butanediol, adipate, and terephthalate copolymer, was obtained from Eastman Chemical Company, Kingsport, Tennessee. Bionolle™ 1050, a polybutylene succinate copolymer, was obtained from Showa Highpolymer Co. Ltd., Tokyo, Japan. The characteristics of the various polyesters are summarized in Table 4.1. Hydroxyapatite (grade Capital S) [3 µm<d<6 µm] was obtained from Plasma Biotal Ltd, Tideswell, England.

Table 4.1. Material properties of polyesters used in this study.

	PCL 787 [a]	PBS [b]	PBTA [c]	PLA [d]
MELT INDEX	4	50	20	-
MN (X 10-5)	0.64	0.34	0.43	1.54
MW (X 10-5)	1.24	0.89	0.78	2.52

[a] poly-ε-caprolactone
[b] poly(butylene succinate)
[c] poly(butylene terephthalate adipate)
[d] poly(lactic acid)

2.2. PROCESSING

The materials processed and their composition is shown in Table 4.2. The composites were compounded in a co-rotating twin-screw extruder [Leistriz LSM 36]. Higher filler content pushed the

torque in the extruder close to the maximum. Hence, each composition had 5% by weight of plasticizer (glycerol) to reduce the torque. The extruded strands were ground by a Coloritron grinder using 5 mm diameter pellets. The resulting composite were injection molded using an ENGEL injection moulding machine to produce tensile test bars. The tensile bars had a neck cross-section area of 2x4 mm^2 and a neck length of 20 mm. The conditions used for moulding are summarized in Table 4.3.

Table 4.2. Processing condition used for compounding the various composites studied.

	PROCESSING CONDITIONS		
MATERIAL	TEMPERATURE PROFILE (°C)	SCREW SPEED (RPM)	TYPE OF MACHINE USED
70PBS-30HA [a]	80/120/140/150/165/175	100	Co-rotating
17.5Ch-52.5PBS-30 HA + 5% glycerol [b]	80/120/140/150/165/175	100	Co-rotating
45Ch-45PBS-10HA + 5% glycerol [c]	80/120/140/150/165/175	100	Co-rotating
40Ch-40PBS-20HA + 5% glycerol [d]	80/120/140/150/165/175	100	Co-rotating
35Ch-35PBS-30HA + 5% glycerol [e]	80/120/140/150/165/175	100	Co-rotating
35Ch-35PBTA-30HA + 5% glycerol [f]	80/120/140/150/165/175	100	Co-rotating
35Ch-35PCL-30HA + 5% glycerol [g]	80/120/140/150/165/175	100	Co-rotating
35Ch-35PLA-30HA + 5% glycerol [h]	175 in first 4 zones, 180 rest	100	Co-rotating

[a] Composite containing 70% by weight of PBS and 30% by weight of hydroxyapatite
[b] Composite containing 17.5% by weight of chitosan, 52.5% by weight of PBS and 30% by weight of hydroxyapatite, processed with 5% by weight of glycerol
[c] Composite containing 45% by weight of chitosan, 45% by weight of PBS and 10% by weight of hydroxyapatite, processed with 5% by weight of glycerol
[d] Composite containing 40% by weight of chitosan, 40% by weight of PBS and 20% by weight of hydroxyapatite, processed with 5% by weight of glycerol
[e] Composite containing 35% by weight of chitosan, 35% by weight of PBS and 30% by weight of hydroxyapatite, processed with 5% by weight of glycerol
[f] Composite containing 35% by weight of chitosan, 35% by weight of PBTA and 30% by weight of hydroxyapatite, processed with 5% by weight of glycerol
[g] Composite containing 35% by weight of chitosan, 35% by weight of PCL and 30% by weight of hydroxyapatite, processed with 5% by weight of glycerol
[h] Composite containing 35% by weight of chitosan, 35% by weight of PLA and 30% by weight of hydroxyapatite, processed with 5% by weight of glycerol

Table 4.3. Injection molding processing conditions for the composites.

MATERIAL	INJECTION SPEED (mm/s)	HOLDING PRESSURE (BAR)	BARREL TEMP. (°C)
70PBS-30HA [a]	28	40	90-120-120-140
17.5Ch-52.5PBS-30 HA + 5% glycerol [b]	28	20	110-130-150-160
45Ch-45PBS-10HA + 5% glycerol [c]	26	20	110-130-150-160
40Ch-40PBS-20HA + 5% glycerol [d]	32	20	110-130-150-160
35Ch-35PBS-30HA + 5% glycerol [e]	30	20	110-130-150-160
35Ch-35PBTA-30HA + 5% glycerol [f]	22	25	110-130-150-160
35Ch-35PCL-30HA + 5% glycerol [g]	42	20	110-130-150-160

[a] Composite containing 70% by weight of PBS and 30% by weight of hydroxyapatite
[b] Composite containing 17.5% by weight of chitosan, 52.5% by weight of PBS and 30% by weight of hydroxyapatite, processed with 5% by weight of glycerol
[c] Composite containing 45% by weight of chitosan, 45% by weight of PBS and 10% by weight of hydroxyapatite, processed with 5% by weight of glycerol
[d] Composite containing 40% by weight of chitosan, 40% by weight of PBS and 20% by weight of hydroxyapatite, processed with 5% by weight of glycerol
[e] Composite containing 35% by weight of chitosan, 35% by weight of PBS and 30% by weight of hydroxyapatite, processed with 5% by weight of glycerol
[f] Composite containing 35% by weight of chitosan, 35% by weight of PBTA and 30% by weight of hydroxyapatite, processed with 5% by weight of glycerol
[g] Composite containing 35% by weight of chitosan, 35% by weight of PCL and 30% by weight of hydroxyapatite, processed with 5% by weight of glycerol

2.3. MECHANICAL PROPERTIES

The tensile properties were determined using a Universal tensile testing machine (Instron 4505 Universal Machine, USA). Tensile stress was taken as the maximum stress in the stress/strain curve. Tensile modulus was estimated from the initial slope of the stress strain curve. Samples were conditioned at room temperature for at least 48 h before testing. A crosshead speed of 5 mm/min was used. The values reported were the average of at least five specimens.

2.4. DIFFERENTIAL SCANNING CALORIMETRY

The DSC experiments were performed in a Perkin-Elmer DSC7 apparatus, using a water cooling accessory and nitrogen as a purge gas (flux gas of ca. 20 $cm^3.min^{-1}$). Both temperature and heat flux were calibrated with Indium (99.99999% purity) at a scanning rate of 20 ºC/min. The samples were obtained by cutting a small piece of material (with ca. 10 mg weight) in the central region of the injection parts. An effort was made to maintain the geometry of the different samples in order to keep the same thermal resistance. All the experiments were performed at 20 ºC/min, starting from room temperature. Only the first run was analyzed, which reflects not only the materials contained in the samples, but also the general morphology developed during processing.

2.5. WIDE ANGLE *(WAXS)* X-RAY SCATTERING

WAXS experiments were performed using X-ray synchrotron radiation (transmission mode) at the Soft Condensed Matter A2 beamline at the HASYLAB (DESY) synchrotron facility in Hamburg, Germany. The experimental setup included a linear detector for 1-DWAXS measurements (distance 23 cm). Cu *Kα* radiation, with a wavelength of λ = 0.154 nm, was employed in the experiments. The injection moulded samples were fixed vertically, and the patterns were acquired at room temperature.

2.6. SCANNING ELECTRON MICROSCOPY

The morphological characterization of the composites was made using a Leica-Cambridge S-360 scanning electron microscope. All the samples were sputter-coated with gold. Several different analyses of the cross-section of the tensile bars were made. These include (i) observations of fractured surfaces after break during the tensile tests and (ii) observations after immersing the samples in liquid nitrogen for one minute and fracturing the sample in the testing zone to analyze the brittle fracture of the composite.

3. RESULTS AND DISCUSSION

3.1. DIFFERENTIAL SCANNING CALORIMETRY

Figure 4.1a shows the DSC scans of the 50/50 wt.-% of chitosan and PLA blend. The glass transition at 60.1 ºC (midpoint) can be easily observed, together with the typical structural relaxation endothermic peak, the exothermic peak corresponding to the cold crystallization process (onset at T_c = 89.2 ºC) and melting peak, with an onset temperature of 155.7 ºC.With the addition of 30%wt of HA in the blend, a drop on T_g (53.6 ºC) was observed.

This may be attributed to an extended chain scission during the processing of the composite (HA/chitosan/PLA), with respect to the blend (chitosan/PLA). This may help explain the decrease of the cold-crystallization temperature (T_c = 83.9 ºC) that is also observed upon the introduction of the HA. However, we believe that the HA particles play an important role as nucleating agents. In fact, it has been reported that composites of PLA/HA produced by solvent casting (where chances of thermal degradation are minimal) exhibit decreasing T_c with increasing HA content [25]. Finally, the composite presents a lower melting temperature (T_m = 148.2 ºC) than the pure PLA (155.3 ºC [26]). The presence of

the HA particles during the cold-crystallization process could lead to the formation of less perfect crystalline structures, that melt at a lower temperatures.

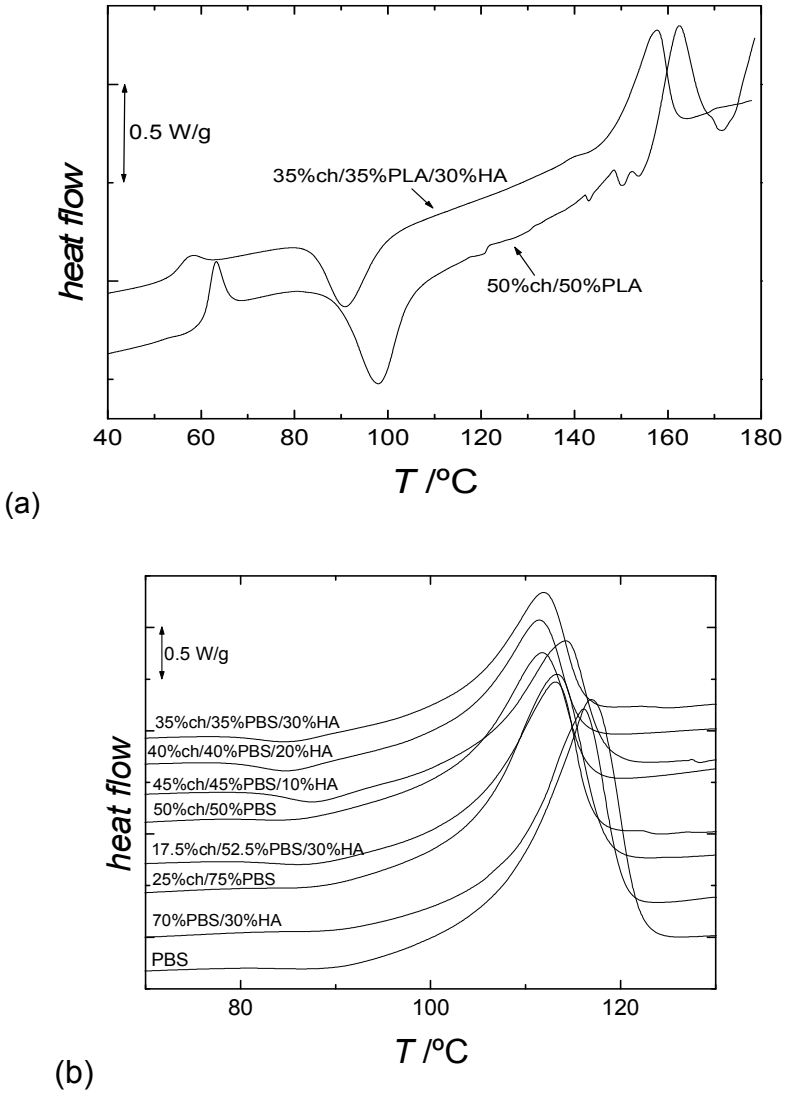

Figure 4.1. Representative DSC thermograms, obtained at 20 ºC.min-1, analyzing the effect of HA addition in (a) PLA and (b) PBS-based materials.

A similar study was performed for the PCL system, where the 50/50 wt.-% chitosan/PCL blend was reinforced with 30%wt HA. In the DSC scans (figure not shown), the melting peak is clearly detected. The inclusion of hydroxyapatite decreased the melting temperature of the 50/50 wt.-% chitosan/PCL blend (Table 4.4). Similar results were reported for PCL reinforced with hydroxyapatite nanocrystals,

processed by solvent casting [27]. From the enthalpy values, the degree of crystallinity of the PCL component in the samples was calculated from the known PCL content and by assuming that the heat of fusion of completely crystalline PCL is 166 $J.g^{-1}$ [28]. The reinforcement of chitosan/PCL by HA increased the degree of crystallinity in the PCL fraction (Table 4.4). In this case, the nucleating effect of the HA particles may be the origin of the enhancement of the degree of crystallization.

Table 4.4. Melting temperature and heat of fusion of the different samples analysed by DSC, and the corresponding crystallinity degree within the synthetic polymer component.

SAMPLE	T_m /ºC	ΔH /$J.g^{-1}$	X%*
50Ch-50PCL [a]	55.2	25.9	31.2
35Ch-35PCL-30%HA [b]	53.5	20.9	36.0
PBS [c]	107.2	73	66.2
70PBS-30HA [d]	107.9	49.9	64.6
25Ch-75PBS [e]	103.4	55.5	67.1
17.5Ch-52.5PBS-30HA [f]	103.7	39.1	67.5
50Ch-50PBS [g]	102.4	31.7	57.5
45Ch-45PBS-10HA [h]	104.6	33.5	67.5
40Ch-40PBS-20HA [i]	103.1	28.7	65.0
35Ch-35PBS-30HA [j]	102.9	30	77.7

*crystallinity in the polyester fraction
[a] Blend containing 50% by weight of chitosan and 50% by weight of PCL
[b] Composite containing 35% by weight of chitosan, 35% by weight of PCL and 30% by weight of hydroxyapatite
[c] poly(butylene succinate)
[d] Composite containing 70% by weight of PBS and 30% by weight of hydroxyapatite
[e] Blend containing 25% by weight of chitosan and 75% by weight of PBS
[f] Composite containing 17.5% by weight of chitosan, 52.5% by weight of PBS and 30% by weight of hydroxyapatite
[g] Blend containing 50% by weight of chitosan and 50% by weight of PBS
[h] Composite containing 45% by weight of chitosan, 45% by weight of PBS and 10% by weight of hydroxyapatite
[i] Composite containing 40% by weight of chitosan, 40% by weight of PBS and 20% by weight of hydroxyapatite
[j] Composite containing 35% by weight of chitosan, 35% by weight of PBS and 30% by weight of hydroxyapatite

The DSC thermograms for the PBS-based materials are shown in Figure 4.1b. Again, the degree of crystallinity of the PBS component was calculated from the known theoretical value of ΔH_m for 100% crystalline PBS, that was estimated to be 110.3 $J.g^{-1}$, calculated on the basis of the group contribution method proposed by Van Krevelen [29]. For PBS and all the blends with chitosan, the introduction of 30%

of HA tends to increase the (onset) melting temperature (Table 4.4). This behavior is different from that found in PCL. The effect of the increase of HA content was analysed for the composite with the same amount of PBS and chitosan. Interestingly, the increase of HA from 10 to 30% tends to decrease T_m (Table 4.4). This behavior indicates that a significant increase in Tm is found with the introduction of a lowquantity ofHAinto the PBS-system, but with a further HA content the melt temperature systematically decreases. An explanation for this finding may be linked to the enhancing of molecular scission upon processing with the increase of the HA content. The degradation of polyester due to the presence of moisture and shear is well documented [30, 31]. As the HA content in the blend increased, the torque and hence the shear stresses increased leading to chain scission of the PBS. A more careful and controlled study is needed to fully elucidate this issue. The introduction of 30%of HA may influence the degree of crystallinity in the PBS fraction: it decreased slightly for pure PBS, increased slightly in the blend of PBS with 25 wt.-% chitosan, and finally increased significantly in the blend of PBS with 50% by weight chitosan (reflected in the reduction of the elastic modulus of this composite with respect to the un-reinforced blend). This indicates that the effect of HA may be dependent on the amount of polysaccharide in the blend. For the particular blend of 50/50 wt.-% chitosan/PBS, the increase of the HA content tends to increase the degree of crystallinity, but the evolution is not progressive. Again, this behavior may be due to the decrease of the molecular weight of PBS during processing with increasing HA.

3.2. MECHANICAL PROPERTIES

The processing parameters for compounding and injection moulding are summarized in Table 4.2 and 4.3. It is well known that extrusion compounding parameters such as screw profile, barrel temperature, and residence time affect the morphology of blends. Similarly, several injection moulding processing parameters, such as injection speed, packing pressure, barrel temperature and mould temperature, may affect the tensile properties. In this study, no attempt was made to optimize properties. Rather, the conditions were selected for ease of processing and visual acceptance of molded parts.

The mechanical properties of composites containing hydroxyapatite with blends of chitosan and various polyesters are summarized in Table 5. Composites containing chitosan, PLA, and hydroxyapatite in the weight ratio of 35:35:30 were also compounded. However, these composites could not be moulded because of their inherent brittleness. The stress-strain behavior is shown in Figure 4.2. The ductility was low, and the composites were brittle. For the low filler content (17.5%Ch-52.5%PBS-30%HA), the

samples strain at constant stress before failing. Addition of hydroxyapatite increased the filler content of the composite and further decreased the tensile strength over chitosan/polyester blends [24].

Table 4.5. Tensile properties of various chitosan polyester blends with hydroxyapatites.

MATERIALS	TENSILE STRENGTH (MPa)	TENSILE MODULUS (GPa)	ELONGATION (%)
PBS [a]	38.6±1.3	0.61±0.01	264±29
PCL [b]	27.3±0.8	0.38±0.02	674±36
PBTA [c]	20.2±0.3	0.08±0.01	1075±37
70PBS-30HA [d]	28.3 ± 0.2	1.04 ± 0.03	13.1 ± 1.7
17.5Ch-52.5PBS-30HA [e]	13.0 ± 0.5	1.05 ± 0.07	4.4 ± 0.2
45Ch-45PBS-10HA [f]	15.9± 0.6	1.85 ± 0.03	1.6 ± 0.2
40Ch-40PBS-20HA [g]	12.1 ± 3.2	1.95 ± 0.03	1.0 ± 0.3
35Ch-35PBS-30HA [h]	13.1 ± 1.4	1.81 ± 0.08	1.2 ± 0.2
35Ch-35PBTA-30HA [i]	11.2 ± 0.4	0.71 ± 0.03	3.3 ± 0.2
35Ch-35PCL-30HA [j]	14.6 ± 0.8	1.45 ± 0.05	1.7 ± 0.2

[a] poly(butylene succinate)
[b] poly-ε-caprolactone
[c] poly(butylene terephthalate adipate)
[d] Composite containing 70% by weight of PBS and 30% by weight of hydroxyapatite
[e] Composite containing 17.5% by weight of chitosan, 52.5% by weight of PBS and 30% by weight of hydroxyapatite
[f] Composite containing 45% by weight of chitosan, 45% by weight of PBS and 10% by weight of hydroxyapatite
[g] Composite containing 40% by weight of chitosan, 40% by weight of PBS and 20% by weight of hydroxyapatite
[h] Composite containing 35% by weight of chitosan, 35% by weight of PBS and 30% by weight of hydroxyapatite
[i] Composite containing 35% by weight of chitosan, 35% by weight of PBTA and 30% by weight of hydroxyapatite
[j] Composite containing 35% by weight of chitosan, 35% by weight of PCL and 30% by weight of hydroxyapatite

The addition of chitosan to polyesters caused a modest decrease (≈20% for 50% chitosan in the blend) in the tensile strength and significant increase in the modulus (≈3-fold). Similar results have been reported by others in the literature [15,17,20]. This is due to incompatibility between the components of the composites that gives rise to low interphase adhesion between the matrix and the dispersed phase, particularly the adhesion of hydroxyapatite to either chitosan or polyester.

The elongation at break shows a marked decrease upon the addition of hydroxapatite (Table 4.5). There is approximately a two orders of magnitude decrease in the elongation at break upon the addition of

30% hydroxyapatite to the polyester. While the pure polyesters underwent plastic deformation, the composites displayed brittle failure. According to Dubnikova et al. [32], there is a critical filler volume fraction (Φ) below which the samples deform by necking. Beyond this critical value, there is negligible shrinkage of the cross-sectional area when deformation occurs.

Predictive equations for tensile strength have been reported [33] and can be used to present a qualitative analysis regarding the adhesion between the filler and the polyester. The volume fraction and the projected area fraction can be related by the equation of Nicolais and Narkis.

$$\sigma_c = \sigma_m\left[1 - K\Phi^{2/3}\right] \qquad (1)$$

where σ_c and σ_m are the tensile strengths of the composite and the polymer matrix respectively and Φ is the volume fraction of the filler.

The parameter, *K*, in the model accounts for the adhesion between the filler and the matrix. The theoretical value of *K* for the extreme case of poor adhesion is 1.21. A value of *K* lower than the theoretical 1.21 indicates some adhesion. Assuming a particle density of hydroxyapatite and polyester to be 3.1 g/cm^3 and 1.2 g/cm^3 respectively, the *K* value (Equation (1)) is close to 1.0 for the PBS and 30% HA blend.

SEM micrographs (see below) indicate that hydroxyapatite and chitosan are dispersed in the continuous polyester phase. An increase in particle size and content results in the reduction of debonding stress due to the formation of micropores. The amount of debonded particles in the matrix, which determines the pore concentration, is a function of particle diameter; the higher the particle diameter, the lower the debonding stress [34]. For these materials, failure occurs immediately following the onset of debonding, and the tensile strength equals the minimum debonding stress [32]. Chitosan/PCL and chitosan/PBS samples with hydroxyapatite displayed a brittle fracture behavior, while chitosan/PBTA with hydroxyapatite displayed a uniform yield. PBTA has very low crystallinity compared to the other polyesters and retains some ductility even at high filler contents.

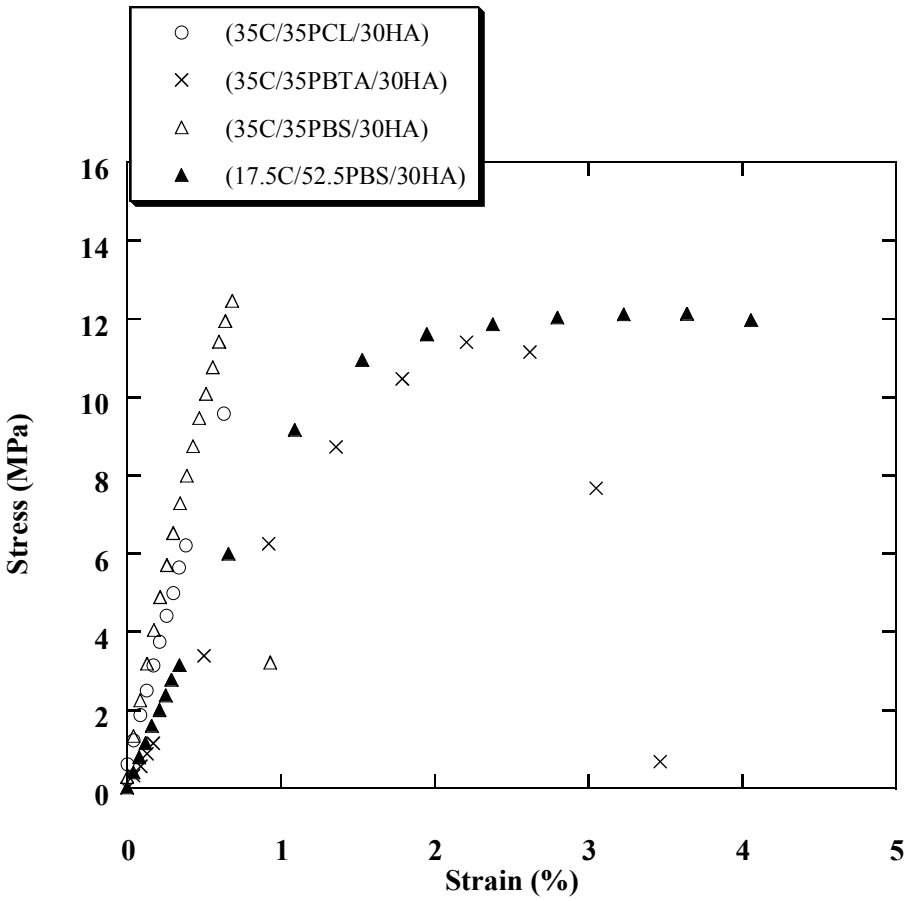

Figure 4.2. Stress versus strain curves for chitosan, polyester and hydroxyapatite composites.

The lack of reinforcing ability of hydroxyapatite with synthetic polymers has been attributed to the lack of chemical interaction of hydroxyapatite with the polymer [9,35,36]. In some instances, coupling agents were used to achieve improved strength [37–39]. In other instances, innovative processing techniques have been used to improve strength [40,41]. The modulus values obtained in this study are in the lower bounds of the properties of bone whose modulus have been reported to range up to 20 GPa [42,43] and could be adequate for minor load bearing applications. Hydrostatic extrusion and oriented molding could be two alternative processing techniques to increase properties further.

The values in Table 4.5 are further reduced because of the added effect of plasticizer, which reduces both the stress and modulus. Bergmann and Owen [17] also observed weak adhesion between hydroxyapatite and polyhydroxybutyrate and poly(hydroxybutyrate-co-valerate). Addition of hydroxyapatite had negligible effect on the modulus, except in the case of chitosan/PCL blend, where it

decreased. This could be due to a combination of lack of reinforcing ability of hydroxapatite due to lack of chemical interaction with the composite as well as the effect of the added plasticizer.

3.3. MORPHOLOGY

The cryogenically-fractured and tensile-stretched specimen cross-section is shown in Figure 4.3 and 4.4. In general, a tensile-stretched specimen cross-section has cavities in two ranges of dimension: one set has diameters less than 4.0 mm and the other has diameters greater than 4.0 mm. Hydroxyapatite crystals have diameters of approximately 3.0 mm. The smaller dimension cavities are more numerous. Many of the cavities have dimensions lower than 3.0 mm, some as lowas 0.5 mm. This could be due to the result of break-down of hydroxyapatite crystals during the compounding process. For all the blends compounded with the hydroxyapatite crystals, it was observed that hydroxyapatite crystals are well distributed within the matrix.

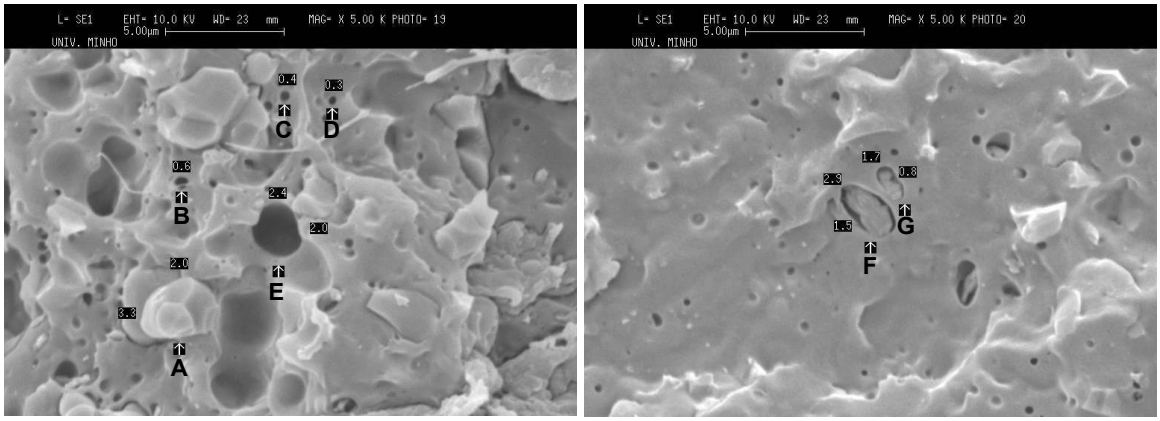

Figure 4.3. 17.5%Chitosan, 52.5% PBS and 30% hydroxyapatite (a) tensile fractured and (b) cryogenically fractured. (A – 3.3x2.0 µm; B – 0.6µm; C – 0.4µm; D – 0.3µm; E – 2.4x2.0µm; F – 1.5x2.9µm; G – 1.7x0.8µm).

The distribution of the hydroxyapatite crystals in the polymer matrix is best visualized by observing the tensilefractured surface in blend with pure polyester (PBS) (Figure 4.4a). The agglomeration of hydoxyapatite crystals is evident since they have dimensions much larger than those observed in blends containing chitosan and polyesters [24]. Similar observations has been reported by Bergmann and Owen [17] in composites of hydroxyapatite and polyhydroxybutyrate and poly(hydroxybutyrate-covalerate). One

reason for the agglomeration in our system could be due to the effect of stresses developed during processing.

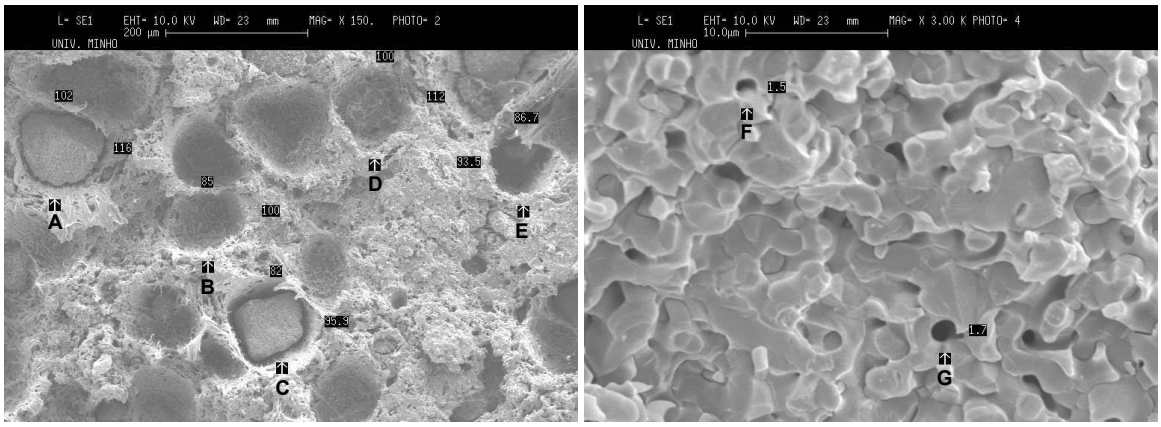

Figure 4.4. 70% PBS and 30% hydroxyapatite (a) tensile fractured and (b) cryogenically fractured. (A – 102.0x116.0µm; B – 85.0x100.0µm; C – 82.0x95.9µm; D – 100.0x112.0µm; E – 93.5x86.7µm; F - 1.5µm; G – 1.7µm)

Composites containing chitosan, polyester, and hydroxyapatite had a much higher viscosity (due to increased filler content), and, hence, the stresses generated were higher than the blend containing hydroxyapatite and PBS. The higher stresses may have resulted in the deagglomeration of the hydroxyapatite crystals in these blends. Another observation is that hydroxyapatite crystals are actually visible in the composite (Figure 4.4a) with pure polyester as opposed to blends containing chitosan and polyesters, where predominantly cavities without the particles are visible. One possible explanation is that pure polyester undergoes shrinkage that results in some adhesion with the hydroxyapatite crystals preventing complete detachment. With the presence of chitosan in the blend, the polyester/chitosan matrix undergoes minimal shrinkage and results in debonding. This also explains the fact that when hydroxyapatite crystals are added, only pure polyester (PBS) experienced an increase in the tensile modulus. Clements and Mas [44] presented expressions from wherein modulus reinforcement can be estimated. For materials that debond and cause voids, the reinforcement factor is typically less than 1.0, irrespective of the aspect ratio of the filler.

The hydroxyapatite crystals have minimal adhesion to the polymer matrix, as is evident from the extensive debonding and the smooth surfaces of the cavities. The number of cavities believed to be as a result of hydroxyapatite crystals is greater than those due to chitosan. As seen in Figure 4.3, the

cavities generated in the tensile-fractured and cryogenically-fractured samples are due to hydroxyapatite. The number of cavities in the tensile-fractured surface is higher than those in the cryogenically-fractured surface. This is probably because chitosan has greater adhesion to the polyester matrix than hydroxyapatite has to the polyester and chitosan matrix. This supports the data from tensile tests that indicate a sharp drop in the tensile strength as hydroxyapatite is added as failure occurs at the initiation of debonding which happens at a lower stress with hydroxyapatite in the blend. Hence, it can be concluded that there is no chemical bonding between the hydroxyapatite crystals and the matrix. It appears that the polymer/chitosan simply flowed around the hydroxyapatite crystals. This could be one reason for minimal modulus reinforcement due to the added hydroxyapatite crystals.

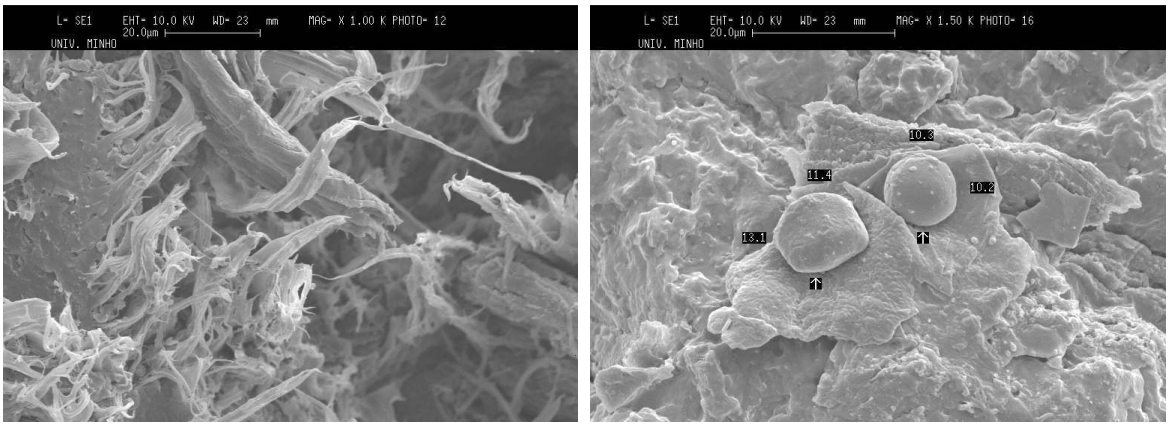

Figure 4.5. 35% chitosan, 35% PBTA and 30% hydroxyapatite (a) tensile fracture, and (b) brittle fracture.

The surfaces of tensile fractured specimens show the typical appearance of brittle failure without visible plastic strain. The only exception is blend with the PBTA, which displayed some plastic deformation (Figure 4.5a). This is probably due to the low crystallinity of the polyester. The surface appears ductile-like with evidence of deformation and stretching of the matrix with submicron size fibrils. For the remaining materials, the morphology is relatively flat with minimal stretching of the matrix. During loading of the composite, deformation is sustainable until failure of the hydroxyapatite crystals occurs (due to debonding) and leads to stress overload of the remaining matrix. The tensile strength is lower than the similar blend composition without hydroxyapatite crystals because of the reduced cross-section area caused by the detached particles. The cryogenically-fractured surface of all hydroxyapatite containing composites breaks in a brittle manner with little stretching of the matrix (Figure 4.5(b)). The

filler content (chitosan and hydroxyapatite) in some cases are as high as 65%, and plastic deformation is not observed on the surface of the fractured specimen. No hydroxyapatite crystals that are bare in the matrix (i.e., have no polymer matrix on them) are observed. Also, the failure of hydroxyapatite particle at the fracture surface is not evident. The absence of bare hydroxyapatite crystals or breaking off at the fracture surface indicates no adhesion of matrix to the hydroxyapatite and results in crystal pull-out during the fracture process.

3.4. WIDE-ANGLE X-RAY SCATTERING

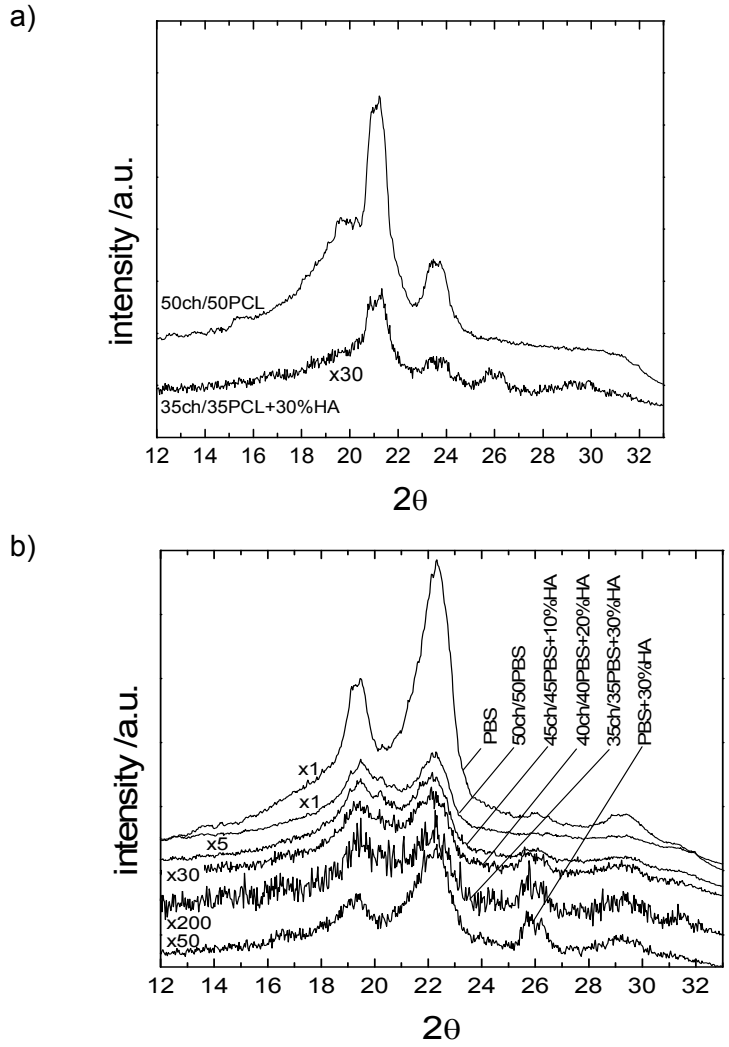

Figure 4.6. WAXS patterns of some PCL-based samples (a) and PBS-based samples (b), where the effect of the addition of HA is investigated. Some patterns were obtained by multiplying the original data by the values indicated near the corresponding lines, for better visualisation.

RepresentativeWAXS patterns on some selected PCL- and PBS-based materials are shown in Figure 4.6a and 4.6b, respectively. In the first case, two main diffractions, at 2θ around 21 and 23º, attributed to the (110) and (200) planes in PCL are detected [45]. The inclusion of HA did not influence the position of the two diffraction peaks of PCL (Figure 4.6a).

The diffraction diagrams for the PBS-based injection moulded parts (Figure 4.6b) display a peak at 2θ≈19.3º, assigned to the (11–1) and (002) planes, a peak of (110) at 2θ≈22.2º, with a shoulder at lower angles (better defined in the blends and composites) associated with the (012) planes, a peak of (12–1) at 2θ≈25.9º and a peak of (111) at 2θ≈29º. An electron diffraction study showed that PBS chains crystallize in monoclinic crystal lattice, with *a* = 0.523nm, *b* = 0.908nm, *c* = 1.079nm and β = 123.87º [46]. It can be seen in Figure 4.6b that the position of the diffraction peaks is not altered with the introduction of chitosan or HA, as observed previously for the PCL system. Moreover, the half-widths of the two main diffraction peaks are maintained, indicating that the PBS crystal sizes do not change significantly with the introduction of HA. Only the intensity of the peaks is altered due to the loss of total crystallinity (with the blending with chitosan), or the intensity of the signal is strongly depressed in the case of the composites due to the strong diffraction of the HA crystals.

4. CONCLUSIONS

Chitosan and hydroxyapatite, an important biomaterial, can be melt blended with several biodegradable polyesters to produce materials with a range of acceptable properties [4]. However, the addition of high volume fraction of fillers (both chitosan and hydroxyapatite) led to processing difficulties that made for poor dispersion, particularly for the HAin the composite. This coupled with the lack of adhesion of HA to the matrix led to reduced mechanical properties over blends of chitosan and polyester [24]. Thus alternative processing techniques [37–41] or the use coupling agents or the functionalization of the ceramic needs to be considered to improve on the properties since the current properties are the lower bound of what is reported for bone.

Addition of HA to chitosan/PLA blends decreased the glass transition temperature as well as the temperature of the onset of crystallization. Melt compounded and injection molded composites of HA, chitosan, and synthetic aliphatic polyester displayed a skin core morphology. The filler domains tend to be enclosed in the inner regions of mouldings, confirming the observation that the continuous phase consists of polyester and the dispersed phase is composed of chitosan/hydroxyapatite domains. Cryogenically- and tensile-fractured surfaces of blends containing hydroxyapatite show extensive

debonding, primarily of hydroxyapatite crystals, indicating poor adhesion between the hydroxyapatite and the chitosan/polyester matrix. This is manifested in reduced tensile strength and tensile modulus of these blends. The diffraction peaks observed using WAXS, are unaffected by the addition of the fillers. The morphological and mechanical properties indicate that the chitosan, ceramic, and polyester are phase-separated systems.

REFERENCES

1. Muzzarelli, R.A.A., Enzymatic synthesis of Chitin and Chitosan, in: Chitin, Pergamon Press, Oxford 1977, p. 5–17.
2. Majeti, N.V., R. Kumar, A review of chitin and chitosan applications. Reactive and Functional Polymers, 2000. 46(1): p. 1-27.
3. Goosen, M.F.A., Applications of Chitin and Chitosan, Technomic Publishing Co. Inc., Pennsylvania 1997.
4. Engleberg, I., and J. Kohn, Physico-mechanical properties of degradable polymers used in medical applications: A comparative study. Biomaterials, 1991. 12(3): p. 292-304.
5. Ratner, B.D., *et al.*, Biomaterials Science: An Introduction to Materials in Medicine, Academic Press 1996.
6. Muller-Mai, C.M., *et al.*, Nanoapatite and organoapatite implants in bone: Histology and ultrastructure of the interface. Journal of Biomedical Materials Research, 1995. 29 (1): p. 9-18.
7. Edwards, J.T., J.B. Brunski and H.W. Higuchi, Mechanical and morphologic investigation of the tensile strength of a bone-hydroxyapatite interface. Journal of Biomedical Materials Research, 1997. 36(4): 454-468.
8. De Groot, K., Medical applications of calciumphospate bioceramics. Journal of the Ceramic Society of Japan, 1991. 99(10): p. 943-953.
9. Deb, S. *et al.*, Hydroxyapatite-polyethylene composites: effect of grafting and surface treatment of hydroxyapatite. Journal of Materials Science: Materials in Medicine, 1996. 7(4): p. 191-193.
10. Huang, J., *et al.*, *In vitro* mechanical and biological assessment of hydroxyapatite-reinforced polyethylene composite Journal of Materials Science: Materials in Medicine, 1997. 8(12): p. 775-779.

11. Wang, M., R. Joseph and W. Bonfield, Hydroxyapatite-polyethylene composites for bone substitution: effects of ceramic particle size and morphology. Biomaterials, 1998. 19(24): p. 2357-2366.
12. Verheyen, C.C.P.M., *et al.*, Evaluation of hydroxylapatite/poly(l-lactide) composites: Mechanical behaviour. Journal of Biomedical Materials Research, 1992. 26(10): p. 1277-1296.
13. Kazuhiko, I., *et al.*, Adhesive bone cement containing hydroxyapatite particle as bone compatible filler. Journal of Biomedical Materials Research, 1992. 26(7): p. 937-945.
14. Serbetci, K., F. Korkusuz and N. Hasirci, Thermal and mechanical properties of hydroxyapatite impregnated acrylic bone cements. Polymer Testing, 2004. 23(2): p. 145-155
15. Cheang, P., and K.A. Khor, Effect of particulate morphology on the tensile behaviour of polymer–hydroxyapatite composites. Materials Science and Engineering A, 2003. 345(1-2): p. 47-54.
16. Luklinska, Z.B. and W. Bonfield, Morphology and ultrastructure of the interface between hydroxyapatite-polyhydroxybutyrate composite implant and bone. Journal of Materials Science: Materials in Medicine, 1997. 8(6): p. 379-383.
17. Bergmann, A., and A. Owen, Hydroxyapatite as a filler for biosynthetic PHB homopolymer and P(HB-HV) copolymers. Polymer International, 2003. 52(7): p. 1145-1152.
18. Vaz, C.M., R.L. Reis and A.M. Cunha, Use of coupling agents to enhance the interfacial interactions in starch–EVOH/hydroxylapatite composites. Biomaterials, 2002. 23(2): p. 629-635.
19. Sousa, R.A., *et al.*, Mechanical performance of starch based bioactive composite biomaterials molded with preferred orientation. Polymer Engineering and Science, 2002. 42(5): p. 1032-1045.
20. Liu, Q., J.R. de Wijn and C.A. van Blitterswijk, Composite biomaterials with chemical bonding between hydroxyapatite filler particles and PEG/PBT copolymer matrix. Journal of Biomedical Materials Research, 1998, 40(3): p. 490-497.
21. Midy, V., M. Dard and E. Hollande, Evaluation of the effect of three calcium phosphate powders on osteoblast cells. Journal of Materials Science: Materials in Medicine, 2001. 12(3): p. 259-265.
22. Heymann, D., J. Guichex and A.V. Rousselle, Ultrastructural evidence in vitro of osteoclast-induced degradation of calcium phosphate ceramic by simultaneous resorption and phagocytosis mechanisms. Histology and Histopathology, 2001. 16(1): p. 37-44.
23. Shirakata, Y., *et al.*, Histocompatible Healing of Periodontal Defects After Application of an Injectable Calcium Phosphate Bone Cement. A Preliminary Study in Dogs. Journal of Periodontology, 2002. 73(9): 1043-1053.

24. Correlo, V.M., *et al.*, Properties of Melt Processed Chitosan and Aliphatic Polyester Blends. Materials Science and Engineering: A, 2005. 403(1-2): p. 57-68.
25. Kesenci, K., *et al.*, Preparation and properties of poly(L-lactide)/hydroxyapatite composites. Journal of Biomaterials Science, Polymer Edition, 2000. 11(6): p. 617-632.
26. Hao, J.Y., M. L.Yuan and X.M. Deng, Biodegradable and biocompatible nanocomposites of poly(-caprolactone) with hydroxyapatite nanocrystals: Thermal and mechanical properties. Journal of Applied Polymer Science, 2002. 86(3): p. 676-683.
27. Honma, T., T. Senda and Y. Inoue, Thermal properties and crystallization behaviour of blends of poly(-caprolactone) with chitin and chitosan. Polymer International, 2003. 52(12): p. 1839-1846.
28. Chen, H.L., L.J. Li and T.L. Lin, Formation of Segregation Morphology in Crystalline/Amorphous Polymer Blends: Molecular Weight Effect. Macromolecules, 1998. 31(7) 2255-2264.
29. van Krevelen, D.W., Properties of Polymers, Elsevier, Amsterdam 1990.
30. Ramkumar, D.H.S., and M. Bhattacharya, Steady shear and dynamic properties of biodegradable polyesters. Polymer Engineering and Science, 1998. 38(9): p. 1426-1435.
31. Jamshidi, K., S.H. Hyon and Y. Ikada, Thermal characterization of polylactides. Polymer, 1988. 29(12): p. 2229-2234.
32. Dubnikova, I.L., V.G. Oshmyan and A.Ya. Greenberg, Mechanisms of particulate filled polypropylene finite plastic deformation and fracture. Journal of Materials Science, 1997. 32(6): 1613-1622.
33. Nielsen, L.E., Mechanical Properties of Polymers and Composites, Marcel Dekker, New York 1974.
34. Albelora, N.D. and P. Mele, Interface and mechanical coupling effects in model particulate composites. Polymer Engineering and Science, 1997. 37(10): p. 1712-1721.
35. Wang, K., S. Deb and W. Bonfield, Chemically coupled hydroxyapatite-polyethylene composites: processing and characterisation. Materials Letters, 2000. 44(2): p. 119-124.
36. Wang, K. and W. Bonfield, Chemically coupled hydroxyapatite–polyethylene composites: structure and properties. Biomaterials, 2001. 22(11): p. 1311-1320.
37. Sousa, R.A., *et al.*, Coupling of HDPE/hydroxyapatite composites by silane-based methodologies. Journal of Materials Science: Materials in Medicine, 2003. 14(6): p. 475-487.
38. Sousa, R.A., *et al.*, Structure Development and Interfacial Interactions in HDPE/HA Composites Moulded with Preferred Orientation. Journal of Applied Polymer Science, 2002. 86(11): p. 2873-2886.

39. Vaz, C.M., R.L. Reis and A.M. Cunha, Use of coupling agents to enhance the interfacial interactions in starch–EVOH/hydroxylapatite composites. Biomaterials, 2003. 23(2): p. 629-635.
40. Wang, M., *et al.*, Hydrostatically extruded HAPEX™. Journal of Materials Science, 2000. 35(4): p. 1023-1030.
41. Ladizesky, N.H., I. M. Ward and W. Bonfield, Hydrostatic extrusion of polyethylene filled with hydroxyapatite. Polymers for Advanced Technologies, 1997. 8(8): p. 496-504.
42. Rho, J.Y., L. Kuhn-Spearing and P. Zioupos, Mechanical properties and the hierarchical structure of bone. Medical Engineering and Physics, 1998. 20(2): p. 92-102.
43. Rho, J.Y., R.B. Ashman and C.H. Turner, Young's modulus of trabecular and cortical bone material: Ultrasonic and microtensile measurements. Journal of Biomechanics, 1993. 26(2): p. 111-119.
44. Clements, B.E. and E.M. Mas, Dynamic mechanical behavior of filled polymers. I. Theoretical developments. Journal of Applied Physics, 2001. 90(11): p. 5522-5534.
45. Chatani, Y., *et al.*, Structural studies of polyesters. III. Crystal structure of poly-ε-caprolactone. Polymer Journal, 1970. 1(5): p. 555-562.
46. Ihn, K.J., E.S. Yoo and S.S. Inn, Structure and morphology of poly(tetramethylene succinate) crystals. Macromolecules, 1995. 28(7): p. 2460–2464.

CHAPTER V.

Water absorption and degradation characteristics of chitosan-based polyesters and hydroxyapatite composites

CHAPTER V.

Water Absorption and degradation characteristics of chitosan-based polyesters and hydroxyapatite composites

Abstract

Blends of chitosan and biodegradable synthetic aliphatic polyesters (polycaprolactone, poly-(butylene succinate), poly[(butylene succinate)-co-adipate], poly[(butylene terephthalate)-co-adipate], and poly(lactic acid)) were injection-molded. These samples were immersed in isotonic solution at 37 ºC for a period of 60 d. The water uptake and the degradation properties, as measured by the loss in tensile strength, were evaluated as a function of time. In this study, the rate and the equilibriumwater uptake were proportional to the amount of chitosan in the blend. The addition of HA to chitosan and polyester significantly reduced the equilibrium water uptake. The water uptake did not follow the classical Fickian phenomena and could be expressed by a two-stage sorption non-Fickian diffusion model. Contact angle measurement was used to quantify the changes in surface hydrophilicity as a function of chitosan and polyester composition. The glycerol contact angle decreased with increasing synthetic components in the blend. The blends and composites also showed increased degradation, as quantified by a loss in their mechanical properties, with increase in natural content. The degradation of properties was directly related to the water uptake of the blends; the higher the water uptake, the higher the degradation. Pure polyesters, while having low water uptake, nevertheless showed significant degradation by a precipitous drop in the strain at break. Among the polyesters, poly(lactic acid) displayed maximum degradation, while polycaprolactone displayed the least.

This chapter is based on the following publication: **Correlo VM**, Pinho ED, Pashkuleva I, Bhattacharya M, Neves NM and Reis RL, 2007, Water absorption and degradation characteristics of chitosan-based polyesters and hydroxyapatite composites, Macromolecular Bioscience, **7(3)**:354-363

1. INTRODUCTION

Water uptake of polymeric implants affects their mechanical properties, degradability, and dimensional stability. These defects have the potential of compromising function and biocompatibility. Water exposure and uptake may decrease the life of an implant due to hydrolysis and microcrack formation. The amount of water uptake is determined by the diffusion coefficient of the material. High diffusion coefficients allow water to penetrate into the matrix enabling water-soluble additives, including growth factors that aid in tissue repair, to be released more rapidly. Studies have also shown that equilibrium water content and the organization of water within the matrix affect cell adhesion [1].

Similarly, the degradation of the polymeric matrix is of importance in the production and use of implantable devices, particularly those involved in bone fixation, bone regeneration, and tissue engineering [2,3]. The rate of degradation of these implants (loss in mechanical properties) should be tailored to the rate of tissue generation. The control of the hydrophilicity of a material helps in controlling the degradation rate of the material [4].

Another important property of a biomaterial is its surface characteristics. There has been major interest in these characteristics since it is the surface of these materials that first comes into contact with the biological surroundings. The change in the surface properties was found to affect the interaction of the surface with biomacromolecules, such as proteins [5–7], and with cells [7–9]. The energy of the surface, which is directly related to its wettability, is a useful parameter that has often correlated strongly with those biological interactions.

We have recently reported on the properties and morphology of chitosan-based polyester blends [10,11]. This work aims at reporting on the water absorption and degradation of the newly developed polymer blends and composites since these properties are critical for their possible applications as biomaterials.

2. MATERIALS AND METHODS

2.1. MATERIALS

The chitosan/polyester blends were compounded in a twin-screw extruder. The polyesters used include poly(ε-caprolactone) (PCL), poly(butylene succinate) (PBS), poly(lactic acid) (PLA), poly(butylenes terephthalate adipate) (PBTA), and poly(butylene succinate adipate) (PBSA). The chitosan used had a degree of deacetylation of approximately 85%. Briefly, the chitosan/polyester blends were prepared by

melt blending in a twin-screw extruder. These blends were then further compounded with hydroxyapatite (HA). In this study, the formulations of chitosan/polyester will be referred to as blends and the formulations containing chitosan/polyester/HA as composites. The details of the processing conditions are summarized elsewhere [10,11]. The extruded strands were ground to 5 mm diameter pellets using a Coloritron grinder. The blends were injection-molded using an ENGEL injection molding machine to produce tensile test bars. The tensile bars had a neck cross-section area of 24 mm^2 and a neck length of 20 mm.

2.2. WATER ABSORPTION

The molded samples were dried in a vacuum oven at 50 ºC until a constant weight was obtained. These samples were immersed in an isotonic solution of NaCl 0.154 M (9 $g.l^{-1}$) and pH 7.4 at 37 ºC for periods of 1, 3, 7, 14, 30, and 60 d. The samples were then removed at specific intervals, gently blotted with tissue paper to remove the excess water on the surface, and the weight recorded. This process was repeated at several time intervals. In order to ensure that no leaching had occurred, samples were dried at the end of the test period and weighed and compared against the original sample weight. Where leaching was found to occur, the data were corrected to account for the weight loss. The parameters D, Φ, and ψ were estimated for the data by non-linear regression routine (provided in Kaleidagraph, Synergy Software, Reading, PA, USA) based on a modified Levenberg–Marquardt algorithm.

2.3. DEGRADATION

The injection-molded samples were immersed in an isotonic saline solution for periods of 1, 3, 7, 14, 30, and 60 d. A solution of 40 ml was used for three samples (one batch). Two batches were used for each selected immersion period. At the end of each immersion period, the solution pH was measured. The weight loss was determined by drying the samples to constant weight and comparing to their initial weight. The tensile bars from the water absorption tests above were subjected to tensile testing using an Instron Universal Tensile Testing Machine. The tensile modulus was the initial slope of the force–deformation curve.

2.4. CONTACT ANGLE

The static contact angle measurements were obtained by the sessile drop method using a contact angle meter OCA15+ with a high-performance image processing system (DataPhysics Instruments, Germany). The liquid (glycerol or CH_2I_2, 1 µL, HPLC grade) was added by a motor-driven syringe at

room temperature. Five samples of each material were used, and six measurements were carried out for each sample. The data presented are an average of five readings. The polarity of the surface and the surface tension were calculated using Kaelble's equation.

3. RESULTS AND DISCUSSION

3.1. WATER ABSORPTION

The fractional water-uptake curves as a function of chitosan content and type of polyesters are shown in Figure 5.1 and 5.2.

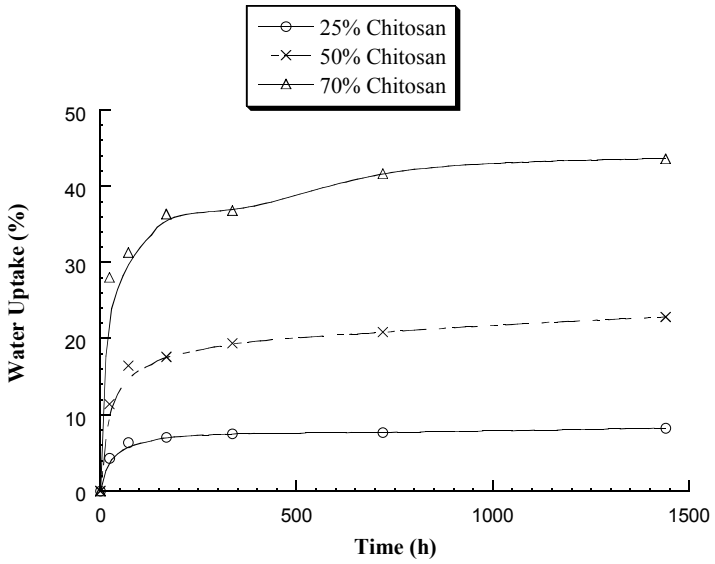

Figure 5.1. Water-uptake as a function of chitosan content for polybutylene succinate/chitosan blends.

As the chitosan content was increased, the water uptake increased and the time required to achieve the equilibrium water content increased. This was an expected result since chitosan is hydrophilic and the aliphatic polyesters are hydrophobic. Similar results are reported in the literature for polyester blends with other natural origin polymers like starch [12,13]. This is primarily due to the presence of amine and hydroxyl groups on the chitosan moiety, which is the most probable site for accommodation of the additional water.

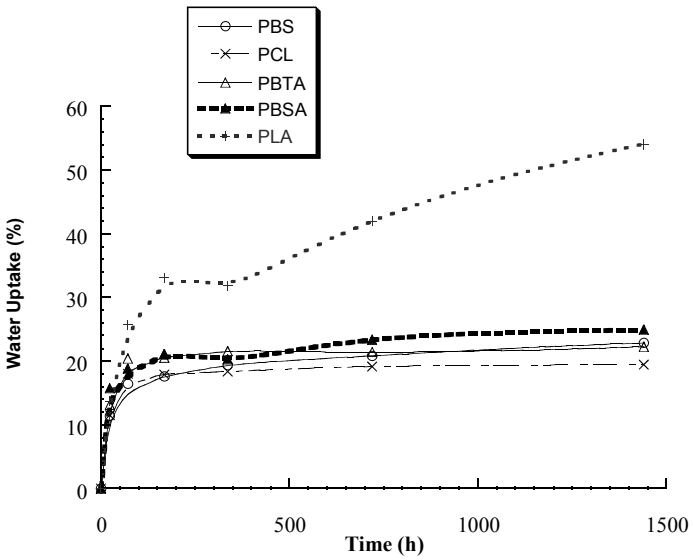

Figure 5.2. Water-uptake for different polyester blends containing 50% chitosan.

The water uptake characteristics of pure polyester (figure not shown) are typical of hydrophobic polymers, with PCL exhibiting the lowest equilibrium water uptake (0.5%) and other polymers at approximately 1.5% at the end of 60 d of immersion. The water absorption curves for blends containing 50% chitosan and different polyesters are shown in Figure 5.2. There is a sharp burst of water intake initially in all of the blends. Of the polyesters tested, the water uptake curves of PBS, PBSA, PCL, and PBTA are similar and have comparable times required to achieve equilibrium water uptake. The lowest equilibrium water content occurred with blends containing PCL. The highest water uptake was experienced with blends containing PLA. It was observed that the water absorption of PLA/chitosan blends does not attain an equilibrium value but displays a two-step kinetics. The first step is similar to other blends where the penetrant is picked up by the hydrophillic chitosan. SEM has shown that materials display a skin–core morphology with the skin being polyester rich while the core is a blend of chitosan and polyester [10]. Since chitosan is hydrophilic, it picks up water that diffuses into the polyester matrix even in the inner regions, increasing the equilibrium water uptake. The second step of the chitosan-PLA water uptake may be explained by the formation of micro-cracks in the surface (visible to the naked eye) of the specimens during the longer degradation stages. The higher water uptake could be the low crystallinity of PLA with respect to PBS, PCL, and PBSA. For PBTA, which is also mostly amorphous, the water absorption is sharply lower and thus can be attributed to the non-formation of micro-cracks. In an elastomerlike material the formation of micro-cracks is highly unlikely.

The addition of HA significantly reduces the equilibrium water uptake (Figure 5.3). Similar results were reported by Santos for BisGMA incorporated with HA [14]. This is due to the decrease in the amount of the hydrophilic component (chitosan) in the composite. However, these composites containing HA showed a significantly sharper uptake of water in the first few hours and achieved equilibrium water uptake much quicker than that of chitosanbased blends (Figure 5.1 and 5.2 versus Figure 5.3).

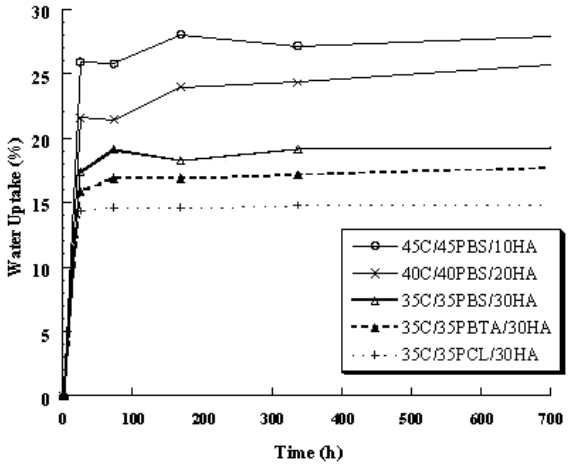

Figure 5.3. Water uptake for polyester / chitosan composites containing hydroxyapatite.

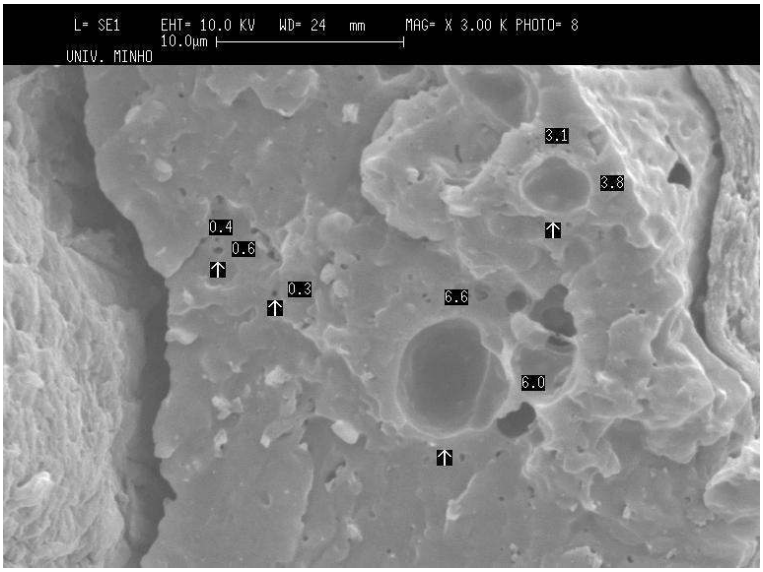

Figure 5.4. SEM image of the tensile fractured surface of the blend 35% chitosan, 35% PBS and 30% hydroxyapatite.

This can be explained from previous morphological observations using SEM that have shown that HA crystals have minimal adhesion to the polyester matrix [11]. This is seen in Figure 5.4 where cavities with smooth surface were formed due to the extensive detaching of HA crystals. This increase can be attributed to the presence of spaces between the HA and thematrix,where the adsorbed water is lodged. The interfaces between the HA crystals and chitosan/polyester matrix will work as micro-voids that will facilitate water diffusion into the specimens and reach chitosan domains easier. This will allow faster water diffusion and consequently a quicker achievement of the equilibrium water uptake or saturation.

The diffusion of a solvent into a polymeric matrix has been modeled by several researchers using Fick's second law, expressed as [14–19]

$$\frac{\partial C}{\partial t} = D\frac{\partial^2 C}{\partial x^2} \tag{1}$$

where *C* denotes the concentration of the diffusing solvent at time *t* along the axis *x*. If the initial concentration of the solvent is zero and the polymer is placed in an infinite bath of the solvent, the solution to Equation (1) is given by [20]

$$\frac{M(t)}{M_{eq}} = 1 - \frac{8}{\pi^2}\sum_{m=0}^{\infty}\frac{1}{(2m+1)^2}\exp\left[-\frac{\pi^2(2m+1)^2}{L^2}Dt\right] \tag{2}$$

Where *M(t)* is the water uptake at time *t*, M_{eq} the water uptake at $t=\infty$, and *L* the thickness of the sample. Adherence to Fickian behavior is determined by testing the conformity to the initial kinetics to $t^{0.5}$ scaling. At small times, when $M(t)/M_{eq}$ is small (<0.60), Equation (2) can be approximated by

$$\frac{M(t)}{M_{eq}} = \frac{4}{L}\sqrt{\frac{Dt}{\pi}} \tag{3}$$

Plots of $M(t)/M_{eq}$ against $t^{0.5}$ were found to be non-linear in the initial stages indicating that the process of solvent uptake follows an anomalous process. When a solvent penetrates a polymer, the movement of polymer chains is not sufficiently rapid to completely homogenize the penetrant's environment. This is particularly true of blends of hydrophilic and hydrophobic polymers where the penetrants have different diffusional mobilities. The relatively similar magnitude of the rates of diffusion and relaxation process leads to anomalous behavior during solvent uptake. On the other hand, when one dominates the other, Fickian diffusion is observed.

Morphological studies have shown that the blend systems are a two-phase system [10]. Hence, one would expect that the water diffusion into the polyester phase is different from that in the chitosan phase and would result in some deviations from the typical Fickian type of water diffusion which was derived for more homogeneous matrices.

Two-stage sorption, a notable non-Fickian phenomenon, has been observed by several authors [21, 22]. Berens and Hopfenberg [21] considered the sorption process as a linear superposition of phenomenologically independent contributions from Fickian diffusion and polymeric relaxation. The diffusion-controlled initial sorption is faster than the relaxation process, thus permitting explicit separation of the sorption process into two independent mechanisms. The resulting modification to Equation (2), assuming a first order relaxation process, results in the expression below:

$$\frac{M_t}{M_\infty} = \phi\left(1 - \frac{8}{\pi^2}\sum_{m=0}\frac{1}{(2m+1)^2}\exp\left(-\frac{(2m+1)^2\pi^2 Dt}{L^2}\right)\right) + (1-\phi)\left[1-\exp\left(-\psi\frac{Dt}{L^2}\right)\right] \qquad (4)$$

where ϕ is a measure of the ratio of the equilibria of the first stage to that of the second stage in the sorption, and ψ is the ratio of the characteristic diffusion time $\left(\frac{L^2}{D}\right)$ to the characteristic time of relaxation.

The diffusion coefficients calculated using Equation (4) are summarized in Table 5.1. The datasets for pure polymers were not considered since the differences between successive data points were too small to be determined with a fair degree of accuracy. The coefficient of determination (R^2) is

significantly higher using Equation (4) than Equation (2). The Fickian diffusion model [Equation (2)] fails in the case of datasets that have a sharp knee. Since ϕ can also be interpreted as the fraction of equilibrium amount of sorption in the unrelaxed polymer in the fully relaxed polymer [15], the higher ϕ values of 50Ch-50PBTA are reflection of low crystallinity of the continuous phase. For blends of chitosan and polyester, the ψ values are similar (0.32 – 0.75), indicating that the characteristic time of relaxation or the exchange between the two different modes is approximately 1.3 – 3.0 times of that of the diffusion time. For composites containing HA, the ratio ranges from 0.24 to 10.63.

Table 5.1. Water uptake parameters for various blend and composites compositions.

MATERIAL COMPOSITION	EQUILIBRIUM WATER CONTENT (%)	D (m^2/h) x 10^8	ϕ	ψ	R^2
25Ch-75PBS [a]	7.7	1.30	0.79	0.63	0.99
50Ch-50PBS [b]	21.4	1.61	0.68	0.52	0.99
50Ch-50PCL [c]	18.9	2.2	0.84	0.38	0.99
50Ch-50PBTA [d]	22.4	1.30	0.92	0.48	0.99
50Ch-50PBSA [e]	23.9	2.56	0.73	0.30	0.99
50Ch-50PLA [f]		0.82	0.49	0.75	0.99
70Ch-30PBS [g]	44.5	4.00	0.68	0.35	0.99
17.5Ch-52.5PBS-30HA [h]	3.9	9.43	0.0006	4.16	0.99
70PBS-30HA [i]	1.8	11.3	0.72	0.094	0.99
45Ch-45PBS-10HA [j]	24.2	17.62	0.88	0.24	0.99
40Ch-40PBS-20HA [l]	19.1	5.46	0.80	0.12	0.99
35Ch-35PBS-30HA [m]	8.3	4.02	0.95	0.39	0.99
35Ch-35PBTA-30HA [n]	11.0	5.21	0.91	0.36	0.99
35Ch-35PCL-30HA [o]	7.5	79.57	0.49	1.70	0.99

[a] Blend containing 25% by weight of chitosan and 75% by weight of PBS
[b] Blend containing 50% by weight of chitosan and 50% by weight of PBS
[c] Blend containing 50% by weight of chitosan and 50% by weight of PCL
[d] Blend containing 50% by weight of chitosan and 50% by weight of PBTA
[e] Blend containing 50% by weight of chitosan and 50% by weight of PBSA
[f] Blend containing 50% by weight of chitosan and 50% by weight of PLA
[g] Blend containing 70% by weight of chitosan and 30% by weight of PBS
[h] Composite containing 17.5% by weight of chitosan, 52.5% by weight of PBS and 30% by weight of hydroxyapatite
[i] Composite containing 70% by weight of PBS and 30% by weight of hydroxyapatite
[j] Composite containing 45% by weight of chitosan, 45% by weight of PBS and 10% by weight of hydroxyapatite
[l] Composite containing 40% by weight of chitosan, 40% by weight of PBS and 20% by weight of hydroxyapatite
[m] Composite containing 35% by weight of chitosan, 35% by weight of PBS and 30% by weight of hydroxyapatite
[n] Composite containing 35% by weight of chitosan, 35% by weight of PBTA and 30% by weight of hydroxyapatite
[o] Composite containing 35% by weight of chitosan, 35% by weight of PCL and 30% by weight of hydroxyapatite

The diffusivity of composites containing chitosan and HA is higher than those without HA even though the equilibrium water uptake is lower. The results imply that the penetrant diffuses and reaches equilibrium faster as the mass of the polymer that adsorbs the solvent decreases (HA has very low water absorption). The interfacial region between the HA and the matrix benefits the transport of the penetrant (diffusant); in consequence, the water diffuses mainly through the HA–matrix interface, reaching the saturation faster than in the blends.

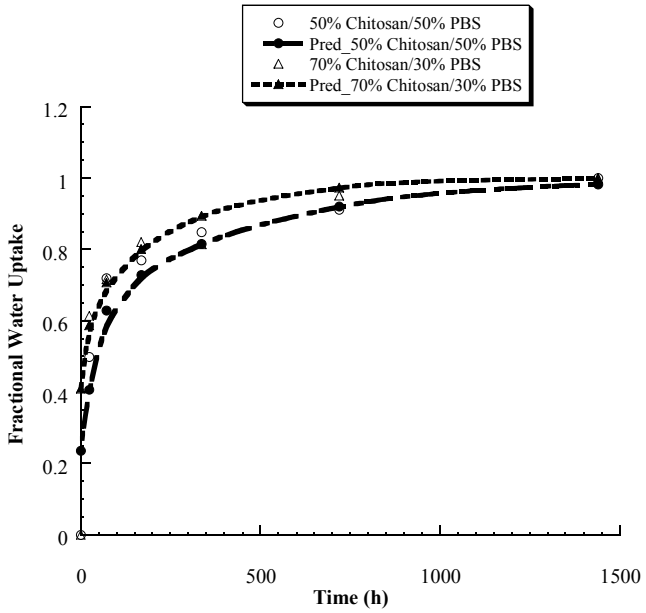

Figure 5.5. Comparison of predicted versus experimentally determined fractional water uptake for two different blend composition.

Using these values for diffusion coefficient, the water uptake profile was simulated using the first two terms and compared to the experimentally measured data. The simulated values are close to the experimentally measured ones for the entire duration (Figure 5.5). Equation (2) is derived under the assumption that the sample is homogeneous. The overall diffusion of water will depend on the degree of crystallinity and the morphology of the blends and is positiondependent. From a morphological point of view, water diffusion is different in the continuous phase (polyester) versus the dispersed phase (chitosan). Hence, when the solvent enters the system, there is a non-homogeneous distribution of the

diffusing solvent inside the polymeric matrix. One of the phases allows the penetrant to diffuse freely while the other immobilizes the penetrant, limiting its movement. The penetrant can become immobilized by reacting with functional groups on the polymers or getting lodged in holes and cavities. Perhaps a more appropriate model would have been the ‘‘dual-mode’’ model [21], which assumes that the transfer between the two modes can be described by a first-order reversible reaction. This leads to different relaxation times of polymer chains and, hence, anomalous effects in polymer–solvent diffusion. Three dimensionless numbers $\left(\theta = \frac{Dt}{L^2}, \phi, \psi\right)$ are used to account for the water uptake in these materials. The relative magnitude of the rates of diffusion and relaxation processes is a major factor in determining the deviations from Fickian sorptions [22].

Visual observations of samples after removal indicate some degree of swelling, particularly in blends containing higher amounts of chitosan (50% and above). The diffusion coefficient increases with the concentration of chitosan due to the increased free volume caused by the swelling effect of the penetrating solvent. Solvent adsorbed can be lodged in holes and cavities, thus hindering the diffusion process. In addition, the penetrating solvent (water) is reversibly bound to the amine and hydroxyl groups in the chitosan domains dispersed within the polyester matrix, leaving only the unbound water to contribute to the diffusion. The largest deviation from Fick’s model and the experimental data is obtained for chitosan and PLA. Of the polyester used in this study, PLA is the only polymer that has a glass transition temperature above the test temperature. The slow relaxation of the polymer chains due to the sorption of the solvent leads to deviation from the Fickian process [23–26].

3.2. CONTACT ANGLE

There are no direct methods to measure surface energy or surface tension of solids. However, a number of indirect empirical and semi-empirical methods have been developed based on contact angle measurements [27,28]. Kaelble’s equation is very often used to determine surface tension of the blends because of its simplicity. Moreover, Kaelble’s equation allows the determination of the polar components of the surface tension by measuring the contact angles of two liquids of known surface tension on the polymer surface:

$$\gamma_{lv1}(1+\cos\theta_1) = 2\sqrt{(\gamma_{lv1}^{d}+\gamma_{sv}^{d})} + 2\sqrt{(\gamma_{lv1}^{p}+\gamma_{sv}^{p})} \quad (5)$$

$$\gamma_{lv2}(1+\cos\theta_2) = 2\sqrt{(\gamma_{lv2}^{d}+\gamma_{sv}^{d})} + 2\sqrt{(\gamma_{lv2}^{p}+\gamma_{sv}^{p})} \quad (6)$$

where the subscripts 1 and 2 represent the liquids glycerol and methyleneiodine, respectively. The polar and dispersion components of the surface tension of the blends are shown in Table 5.2 and were obtained after solving Equation (5) and (6). The increase in the polar component is an indication of an increase in the polar groups existing on the surface.

Table 5.2. Contact angle values (θ1 with glycerol, θ2 with methyleneiodine), and surface tension components for chitosan and its blends with synthetic polyesters.

MATERIAL	θ_1 [deg]	θ_2 [deg]	γ^p [mN m^{-2}]	γ^d [mN m^{-2}]	γ [mN m^{-2}]
PLA [a]	70.47	48.76	5.14	34.97	40.11
Chitosan (Ch)	68.67	51.18	6.22	33.6	39.82
PBTA [b]	63.61	26.34	4.84	45.66	50.50
50Ch-50PBTA [c]	73.60	48.64	4.04	35.03	39.07
PCL [d]	66.53	33.09	4.51	42.89	47.40
50Ch-50PCL [e]	69.92	41.06	4.29	39.07	43.36
PBS [f]	67.23	45.53	5.85	36.73	42.58
70Ch-30PBS [g]	69.95	37.33	3.97	40.93	44.90
50Ch-50PBS [h]	61.30	40.02	7.32	39.60	46.92
25Ch-75PBS [i]	57.24	34.86	8.20	42.09	50.29

[a] poly(lactic acid)
[b] poly(butylene terephthalate adipate)
[c] Blend containing 50% by weight of chitosan and 50% by weight of PBTA
[d] poly-ε-caprolactone
[e] Blend containing 50% by weight of chitosan and 50% by weight of PCL
[f] poly(butylene succinate)
[g] Blend containing 70% by weight of chitosan and 30% by weight of PBS
[h] Blend containing 50% by weight of chitosan and 50% by weight of PBS
[i] Blend containing 25% by weight of chitosan and 75% by weight of PBS

PLA was used as a standard since it is a widely used biomaterial. Chitosan has a surface tension value similar to PLA (Table 5.2). Blending of chitosan with synthetic polyesters resulted in an increase in the surface tension over that of pure chitosan except in the case of chitosan/PBTA where the surface tension was mostly unaffected. This was expected since those blends have been showing skin–core morphology with the skin being rich in polyester [10]. The contact angle's values however were different from the ones measured for the pure synthetic polyesters. For PBTA and its blend with chitosan, which is mostly amorphous, the most significant difference was observed (surface tension of 50.50 and 39.07 $mN.m^{-2}$ respectively were calculated). A possible explanation for those observations could be an interaction such as hydrogen bonding between both the components that tie up the polar groups.

When the total surface free energies of the blends were separated into dispersive and polar components, the polar components exhibited a value close to that measured for pure synthetic polyesters. The magnitude of the dispersive components increased. The values obtained for the respective blends were between those of chitosan and those of polyesters, as was expected.

The influence of the chitosan/synthetic polyester ratios on the changes of surface hydrophilicity were studied for chitosan and PBS blends. Three different compounds with varying amounts of chitosan (Table 5.2) were studied. A decrease in the glycerol contact angle values was observed with the increase in synthetic component percentage. As a result, the highest surface tension of 50.29 $mN.m^{-2}$ was obtained for the lowest amount of chitosan in the blend chitosan/PBS (25:75). However, a different behavior for these blends was observed compared to the other two blends containing higher percentages of chitosan. Large changes in the polar component of the surface tension values from 3.97 to 8.20$mN.m^{-2}$ were observed. There are two possible reasons for this observation. The first is related to the shorter aliphatic chain of PBS, and the second is the possible interaction/chemical bond between PBS and chitosan. In both cases, a reduced flexibility of the chain results in a more ordered and oriented surface structure. Moreover, it should be noted that the wettability could not always be directly correlated to the surface composition [29]. When subjected to a change in environmental conditions, such as temperature or incubation medium, the surface composition can be altered by movements of certain components or groups to the surface [30]. Surface composition can vary during the measurements due to the possible interactions between the two phases; glycerol,which has hydroxyl groups, could form hydrogen bondswith the hydroxyl groups from thematerial and in this way orient them from the bulk to the surface. These interactions can depend on both the –OH end groups concentration and the mobility of the block to which the –OH belongs. On the other hand, diiodomethane and air do not have this

ability. Hence, there is no interaction, which moves these groups to the material surface, thus affecting wettability.

3.3. DEGRADATION

Pure polyesters show a very low percentage of water uptake. During the 60 d of immersion in the isotonic saline solution, the maximum water uptake was less than 1.5% for all of them and the weight loss of the pure polyesters was almost insignificant - at less than 0.5%. These results would indicate that there was minimal degradation. However, a plot of strain versus time curve for PBS immersed for different time periods in isotonic saline solution indicates that the degradation does occur (Figure 5.6). While the ultimate tensile strength (UTS) and the modulus (measured as the slope of the stress versus strain curve) remained invariant with time, a sharp decrease in the elongation to break was observed. The strain at break, decreased by over an order of magnitude after 60 d in an isotonic saline solution. Other polyesters showed a decrease in both strain and stress at break, indicating that there is a loss of mechanical properties without any appreciable weight loss.

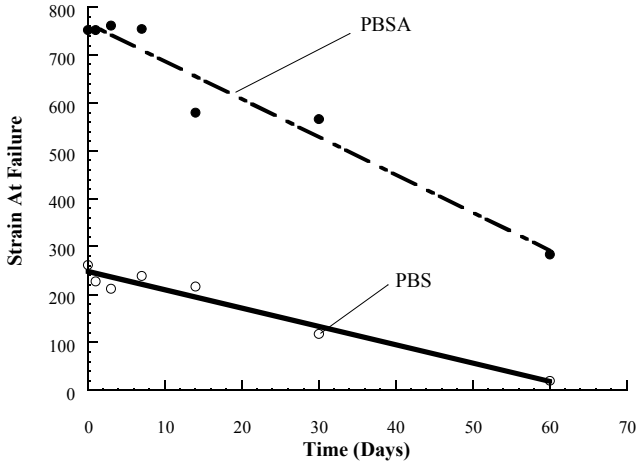

Figure 5.6. Strain at failure versus time of poly (butylenes succinate) and poly (butylene succinate adipate) as a function of immersion time in isotonic saline solution.

Of the other polyesters, PLA had the largest decrease in tensile strength (15%) and modulus (25%) while PCL had the least. The rate of hydrolytic degradation for aliphatic polyesters depends primarily on the kinetics of the cleavage of the ester bonds. Furthermore, the degradation is much faster in amorphous domains than in crystalline domains, as water penetration is easier within a disordered network of polymer chains. The difference in the degradation rate between PLA and PCL is probably related to the crystallinity of the two polyesters. Hence, the low rate of degradation observed for PCL is expected since it has the highest crystallinity, which makes it resistant to hydrolytic degradation. An ester bond within a crystalline domain is much more resistant than the same bond within an amorphous domain. Initial degradation also causes an increase in the number of carboxylic ends, which autocatalyzes the ester hydrolysis. The changes in strain at break are a result of chain scission. Using a similar reasoning, degradation is faster in amorphous domains above the glass transition temperature than below the glass transition temperature because of the enhanced mobility of chain segments. The decrease in weight was insignificant because the degradation occurred without any leaching.

The change in the UTS as a function of immersion time for various blend compositions is shown in Figure 5.7. The UTS was normalized with respect to the initial tensile strength. For blends with the same chitosan content [Figure 5.7(a)], the least degradation in terms of mechanical properties occurred for chitosan/PCL blends, while the most severe degradation occurred for chitosan/PLA blends. This is related to the fact that PCL is more crystalline and consequently less affected by hydrolytic degradation. PLA, on the other hand, is well known to be susceptible to hydrolytic degradation [31,32]. The water uptake of chitosan/PCL blends is significantly lower than that of chitosan/PLA, and this leads to increased hydrolytic degradation of the latter. Blends containing PBS, PBSA, and PBTA show a similar degradation rate, with PBTA having a slightly higher initial rate.

As the chitosan content increased [Figure 5.7(b)], the rate of decay of tensile strength increased. Blends containing 25% chitosan with PBS had a degradation rate similar to that of blends containing 50% chitosan with PCL, while blends containing 70% chitosan with PBS had a degradation rate similar to that of 50%chitosan with PLA (Figure 5.7). The same holds true for the modulus. This was a result of increased hydrolytic degradation due to increased water absorption. The deformation at break increased after degradation stages due to the presence of residual moisture that worked as a plasticizer. This residual water also contributes to the loss of stiffness. The loss in properties is primarily the effect of chitosan, which degrades and leaches out into the solution.

a)

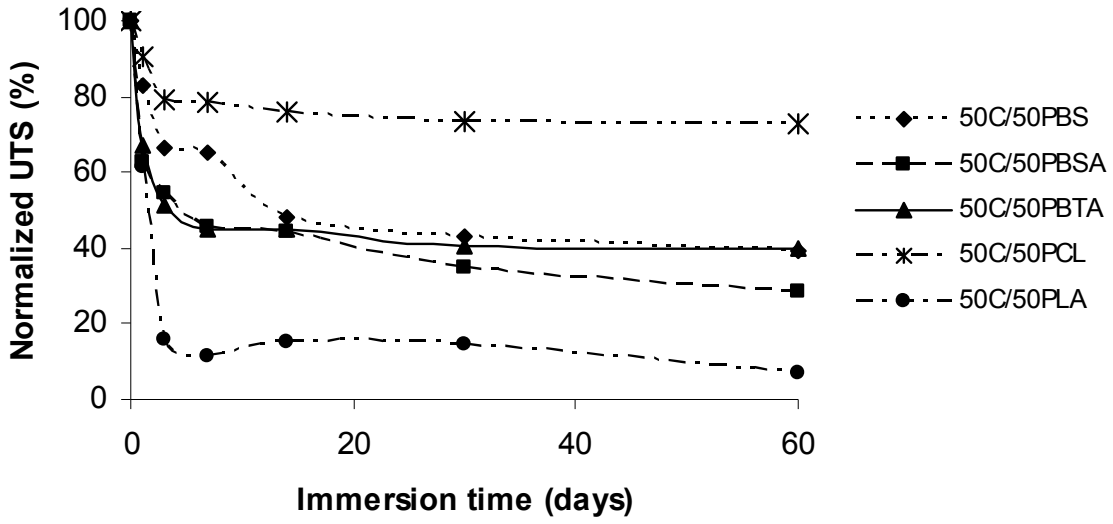

b)

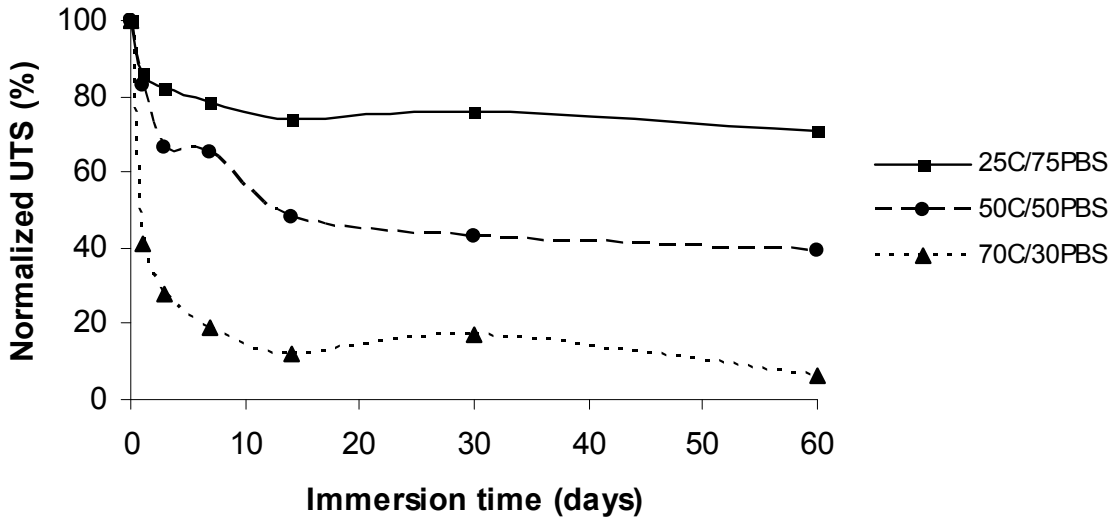

Figure 5.7. Degradation of mechanical properties of polyester/chitosan blends as a function of immersion time in isotonic saline solution.

a) different polyester blends containing 50% chitosan; b) chitosan/PBS blends with different chitosan amounts.

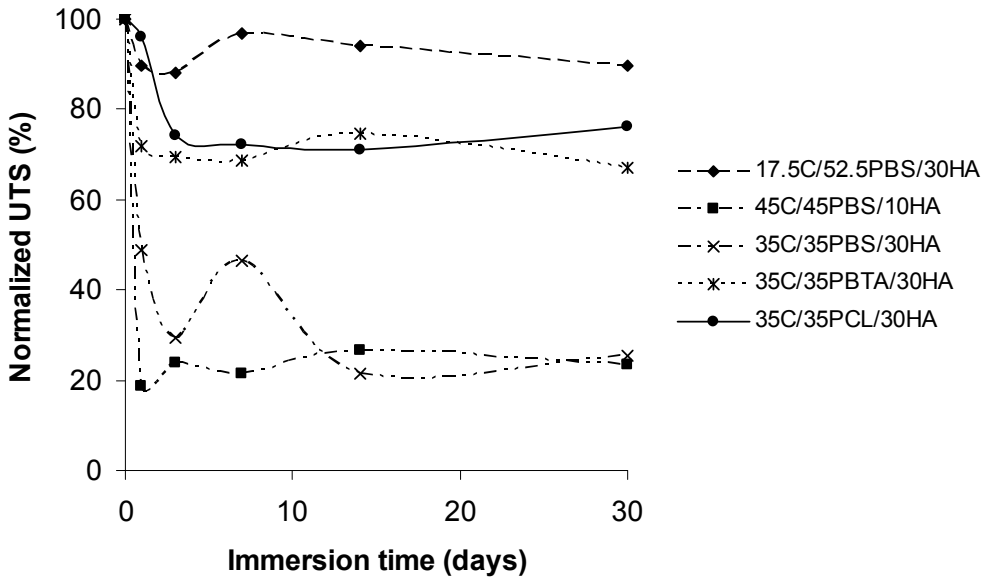

Figure 5.8. Degradation of mechanical properties of polyester/chitosan/hydroxyapatite blends as a function of immersion time in isotonic saline solution.

The change in mechanical properties during degradation as a function of HA content is given in Figure 5.8. For composites containing 30% HA by weight, those blended with chitosan/PBTA showed a lower percentage loss than those blended with chitosan/PBS. There appears to be a little difference in the final value of the normalized tensile strength as a function of HA content. It should be noted that even though the normalized tensile strength is higher in some cases for composites containing HA, the actual tensile strength for composites containing HA is always lower than those without HA. The kinetics of degradation of the system was investigated by evaluating a plot of property loss with time. The rate of change of a component, P is given by

$$-\frac{d[P]}{dt} = k[P]^n$$

Hence, a linear semi-log plot of *P* versus time can be considered to follow a first-order kinetics. This appears to be the case of most of the data (with the exception of PCL and blends containing PCL). There appears to be some scatter in the data which do not lend to the estimation of the time constant (*k*) with any reasonable degree of confidence. The fit for blends containing HA is poor, primarily because of the scatter in the data (Figure 5.8).

In terms of weight loss, the degradation behavior of all the chitosan/polyester blends and composites is typical of other natural-based biodegradable polymers [33–37]. For all the blends and composites, there are two different degradation stages (Figure 5.7 and 5.8). The first degradation stage, between 0 and 7 d, is characterized by a very fast water uptake and weight loss. In this stage, the mechanism responsible for this sharp increase in weight loss is a physical phenomenon. The higher amount of water uptake is responsible for the fast leaching of low molecular weight polymeric chains resulting from the thermomechanical degradation during processing. At the same time, the material swells and the water penetrates into the interface between the hydrophobic matrix and the hydrophilic disperse phase, releasing chitosan to the solution (and in some cases also HA). The chitosan release into the solution was responsible for the pH increase during the degradation periods (data not shown). This was independently verified by immersing 3.5 g of chitosan in 100 ml of distilled water (pH = 5.7) or buffer solution (pH = 7.7). After 2 h, the pH of both solutions increased significantly (10.0 for distilled water and 9.4 for the buffer). The chitosan release into the solution and consequent pH increase may influence the kinetics of degradation of polyesters. Wu et al. [38] have shown that PLGA scaffolds coated with chitosan absorbed more water but had a slower degradation ratio than uncoated scaffolds. The release of chitosan material causes an increase in the pH. This effect can neutralize the acidity associated with the degradation of PLGA. Thus, the degradation of chitosan can hinder the PLGA autocatalytic degradation and therefore retards its degradation kinetics.

The second degradation stage, between 15 and 60 d, corresponds to stabilization in water uptake andweight loss. The principal process involved in theweight loss during this period is chemical degradation (hydrolysis). The weight loss is less pronounced because low molecular weight polymeric chains resulting from the thermal degradation and the chitosan particles were released during the first stage. In this stage, the weight loss slows down because only low molecular weight fractions resulting from the hydrolysis of the polyesters are released and the pH decreases. The polyester degradation proceeds by chain scission resulting from hydrolysis of the ester links until the molecular weight has decreased to the point where fragments are small enough to diffuse from the polymer matrix into the

solution. Both these stages are characterized by a pronounced decrease in the UTS and modulus for all the blends. The strain at break for blends increased in all cases. Although the moisture present in the samples was stabilized before testing, some residual moisture was present. The residual moisture probably worked as a plasticizer.

The composites containing HA experienced higher weight loss. The weight loss increases as the HA content increases. This is related to the preferential attack at the polymeric–ceramic interface resulting in leaching of HA to the solution. Similar results were reported for other biodegradable polymers reinforced with HA [34,35]. During the extrusion processing of blends containing HA, 5% glycerol was added to enhance the plasticization process. The glycerol was released in the first degradation stage, contributing to the higher weight loss of chitosan-based blends containing HA. Furthermore, morphological studies of composites indicate poor adhesion between the HA and the matrix [11]. Hence, during the sharp initial uptake of water due to the preferential location of chitosan in the outer circumference of the core, the solvent molecules penetrate the cavities between the HA and the matrix. This would lead to loosening of the HA from the matrix leading to increase in leaching and weight loss. Since the addition of chitosan to the blends, results in higher water uptake (Figure 5.1), it also leads to higher weight loss. The blends with 70% chitosan have the highest weight loss (except the ones with HA), and the blends with 25% chitosan have the lowest weight loss. The increase in weight loss with the increase in chitosan present in the blend can be due to two mechanisms: both polyesters and chitosan degrade by hydrolysis. Higher water uptake promotes the hydrolysis and consequently the weight loss increases. Higher water uptake also promotes the erosion and diffusion of the chitosan particles from the matrix into the solution. The pH increased as a result of the release of chitosan particles into the solution. In the first degradation stage, the pH was higher for the blend containing 70 chitosan/30 PBS because the amount of chitosan released to the solution was higher. The fact that chitosan amount affects the degradation behavior of the blend is an important result because by controlling the chitosan percentage it is possible to tailor the degradation rate of the blend. In terms of weight loss, the blends containing the same amount of chitosan but different polyesters had a similar behavior.

4. CONCLUSIONS

The water absorption and degradation characteristics of chitosan-based polyesters and HA composites were studied. Pure polyesters showed hydrophobic behavior with low water uptake and displayed a decrease in the mechanical properties without any appreciable weight loss. Among the various

polyesters studied, PLA showed the largest decrease in mechanical properties while PCL showed the least.

Increased chitosan content increased the water uptake and diffusion coefficient of the blends. For blends with the same chitosan content, the lowest equilibrium water content was observed in blends containing PCL, and the highest water uptake was experienced by the blends containing PLA. The water absorption of all blends and composites deviated from the Fickian diffusion model and was modeled using a two-stage sorption. Composites containing HA had a lower water uptake than blends containing Chitosan but achieved equilibrium water uptake much faster than the blends.

Increased chitosan content significantly reduced the mechanical properties and increased the weight loss as a function of immersion time. Chitosan/PCL showed the lowest degradation among the different blends with the same chitosan amount, whereas chitosan/PLA showed the most severe property degradation (corresponding to the lowest and the highest water uptake, respectively). This observation is an indication that the degradation of properties with immersion time was directly related to the water uptake of the blends. The composites containing HA experienced larger weight loss. The weight loss also directly correlates with the HA content, as expected.

REFERENCES

1. Scotchford, C.A., *et al.*, Water uptake and protein release characteristics of a new methacrylate-based polymer system. Polymer, 1997. 38(15): p. 3869-3874.
2. Suarez, N., S. Brocchini and J. Kohn, The study of water uptake in degradable polymers by thermally stimulated depolarization currents. Biomaterials, 1998. 19(24): p. 2347-2356.
3. Lu, L., C.A. Garcia and A.G. Mikos, In vitro degradation of thin poly(DL-lactic-co-glycolic acid) films. Journal of Biomedical Materials Research, 1999. 46(2): p. 236-244.
4. Lydon, M.J., T.W. Minett and B.J. Tighe, Cellular interactions with synthetic polymer surfaces in culture. Biomaterials, 1985. 6(6): p. 396-402.
5. Sashiwa, H., et al., Chemical Modification of Chitosan: Preparation and Lectin Binding Properties of α-Galactosyl-chitosan Conjugates. Potential Inhibitors in Acute Rejection following Xenotransplantation. Biomacromolecules, 2000. 1(3): p. 303-305.

6. Chapman, R.G., et al., Polymeric Thin Films That Resist the Adsorption of Proteins and the Adhesion of Bacteria. Langmuir, 2001. 17(4): p. 1225-1233.
7. Khang, G., *et al.*, Interaction of different types of cells on physicochemically treated poly(L-lactide-co-glycolide) surfaces. Journal of Applied Polymer Science, 2002. 85(6): p. 1253-1262.
8. Schamberger, P.C. and J.A. Gardella, Surface chemical studies of aging and solvent extraction effects on plasma-treated polystyrene. Colloids and Surfaces B: Biointerfaces,1994. 3(4): p. 203-215.
9. Koyano, T., *et al.*, Attachment and growth of cultured fibroblast cells on PVA/chitosan-blended hydrogels. Journal of Biomedical Materials Research, 1998. 39(3): p. 486-490.
10. Correlo, V.M., *et al.*, Properties of melt processed chitosan and aliphatic polyester blends. Materials Science and Engineering: A, 2005. 403(1-2): p. 57-68.
11. Correlo, V.M., *et al.*, Hydroxyapatite Reinforced Chitosan and Polyester Blends for Biomedical Applications. Macromolecular Materials and Engineering, 2005. 290(12): p. 1157-1165.
12. Mani, R. and M. Bhattacharya, Properties of injection moulded blends of starch and modified biodegradable polyesters. European Polymer Journal, 2001. 37(3): p. 515-526.
13. Wang, H., X. Sun and P. Seib, Mechanical properties of poly(lactic acid) and wheat starch blends with methylenediphenyl diisocyanate. Journal of Applied Polymer Science. 2002. 84(6): p. 1257.-1262
14. Santos, C., *et al.*, Water absorption characteristics of dental composites incorporating hydroxyapatite filler. Biomaterials, 2002. 23(8): p. 1897-1904.
15. Sun, Y.M., Sorption/desorption properties of water vapour in poly(2-hydroxyethyl methacrylate): 2. Two-stage sorption models. Polymer, 1996. 37(17): p. 3921-3928.
16. Han, H., C.C. Gryte and M. Ree, Water diffusion and sorption in films of high-performance poly(4,4'-oxydiphenylene pyromellitimide): effects of humidity, imidization history and film thickness. Polymer, 1995. 36(8): p. 1663-1672.
17. Nogueira, P., *et al.*, Effect of water sorption on the structure and mechanical properties of an epoxy resin system. Journal of Applied Polymer Science, 2001. 80(1): p. 71-80.
18. Asaoka, K. and S. Hirano, Diffusion coefficient of water through dental composite resin. Biomaterials, 2003. 24(6): p. 975-979.
19. Sideridou, I., *et al.*, Water sorption characteristics of light-cured dental resins and composites based on Bis-EMA/PCDMA. Biomaterials, 2004. 25(2): p. 367-376.

20. Crank, J., Mathematics of Diffusion, Second edition, Oxford University Press. Great Calendron Street Oxford OX2 6DP 1975.
21. Berens, A.R. and H.B. Hopfenberg, Diffusion and relaxation in glassy polymer powders: 2. Separation of diffusion and relaxation parameters. Polymer, 1978. 19(5): p. 489-496.
22. Joshi, S. and G. Astarita, Diffusion-relaxation coupling in polymers which show two-stage sorption phenomena. Polymer, 1979. 20(4): p. 455-458.
23. Vrentas, J.S. and J.L. Duda, Diffusion in polymer-solvent systems. III. Construction of Deborah number diagrams. Journal of Polymer Science: Polymer Physics Edition, 1977. 15(3): 441-453.
24. McCall, D.W., *et al.*, Solubility and diffusion of water in low-density polyethylene. Macromolecules, 1984. 17(9): p. 1644-1649.
25. Valles, J.L. and J.W. Halley, Molecular dynamics model of absorption of water in polymers. Journalof Chemical Physics, 1990. 92(1): p. 694-698.
26. Vrentas, J.S., C.M. Jarzebski and J.L. Duda, A Deborah number for diffusion in polymer-solvent systems. AIChE Journal, 1975. 21(5): p. 894-901.
27. Ratner, B.D., Surface properties of materials, in: Biomaterials Science: An introduction to Materials in Medicine, B. D. Ratner, A. Hoffman, F. Schoen, J. Lemon, Eds., Academic Press, New York 1996, Vol. 1 , p. 21.
28. Ch.-M. Chan, Contact angle measurement, in: Polymer Surface Modification and Characterization, Hanser Publishers, Munich 1994.
29. Toselli, M., *et al.*, Poly(ε-caprolactone)-poly(fluoroalkylene oxide)-poly(ε-caprolactone) block copolymers. 2. Thermal and surface properties. Polymer, 2001. 42(5):, p. 1771-1779.
30. Santerre, J.P. and R.S. Labow, The effect of hard segment size on the hydrolytic stability of polyether-urea-urethanes when exposed to cholesterol esterase. Journal of Biomedical Materials Research, 1997. 36(2): 223-232.
31. Ramkumar, D.H.R. and M. Bhattacharya, Steady shear and dynamic properties of biodegradable polyesters. Polymer Engineering and Science, 1998. 38(9): p. 1426-1435.
32. Jamshidi, K., S.H. Hyon and Y. Ikada, Thermal characterization of polylactides. Polymer, 1988. 29(12): p. 2229-2234.
33. Reis, R.L., *et al.*, Processing and in vitro Degradation of Starch/EVOH Thermoplastic Blends. Polymer International, 1997. 43(4): p. 347-352.

34. Demirgo¨z, D., *et al.*, Chemical modification of starch based biodegradable polymeric blends: effects on water uptake, degradation behaviour and mechanical properties. Polymer Degradation and Stability, 2000. 70(2): p. 161-170.
35. Alberta Araújo, M., *et al.*, *In-vitro* degradation behaviour of starch/EVOH biomaterials. Polymer Degradation and Stability, 2001. 73(2): p. 237-244.
36. Vaz, C.M., A.M. Cunha and R.L. Reis, Degradation model of starch-EVOH+HA composites. Materials Research Innovations, 2001. 4(5-6): p. 375.
37. Azevedo, M.C., *et al.*, Development and properties of polycaprolactone/hydroxyapatite composite biomaterials, Journal of Materials Science-Materials in Medicine, 2003. 14(2): p. 103-107.
38. Wu, Y.-C., *et al.*, Bone tissue engineering evaluation based on rat calvaria stromal cells cultured on modified PLGA scaffolds. Biomaterials, 2006. 27(6): p. 896-904.

CHAPTER VI.

Melt-based compression-molded scaffolds from chitosan–polyester blends and composites: morphology and mechanical properties

CHAPTER VI.

Melt-based compression-molded scaffolds from chitosan–polyester blends and composites: morphology and mechanical properties

Abstract

Blends of chitosan and synthetic aliphatic polyesters (polybutylene succinate, polybutylene succinate adipate, polycaprolactone, and polybutylene terepthalate adipate) were compounded with and without hydroxyapatite, a bioactive mineral filler known to enhance osteoconduction. The blends and composites were compression molded with two different granulometric salt sizes (63–125 μm and 250–500 μm) having different levels of salt content (60, 70, and 80%) by weight. By leaching the salt particles, it was possible to produce porous scaffolds with distinct morphologies. The relationship between scaffold morphology and mechanical properties was evaluated using scanning electron microscopy, microcomputed tomography, compression testing, differential scanning calorimetry, small-angle X-ray scattering (SAXS), and wide-angle X-ray scattering. The produced scaffolds are characterized by having different morphologies depending on the average particle size and the amount of NaCl used. Specimens with higher porosity level have a less organized pore structure but increased interconnectivity of the pores. The stress–strain curve under compression displayed a linear elasticity followed by a plateau whose characteristics depend on the scaffold polymer composition. A decrease in the salt particle size used to create the porosity caused in general a decrease in the mechanical properties of the foams. Composites with hydroxyapatite had a sharp reduction in yield stress, modulus, and strain at break. The melting temperature decreased with increased chitosan content. SAXS results indicate no preferential crystalline orientation in the scaffolds. Cytotoxicity evaluation were carried out using standard tests (accordingly to ISO/EN 10993 part 5 guidelines), namely MTS test with a 24-h extraction period, revealing that L929 cells had comparable metabolic activities to that obtained for the negative control.

This chapter is based on the following publication: **Correlo VM**, Boesel LF, Pinho ED, Costa-Pinto AR, Alves da Silva ML, Bhattacharya M, Mano JF, Neves NM and Reis RL, 2008, Melt-based compression moulded scaffolds from chitosan-polyester blends and composites: morphology and mechanical properties, Journal of Biomedical Materials Research: Part A (DOI - 10.1002/jbm.a.32221)

---

1. INTRODUCTION

Tissue engineering has recently boosted the interest in producing porous structures for scaffolding in tissue regeneration. The underlying principle in tissue engineering is that cells isolated from a patient are cultured, expanded, and even induced to differentiate in vitro in a cell culture. Still in vitro, the cells are seeded onto a scaffold being further matured in vitro, eventually in dynamic culture conditions, after which is implanted back into the patient defect to act as an inductor for regeneration of the tissue [1]. The porous scaffold provides surface area for further cell expansion and colonization of the whole volume, favoring diffusion of nutrients and metabolites and providing temporary support for the cells.

Ideal scaffolding materials for use in hard tissue engineering must satisfy certain requirements. The materials (and their degradation products) must be noncytotoxic and allow production of biocompatible structures adapted to the tissue to be regenerated. The materials should be biodegradable with an adjustable degradation rate that should match closely the rate of tissue regeneration. The scaffold must also possess mechanical properties adequate to support morphogenesis of the neotissue and also to allow for manipulation of the device. It should provide appropriate surface chemistry to facilitate cell attachment, proliferation, and differentiation. Moreover, it should possess the appropriate pore size and interconnected pore network to facilitate extracellular matrix production and tissue ingrowth, enable vascularization to develop, improve oxygen and nutrients supply, and metabolite removal [2].

Materials that have been evaluated for use in tissue engineering constructs include synthetic polymers, natural polymers, ceramics, metals, and many combinations of the aforementioned types. However, it is highly desirable that the constructs biodegrade, enabling designing temporary systems that maintain available space for the regenerated tissue. Biodegradable aliphatic polyesters such as poly(lactic acid), poly(glycolic acid), polycaprolactone (PCL), and their copolymers are the most widely used synthetic polymers in the field of bone and cartilage tissue engineering.

A natural polymer that has received increased attention in the biomedical field is chitosan. Chitosan can be obtained by alkaline deacetylation of chitin, the second most abundant natural polysaccharide being extracted mainly from the exoskeleton of shellfish [3]. Because of the *N*-acetyl glucosamine repeating units, the chitosan structure is similar to glucosaminoglycans and seems to mimic their functional behavior. The scientific basis for the utility of *N*-acetylglucosamine in enhancing the promotion of wound healing is well documented [4,5].

Studies have been devoted to produce blends of synthetic polymers with chitosan to combine the superior mechanical properties of the synthetic polymers with the biocompatibility and biological interactions of the natural polymer [6,7]. The properties of a scaffold depend not only on the selected material but also on the technology used for its processing. Methods based on the leaching of soluble particulates are widely employed in the fabrication of 3-D porous structures (scaffolds) [8–20]. By these methods, the porosity can be controlled by varying the amount of leachable particles. The pore size and pore morphology can be adjusted, independent of the porosity, by using particles of different sizes and different morphologies [8,9]. To improve the structure and to increase the pore interconnectivity of the porous scaffold, particulate leaching has been used in combination with other techniques, namely: solvent casting [9,10], gas forming [11,12], freeze-drying [13], injection molding [14], extrusion [15] and compression molding [8,16,17]. Some of these methods require the use of organic solvents (e.g., solvent casting followed by particulate leaching). Residual traces of organic solvents used in the process may remain entrapped in the scaffold and eventually damage the cells seeded onto the scaffolds or tissues at the transplantation site [18,19].

Significant efforts have been made to manufacture porous scaffolds without organic solvents for tissue engineering applications [11,12,18–20]. One such technology involves melt-based compression molding followed by particulate leaching. The process involves physically mixing a polymer (usually in the powder form) with defined amounts of calibrated leachable particles and loading this powder onto a mold. This is followed by the application of heat and pressure (compression) that result in the melting of the polymeric phase. The compression maximizes the packing of the mixture. The heating process causes the fusion of the polymer particles and promotes the formation of a continuous polymeric network that provide mechanical stability to the structure. The last stage consists in immersing the molded polymer–porogen composite in a solvent that selectively dissolves the porogen agent. This methodology has been successfully applied in the production of natural origin starch-based scaffolds [21].

This study reports on the production of novel scaffolds made from blends of chitosan and biodegradable synthetic aliphatic polyesters produced by the melt-based routine involving compression molding and salt leaching. The motivation for this work was to develop and to produce a new range of chitosan based scaffolds using novel polymeric matrices in an established melt processing technology. Most of the approaches reported in the literature to produce scaffolds from chitosan-based blends or composites involve the use of solvents, this work being the first reporting the use of a melt-based route. Moreover, the methodologies described in this article are very versatile and avoid the drawbacks associated with

solvents and allows producing a large variety of scaffolds with a wide range of porosities and pore morphologies using different polymers. The scaffolds were made with different pore sizes and porosity, aiming at applications in bone and cartilage tissue engineering. We report herein the mechanical and thermal properties and morphology of the newly developed 3-D constructs.

2. MATERIALS AND METHODS

2.1. MATERIALS

The polyesters used in this study include poly-ε-caprolactone (PCL), poly(butylene succinate) (PBS), poly(butylenes terepthalate adipate) (PBTA), and poly(butylene succinate adipate) (PBSA). The chitosan used had a degree of deacetylation of ≈85%. Polycaprolactone resins PCL 787 (MFI ≈ 4), commercially available as TONE™ polymer, were obtained from Union Carbide Chemicals and Plastics Division, Bound Brook, New Jersey. Eastar Bio Copolyester 14766™, a butanediol, adipate, and terephthalate copolymer (MFI ≈ 20), was obtained from Eastman Chemical Company, Kingsport, Tennessee. Bionolle™ 1050, a PBS copolymer (MFI ≈ 20), was obtained from Showa Highpolymer Co. Ltd., Tokyo, Japan. The melt flow indices were determined using ASTM test method D 1238 at 190 ºC using a 2.16 kg load. Hydoxyapatite (grade Capital S) was obtained from Plasma Biotal Ltd. (U.K).

2.2. PROCESSING OF SCAFFOLDS

The chitosan/polyester blends and composites were compounded in a twin-screw extruder. The details of the processing conditions are described elsewhere [22,23]. Salt was obtained from a local grocery store. The group of the larger range of NaCl particles (250–500 μm) was obtained by sieving the raw material. The second group (63–125 μm) was obtained by grinding the raw material that was further sieved. The compounded blends or composites were ground, mixed with salt, loaded into a mold that was further heated, and compression molded into discs. The salt content was 60 and 80% by weight for blends and 60 and 70% by weight for composites containing hydroxyapatite (HA).

The aim of using two different salt amounts and two different salt particle size ranges was to produce scaffolds with varying amounts of porosity and pore sizes and analyze the effect of these parameters on the morphology and mechanical of the developed scaffolds. Some scaffolds were selected to analyze the effect of compression-molding processing method on the crystallinity and thermal properties of the polyester part.

The compression-molded discs were further sliced to obtain cubes with nominal dimensions of 5 mm. The cubes were then immersed in distilled water to leach out the porogen. The water was replaced daily. Preliminary studies had shown that immersing for a period of 6 days would enable the entire salt to leach out. The cubes were dried to constant weight and used for further testing. The various scaffolds composition, levels of porosity and pore size are summarized in Table 6.1.

Table 6.1. Composition, porosity and pore size of the scaffolds produced from chitosan-polyester blends and salt particle size ranging from 63 -125μm or 250 -500μm.

COMPOSITION	SALT PARTICLE SIZE (μm)	SALT CONTENT (WT%)	POROSITY (%)	PORE SIZE (μm)
25C-75PBS [a]	63-125	60	-	-
		80	-	-
	250-500	60	57.8±3.0	226.0±16.9
		80	74.2 ±2.3	236.2±7.4
50C-50PBS [b]	63-125	60	54.3 ±1.4	109.3±2.6
		80	78.6±2.5	276.8±52.5
	250-500	60	57.7±6.6	199.3±5.3
		80	77.4±2.2	280.5±42.9
50C-50PBTA [c]	63-125	60	54.6±1.5	125.4±1.4
		80	75.8±1.8	258.5±15.8
	250-500	60	55.7±4.6	202.2±3.7
		80	73.4±4.7	232.2±4.9
50C-50PCL [d]	63-125	60	58.1±3.0	154.2±13.1
		80	80.6±1.9	336.0±35.5
	250-500	60	62.8±2.1	212.8±6.8
		80	76.9±7.4	266.3±32.7
70C-30PBS [e]	63-125	60	47.9±0.7	98.6±2.3
		80	-	-
	250-500	60	51.7±1.9	221.3±4.2
		80	-	-

[a] Blend containing 25% by weight of chitosan and 75% by weight of PBS
[b] Blend containing 50% by weight of chitosan and 50% by weight of PBS
[c] Blend containing 50% by weight of chitosan and 50% by weight of PBTA
[d] Blend containing 50% by weight of chitosan and 50% by weight of PCL
[e] Blend containing 70% by weight of chitosan and 30% by weight of PBS

2.3. MECHANICAL PROPERTIES

Uniaxial compression tests were performed on the cubic scaffolds using a Universal tensile testing machine (Instron 4505 Universal Machine, USA). Each specimen measured 5 mm in the direction of

testing and was 5 mm square in crosssection. Samples were conditioned at room temperature for at least 48 h before testing. A crosshead speed of 2 $mm.min^{-1}$ was used in the compression tests. The values reported are the average of at least five specimens per condition. The compressive modulus was determined in the most linear region of the stress–strain graph and in the cases that the yield stress was not clear it was calculated as the stress at the intersection of a line drawn parallel to the linear region and intercepting the *x*-axis at 1% strain.

2.4. MORPHOLOGICAL ANALYSIS

The cross-section of all the developed scaffolds was analyzed using a Leica-Cambridge S-360 scanning electron microscope (SEM) for preliminary assessments on the morphology of the scaffolds. All the samples were sputtercoated with gold prior to SEM observations. Microcomputed tomography (μCT) equipment (SkyScan, Belgium) was used as a nondestructive technique for a very detailed analysis of the morphology of the developed scaffolds using only chitosan-based blends. Four scaffolds of each condition were scanned in high-resolution mode of 8.7 μm *x/y/z* and an exposure time of 1792 ms. The energy parameters defined in the scanner were 63 keV with a current of 157 μA. Isotropic slice data were obtained by the system and reconstructed in 2-D images. These slice images were compiled and analyzed to render 3-D images and obtain quantitative architecture parameters. A μCT analyser and a μCT Volume Realistic 3-D Visualization, both from SkyScan, were used as image processing tools for both μCT reconstruction and to create/visualize the 3-D representation. Regions of interest (square of 4.5x4.5 mm^2) were selected in each slice image and thresholded to eliminate background noise. This threshold (to distinguish polymer material from pore voids) was chosen and maintained constant for all the scanned specimens and samples. The threshold was also inverted to obtain pore volume and to analyze both the pore morphology and its interconnectivity.

2.5. DIFFERENTIAL SCANNING CALORIMETRY

The differential scanning calorimetry (DSC) experiments were performed in a Perkin-Elmer DSC7 apparatus using a water cooling accessory and nitrogen as a purge gas (flux gas of ca. 20 cm^3/min). Both temperature and heat flux were calibrated with indium (99.99999% purity) at a scanning rate of 208C/min. The samples were obtained by cutting a small piece of the scaffold, with about 10 mg weight. All the experiments were performed at 208C/min, starting from room temperature. Only the first run samples were analyzed, which reflects both the type of existing materials and the general morphology developed during processing.

2.6. CRYSTALLINITY

Wide-angle X-ray scattering (WAXS) and small-angle Xray scattering (SAXS) experiments on some representative scaffolds were performed using X-ray synchrotron radiation at the Soft Condensed Matter A2 beamline of DESYHASYLAB (Hamburg, Germany). The experimental setup includes a MARCCD detector for acquiring two-dimensional SAXS patterns (sample-to-detector distance being 280 cm) and a linear detector for 1D WAXS measurements (distance 23 cm).

2.7. CELL CYTOTOXICITY ASSAYS

A rat lung fibroblast cell line -L929-, acquired from the European Collection of Cell Cultures, was used to perform cytotoxicity tests. Cells were grown as monolayers in Dulbecco's modified eagle's medium (Sigma, St. Louis, MO) supplemented with 10% fetal bovine serum (Biochrom, Berlin, Germany) and 1% of antibiotic–antimycotic mixture (10,000 U/mL penicillin G sodium; 10,000 U/mL streptomycin sulphate; 25 µg/mL amphotericin B) (Gibco, Invitrogen, USA). Trypsin/EDTA (0.25% w/v trypsin/0.02% EDTA, Sigma) was used to detach the cells from the culture flasks before the experiments were conducted. Cells were seeded in 96-well plates (n = 6) at a density of 1.8 x 10^4 cells/well and incubated for 24 h at 37 ºC, in a humidified atmosphere with 5% CO_2.

The ratio of material weight to extract fluid was constant and equal to 0.25 g/mL. Latex rubber was used as a positive control of cell death, because it has a strong cytotoxic effect leading to extensive cell death. The ratio of latex material outer surface to extraction fluid was 2.5 cm^2/mL. Culture medium was used as negative control of cytotoxicity, considered to be the ideal situation of cell growth. Test scaffolds (n = 6) and positive control were extracted for 24 h at 37 ºC, using complete culture medium as the extraction fluid. Before the tests, culture medium was removed from wells with cells adhered, and an identical volume (200 µL) of extraction fluid was added. The cells were left to proliferate in the extract fluid for 72 h. After this period, the extraction fluid was removed, and the serum-free culture medium without phenol red and a substrate-3-(4,5-dimethylthiazol-2-yl)-5(3-carboxymethoxyphenyl)-2(4-sulfofenyl)-2*H*-tetrazolium (MTS; CellTiter 96 One solution Cell Proliferation Assay kit; Promega, Madison, WI), in a proportion of 5:1, was added to each well. This reaction is based on the reduction of MTS, into a brown formazan product by an enzyme—dehydrogenase—active in all viable cells.

Cells were then incubated for 3 h at 37 ºC in a humidified atmosphere containing 5% CO_2. After this period, optical density (OD) was measured with a plate reader (Biotek, model Synergy HTi) at 490 nm. The mean OD value obtained was standardized taking into account the values for the negative control.

3. RESULTS AND DISCUSSION

3.1. MORPHOLOGICAL CHARACTERIZATION

The cross-sectional pore morphology of scaffolds after salt leaching was analyzed using SEM.

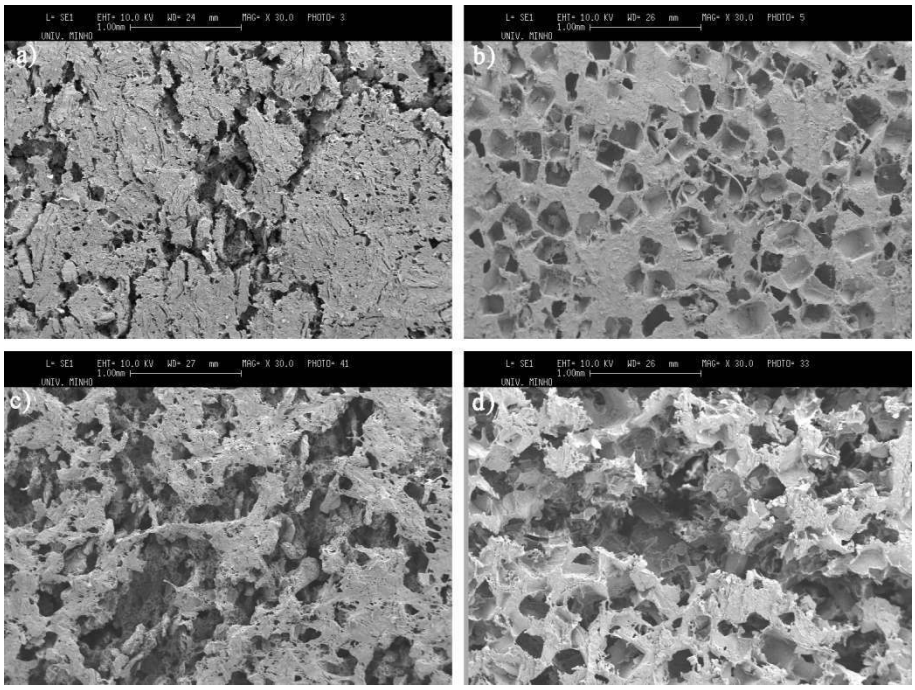

Figure 6.1. Representative SEM images of the scaffolds obtained with different amounts of salt and different granulometric size particles: a) 60 wt% of NaCl particles with size 63-125 μm; b) 60 wt% of NaCl particles with size 250-500 μm; c) 80 wt% of NaCl particles with size 63-125 μm; d) 80 wt% of NaCl particles with size 250-500 μm.

No significant morphological differences were observed between the scaffolds of different polymeric materials produced with both the same range of particle size and same amount of salt. This indicates that material composition does not significantly affect the morphology of the developed scaffolds. However, variations in the amount and/or in the range of NaCl average particle size affected the porosity and pore structure of the scaffolds.

Considering that material composition did not affect porosity and pore morphology, the produced scaffolds were divided into four groups in order to analyze the effect of the other two variables (salt amount and range of salt particle size) into pore morphology and porosity. Representative SEM images of the four different groups are presented in Figure 6.1. Qualitative analysis of the scaffolds architecture can be made by studying these images. Increasing the amount of salt particles resulted in an increased porosity and interconnectivity in both salt particle size ranges. Using salt particles with different size range also affected the pore morphology. In the case of using larger salt particle size (250–500 μm), the pores in the scaffolds mimic the cubic salt crystals with a narrow distribution of average pore size that is consistent with the size of the particles used [Fig. 6.1(b,d)].

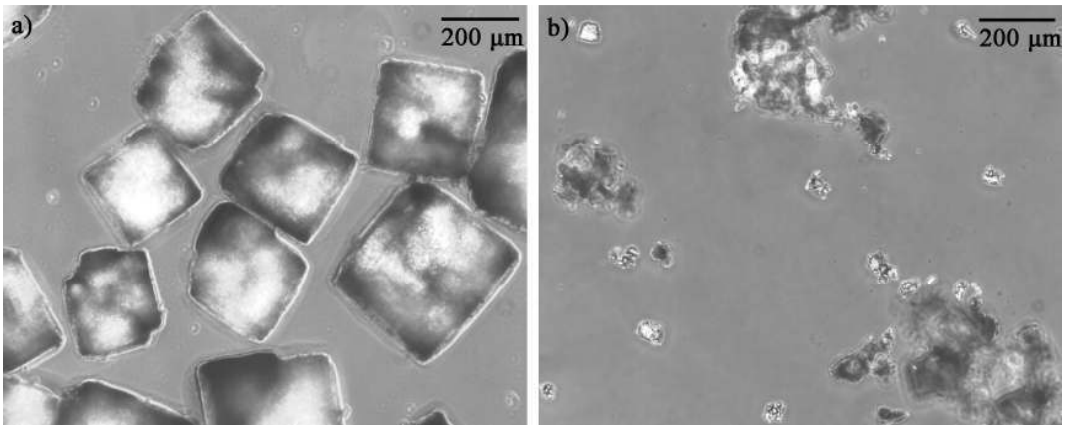

Figure 6.2. Optical microscopy using phase contrast mode images of the different salt particles: a) particle size between 250-500 μm; b) particle size between 63-125 μm.

Scaffolds obtained using smaller salt particles (63–125 μm) do not show a clear relation between the pore structure and the particle shape [Fig. 6.1(a,c)]. In these cases, a larger pore size distribution is observed. The average pore size is larger than the particle size used, probably because of clustering of the smaller porogen particles in aggregates. Although there are pores with sizes in the range of 63–125 μm as the porogen, when 80% of salt was used, the majority of the pores have a significantly larger size. These larger pore sizes were observed probably due to aggregate formation of the salt particles that were not disrupted during the mixing process. This observation may be connected with a tendency of the smaller NaCl grains to aggregate in the presence of trace amounts of moisture. To better understand these results, both groups of particles used in this study were analyzed by optical

microscopy using phase contrast mode (Fig. 6.2), where the tendency to produce aggregates is confirmed.

The grinding procedure also affected the morphology of the salt particles. The morphology of the larger particles (just sieved) presented almost perfect cubic shape [Fig. 6.2(a)]. Conversely, the smaller particles presented an irregular morphology because of the grinding process that mechanically fragmented the crystals into smaller pieces [Fig. 6.2(b)]. It was also difficult to observe individual particles when this group was analyzed, as most of them were aggregated in clusters. This indicates that the small particle size had a tendency to aggregate in the presence of humidity, probably because of the larger surface area of the particles. Attempts were made to minimize the agglomeration of smaller particles, such as grinding the polymeric blends to a size similar to the porogen used. This methodology was used for all the scaffolds. This procedure reduced the agglomeration but did not completely eliminate its effects.

Recently, μCT was employed for the observation and analysis of 3-D porous scaffolds [24]. Its advantages include the fact that it is a nondestructive technique that allows analysis the scaffold interior as opposed to SEM that requires sectioning. μCT allows visualizing and measuring the complete three-dimensional volume of the structures without any further sample preparation or chemical fixation.

The 3-D scaffolds structure of chitosan-based blends was analyzed using X-ray and μCT. For each processing condition, four scaffolds were scanned and analyzed. A representative 2-D X-ray image on the region of interest (a square of 4.5 x 4.5 mm) of the four groups of scaffolds is shown in Figure 6.3. The white regions of these images correspond to material-rich regions, whereas the darker areas correspond to pores. Previous SEM observations were confirmed by analyzing these 2-D μCT images, where a substantial difference exists between porous structures obtained with 60 and 80% by weight of salt. Pores resulting from the leaching of the larger range of particle size have cubic shape [Fig. 6.3(b,d)], particularly the pores obtained using 60% of salt that have a very narrow distribution of pore dimensions. The specimens with larger porosity have less organized pore structure, probably because of contacting adjacent particles. As a result, an increased interconnectivity of pores is observed. Samples obtained using the smaller particle sizes have pores with relatively unrelated shape [Fig. 6.3(a,c)]. The pores on those scaffolds indicate the leaching of clusters of particles. The resulting pores resemble small tunnels interconnected across the entire scaffold volume.

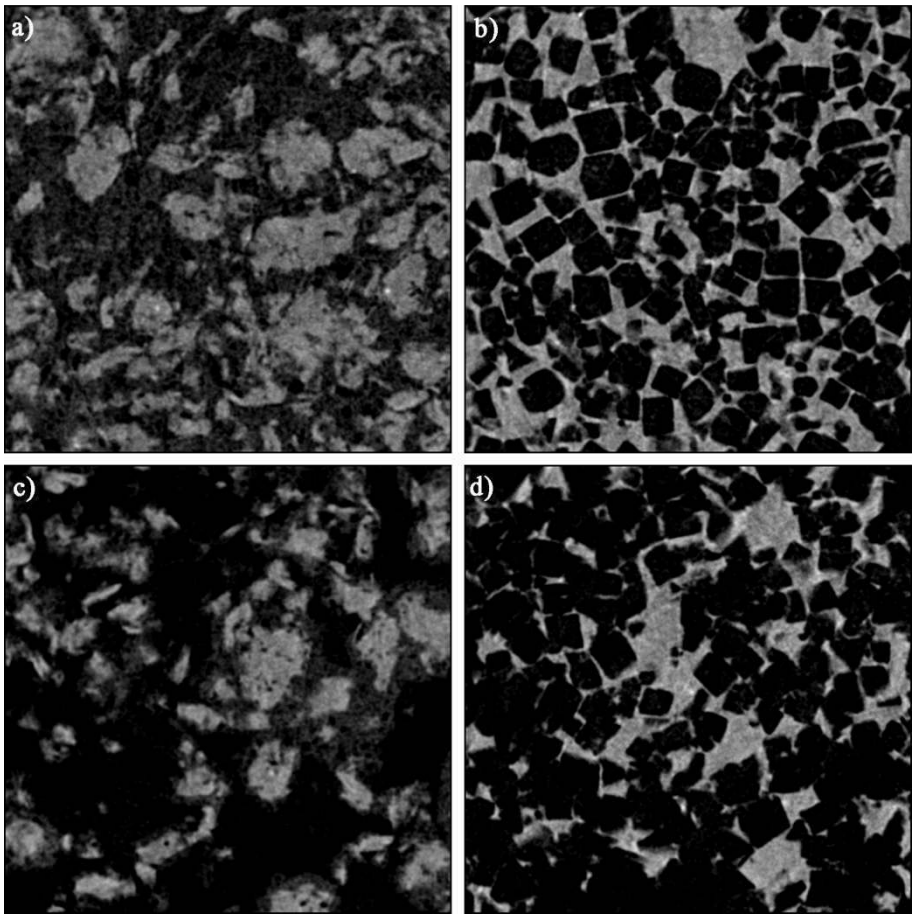

Figure 6.3. Representative 2-D μCT images (corresponding to the region of interest) of the scaffolds obtained using chitosan based blends with different amounts of salt and different granulometric size particles: a) 60 wt% of NaCl particles with size 63-125 μm; b) 60 wt% of NaCl particles with size 250-500 μm; c) 80 wt% of NaCl particles with size 63-125 μm; d) 80 wt% of NaCl particles with size 250-500 μm.

Because of the probable agglomeration, it appears that the scaffolds obtained with the smaller particle sizes possess higher interconnectivity than the ones obtained using the larger particle size. This is consistently observed for both porosities.

The images of the region of interest were threshold and binary images were obtained (figure not shown). For all the analyzed scaffolds, a dynamic threshold ranging from 255–60 gray scale values was used to distinguish polymer material from pore voids. This setting was used for all the scanned specimens. Individual 2-D analysis of the binary images (with a region of interest of 4.5 x 4.5 mm^2) obtained along the scaffold cross-section consisting of 300 slices was performed for morphometry calculations.

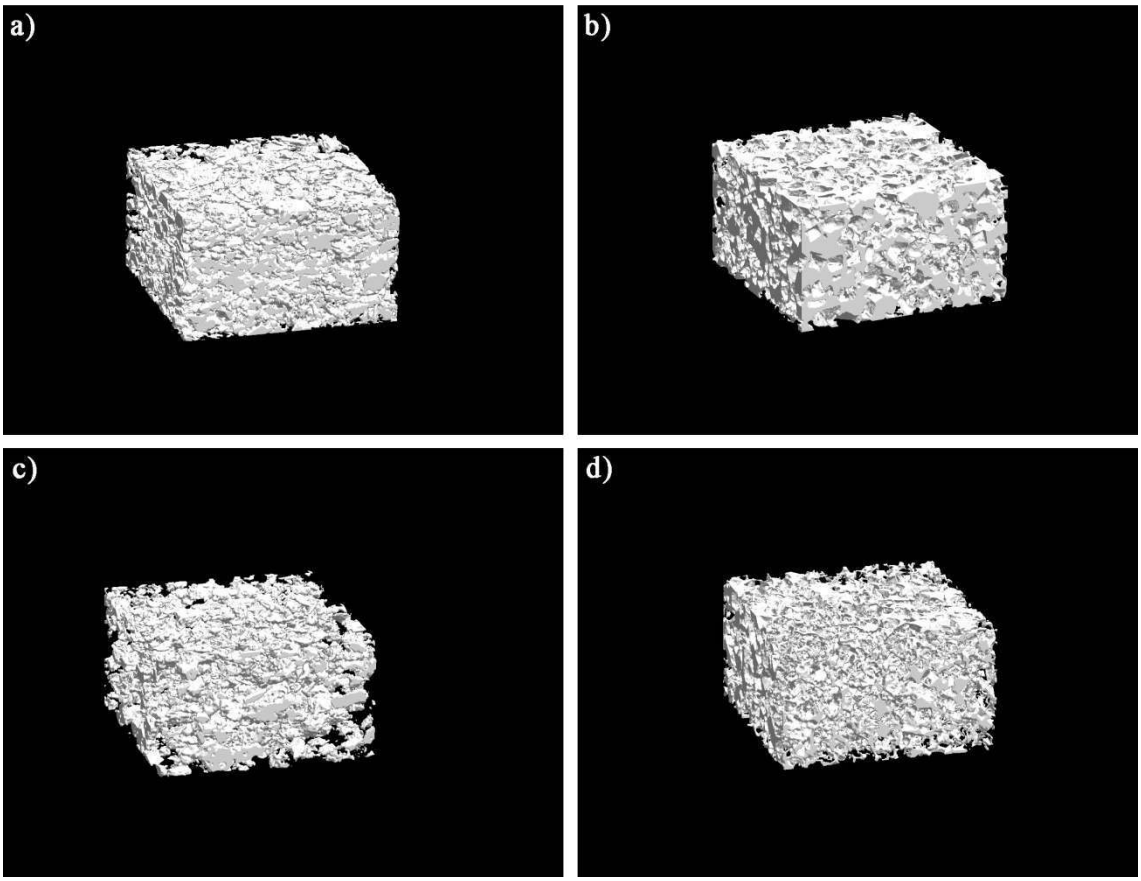

Figure 6.4. Representative 3-D μCT images of the entire scaffolds obtained using chitosan based blends with different amounts of salt and different granulometric size particles: a) 60 wt% of NaCl particles with size 63-125 μm; b) 60 wt% of NaCl particles with size 250-500 μm; c) 80 wt% of NaCl particles with size 63-125 μm; d) 80 wt% of NaCl particles with size 250-500 μm

The total porosity and pore size of each scaffold specimen (Table 6.1) was obtained as the average of the individual porosity and pore size of the 300 slices of each scaffold. For each condition, four scaffolds were analyzed. As expected, the volumetric porosity depends on the amount of porogen particles used, and in all the cases was very similar to the amount of salt used, whereas no significant influence of the NaCl particle size was observed on those results. The average pore size of the scaffolds is strongly affected by both particle size and particle amount. In scaffolds prepared with 60 wt % of salt with a particle size range of 250–500 μm, the observed average pore size is smaller than expected. This result indicates that the sieving process is not sufficiently accurate to allow controlling the pore size in the scaffolds after porogen removal. When the amount of salt was set at 80 wt %, there was a marginal

increase on the average pore size. However, this variation was more pronounced when 80 wt % of salt with particle size of 63–125 μm was used, being in most of the cases larger than when the porogen particles with the granulometric size range of 250–500 μm was used. This is a clear indication that the smaller particles are more prone to agglomeration probably because of the environmental humidity. This result also confirms previous SEM observations, where smaller porogen particles led to larger average pore size in the scaffolds.

Using a μCT-analyser (CTan), 3-D models of the different scaffolds were made using a square region of interest (4.5 x 4.5 mm2) and a length of 300 slices (Fig. 6.4). To analyze the morphology in the bulk of the scaffold, 3-D models were made using only 50 slices (figure not shown). In both cases, a dynamic threshold in the range 255-60 gray scale was used. No significant differences were observed between the bulk and the global morphology of the scaffolds. As expected, the architecture of the scaffolds is deeply affected by the amount of salt and by the salt particle size range used.

By inverting the threshold, a negative image of the scaffolds was created (figure not shown). This image corresponds to the volume of the pores and allowed to visualize the pore morphology and also to evaluate pore interconnectivity. As observed previously, the morphology of the pores changed when salt amount and particle size range were varied. The pores obtained using the larger range of particles mimicked the perfect cubic shape of the NaCl particles used (figure not shown). As the porosity was increased from 60 to 80%, this effect was less visible due to the increased number of contact points between the adjacent particles, causing more difficulties in identifying pores with perfect cubic shape. This effect resulted in the improvement of the interconnectivity. The pores produced with the smaller range of porogen particles resulted mostly from the leaching of clusters of NaCl particles. These pores have an undefined morphology with a larger distribution of average pore diameter.

The use of smaller range of particles also resulted in scaffolds with a higher degree of interconnectivity of the pore network. This is particularly visible when the higher porosity scaffolds were analyzed.

3.2. MECHANICAL PROPERTIES

The nominal stress–nominal strain curve for the various polyesters and their blends for differing porosities and pore sizes are shown in Figures 6.5–6.9. Stress is defined as the load per total area of the specimen, while strain is calculated on the entire structure and not on the microscopic strain in the cell walls. The compressive modulus was calculated as the slope of the most linear region of the stress–

strain curve prior to the yield point. The compressive stress was calculated as the maximum stress prior to the collapse of the porous construct. All tests were conducted on the specimen with identical dimensions, since the specimen size affects its mechanical properties [25].

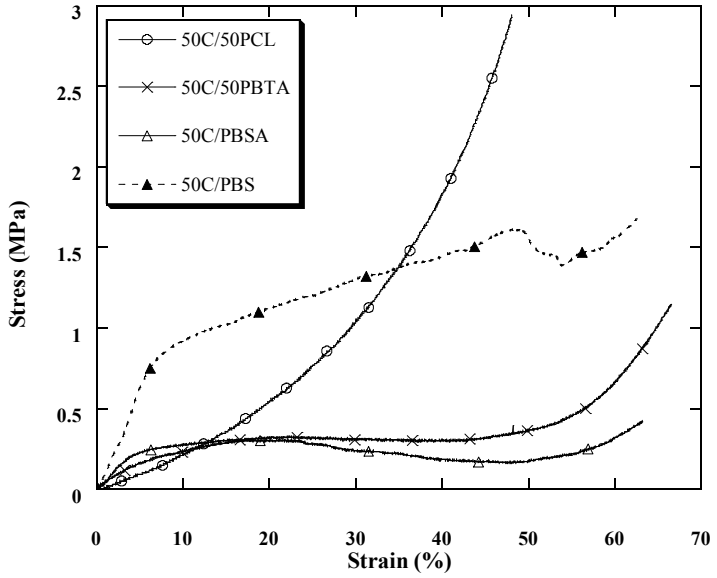

Figure 6.5. The effect of polyester type on the stress-strain plot of scaffolds having 50% chitosan and a porosity of 80% with particle size range between 63-125 μm.

The stress–strain curves of most of the scaffolds exhibit qualitative characteristics similar to that of metallic or polymeric foams [26–28]. The shape of the curve varies with the amount of porosity, pore size, composition, and the type of polyester. At the initial stage of compression, an elastic region is observed that is followed by a peak stress for scaffolds obtained with all materials. This linear elastic region is related to cell-edge bending in open-cell foams [26]. The peak stress is typically associated with the beginningof crack initiation where the cell walls start to buckle. A distinct yield point after the elastic region may be observed in some cases. After this initial stage, the curve changes to a regime of very strong plastic flow characterized by a significant change in the slope of the stress versus strain curve. For some compositions (Fig. 6.5), the curve is horizontal, that is, the stress does not change during large strain levels (blends containing PBTA and PBSA). In other compositions, the plastic regime is not associated with a flat plateau, but the stress continues to monotonically increase with strain (blends

containing PCL Fig. 6.5). In this region, as stress increases, the cells begin to collapse by elastic buckling, yielding, or fracture, depending on the nature of the predominant cell wall material [29]. This region corresponds to a high-energy absorption, where the space occupied by the hollow pores is filled by materials that are being compressed. Following the extended plateau regime (Fig. 6.5), the stress–strain curve changes into the regime of densification. In this regime, the cell wall touches each other cell walls, and it is accompanied by a steep increase in stress. At higher strain, the rupture causes the cell walls to break into small pieces, squeezing it and causing the stress to increase.

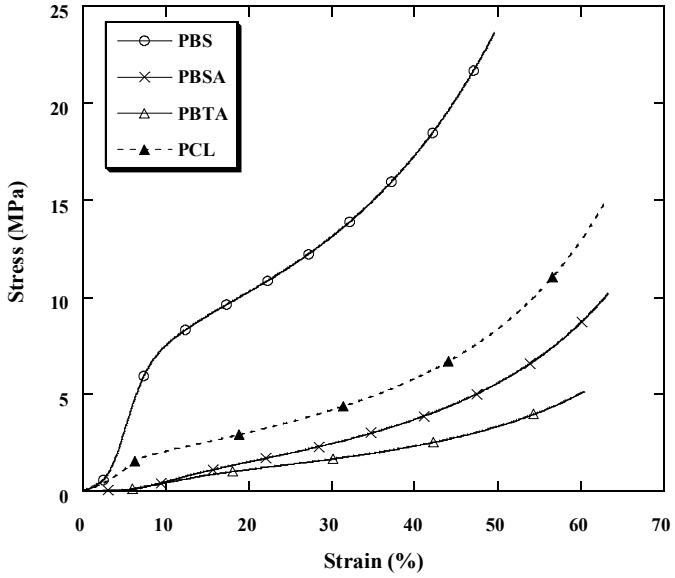

Figure 6.6. Stress-strain plot of polyester scaffolds with 60% porosity with particle size range between 250-500 μm.

Pure polyesters display a smooth stress–strain curve (Fig. 6.6). In these samples, the yield points are less obvious. The plateau stress is not identifiable in these scaffolds as the materials did not fracture; rather, the scaffolds continue to strain harden at all strains. This behavior is also observed for blends containing 25% chitosan and 75% PBS (Fig. 6.7) and the low-porosity blends of 50% chitosan and 50% PBTA (figure not shown). In these materials, a partial collapse of some parts of the scaffolds was observed while the remaining part still behaved elastically. Alternately, the cell walls could undergo plastic yielding throughout the deformation range. The strain at which densification occurs for pure polyesters is larger than those that occur in the blends.

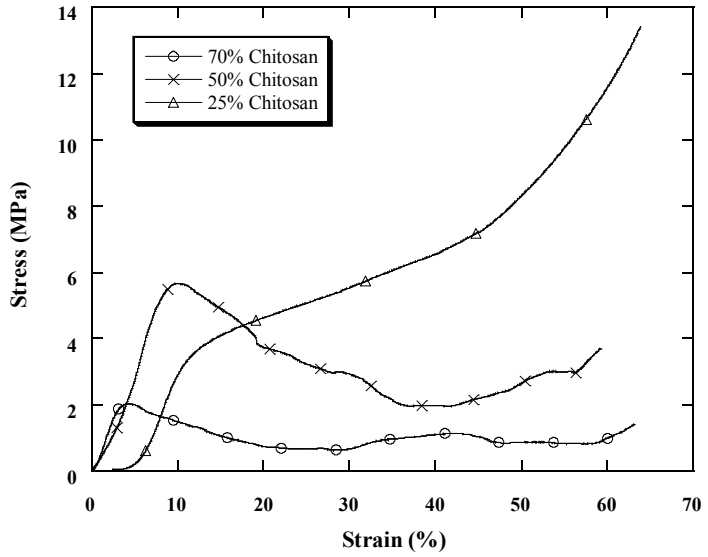

Figure 6.7. Effect of chitosan content on polybutylene succinate scaffold with a porosity of 60% with particle size range between 250-500 μm.

The stress–strain curves for blends of chitosan and polyester are shown in Figures 6.5 and 6.7. The stress–strain behavior is affected by the type of polyester used in the blend. For blends of 50% chitosan/50% PCL (at ~60% and ~80% porosity), 50% chitosan/PBTA (~60% porosity), and 25% chitosan/75% PBS (~60% and ~80% porosity), the stress–strain behaviour is similar to that of the pure polyester. For the scaffolds produced using larger salt particle size, as the chitosan content increased, the modulus increased. The yield stress reached a maximum with 50% of chitosan, decreasing for the material with 70% of chitosan (Fig. 6.7). For the scaffolds obtained with smaller particles, both the yield stress and modulus decreased with increasing chitosan content. The addition of HA causes a significant reduction in both the strength and the modulus. These are immiscible blends, and earlier studies have already shown [23] that HA displays poor adhesion to the chitosan/polyester matrix.

The values for the compressive yield stress and modulus for various specimens are listed in Table 6.2.

Table 6.2. Mechanical properties of the scaffolds produced from chitosan-polyester blends and salt particle size ranging from 63 -125μm or 250 -500μm.

Composition	Salt particle size (μm)	Salt content (wt%)	Compressive Modulus (MPa)	Yield stress (MPa)
PCL [a]	63-125	60	32.4±19.9	1.5±0.4
		80	2.7±1.4	0.05±0.01
	250-500	60	48.1±17.7	3.1±2.9
		80	5.3±1.7	0.5±0.2
PBTA [b]	63-125	60	-	-
		80	-	-
	250-500	60	7.0±2.0	0.5±0.1
		80	4.0±3.0	0.2±0.1
PBSA [c]	63-125	60	-	-
		80	-	-
	250-500	60	19.0±11.0	2.4±0.9
		80	7.0±4.0	0.2±0.1
PBS [d]	63-125	60	106.3±44.6	6.3±3.5
		80	12.7±4.4	0.3±0.2
	250-500	60	212.2±77.5	14.9±7.2
		80	-	-
25Ch-75PBS [e]	63-125	60	106±34	9.9±3.1
		80	9.0±3.0	0.3±0.2
	250-500	60	64.3±22.9	2.8±0.5
		80	12.4±3.3	0.4±0.3
50Ch-50PBS [f]	63-125	60	39.0±7.4	1.1±0.5
		80	1.7±0.4	0.05±0.01
	250-500	60	87.4±21.6	3.8±1.4
		80	12.1±3.3	0.4±0.1
50Ch-50PBSA [g]	63-125	60	6.2±2.8	0.43±0.2
		80	0.5±0.1	0.02±0.01
	250-500	60	14.0±6.4	0.9±0.4
		80	5.6±3.3	0.2±0.1
50Ch-50PBTA [h]	63-125	60	7.9±02.5	0.1±0.03
		80	1.6±0.3	0.02±0.01
	250-500	60	21.8±7.8	1.1±0.8

		80	6.3±1.3	0.3±0.1
50Ch-50PCL [i]	63-125	60	42.0±12.8	1.3±0.8
		80	5.7±3.1	0.05±0.02
	250-500	60	53.1±23.7	2.2±1.6
		80	5.5±3.3	0.1±0.05
70Ch-30PBS [j]	63-125	60	9.0±2.3	0.1±0.05
		80	3.0±1.8	0.08±0.01
	250-500	60	47.0±27.1	1.1±0.7
		80	5.0±5.0	0.04±0.02

[a] poly-ε-caprolactone
[b] poly(butylene terephthalate adipate)
[c] poly(butylene succinate adipate)
[d] poly(butylene succinate)
[e] Blend containing 25% by weight of chitosan and 75% by weight of PBS
[f] Blend containing 50% by weight of chitosan and 50% by weight of PBS
[g] Blend containing 50% by weight of chitosan and 50% by weight of PBSA
[h] Blend containing 50% by weight of chitosan and 50% by weight of PBTA
[i] Blend containing 50% by weight of chitosan and 50% by weight of PCL
[j] Blend containing 70% by weight of chitosan and 30% by weight of PBS

At similar pore size, increasing the porosity decreased the yield stress and the modulus. This was an expected result, since a higher amount of porosity corresponds to a smaller volume of material sustaining the stress. Scaffolds prepared using larger particle size ranges show higher compressive modulus than the ones prepared using particles of lower size (with the exception of PBTA blends). Similar results were reported in the literature by other research groups [30,31]. This result is in accordance with the previous morphological analyses showing that the scaffolds prepared with larger particle size possess pores with a more organized and defined structure and apparently having lower interconnectivity than do the ones prepared using smaller particle size. Pore interconnectivity makes the structure more brittle, reducing scaffold stiffness. Decreasing the salt particle size also decreased the yield stress of the foams. Gibson and Ashby [29] analyzed the collapse stress of porous metal and concluded that the collapse stress is unaffected by the pore size. Following the analysis outlined by Landers *et al.* [32] it can be shown that for scaffolds having the same porosity the strut diameter is proportional to the pore size. Euler's buckling load is proportional to the fourth power of strut diameter and inversely proportional to the square of strut length (which approximately equals pore size). Hence, scaffolds with smaller pore size have reduced yield strength (Table 6.2). In addition, it has been reported that cell wall curvature reduces the mechanical properties below values that would be expected if the walls were planar [26]. It is apparent that the shape of larger salt particles is cubical while that of the smaller size salt particle is less defined but without sharp edges (Fig. 6.2). This results in a scaffold with

planar walls for larger salt particle [Fig. 6.3(b,d)] versus rounder walls for smaller particle size [Fig. 6.3(a,c)].

The addition of chitosan content into the blends increased the compressive modulus of the scaffolds produced using the PCL and PBTA blends. In the case of the scaffolds produced using PBS and PBSA blends, the addition of chitosan resulted in an opposite effect. This behavior was observed independently of the pore size for both cases. The chitosan content caused a small variation in the yield stress but a significant difference in the strain at yield (data not shown). This observation is common for all the samples, independent of composition and porosity, except for samples containing 70% chitosan. The stress–strain diagrams show no yielding point. The stress decreases sharply after the peak, and at ~20–30% strain, the samples collapsed (stress ~0). The scaffolds produced with other brittle materials (50% chitosan/50% PBS, and 70% chitosan/30% PBS) have an oscillating plateau region. This region is marked by progressive collapse occurring as a result of continued deformation of existing cracks as well as by the formation of new ones. As strain progresses, the structure is further compressed, and densification causes the stress to raise again until the next fracture that releases the stress again. This is responsible for the oscillations in stress. The drop in stress is observed for stress levels between 50 and 60% of the peak stress. Reproducibility, particularly for the high porosity samples of the aforementioned blends, is poor. This is probably because of difficulties in cutting the specimens as well as by any unintended anisotropy of the pore structure. During the early stages of compression, at the initiation of crack, the brittle nature of the scaffolds leads to the formation of powder material and some mass loss due to fragments detaching from the scaffolds.

The stress–strain curves of scaffolds obtained using composites containing chitosan/polyester and HA are shown in Figures 6.8 and 6.9. These scaffolds were produced using just the higher salt particle size range. The value for yield strength and compressive modulus is given in Table 6.3. Composites of chitosan and hydoxyapatite with either PCL or PBTA are able to carry loads to strains well beyond their ultimate strains. The exceptions are composites containing 50% chitosan and PBS with HA (Fig. 6.8) where a linear increase is observed after which the stress decreases for increasing strains. In these materials, the densification process, apparent in the more ductile material, seems to be absent.

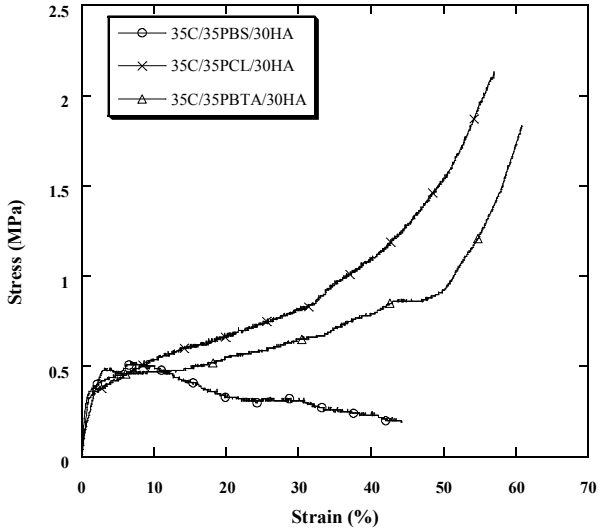

Figure 6.8. Effect of polyester type on the stress-strain behavior of 70% porosity scaffolds.

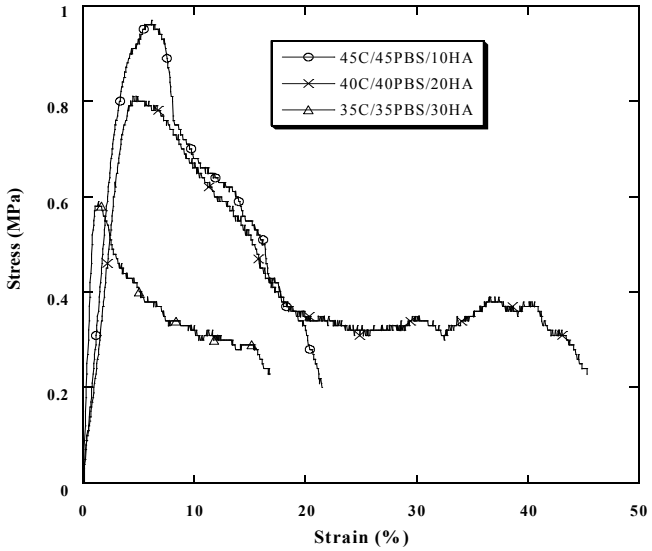

Figure 6.9. Effect of hydroxyapatite content on the stress-strain behavior of 60% porosity scaffolds.

The specimens fail by a brittle process and an abrupt loss of load carrying capacity after attaining peak stress. The failure initiates in the region having the lowest density or clusters of defects or weaker regions. The probability of weak regions is significantly higher in the highporosity samples than in samples with lower porosity. As the HA content in the blend increased (Fig.6.9), both yield stress and strain at failure decreased. Addition of HA led to a decrease in the compressive yield stress for all blends. The compressive modulus was also lower for blends containing HA, except for scaffolds containing PCL. Similar results were observed on compact injection-molded tensile testing samples [23]. Morphological observations using SEM indicate [23] that HA particles have minimal adhesion to the chitosan/polyester matrix and debond easily during deformation, thus not contributing significantly to the stiffening of the material.

Table 6.3. Mechanical properties of scaffolds containing hydroxyapatite produced using salt particles with size ranging from 250 - 500μm.

Composition	Salt content (%)	Compressive Modulus (MPa)	Yield stress (MPa)
70PBS-30HA [a]	60	100±19	4.6±1.8
	70	52±20	1.3±1.1
17.5Ch-52.5PBS-30HA [b]	60	67±14	2.7±0.5
	70	35±25	0.9±0.5
45Ch-45PBS-10HA [c]	60	39±9	0.3±0.2
	70	21±10	0.2±0.1
40Ch-40PBS-20HA [d]	60	85±9	0.6±0.4
	70	25±11	0.4±0.1
35Ch-35PBS-30HA [e]	60	48±12	0.6±0.2
	70	38±29	0.5±0.3
35Ch-35PCL-30HA [f]	60	102±18	2.1±0.7
	70	74±27	0.5±0.2
35Ch-35PBTA-30HA [g]	60	43±5	0.5±0.1
	70	25±18	0.1±0.04

[a] Composite containing 70% by weight of PBS and 30% by weight of hydroxyapatite
[b] Composite containing 17.5% by weight of chitosan, 52.5% by weight of PBS and 30% by weight of hydroxyapatite
[c] Composite containing 45% by weight of chitosan, 45% by weight of PBS and 10% by weight of hydroxyapatite
[d] Composite containing 40% by weight of chitosan, 40% by weight of PBS and 20% by weight of hydroxyapatite
[e] Composite containing 35% by weight of chitosan, 35% by weight of PBS and 30% by weight of hydroxyapatite
[f] Composite containing 35% by weight of chitosan, 35% by weight of PCL and 30% by weight of hydroxyapatite
[g] Composite containing 35% by weight of chitosan, 35% by weight of PBTA and 30% by weight of hydroxyapatite

The foams can be construed to be made up of interconnected beams. In open-cell foams, the cell edges initially deform by bending. Cell struts in foams subjected to compressive loading fail either by elastic buckling when the maximum compressive stress exceed the Euler buckling load, or by crushing when the maximum stress exceeds the modulus of rupture [33], that is, the strength of foams is dependent on the strength of the struts parallel to the direction of the applied load. Euler buckling load depends on the elastic modulus and slenderness of the individual cell walls. Hence, materials with lower elastic modulus also display lower compressive yield strength. Brittle crushing occurs when the critical skin stress exceeds the cell-wall modulus. The failure stress and cell-wall modulus depend on cell size, relative density, and Weibull modulus, which is related to the properties of cracks and flaw size distribution within brittle solids [29]. The elastic buckling strength of foams is given as follows [29]:

$$\sigma_b = \frac{n^2 \pi^2 E_s}{12} \left(\frac{\rho_{FOAM}}{\rho_{SOLID}} \right)^2 \quad (1)$$

where E_s is the elastic modulus of the solid cell struts (assumed in our case to be equal to the modulus of the solid material) and n^2 is the end constraint factor that depends on stress state and buckling mode. The value of n^2 for biaxial compression is taken to be 0.36. The buckling stress computed from Eq. (1) (data not shown) when compared to experimentally measured yield yielded a correlation coefficient r^2 = 0.925. Possible reasons for deviations include inhomogeneous density distribution leading to density gradient [28], kinks and wriggles in cell walls [34] or nonuniform material distribution in cell walls [35].

3.3. DIFFERENTIAL SCANNING CALORIMETRY

For DSC analyses, scaffolds from chitosan/PBS blends and processed using salt particles of higher size range and with 60% porosity were selected. Normalized DSC scans of PBS-based materials were shown in Figure 6.10. The melting peak of the PBS fraction is visible in the thermograms, and the corresponding melting temperature and melting enthalpy are shown in Table 6.4.

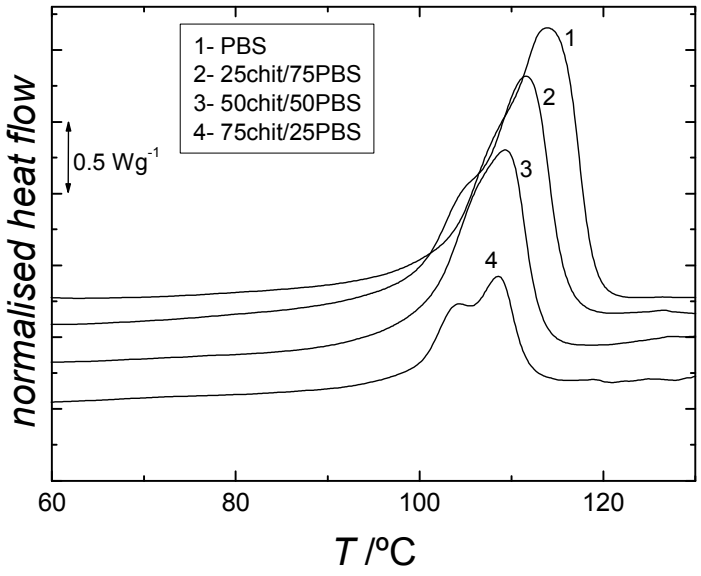

Figure 6.10. Normalised DSC thermograms (heat flow divided by the sample mass) of some PBS-based scaffolds of 60% porosity, obtained at 20 ºC.min^{-1}.

Table 6.4. Melting temperature and heat of fusion of the PBS-based scaffold materials. The degree of crystallinity within the PBS fraction is also included.

MATERIAL	T_m (ºC)	ΔH (J/g)	x %
PBS [a]	104.3	60.8	55.1
25Ch-75PBS [b]	102.3	52.9	63.9
50Ch-50PBS [c]	100.1	37.5	68.0
75Ch-25PBS [d]	99.3	19.6	71.1

[a] poly(butylene succinate)
[b] Blend containing 25% by weight of chitosan and 75% by weight of PBS
[c] Blend containing 50% by weight of chitosan and 50% by weight of PBS
[d] Blend containing 70% by weight of chitosan and 30% by weight of PBS

The crystallinity degree of the PBS component was calculated by knowing the theoretical value of ΔH_m for 100% crystalline PBS, that was taken as 110.3 J/g, calculated on the basis of the group contribution method proposed by Van Krevelen [36]. The melting temperature is found to decrease with increasing chitosan content, as detected before in injection-molded samples with the same composition [22]. The same trend was also observed in blends of poly(3-hydrpxybutyrate) and chitosan [37] and attributed to

strong intermolecular interactions between the chitosan and the polyester chains, resulting in thinner lamellar thickness crystals. However, despite this reduction of crystalline perfection, it was found that the total degree of crystallinity in the PBS fraction increased with increasing chitosan content. This suggests that, in this case, chitosan could act as a nucleating agent for PBS. The results (Fig. 6.10) also suggest that the melting peak may reflect the presence of two processes as, with increasing chitosan content a lower temperature shoulder is progressively enhanced. This may be an indication that chitosan may induce, in fact, the development of crystalline structures with a different lamellar morphology than that appearing in pure PBS. As such structures melt at lower temperatures, they should be composed of thinner lamellae. Comparing the thermal behavior of the scaffolds and the injection-molded compact samples made of the same materials [22], we may conclude that the former present lower melting temperature, indicating that shear can induce the production of more perfect/thicker crystalline structures.

3.4. CRYSTALLINITY

Small angle X-ray scattering

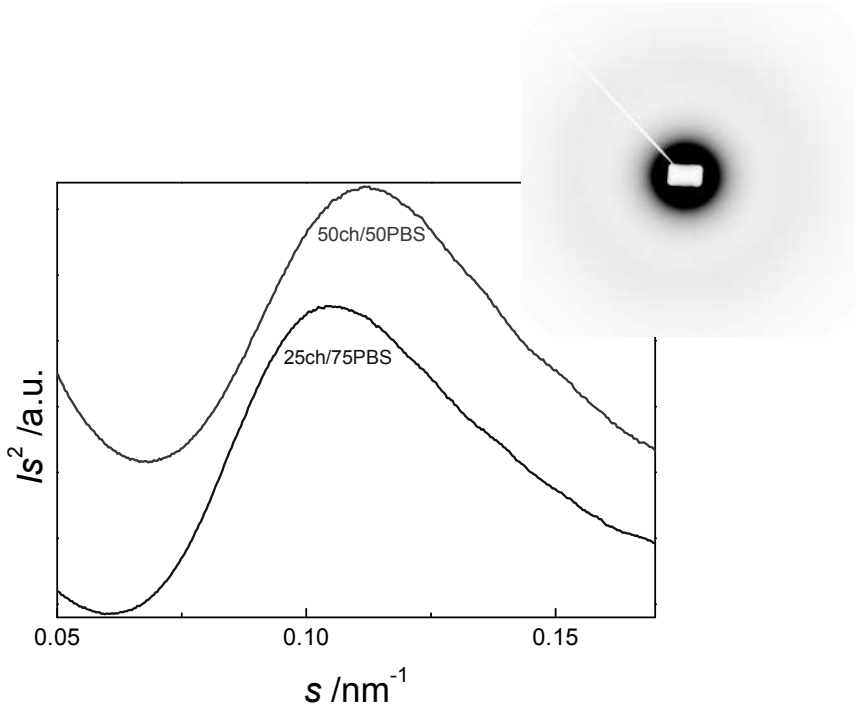

Figure 6.11. Lorentz-corrected SAXS profiles of some chitosan/PBS blends (60% porosity), where the effect of chitosan content is investigated. Inset: 2-D-SAXS pattern for the 25/75 chitosan/PBS blend.

SAXS may provide further insights on the microstructure at the lamellae scale. The inset of Figure 6.11 shows, as a representative result, the 2-D SAXS pattern of the 25/75 chitosan/PBS sample. As found in all the analyzed scaffolds, the results are consistent with the conventional lamellar structure, where the well-defined Debye ring is indicative that no preferential crystalline orientation exists. The 2-D patterns were integrated using the X-ray software, version 1.0, allowing obtaining the intensity as a function of the scattering vector, s. Figure 6.11 shows some Lorentz-corrected scattering profiles for some analyzed PBS-based materials. The position of the peaks were used to calculate the average long period, $L=1/s_{max}$. A slightly higher value of L was found for the 50/50 chitosan/PBS scaffold (L = 9.6 nm) with respect to the other two materials (L = 8.9 nm). An interesting result arises when one compares the morphology of such materials with those processed by injection molding, where the long period was found to be around 7.5 nm [22]. This finding demonstrates the importance of the processing conditions on the developed morphology.

Wide angle X-ray scattering

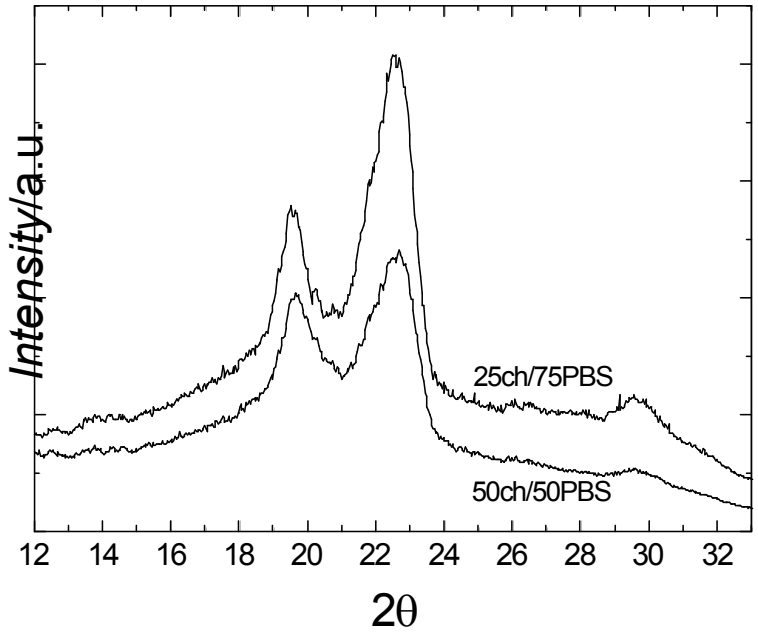

Figure 6.12. WAXS patterns for two different blends of chitosan and PBS (25/75 and 50/5) of scaffolds with 60% porosity.

Figure 6.12 shows the diffraction diagrams for some PBS-based scaffolds. The typical diffraction features of PBS are observed: peak at 2θ ≈ 19.3º, assigned to the (111) and (002) planes, a peak of

(110) at 2θ ≈ 22.2º, with a shoulder at lower angles associated with the (012) planes, a peak of (121) at 2θ ≈ 25.9º and a peak of (111) at 2θ ≈ 29º. An electron diffraction study showed that PBS chains crystallize in monoclinic crystal lattice, with *a* = 0.523 nm, *b* = 0.908 nm, *c* = 1.079 nm, and *β* = 123.87º [38]. No change in peak position is found when the chitosan content changes. However, a close inspection on the half-width of the two major diffraction peaks, *β*, leads to the conclusion that the peaks are broader for the blend with 50% chitosan than the blend with 25% chitosan. This would indicate that the size of the crystalline structures, L_{hkl}, is higher in the sample richer in PBS, as L_{hkl} is intimately related to b by the Scherrer's equation [39]: $L_{hkl} = k\lambda/(\beta \cos \theta)$, where *k* is an instrument constant and λ is the wavelength of radiation used. This result correlates well with the DSC results, where from the analysis of the melting temperatures, it was possible to conclude that, with increasing chitosan content in the blends, the global crystalline structure of PBS would be more imperfect or characterized by thinner lamellae.

3.5. CYTOTOXICITY EVALUATION

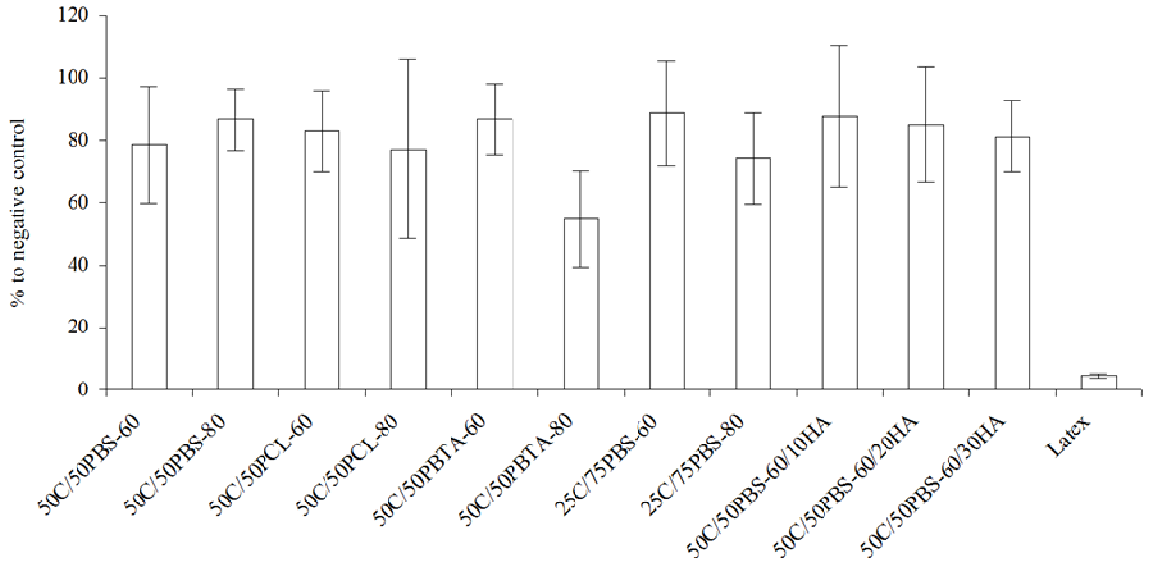

Figure 6.13. Cytotoxicity results of the 72h extracts of scaffolds with pore size ranging between 250-500μm, namely 50C/50PBS-60, 50C/50PBS-80, 50C/50PCL-60, 50C/50PCL-80, 50C/50PBTA-60, 50C/50PBTA-80, 25C/75PBS-60, 25C/75PBS-80, 50C/50PBS/10HA-60, 50C/50PBS/20HA-60, 50C/50PBS/30HA-60 and positive control of cell death, latex. Results are based on optical density measurements, at O.D. of 490nm and normalized for the negative control (n=6; ±sd; $p<0.05$).

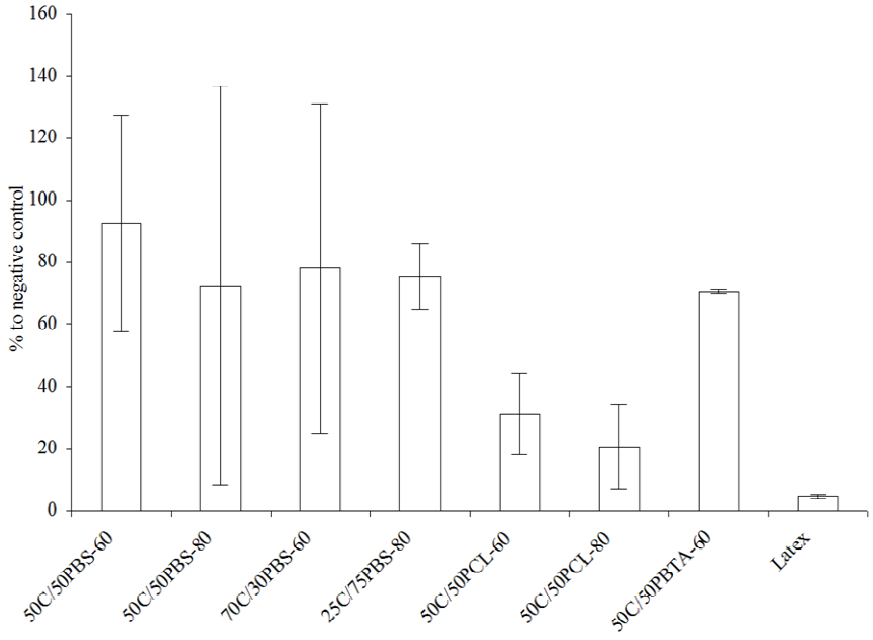

Figure 6.14. Cytotoxicity results of the 72h extracts of scaffolds with pore size ranging between 63-125μm, namely 50C/50PBS-60, 50C/50PBS-80, 70C/30PBS-60, 25C/75PBS-80, 50C/50PCL-60, 50C/50PCL-80, 50C/50PBTA-60 and positive control of cell death, latex. Results are based on optical density measurements, at O.D. of 490nm and normalized for the negative control (n=6; ±sd; $p<0.05$).

Cytotoxic tests are a very important tool to evaluate a biomaterial in terms of toxic effect over cell growth and viability. L929 cells were exposed to extracts from the scaffolds for 72 h and the cellular response evaluated by MTS viability assay. In general, the MTS test results showed that L929 cells produced large amounts of a brown formazan product after incubation with the tested extracts. These results demonstrated that cells were viable, once they were able to incorporate and metabolize the substrate.

All materials, except the scaffolds composed by 50C/50PCL-60, 50C/50PCL-80 with pore size ranging between 63 and 125 μm (Fig. 6.14), presented a high percentage of cell viability. The extracts of scaffolds with larger pores (Fig. 6.13) showed cellular viability higher than 50% relative to the negative control. Extracts of scaffolds composed with HA (Fig. 6.13), irrespective of the percentage of HA, evidenced no adverse effects on cell viability and shown high values of cellular viability of 80% with respect to negative control. A significant variability in the results of cytotoxicity of extracts from scaffolds of the same blend mixture was observed, with pore sizes ranging between 63 and 125 μm (Fig. 6.14), evidenced by large standard deviation bars. This observation may be related with the morphology of the scaffolds, namely the pore size. Those scaffolds were produced by salt leaching using finer salt

particles. The porogen size being smaller it may be more difficult to leach out all the salt particles, and it might be possible to have more particles entrapped in the scaffold structure. This may significantly influence the toxicity by the leachable components released to the extract that will be in direct contact with cells.

Blends with PBS show the highest results of cell viability. In fact, an increase on the percentage of polyester is observed not to have direct influence in cell viability. A recent study of our group [40] reports the osteogenic behavior of mesenchymal stem cells (MSCs) seeded and cultured onto 60% porosity scaffolds produced with 50C/50PBS, 50C/50PCL, and 50C/50PBTA. The porogen size was in the range of 250–500 μm. Results evidenced a remarkable cell behavior upon those chitosan-based scaffolds, in terms of cell adhesion and viability, as well the formation of mineralized extracellular matrix. The same compounds, but with 80% porosity and porogen particles with size of 65–125 μm, were studied for chondrogenic applications, with MSC differentiation toward a chondrogenic lineage [41], also showing excellent cell viability and activity when seeded at the surface of those materials.

The present study has shown only in one case, PCL/chitosan with smaller pore size, high values of toxicity of extracts from the scaffolds. However, it must be noted that this result was not confirmed for the same material in scaffolds with larger pore size. Thus, this exception in terms of cytotoxicity of extracts must be specifically caused by either the morphology of the scaffold or the preparation method and probably not by the materials.

Thus, the results herein reported of cytotoxicity of extracts from the scaffolds produced from novel developed chitosan-based blends show overall good viability of the cells (greater than 50% of the values of negative control) and those scaffolds will be further developed for various tissue engineering applications.

4. CONCLUSIONS

In the present study, chitosan-based porous scaffolds with different architectures were produced by melt-based compression molding followed by salt leaching. The microarchitecture of the developed scaffolds was accessed by SEM and μCT. By changing both the amount and average particle size of the porogen agent used, it was possible to prepare scaffolds with different macroscopic architecture using a melt-based approach. As expected, the amount of porosity was inversely proportional to the final mechanical properties of the developed scaffolds. For the scaffolds produced using similar particle

size range, increasing the porosity decreased the yield stress and the compression modulus. Scaffolds prepared using particles of smaller size were observed to have lower compressive modulus than the ones prepared using a larger particle size range. Although contrary to the expected result, it was shown by analyzing the morphology to be consistent with the pore interconnectivity observed. Addition of chitosan increased the compressive modulus of the scaffolds produced using PCL and PBTA, but reduced the compressive modulus of those developed using PBS and PBSA. Addition of HA led to a decrease in the compressive yield stress and compressive modulus, probably because of the low interface adhesion. Thermal properties of chitosan-PBS-based scaffolds were analyzed, and it was found that the melting temperature decreased with increasing chitosan content. Microstructure analysis (WAXS and SAXS) demonstrated that with increasing chitosan content in the chitosan-PBS blends, the global crystalline structure of PBS would be more imperfect or characterized by thinner lamellae. Cytotoxic evaluation by means of MTS test revealed that L929 cells had similar metabolic activities to that obtained by the negative control. Therefore, the leachables released from the tested scaffolds could be considered as nontoxic and clearly cytocompatible.

REFERENCES

1. Langer, R. and J.P. Vacanti, Tissue Engineering. Science, 1993. 260: p. 920–926.
2. Hutmacher, D.W., Scaffold design and fabrication technologies for engineering tissues - State of the art and future perspectives. Journal of Biomaterials Science, Polymer Edition, 2001. 12(1): p. 107-124.
3. Muzzarelli, R.A.A., Chitin, Pergamon Press, New York, 1977.
4. Klokkevold, P.R., *et al.*, Osteogenesis enhanced by chitosan (poly-N-acetyl glucosaminoglycan) in vitro, Journal of periodontology, 1996. 67(11): p. 1170-1175.
5. Peluso, G., Chitosan-mediated stimulation of macrophage function. Biomaterials,1994. 15(15): p. 1215–1220.
6. E. T. Baran, R. L. Reis. Use of chemically modified chitosan and other natural-origin polymers in tissue engineering and drug delivery, in: Biodegradable Systems in Tissue Engineering and Regenerative Medicine, Boca Raton, CRC Press, 2005, p. 325–335.
7. Sarasam, A. and S.V. Madihally, Characterization of chitosan–polycaprolactone blends for tissue engineering applications. Biomaterials, 2005. 26(27): p. 5500–5508.

8. Zhang, J., *et al.*, A comparative study of porous scaffolds with cubic and spherical macropores. Polymer, 2005. 46(13): p. 4979–4985.
9. McGlohorn, J.B., *et al.*, Evaluation of smooth muscle cell response using two types of porous polylactide scaffolds with differing pore topography. Tissue Engineering, 2004. 10(3-4): p. 505-514.
10. Lee, W.K. *et al.*, Novel poly(ethylene glycol) scaffolds crosslinked by hydrolyzable polyrotaxane for cartilage tissue engineering. Journal of Biomedical Materials Research Part A, 2003. 67(4): p. 1087–1092.
11. Kim, S.S., *et al.*, Poly(lactide-co-glycolide)/hydroxyapatite composite scaffolds for bone tissue engineering. Biomaterials, 2006. 27(8): p. 1399–1409.
12. Riddle, K.W. and D.J. Mooney, Role of poly(lactide-co-glycolide) particle size on gas-foamed scaffolds. Journal of Biomaterials Science, Polymer Edition, 2004. 15(12) 1561–1570.
13. Hou, Q., D.W. Grijpma and J. Feijen, Preparation of interconnected highly porous polymeric structures by a replication and freeze-drying process. Journal of Biomedical Materials Research Part B, 2003. 67(2): p. 732–740.
14. Wu, L., D. Jing and J. Ding, A “room-temperature” injection molding/particulate leaching approach for fabrication of biodegradable three-dimensional porous scaffolds. Biomaterials, 2006. 27(2): p. 185–191.
15. Jeong, S.I., et al., Manufacture of elastic biodegradable PLCL scaffolds for mechano-active vascular tissue engineering. Journal of Biomaterials Science, Polymer Edition, 2004. 15(5): p. 645–660.
16. Wu, L., *et al.*, Fabrication of three-dimensional porous scaffolds of complicated shape for tissue engineering. I. Compression molding based on flexible-rigid combined mold. Tissue Engineering, 2005. 11 (7-8): p. 1105–1114.
17. Malda, J., *et al.*, The effect of PEGT/PBT scaffold architecture on the composition of tissue engineered cartilage. Biomaterials, 2005. 26(1): p. 63–72.
18. Lee, S.H., *et al.*, Thermally produced biodegradable scaffolds for cartilage tissue engineering. Macromolecular Bioscience, 2004. 4(8,9): p. 802–810.
19. Jung, Y., *et al.*, A poly(lactic acid)/calcium metaphosphate composite for bone tissue engineering. Biomaterials, 2005. 26(32): p. 6314–6322.
20. Sun, J., *et al.*, Macroporous poly(3-hydroxybutyrate-co-3-hydroxyvalerate) matrices for cartilage tissue engineering. European Polymer Journal, 2005. 41(10): p. 2443–2449.

21. Gomes, M.E., *et al.*, Alternative tissue engineering scaffolds based on starch: processing methodologies, morphology, degradation and mechanical properties. Materials Science and Engineering: C, 2002. 20 (1-2): p. 19–26.
22. Correlo V.M., *et al.*, Properties of melt processed chitosan and aliphatic polyester blends. Materials Science and Engineering: A, 2005. 403(1-2): p. 57–68.
23. Correlo, V.M., *et al.*, Hydroxyapatite Reinforced Chitosan and Polyester Blends for Biomedical Applications. Macromolecular Materials and Engineering, 2005. 290(12): p. 1157–1165.
24. Ho, S.T. and D.W. Hutmacher, A comparison of micro CT with other techniques used in the characterization of scaffolds. Biomaterials, 2006. 27(8): p. 1362–2376.
25. Koza, E., *et al.*, Compressive strength of aluminium foams. Materials Letters, 2003. 58: p. 132–135.
26. Gibson, L.J., Mechanical behavior of metallic foams. Annual Review of Materials Science, 2000. 30: p. 191–227.
27. Banhart, J. and J. Baumeister, Deformation characteristics of metal foams. Journal of Materials Science, 1998. 33(6): p. 1431–1440.
28. Beals, J.T. and M.S. Thompson, Density gradient effects on aluminium foam compression behaviour. Journal of Materials Science, 1997. 32(13): p. 3595–3600.
29. Gibson, L.J. and M.F. Ashby, Cellular Solids Structure and Proper-AQ3 ties, 2nd ed. Cambridge University Press, 1997.
30. Burdick, J.A., *et al.*, An initial investigation of photocurable three-dimensional lactic acid based scaffolds in a critical-sized cranial defect. Biomaterials, 2003. 24(9): p. 1613–1620.
31. Ma, P.X., J.W. Choi, Biodegradable polymer scaffolds with well-defined interconnected spherical pore network. Tissue Engineering, 2001. 7(1): p. 23–33.
32. Landers, R., *et al.*, Fabrication of soft tissue engineering scaffolds by means of rapid prototyping techniques. Journal of Materials Science, 2002. 37(15): p. 3107–3116.
33. Huang, J.S. and C.Y. Chou, Survival probability for brittle isotropic foams under multiaxial loading. Journal of Materials Science, 2000. 35(15): p. 3881–3887.
34. Grenestedt, J.L., Influence of wavy imperfections in cell walls on elastic stiffness of cellular solids. Journal of the Mechanics and Physics of Solids, 1998. 46(1): p. 29–50.
35. Simone, A.E. and L.J. Gibson, Aluminum foams produced by liquid-state processes. Acta Materialia, 1998. 46(9): p. 3109–3123.
36. Van Krevelen D.W., Properties of Polymers. Amsterdam: Elsevier; 1990.

37. Cheung, M.K., K.P.Y. Wan and P. H. Yu, Miscibility and morphology of chiral semicrystalline poly-(R)-(3-hydroxybutyrate)/chitosan and poly-(R)-(3-hydroxybutyrate-co-3-hydroxyvalerate)/chitosan blends studied with DSC, 1H T1 and T1 CRAMPS. Journal of Applied Polymer Science, 2002. 86(5): p. 1253–1258.
38. Ihn, K.J., E.S. Yoo and S.S. Inn, Structure and morphology of poly(tetramethylene succinate) crystals. Macromolecules, 1995. 28(7): p. 2460–2464.
39. L. E. Alexander, X-ray Diffraction Methods in Polymer Science, New York, Wiley Interscience, 1969, pp. 137.
40. Costa-Pinto, A.R., *et al.*, Adhesion, Proliferation and Osteogenic Differentiation of a Mouse Mesenchymal Stem Cell line (BMC9) Seeded on Novel Melt Based Chitosan/Polyester 3D Porous Scaffolds. Tissue Engineering, 2007. 14(6): p. 1049-1057
41. Oliveira J.T., *et al.*, Assessment of the suitability of chitosan/polybutylene succinate scaffolds seeded with mouse mesenchymal progenitor cells for a cartilage tissue engineering approach. Tissue Engineering, 2007. 14(10): p. 1651-1661.

CHAPTER VII.

Melt processing of chitosan-based fibers and fiber-mesh scaffolds for the engineering of connective tissues

CHAPTER VII.

Melt processing of chitosan-based fibers and fiber-mesh scaffolds for the engineering of connective tissues

Abstract

Three-dimensional porous scaffolds play a pivotal role in tissue engineering of human tissues like for instances bone and cartilage. The scaffold provides the necessary support for cells to attach, proliferate and maintain their differentiated phenotype. Numerous techniques have been used to produce porous scaffolds including fiber bonding methodologies. We report herein the production of chitosan based fibers and chitosan fiber mesh structures by melt processing (solvent-free) to be used as tissue engineering scaffolds. Fibers from a blends of chitosan with poly(butylene succinate) (Ch- PBS) in two different ratios (25/75 wt% and 50/50wt%) and chitosan with poly(butylene terephthalate adipate) (Ch-PBTA) (50/50 wt%) were produced using a micro-extruder. The surface roughness of the fibers is directly proportional to the chitosan content. Conversely, the mechanical performance (tensile strength and modulus) is inversely correlated with the chitosan fraction. The type of polyester used clearly affected the mechanical properties of both the fibers and the scaffolds. The melt based approach used to produce the scaffolds did not change the main characteristics of the fibers including its surface roughness and microporosity. Moreover, no significant morphological differences were observed between scaffolds produced with fibres of different composition. The porosity, pore size, interconnectivity and mechanical performance of the scaffolds are all within the range required for various tissue engineering applications. Biological assessment was performed in direct contact assays, using a human osteosarcoma cell line (SaOs-2). Cells were able to fully colonize the scaffold, not only at the surface but also in the inner porous structure of the different scaffolds. Furthermore, the cells showed high indexes of viability in all the scaffold types. The results give us confidence to further develop those scaffolds for various tissue engineering applications.

This chapter is based on the following publication: **Correlo VM**, Costa-Pinto AR, Sol P, Covas JA, Bhattacharya M, Mano JF, Neves NM and Reis RL, 2009, Melt processing of chitosan-based fibers and fiber-mesh scaffolds for the engineering of connective tissues, Acta Biomaterialia, *submitted*

---

1. INTRODUCTION

In the last two decades, tissue engineering (TE) has emerged as a promising alternative to treat or replace tissues and organs that lose their function either by disease or by trauma. The most studied strategy involves the use of an artificial extracellular matrix (the scaffold) frequently intended to be temporary and thus produced from biodegradable or bioresorbable polymers. The scaffold will support the cell attachment, growth and proliferation, and acts as a template to guide the morphogenesis of the new tissue [1, 2].

A successful scaffold needs to combine different specific requirements. Among those the chemical composition and the surface chemistry have been suggested to play important roles in promoting the proliferation and differentiation of cells [3]. Moreover, the porous architecture and morphology of the scaffold including the amount of porosity [4], pore size [5], pore accessibility and pore tortuosity [6] are widely recognized to be important parameters conditioning the formation of new tissue. Many characteristics of the scaffolds are dictated by the processing method used in its production.

Fiber-based scaffolds were among the first templates proposed for tissue engineering [7, 8]. The fibers can be produced by wet [9] or dry–wet spinning [10] from polymeric solutions or by melt spinning [11]. The fibers can be further processed by a great variety of processing methods involving knitting [12, 13], physical bonding (by the combined application of pressure and temperature) [14]. The aim is to create an interconnected 3-D porous structure with a large surface area for cell attachment and proliferation. Several studies have shown that scaffolds produced from fibers have adequate porous interconnectivity and mechanical properties for various tissue engineering applications [4, 15].

Although fibre mesh chitosan based scaffolds [16, 17] and some chitosan blend fibers [18, 19] have been produced from polymeric solutions (wet spinning), to the best of the authors knowledge, no reports exist in the literature on the production of chitosan fiber mesh scaffolds using melt processing methods.

The main aim of the present work is to report on the production of chitosan based fibers and chitosan fiber mesh scaffolds using only melt based technology and its mechanical and morphological characterization. We have also assessed its biological performance using osteoblastic like cells to conclude about the potential of those scaffolds to be used as templates for the engineering of connective tissues.

2. MATERIALS AND METHODS

2.1. FIBERS PRODUCTION

Blends of chitosan with poly(butylene succinate) (Ch-PBS) at two different ratios (25/75 wt% and 50/50wt%) and blends of chitosan with poly(butylene terephthalate adipate) (Ch-PBTA) (50/50 wt%) were compounded on a twin screw extruder. Processing parameters used in this compounding stage were detailed previously elsewhere [20]. The chitosan based blends were extruded into fibers, by using a prototype single screw micro-extruder [21] coupled to a capillary die. Although the machine is capable of producing extrudates with only a few grams of material in powder form, it was designed to induce thermo-mechanical stresses of the same order of magnitude of those developed in bigger machines. Moreover, the screw contains a multi-pass barrier section that greatly improves the dispersive mixing capacity.

2.2. SCAFFOLDS PRODUCTION

The scaffolds were fabricated into mesh structures by a fiber compression method. Briefly, the extruded fibers were chopped in 1 cm long sections and loaded into a mould. The mould is heated above the melting temperature (T_m) of the thermoplastic composite during a specific time period. The next step involves applying pressure to allow the fibers to weld at the junctions forming a stable fiber mesh structure. The porous mesh structure is further cut into 1.5 mm thick discs, with diameter of 7 mm.

2.3. OPTICAL MICROSCOPY

To analyze the chitosan phase distribution within the fibers, cross sections were prepared and analyzed in a procedure similar to the one reported in a previous study [20]. Briefly, chitosan based fibers were mounted in epoxy resin. After the curing stage, thin slices of material were removed from the surface of the fibers entrapped in the epoxy resin using a microtome. The procedure continued until approximately half the diameter of the fibers was sliced. After this procedure, the fibers with the exposed surface were stained with a 0.10 (w/v) eosin solution for 10 min at 32±0.5 ºC. Stained samples were examined by light microscopy (Olympus BH-2) in reflection. Photomicrographs of the stained surfaces were obtained using a digital camera Olympus DP11 directly mounted in the microscope.

2.4. SCANNING ELECTON MICROSCOPY

The morphology of the produced chitosan based fibers and fiber mesh scaffolds was analyzed using a Leica-Cambridge S-360 (UK) scanning electron microscope (SEM). Previously to the SEM analysis, all the samples were sputter-coated with gold (Fisons Instruments, Sputter Coater SC502, UK).

2.5. MICRO-COMPUTED TOMOGRAPHY

Chitosan-based fiber mesh scaffolds were analyzed using a high-resolution micro-computed tomography (μCT) Skyscan 1072 scanner (Skyscan, Kontich, Belgium). Five scaffolds of each condition were scanned in high resolution mode using a pixel size of 8.24μm and integration time of 2.0 ms. The X-ray source was set at 80 keV of energy and 124 μA of current. For all the scanned specimens representative data sets of 150 slices were transformed into binary using a dynamic threshold of 60-255 (grey values) to distinguish polymer material from pore voids. This data was used for morphometric analysis (CT Analyser v1.5.1.5, SkyScan). The morphometric analysis included quantifying the porosity and mean pore size quantification (Table 7.3). 3-D virtual models of representative regions in the bulk of the scaffolds were also created, visualized and registered using both image processing softwares (ANT 3-D creator v2.4, SkyScan).

2.6. MECHANICAL TESTS

The tensile properties of the produced fibers were determined using a Universal tensile testing machine (Instron 4505 Universal Machine, USA). A crosshead speed of 5 $mm.min^{-1}$ was used up to rupture of the fiber. The results presented in Table 7.2 are the average of the testing of 10 specimens.

The compression testes of the developed chitosan based fiber mesh scaffolds were performed using a Universal tensile testing machine (Instron 4505 Universal Machine, USA). The tests were performed under compression loading using a crosshead speed of 2 $mm.min^{-1}$ until 60% strain was reached. The results presented in Table 7.3 are the average of at least five specimens.

Both the tensile and the compressive modulus were determined in the most linear region (between 0 and 1% strain) of the stress–strain curve using the secant method.

2.7. CELL CULTURE

A human osteoblast cell line (SaOs-2) was used to conduct the cell culture studies. Cells were grown as monolayer cultures in a culture medium consisting of DMEM medium, 10% FBS and 1% antibiotic/antimycotic mixture. When the adequate cell number was obtained, cells were detached with trypsin, centrifuged and ressuspended in cell culture medium. Cells were seeded at a density of 2,5x105cells/scaffold under static conditions, using for this purpose 1mL of cell suspension. Two hours after seeding, the cell seeded scaffolds were changed into new plates and 1 ml of culture medium was added to each well. The cell seeded scaffolds were maintained in a humidified atmosphere at 37ºC, containing 5% CO_2 during the remaining testing period.

2.7.1. Cell adhesion and morphological analysis by SEM

Cell adhesion, morphology and average distribution at the surface and at the bulk of the scaffolds were also analysed by SEM, after 24, 48, 72 hours and 7 days of culture. Cell-seeded scaffolds were washed in 0.15 M phosphate buffered saline and fixed in 2.5% glutaraldehyde in phosphate buffered saline. After rinsing 3 times in phosphate buffered saline, the constructs were dehydrated using a series of graded ethyl alcohols (30, 50, 70, 90, 100% ethanol) for 15 minutes each, twice. The samples were further subjected to 2 changes for 15 minutes each with 100% hexamethyldisilazane (HDMS; Electron Microscopy Sciences, Washington, USA). Finally HDMS was removed and let to air dry for 2h. Afterwards, the constructs were sputter coated with gold (Fisons Instruments, Sputter Coater SC502, UK) and analyzed with a Leica Cambridge S360 (UK) scanning electron microscope.

2.7.2. Cell viability by MTS assay

Cell viability was assessed after 24, 48, 72 hours and 7 days, using the MTS test. Cells cultured onto tissue culture polystyrene (TCPS) with standard culture medium were used as negative control. At each time point, cell-seeded scaffolds (*n*=3) were rinsed in 0.15M phosphate buffered saline (Sigma, USA) and immersed in a mixture consisting of serum-free cell culture medium and MTS reagent at 5:1 ratio and incubated for 3h at 37 ºC in a humidified atmosphere containing 5% CO2. After this, 200 µl (*n*=3) were transferred to 96 well plates and the optical density (O. D.) determined at 490 nm.

3. RESULTS AND DISCUSSION

3.1. FIBERS PRODUCTION AND CHARACTERIZATION

Usually, fibre or monofilament melt extrusion involves two stages: i) initially, the melt is forced through the die and a circular extrudate is obtained, ii) then this extrudate is stretched axially while being cooled down by forced convection/immersion in a water tank, in order to induce some degree of molecular orientation and thus improve the molecular properties. Simultaneously, the final diameter of the fibres/monofilaments becomes significantly smaller than that of the initial extrudate.

Unfortunately, fibers with high chitosan content cannot withstand the usual drawing ratios involved in conventional extrusion, which means that it is necessary to use capillary dies to obtain immediately small diameter extrudates. However, since chitosan particles are usually around 400μm in size, this limits the lowest die diameter to adopt, if operation steady state is to be achieved.

In this work, the chitosan-based fibers were produced using a prototype micro-extruder that could be coupled to capillary dies of different diameters. The extrudates were air-cooled without any significant stretch and winded. The extruder operating conditions are summarized in Table 7.1.

Table 7.1. Processing conditions of chitosan based fibers using a micro-extruder.

COMPOSITION	BARREL TEMPERATURE (°C)	SCREW SPEED (RPM)
25Ch-75PBS [a]	140-150	35
50Ch-50PBS [b]	140-155	35
50Ch-50PBTA [c]	155-160	35

[a] Blend containing 25% by weight of chitosan and 75% by weight of PBS
[b] Blend containing 50% by weight of chitosan and 50% by weight of PBS
[c] Blend containing 50% by weight of chitosan and 50% by weight of PBTA

The morphology of the obtained fibers was analyzed by SEM and representative micrographs are shown in Figure 7.1. Chitosan based fibers present a peculiar morphology that is clearly affected by the particulate chitosan content. As the chitosan content increases, the surface roughness also increases creating some level of microporosity at the surface (Figs 7.1a and 7.1b).

To confirm what was the main parameter controlling the surface roughness, the fibers were mounted in epoxy resin and sliced to obtain longitudinal sections of the fibres. The sections were further immersed in eosin solution aiming at staining the chitosan domains and analyzing them by optical microscopy. The images of the stained longitudinal sections are shown in Figure 7.2. As observed on previous studies [20]

for injection molded samples, the fibers are composed of a continuous phase consisting of the polyester that surrounds the chitosan particles or domains (dispersed phase appearing in orange in the images).

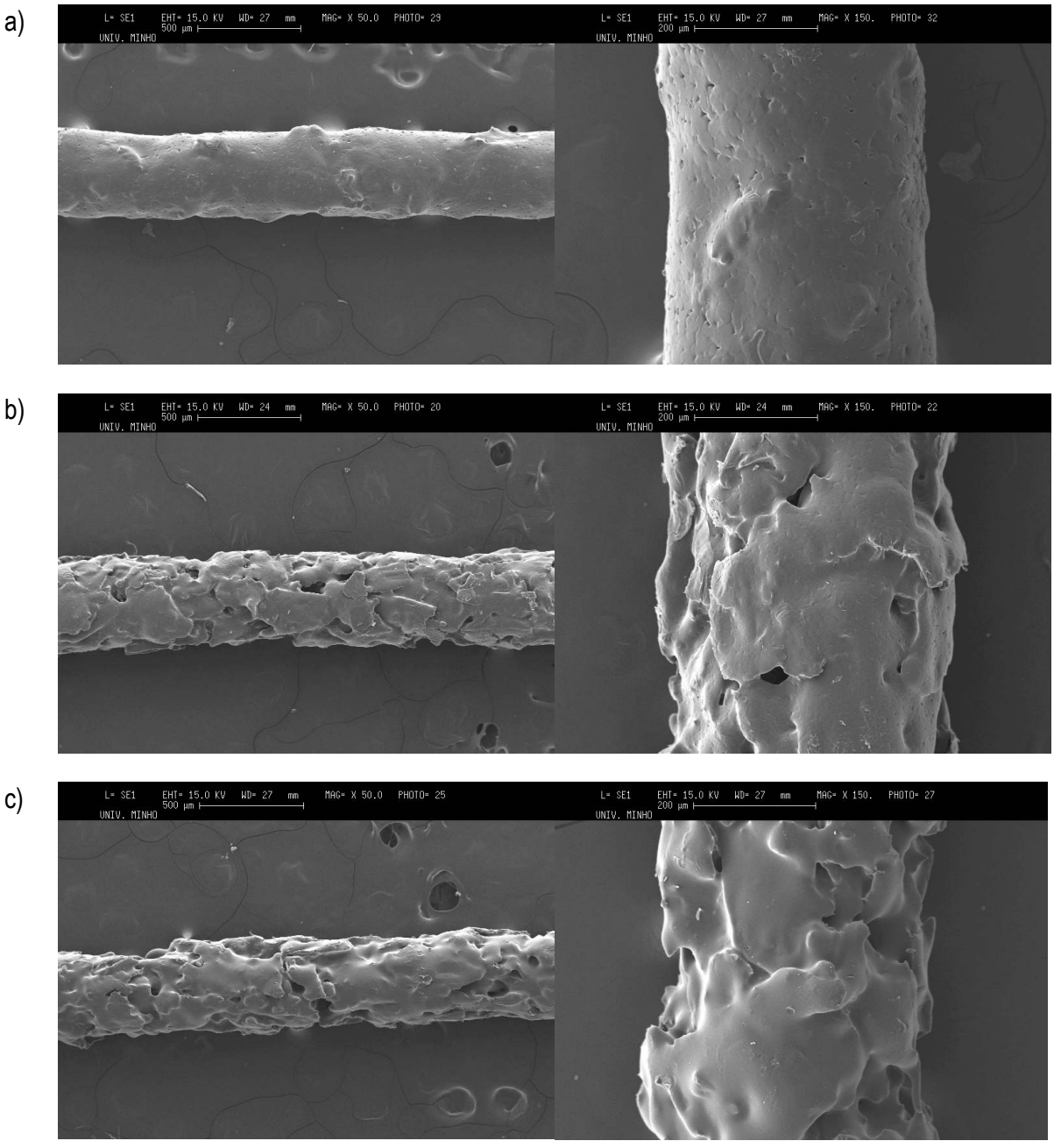

Figure 7.1. SEM images of the morphology of the fibers: a) Fiber of the blend 25Ch-75PBS; b) Fiber of the blend 50Ch-50PBS; c) Fiber of the blend 50Ch-50PBTA.

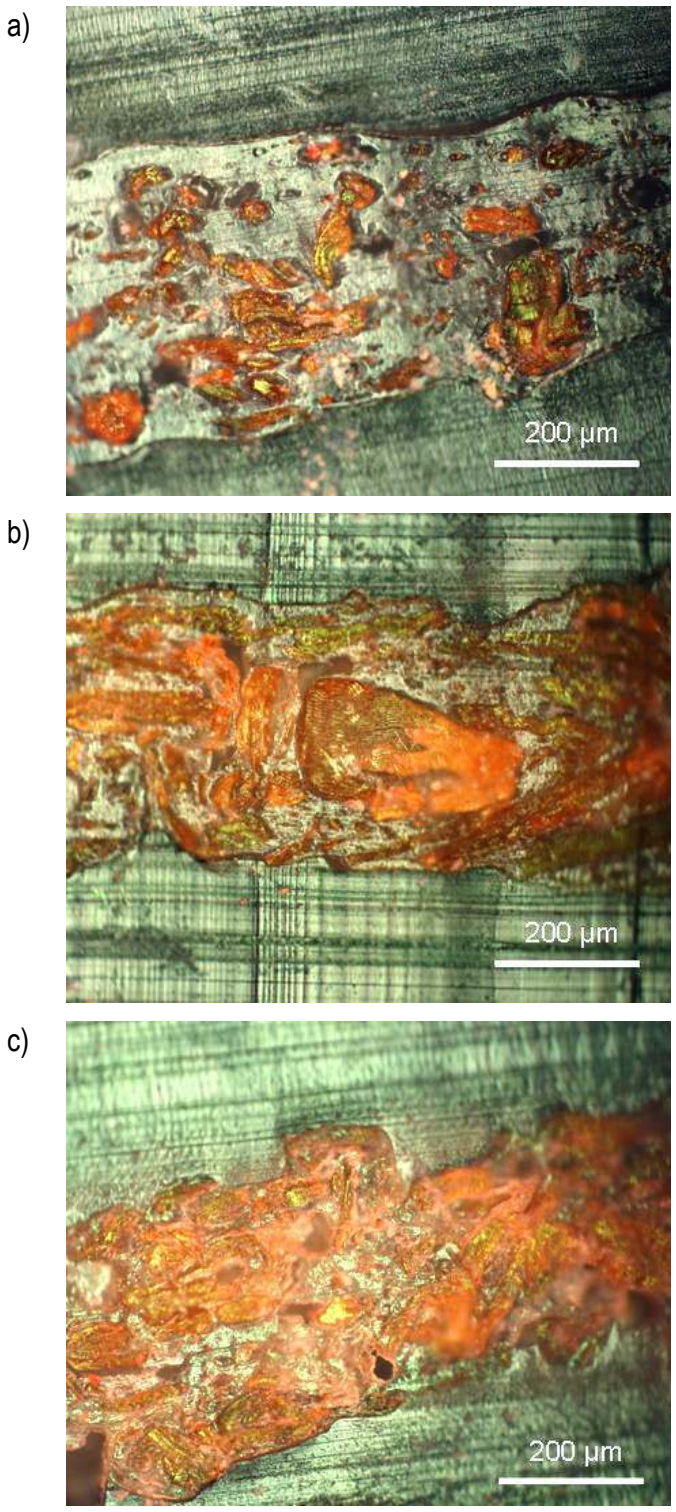

Figure 7.2. Optical microscopy micrographs of longitudinal sections of the fibers after being stained with eosin: a) 25Ch-75PBS; b) 50Ch-50PBS; c) 50Ch-50PBTA.

No significant differences are observed between fibers produced with the same content of chitosan and different polyesters (Figs 7.2b and 7.2c). The fibers produced with PBS with different contents of chitosan present significant morphological differences (Figs 7.2a and 7.2b). Thus, it is very clear to conclude that as the chitosan content increases, the chitosan domains aggregate and are more predominant, causing an increase on the fiber surface roughness. As the chitosan amount increases, there is less polyester available to embed and surround all the chitosan domains, exposing the chitosan phase at the surface and increasing the surface roughness.

The mechanical performance of the different fibers, determined in tensile tests, is shown in Table 7.2. As expected, both the fibres obtained with various chitosan contents and with different polyesters have significant differences on the mechanical performance. The fibers obtained from Ch-PBS, as the chitosan content increases the ultimate tensile strength (UTS) and the modulus decreases significantly. These results are not in accordance with the properties obtained by us in previous studies [20]. The difference on the results may be explained by the specific processing routine and to the constraints caused by the 2-D fibrous geometry with small diameters. Those small cross-section dimensions when using larger chitosan contents (50%wt) may lead to the formation of chitosan-rich aggregates with dimensions close to the diameter of the fiber. Those aggregates may reduce the quality of the interface with the polyester phase (the continuous phase) leading to a lower efficiency of stress transfer to the chitosan phase. Furthermore, the surface roughness also indirectly affects the evaluation of the mechanical properties by the over-estimation of the cross-section area of the fibers.

Table 7.2. Mechanical properties of the chitosan based fibers.

COMPOSITION	UTS (MPa) [d]	E_S (MPa) [e]	ε (%) [f]
25Ch-75PBS [a]	13.9 ± 3.0	795.2 ± 178.2	2.7 ± 0.5
50Ch-50PBS [b]	5.9 ± 2.3	499.7 ± 92.0	2.7 ± 0.9
50Ch-50PBTA [c]	5.3 ± 0.4	268.9 ± 46.3	3.6 ± 0.9

[a] Blend containing 25% by weight of chitosan and 75% by weight of PBS
[b] Blend containing 50% by weight of chitosan and 50% by weight of PBS
[c] Blend containing 50% by weight of chitosan and 50% by weight of PBTA
[d] Ultimate tensile stress
[e] Secant modulus
[f] Strain at break

From the group of fibers with the similar chitosan content, the ones produced with PBS have higher modulus and UTS than the ones produced with PBTA. This result was expected since it confirms the differences in modulus of the two polyesters. Similarly, the elongation at break was by the same reasons higher in the case of Ch-PBTA fibers. Those results are all consistent with the fact that PBTA is a more compliant matrix than PBS.

3.2. SCAFFOLDS PRODUCTION AND CHARACTERIZATION

Scaffolds were produced only with fibers having a chitosan/polyester ratio of 50/50 wt. Fiber mesh scaffolds were produced after cutting, heating and compressing the extruded fibers. The porous morphology of the novel chitosan based fiber mesh scaffolds was analysed by SEM (Fig. 7.3). The SEM migrographs allows concluding that the fiber compression process was successful in welding the fibers together into a mesh structure. It is also clear fom the SEM micrographs that no significant differences are detected between the Ch-PBS and the Ch-PBTA fiber mesh scaffolds. In both cases, the characteristic roughness of the fibers was maintained after the production of the scaffolds. The surface microporosity is preserved after the production of the scaffolds.

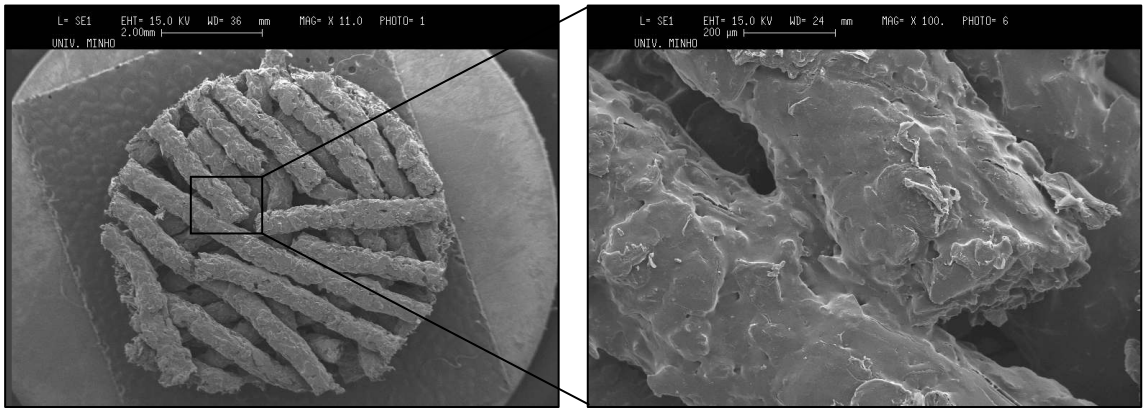

Figure 7.3. SEM micrographs of Ch-PBS (50/50wt%) fiber mesh scaffolds

A more detailed and quantitative analysis of the internal structure of the scaffolds was performed by micro-computed tomography (µCT). µCT images (2-D and 3-D) of the Ch-PBS fiber mesh scaffold are shown in Figures 7.4 and 7.5.

Most details observed in SEM micrographs were further confirmed in the μCT analysis. No significant differences were observed between both types of scaffolds by this very accurate technique. Furthermore, μCT allowed to confirm the existence of micropores (<20μm) on the fibers composing the scaffolds. Interestingly, these small pores are not only confined at the surface, but are also observed in the inner structure of the fibers (Figs 7.4 and 7.5). The presence of those micropores can cause an increase of the surface area what usually facilitates the cell adhesion. In fact, smoother surfaces are frequently less efficient in allowing the adherence of cells to the surface of fibers. Although the fibers were not specifically intended to have rougher surfaces, its surface morphology is interesting in facilitating the interaction with cells. This characteristic imight be very positive for the envisaged application.

Controlling cell adhesion and proliferation at the surface of scaffolds constitutes a key issue for tissue engineering. Surface topography, including the surface roughness, is recognized as a parameter that may have a dramatic influence over the cellular behavior. Different studies concluded that an increase in the surface roughness (keeping constant the surface chemistry) resulted in an improvement on cell adhesion, proliferation and differentiation of bone cells [22, 23].

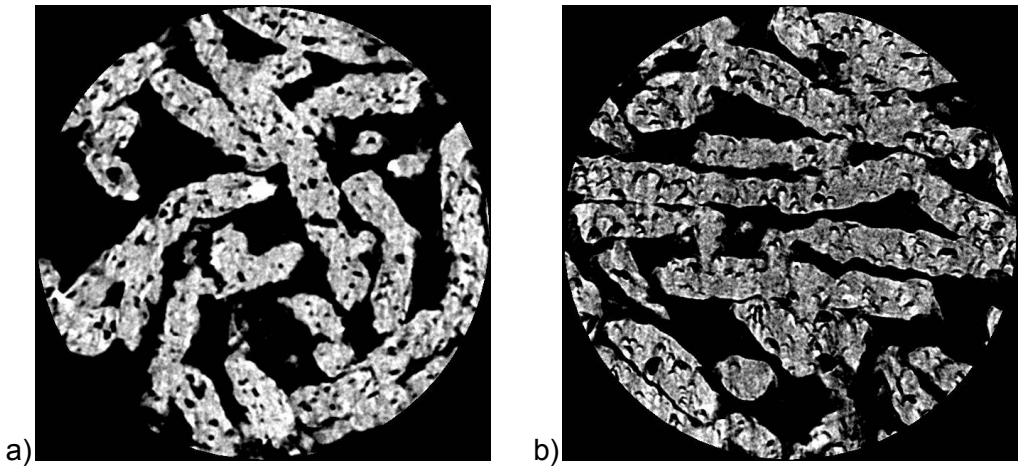

Figure 7.4. Representative 2-D μCT images of: a) Ch-PBS fiber mesh scaffold; b) Ch-PBTA fiber mesh scaffold

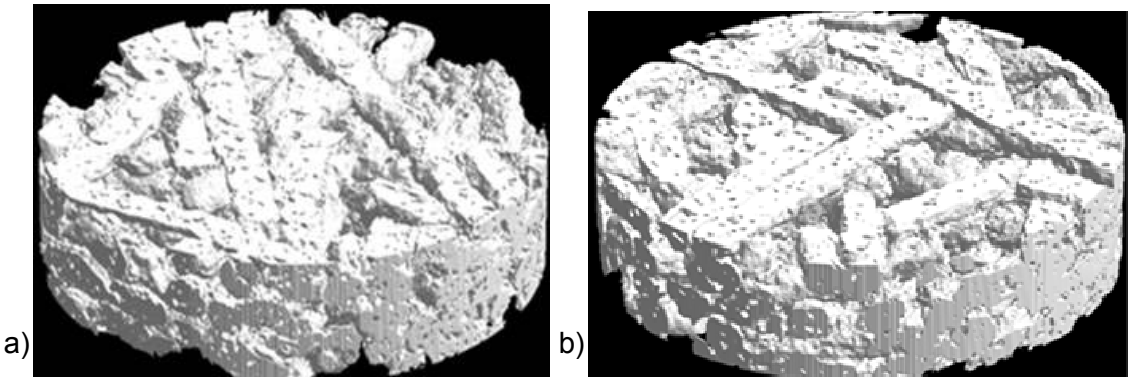

Figure 7.5. Representative 3-D μCT images of: a) Ch-PBS fiber mesh scaffold; b) Ch-PBTA fiber mesh scaffold

More recently, due to the advances in microfabrication it has been even more emphasized the analysis of the effects of nano-structured topographies. For example, endothelial cells and osteoblasts were shown to preferentially adhere to both nanometer and sub-micron structured titanium surfaces when compared to flat (smooth) titanium surfaces [24]. Other study used pit-patterned surfaces of polystyrene (PS) film with diameters 2.2 and 0.45 mm and islands-patterned (with similar dimensions) on PLLA surfaces. The results also confirm that the cell adhesion is enhanced in PLLA and PS surfaces with nano-scale and micro-scale roughnesses compared to the smooth surfaces on the same materials [25].

As previously referred, micro-porosity is also a parameter with a favorable affect on cell adhesion and proliferation [26, 27]. One probable hypothesis is that the micropores significantly increase the surface area of the material and this may enhance the protein adsorption process creating a larger number of anchorage points for cells. This effect contributes to the increase on the opportunities for cell adhesion and for proliferation.

An ideal scaffold should meet a large number of requirements that enable for their use in the tissue engineering of connective tissues. Three of these prerequisites are related with the degree of porosity, the pore dimensions and the level of interconnectivity of the porosity. The results of the morphological analysis are shown in Figures 7.3,7. 4 and 7.5 and confirm that the novel fiber mesh scaffold exhibits a good level of interconnectivity. The interconnectivity enables for an easy access of cells, nutrients and metabolite removal from the whole volume of the scaffold porous structure. The observed interconnectivity (also favoured by the fiber structure that limits the packing level) is suitable for an adequate support of cell attachment, growth and proliferation. The porosity and pore size of the scaffolds was determined by μCT and the results are shown in Table 7.3. An extensive porous area is

an advantage by facilitating the penetration of cells into the bulk of the scaffold, keeping the viability of cells by the diffusion of nutrients and removal of metabolic residues.

In addition to the requirements related with the porosity, other important scaffold features are related to their mechanical properties. Scaffolds should possess sufficient initial mechanical strength and stiffness to ensure minimal mechanical function. The minimum level of mechanical properties is related with the easy manipulation of the scaffold but also to the structural integration with the extracellular matrix of the tissue that intends to repair or regenerate. It is not strictly necessary that the mechanical properties of the scaffolds perfectly match the ones of the healthy tissue, but the stiffness and strength should be compatible with the stresses existing at the healing site [28].

The values of compressive modulus for both types of scaffolds are shown in Table 7.3. In both cases the scaffolds stiffness are within the range of modulus of the human cancellous bone and human cartilage and considerably lower than that of human cortical bone [29]. In any case, the mechanical properties, pore sizes and level of porosity are all compatible with the values required for the regeneration of bone and cartilage.

Table 7.3. Porosity, pore size and mechanical properties of the chitosan based fiber mesh scaffolds.

SCAFFOLD COMPOSITION	MACROPOROSITY (%)	PORE SIZE (μm)	E_S (MPa) [c]
50Ch-50PBS [a]	44.8 ± 2.1	260.4 ± 27.0	32.6±12.8
50Ch-50PBTA [b]	48.3 ± 4.6	246.0 ± 48.5	12.4 ±4.6

[a] Blend containing 50% by weight of chitosan and 50% by weight of PBS
[b] Blend containing 50% by weight of chitosan and 50% by weight of PBTA
[c] Secant modulus

3.3. CELL ADHESION RESULTS

SEM images allowed to determine that SaOs-2 cells were able to adhere to the surface of both types of chitosan-polyester based scaffolds (Fig. 7.6).

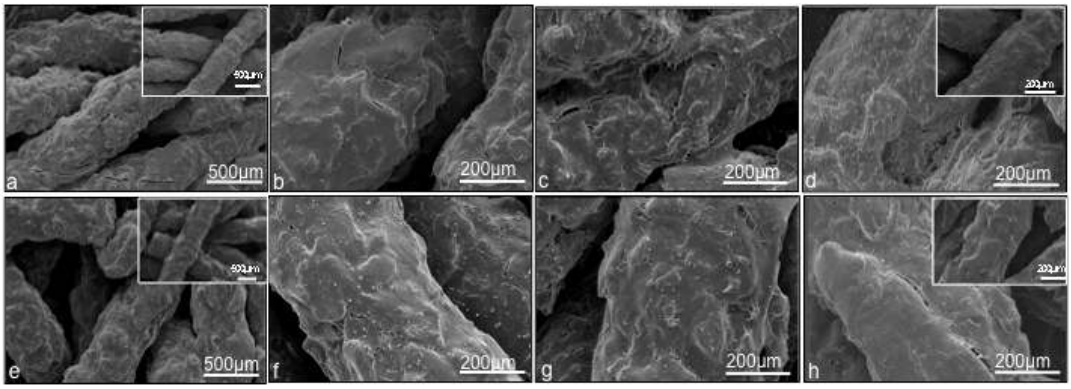

Figure 7.6. SEM micrographs of SaOs-2 cells morphology and adhesion at the surface of Ch-PBS scaffolds after a)1, b)2, c)3 and d)7 days of culture; and onto Ch-PBTA scaffolds after e)1, f)2, g)3 and h)7 days of culture. Lower figures correspond to the non-seeded of each type scaffolds.

Already after 1 day of cell culture, extensive cell colonization can be observed (Figs 7.6a and 7.6e). Cells completely covered the microfibers surfaces (Figs 6b and 6f) on both scaffold formulations. After 1 week of culture, further development of cell numbers and surface density are observed (Figs 7.6d and 7.6h), indicating that the SaOS-2 cells massively adhered and proliferated within both types of chitosan based scaffolds. It is also notorious a progressive and extensive cell proliferation over time (Fig. 7.6).

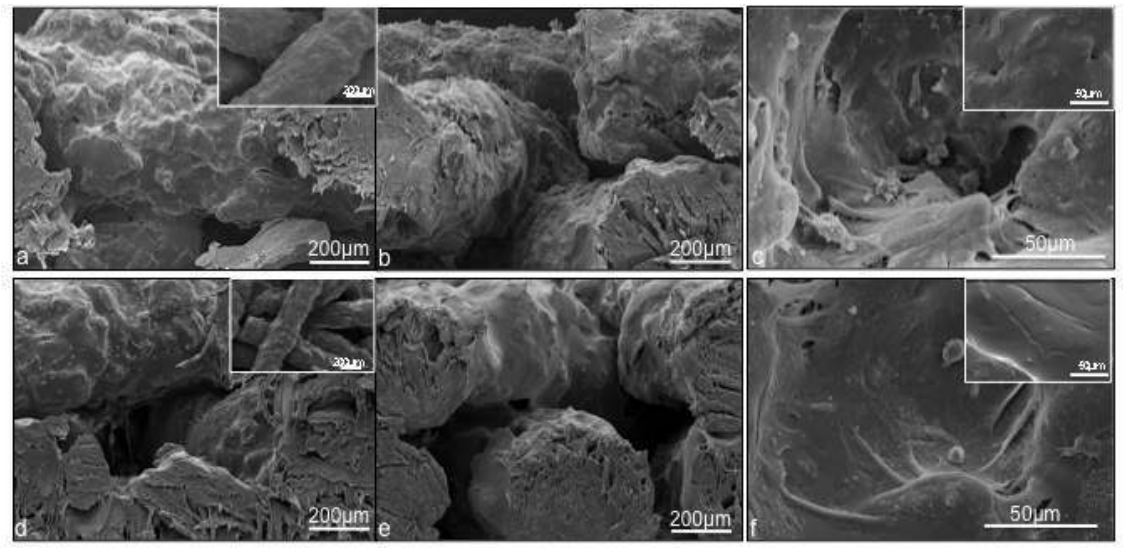

Figure 7.7. SEM micrographs of the cross-sections of cell cultured Ch-PBS scaffolds after a) 3 and b) days; and Ch-PBTA scaffolds after d)3 and e)7 days. High magnifications micrographs of the cell cultured Ch-PBS e) and Ch-PBTA f) at 3 days of culture. Lower figures correspond to the non-seeded of each type scaffolds.

It should be highlighted that the porosity size and interconnectivity are both adequate, since no pore occlusion was observed. The cells also proliferated to the interior regions of the scaffolds, as can be observed on Figure 7.7. At higher magnifications it is possible to observe already some extracellular matrix (ECM) produced by the cells (Figs 7.7c and 7.7f).

The present scaffold formulations were previously explored using other processing methodologies such as compression moulding followed by salt leaching [30]. Direct cell contact assays with those scaffolds showed to promote the attachment, proliferation and osteogenic differentiation of a mouse mesenchymal stem cell line [31]. A different study using the same source of cells showed that these cells cultured on those scaffolds, also differentiated into the chondrogenic lineage and maintained full viability [32]. However those previous scaffolds did showed limitations in the porosity size and interconnectivity. The present fiber based scaffolds showed a strong improvement both in the porosity and on the morphology and mechanical properties. Therefore, this study provides the first biological evaluation of the enhanced efficacy of these novel 3-D fibrous structures to support cell viability and proliferation.

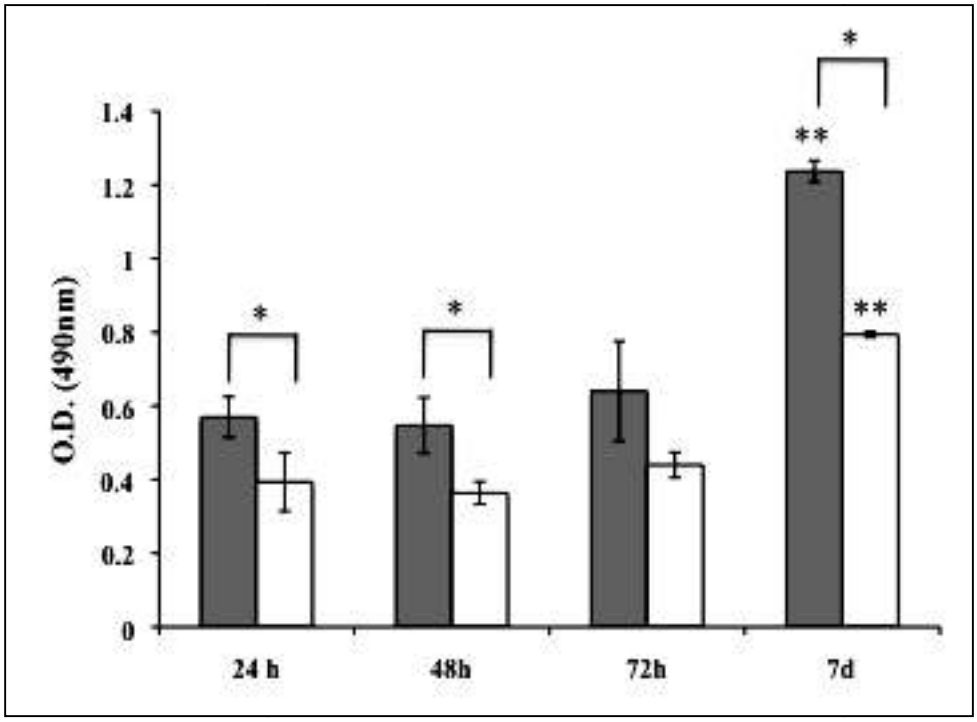

Figure 7.8. Viability of the SaOs-2 cells seeded and cultured onto the Ch–PBS (grey), Ch–PBTA (white) following 24, 48 and 72h and 7 days after cell seeding. Single asterisk (*) indicates a significant difference ($p<0.05$) between conditions at the same time point. Double asterisks (**) indicate a significant difference ($p<0.05$) of each material for 7days compared with the other time points.

In our previous studies evaluating the potential cytotoxicity of leached extracts from the developed scaffolds have we observed a non-cytotoxic effect when fibroblastic cell line was cultured during 72 h of incubation period (data not presented). This evaluation of the viability/activity of the cells seeded on the scaffolds since the initial seeding until the implantation is a subject of critical importance for the development and optimization of bone tissue-engineered constructs [33]. We herein also analysed the cell viability on the scaffolds during this experiments by the MTS test. This assay follows the reduction of substrate, 3-(4,5-dimethylthiazol-2-yl)-5(3-carboxymethoxyphenyl)-2(4-sulfofenyl)-2H-tetrazolium (MTS), into a brown formazan product by dehydrogenase enzymes active only in the viable cells. The results showed that the tested SaOs-2 were able to reduce MTS, showing increasing metabolic rates with increasing time of culture (Fig. 7.8), and denoting a high viability and proliferation profile.

Cells at the surface of the Ch-PBS scaffolds showed the highest values in terms of cell viability for all time periods when compared with the Ch-PBTA scaffolds in particular for the longer time point.

The results show a continuous development of the cell seeded population over the time period in culture at the surface of both scaffolds. It is clear that the attachment of cells is easier in the case of Ch-PBS scaffold, since in the earliest time point we observe a significantly larger cell activity on those scaffolds. The two initial time points show a comparable cell activity in both scaffold types. However, longer time points clearly confirm that the Ch-PBS outperforms the Ch-PBTA scaffolds. This result also confirms data obtained in the SEM analysis of the constructs scaffold/cells.

4. CONCLUSIONS

This study evidenced that it is possible to produce chitosan based fibers and chitosan based porous scaffolds using only melt based technologies and avoiding completely the use of solvents. The chitosan content in the blends plays an important role on the morphology and mechanical properties of the fibers: as the chitosan content cause increase in roughness but decrease in the mechanical properties. The scaffolds produced by fiber hot compression have shown an interesting distribution of micro and macroporosity that can play an important role on cell adhesion and proliferation. Morphological analysis confirmed that the fiber mesh scaffold exhibit adequate pore size and interconnectivity allowing for the penetration of cells into the bulk of the porous scaffold. The mechanical performance of both scaffolds is within the range of properties of the human cancellous bone and the human cartilage. Moreover, the

results obtained in direct contact assays revealed that the two types of chitosan-based fiber mesh scaffolds promoted the adhesion, proliferation and migration of the osteoblastic like cells into the interior of the scaffolds. In addition the Ch-PBS composite showed enhanced biological performance in terms of a more massive production of ECM, and in terms of viability numbers.

In conclusion we can say that these novel chitosan based fibrous scaffolds processed by melt in a completely solvent-free routine herein described evidenced properties of great interest to be used in solutions involving the engineering of connective tissues.

REFERENCES

1. Hutmacher, D.W. and S. Cool, Concepts of scaffold-based tissue engineering-the rationale to use solid free-form fabrication techniques. Journal of Cellular and Molecular Medicine, 2007. 11(4): p. 654-669.
2. Williams, D.F., Biomaterials and tissue engineering in reconstructive surgery. Sadhana-Academy Proceedings in Engineering Sciences, 2003. 28: p. 563-574.
3. Hutmacher, D.W., et al., State of the art and future directions of scaffold-based bone engineering from a biomaterials perspective. Journal of Tissue Engineering and Regenerative Medicine, 2007. 1(4): p. 245-260.
4. Gomes, M.E., et al., Influence of the porosity of starch-based fiber mesh scaffolds on the proliferation and osteogenic differentiation of bone marrow stromal cells cultured in a flow perfusion bioreactor. Tissue Engineering, 2006. 12(4): p. 801-809.
5. Griffon, D.J., et al., Chitosan scaffolds: Interconnective pore size and cartilage engineering. Acta Biomaterialia, 2006. 2(3): p. 313-320.
6. Malda, J., et al., The effect of PEGT/PBT scaffold architecture on the composition of tissue engineered cartilage. Biomaterials, 2005. 26(1): p. 63-72.
7. Freed, L.E., et al., Neocartilage Formation Invitro and Invivo Using Cells Cultured on Synthetic Biodegradable Polymers. Journal of Biomedical Materials Research, 1993. 27(1): p. 11-23.
8. Mikos, A.G., et al., Preparation of Poly(Glycolic Acid) Bonded Fiber Structures for Cell Attachment and Transplantation. Journal of Biomedical Materials Research, 1993. 27(2): p. 183-189.

9. Pashkuleva, I., et al., Starch/ethylene-co-vinyl alcohol fiber mesh scaffolds: Production, characterization and surface modification. Tissue Engineering Part A, 2008. 14(5): p. OP260.
10. Lazzeri, L., et al., Biodegradable hollow microfibres to produce bioactive scaffolds. Polymer International, 2005. 54(1): p. 101-107.
11. Pavlov, M.P., et al., Fibers and 3-D mesh scaffolds from biodegradable starch-based blends: Production and characterization. Macromolecular Bioscience, 2004. 4(8): p. 776-784.
12. Chen, X., et al., Ligament regeneration using a knitted silk scaffold combined with collagen matrix. Biomaterials, 2008. 29(27): p. 3683-3692.
13. Liu, H.F., et al., The interaction between a combined knitted silk scaffold and microporous silk sponge with human mesenchymal stem cells for ligament tissue engineering. Biomaterials, 2008. 29(6): p. 662-674.
14. Gomes, M.E., et al., Starch-poly(epsilon-caprolactone) and starch-poly(lactic acid) fibre-mesh scaffolds for bone tissue engineering applications: structure, mechanical properties and degradation behaviour. Journal of Tissue Engineering and Regenerative Medicine, 2008. 2(5): p. 243-252.
15. Gomes, M.E., et al., Effect of flow perfusion on the osteogenic differentiation of bone marrow stromal cells cultured on starch-based three-dimensional scaffolds. Journal of Biomedical Materials Research Part A, 2003. 67A(1): p. 87-95.
16. Cunha-Reis, C., et al., Influence of porosity and fibre diameter on the degradation of chitosan fibre-mesh scaffolds and cell adhesion. Journal of Materials Science-Materials in Medicine, 2007. 18(2): p. 195-200.
17. Tuzlakoglu, K., et al., Production and characterization of chitosan fibers and 3-D fiber mesh scaffolds for tissue engineering applications. Macromolecular Bioscience, 2004. 4(8): p. 811-819.
18. Fan, L.H., et al., Preparation and properties of alginate/carboxyrnethyl chitosan blend fibers. Carbohydrate Polymers, 2006. 65(4): p. 447-452.
19. Wang, Q., et al., Chitosan/polyethylene glycol blend fibers and their properties for drug controlled release. Journal of Biomedical Materials Research Part A, 2008. 85A(4): p. 881-887.
20. Correlo, V.M., et al., Properties of melt processed chitosan and aliphatic polyester blends. Materials Science and Engineering a-Structural Materials Properties Microstructure and Processing, 2005. 403(1-2): p. 57-68.
21. Covas, J.A. and P. Costa, A miniature extrusion line for small scale processing studies. Polymer Testing, 2004. 23(7): p. 763-773.

22. Kawahara, H., et al., In vitro study on bone formation and surface topography from the standpoint of biomechanics. Journal of Materials Science-Materials in Medicine, 2004. 15(12): p. 1297-1307.
23. Korovessis, P.G., D.D. Deligianni, and L.G. Lenke, Role of surface roughness of titanium versus hydroxyapatite on human bone marrow cells response. Journal of Spinal Disorders & Techniques, 2002. 15(2): p. 175-183.
24. Khang, D., et al., The role of nanometer and sub-micron surface features on vascular and bone cell adhesion on titanium. Biomaterials, 2008. 29(8): p. 970-983.
25. Wan, Y.Q., et al., Adhesion and proliferation of OCT-1 osteoblast-like cells on micro- and nano-scale topography structured pply(L-lactide). Biomaterials, 2005. 26(21): p. 4453-4459.
26. Bignon, A., et al., Effect of micro- and macroporosity of bone substitutes on their mechanical properties and cellular response. Journal of Materials Science-Materials in Medicine, 2003. 14(12): p. 1089-1097.
27. Hing, K.A., et al., Microporosity enhances bioactivity of synthetic bone graft substitutes. Journal of Materials Science-Materials in Medicine, 2005. 16(5): p. 467-475.
28. Hutmacher, D.W., Design and Fabrication of scaffolds via Solid Free-Form Fabrication, in Biodegradable Systems for Tissue in Engineering and Regenerative Medicine, R.L.R.a.J.S. Roman, Editor. 2004, CRC Press, Boca Raton p. 67-89.
29. Yang, S.F., et al., The design of scaffolds for use in tissue engineering. Part 1. Traditional factors. Tissue Engineering, 2001. 7(6): p. 679-689.
30. V. M. Correlo, L.F.B.E.P.A.R.C.-P.M.L.A.d.S.M.B.J.F.M.N.M., Melt-based compression-molded scaffolds from chitosan-polyester blends and composites: Morphology and mechanical properties. 2008. p. NA.
31. Costa-Pinto, A.R., et al., Adhesion, proliferation, and osteogenic differentiation of a mouse mesenchymal stem cell line (BMC9) seeded on novel melt-based chitosan/polyester 3-D porous scaffolds. Tissue Engineering Part A, 2008. 14(6): p. 1049-1057.
32. Oliveira, J.T., et al., Assessment of the Suitability of Chitosan/PolyButylene Succinate Scaffolds Seeded with Mouse Mesenchymal Progenitor Cells for a Cartilage Tissue Engineering Approach. Tissue Engineering Part A, 2008. 14(10): p. 1651-1661.
33. Wilson, C.E., et al., Evaluating 3-D bone tissue engineered constructs with different seeding densities using the alamarBlue (TM) assay and the effect on in vivo bone formation. Journal of Materials Science-Materials in Medicine, 2002. 13(12): p. 1265-1269.

SECTION 4.

CHAPTER VIII.

Summary and general conclusions

CHAPTER VIII.

Summary and general conclusions

1. SUMMARY AND GENERAL CONCLUSIONS

Considerable effort has been directed towards the development of scaffolds using natural polymers for bone and for cartilage tissue engineering. Nevertheless, the use of natural polymers still has some disadvantages that limit their application. Even tought chitosan exhibit a range of properties that make it suitable for use as alternatives to currently used biomaterials, its mechanical properties and processability are less than ideal which precludes its use as material in load bearing applications. The development of hybrid materials that combine naturally occurring polymers with biocompatible synthetic polymers is expected to minimize the mismatch of mechanical properties and preserve biocompatibility. Little research has been conducted in the melt blending of synthetic polyester and chitosan. The main objective of this thesis was to: i) compound and evaluate the properties of chitosan and biodegradable aliphatic polyesters blends and composites processed using melt based technologies; ii) study the water absorption and degradation characteristics of the produced blends and composites; iii) produce chitosan-based scaffolds with different architectures by melt based technologies.; iv) to evaluate their cytotoxic behaviour and conduct direct contact assays aiming to validate their potential use in bone or cartilage tissue engineering applications.

The general conclusions of the research work produced in the present thesis, which extends from Chapter III to VII, are summarized as follows:

1.1. PROPERTIES OF MELT PROCESSED CHITOSAN AND ALIPHATIC POLYESTER BLENDS

Chapter III describes for the first time the processing of chitosan-polyester based blends using melt based methods. In this work, chitosan was melt blended with several aliphatic polyesters including PCL, PBS, PLA, PBTA, and PBSA. Morphological analysis has shown that chitosan displayed intermediate adhesion to the polyester matrix and its addition to the blends decreased the tensile strength but increased the tensile modulus. The same analysis indicated that the skin layer of injected samples is polyester rich, while the core is a blend of chitosan and polyester. The chitosan phase agglomerated into spherical domains or were clustered into sheaths. Pull-out of chitosan particles was evident in tensile-fractured surfaces for blends of chitosan with ductile polymers but absent in the blends with PLA.

With this study allowed to conclude that it was possible to produce chitosan based belnds with interesting properties.

1.2. HYDROXYAPATITE REINFORCED CHITOSAN AND POLYESTER BLENDS FOR BIOMEDICAL APPLICATIONS

Chapter IV reports the preparation of hydroxyapatite, chitosan, and aliphatic polyester composites by melt blending methods. The polyesters include PCL, PLA, PBS, and PBTA. These composites were injection molded and evaluated for thermal, morphological, and mechanical properties. The addition of hydroxyapatite decreased the crystallinity in chitosan/PBS blends, while in blends containing chitosan/PCL, the crystallinity increased. The two main diffraction peaks observed using WAXS are unaffected by the amount of chitosan or hydroxyapatite. The produced materials presented a range of acceptable properties but the addition of high volume fraction of fillers (both chitosan and hydroxyapatite) led to processing difficulties that made for poor dispersion, particularly for the HAin the composite. This coupled with the lack of adhesion of HA to the matrix led to reduced mechanical properties over blends of chitosan and polyester. Thus alternative processing techniques or the use coupling agents or the functionalization of the ceramic needs to be considered in order to improve on the properties since the current properties are the lower bound of what is reported for bone.

1.3. WATER ABSORPTION AND DEGRADATION CHARACTERISTICS OF CHITOSAN-BASED POLYESTERS AND HYDROXYAPATITE COMPOSITES

The work described on Chapter V aims at reporting on the water absorption and degradation of the newly developed polymer blends and composites since these properties are critical for their possible applications as biomaterials. The water uptake and the degradation properties, as measured by the loss in tensile strength, were evaluated as a function of time. In this study, the rate and the equilibriumwater uptake were proportional to the amount of chitosan in the blend. Increased chitosan content increased the water uptake and diffusion coefficient of the blends. For blends with the same chitosan content, the lowest equilibrium water content was observed in blends containing PCL, and the highest water uptake was experienced by the blends containing PLA. The addition of HA to chitosan and polyester significantly reduced the equilibrium water uptake. The water uptake did not follow the classical Fickian diffusion laws and could be expressed by a two-stage sorption non-Fickian diffusion model. Contact angle measurement was used to quantify the changes in surface hydrophilicity as a function of chitosan and polyester composition. The glycerol contact angle decreased with increasing synthetic components in the blend. The blends and composites also showed increased degradation, as quantified by a loss in

their mechanical properties, with increase in natural content. The degradation of properties was directly related to the water uptake of the blends; the higher the water uptake, the higher the degradation. Pure polyesters, while having low water uptake, nevertheless showed significant degradation by a precipitous drop in the strain at break. Among the polyesters, poly(lactic acid) displayed maximum degradation, while polycaprolactone displayed the least.

1.4. MELT-BASED COMPRESSION-MOLDED SCAFFOLDS FROM CHITOSAN–POLYESTER BLENDS AND COMPOSITES: MORPHOLOGY AND MECHANICAL PROPERTIES

On what concerns to the production of novel scaffolds made from blends of chitosan and biodegradable synthetic aliphatic polyesters produced by the melt-based routine involving compression molding and salt leaching the following remarkes can be made. By changing both the amount and average particle size of the porogen agent used, it was possible to prepare scaffolds with different macroscopic architecture using a melt-based approach. The mechancial properties of the produced scaffolds could be taylored by varying the type and amount of porogen used: i) for the scaffolds produced using similar particle size range, increasing the porosity decreased the yield stress and the compression modulus; ii) for scaffolds prepared using particles of smaller size were observed to have lower compressive modulus than the ones prepared using a larger particle size range. Although contrary to the expected result, it was shown by analyzing the morphology to be consistent with the pore interconnectivity observed. Addition of chitosan increased the compressive modulus of the scaffolds produced using PCL and PBTA, but reduced the compressive modulus of those developed using PBS and PBSA. Addition of HA led to a decrease in the compressive yield stress and compressive modulus, probably because of the low interface adhesion. Thermal properties of chitosan-PBS-based scaffolds were analyzed, and it was found that the melting temperature decreased with increasing chitosan content. Cytotoxic screening by means of MTS test revealed that L929 cells had similar metabolic activities to that obtained by the negative control. Therefore, the leachables released from the tested scaffolds could be considered as nontoxic and clearly cytocompatible.

1.5. MELT PROCESSING OF CHITOSAN-BASED FIBERS AND FIBER-MESH SCAFFOLDS FOR THE ENGINEERING OF CONNECTIVE TISSUES

Three-dimensional porous scaffolds play a pivotal role in tissue engineering of human tissues like bone and cartilage. The scaffold provides the necessary support for cells to attach, proliferate and maintain their differentiated phenotype. Numerous techniques have been used to produce porous scaffolds

including fiber bonding. In Chapter VII we report the production of chitosan based fibers and chitosan fiber mesh scaffolds by melt processing (solvent-free) to be used as tissue engineering templates. As observed in the previous studies, the chitosan content in the blends plays an important role on the morphology and mechanical properties of the fibers: as the chitosan content cause increase in roughness but decrease in the mechanical properties. The scaffolds produced by fiber hot compression have shown an interesting distribution of micro and macroporosity that can play an important role on cell adhesion and proliferation. Morphological analysis confirmed that the fiber mesh scaffold exhibit adequate pore size and interconnectivity allowing for the penetration of cells into the bulk of the porous scaffold. The mechanical performance of both scaffolds is within the range of properties of the human cancellous bone and the human cartilage. Moreover, the results obtained in direct contact assays revealed that the two types of chitosan-based fiber mesh scaffolds promoted the adhesion, proliferation and migration of the osteoblastic like cells into the interior of the scaffolds. In addition the Ch-PBS blends showed enhanced biological performance in terms of a more massive production of ECM, and in terms of viability numbers.

The main motivation for the work described on this thesis was to develop and to produce a new range of chitosan based scaffolds using novel polymeric matrices in an established melt processing technology. Most of the approaches reported in the literature to produce scaffolds from chitosan-based blends or composites involve the use of solvents, being this work the first reporting the use of a melt-based route. Moreover, the methodologies described in this thesis are very versatile and avoid the drawbacks associated with solvents and allows producing a large variety of scaffolds with a wide range of porosities and pore morphologies using different polymers. The scaffolds were made with different methods allowing to obtain scaffolds with different architectures and consequentely with different pore sizes and porosity.

As a final remark, we can say that this thesis is a '*proof-of-concept'* showing that these materials (novel chitosan based blends and composites) and scaffolds processed by melt in a completely solvent-free routine herein described evidenced properties of great interest to be used in solutions involving the engineering of connective tissues.